

STRATIATIONS IN A PLASMA COLUMN

by

ROBERT MELSON PERKIN

Royal Holloway College

U. N. C. LIBRARY	
CLASS	TBPP
No	Per
ACC No	133,715
DATE ACQ	NOV. '76

This thesis is submitted in partial fulfilment
for the requirements for the Degree of Doctor
of Philosophy in the University of London

April, 1976

ProQuest Number: 10097423

All rights reserved

INFORMATION TO ALL USERS

The quality of this reproduction is dependent upon the quality of the copy submitted.

In the unlikely event that the author did not send a complete manuscript and there are missing pages, these will be noted. Also, if material had to be removed, a note will indicate the deletion.



ProQuest 10097423

Published by ProQuest LLC(2016). Copyright of the Dissertation is held by the Author.

All rights reserved.

This work is protected against unauthorized copying under Title 17, United States Code.
Microform Edition © ProQuest LLC.

ProQuest LLC
789 East Eisenhower Parkway
P.O. Box 1346
Ann Arbor, MI 48106-1346

ABSTRACT

An investigation into wave interactions between self-excited ionization waves - striations - in the positive column of a direct current argon discharge is described.

Since such self-excited ionization waves are determined by the ionization processes in the discharge, they are inherently nonlinear and a variety of nonlinear effects may be observed.

After reviewing the theory and experimental observations for small amplitude linear ionization waves in gas discharges, experimental data obtained from an argon discharge, 5 cm in diameter, 110 cms in length, run at gas pressures between 0.1-1.5 torr and discharge currents of 20-250 mA, are presented.

Linear interactions between large amplitude self-excited waves of the same frequency, and nonlinear mode coupling between waves of different frequencies and wave numbers are reported and the characteristics of each wave type are described. In order to interpret some of the phenomena observed for the self-excited waves, experiments where an external alternating voltage was applied across the discharge were performed.

Following a general discussion of wave modulation the wave-wave mode coupling is interpreted as due to nonlinear interactions which may arise during the initial nonlinear growth of ionization waves.

A physical model for the nonlinear behaviour is described. By including a nonlinear term in the basic theory of striations expressions are derived which account for the mode-coupling and support the physical interpretation.

Theoretical techniques previously used to describe the nonlinear behaviour of water waves are outlined, and then applied to ionization waves to predict further nonlinear effects which could not be obtained from the modified linear theory.

Finally, a general overall view of two-wave interactions between ionization waves in a discharge is presented using, as an example, the results from a neon discharge. The experimental observations are related to the linear and nonlinear growth of the waves.

C O N T E N T S

	<u>Page</u>
ABSTRACT	2
ACKNOWLEDGEMENTS	8
 <u>CHAPTER I</u> 	
<u>INTRODUCTION</u>	
1.1 INTRODUCTION	9
 <u>CHAPTER II</u> 	
<u>REVIEW</u>	
2.1 INTRODUCTION	13
2.2 HISTORICAL SURVEY	13
2.3 SMALL AMPLITUDE STRIATIONS	17
2.4 DERIVATION OF THE HYDRODYNAMIC EQUATION FOR STRIATIONS	21
2.5 PHYSICAL MECHANISM OF BACKWARD WAVES	27
2.6 LIMITATION OF THE BASIC DIFFUSION MODEL	31
2.7 WAVE VARIETIES AT LOW CURRENTS: EFFECT OF THE ELECTRON GAS	32
2.8 LARGE AMPLITUDE STRIATIONS AND NONLINEAR EFFECTS	36
2.9 MODE-COUPLING AND MODULATION OF SELF-EXCITED WAVES	42
2.10 FACTORS INFLUENCING MOVING STRIATIONS	44
2.11 THE UNIFORM GLOW DISCHARGE	46
 <u>CHAPTER III</u> 	
<u>EXPERIMENTAL APPARATUS AND MEASURING TECHNIQUES</u>	
3.1 INTRODUCTION	50
3.2 DISCHARGE TUBE AND VACUUM APPARATUS	50
3.3 ELECTRICAL CIRCUIT	52
3.4 ARTIFICIAL EXCITATION OF STRIATIONS	53
3.5 FILLING THE SYSTEM WITH GAS	54
3.6 RUNNING THE DISCHARGE	54
3.7 DOUBLE LANGMUIR PROBE	54
3.8 DETECTION OF THE WAVES	57
3.9 CAPACITIVE PICK-UP PROBE	57
3.10 PHOTOMULTIPLIER	57
3.11 SPECTRUM ANALYSER	58
3.12 SPACE-TIME DISPLAY	59
3.13 SPACE-TIME DISPLAY FOR IRREGULARLY MOVING STRIATIONS	60

C O N T E N T S

(continued)

Page

CHAPTER IV

EXPERIMENTAL OBSERVATIONS OF SELF-EXCITED WAVES
IN THE ARGON DISCHARGE

4.1	INTRODUCTION	62
4.2	LINEAR INTERACTIONS: CHARACTERISTICS OF THE SELF-EXCITED WAVES WITH A FUNDAMENTAL FREQUENCY IN RANGE (b): 1 - 5 KHz	64
4.3	LINEAR INTERACTIONS: SYNCHRONOUS OSCILLATIONS	78
4.4	LINEAR INTERACTIONS: CHARACTERISTICS OF THE WAVES IN FREQUENCY RANGE (a)	81
4.5	NONLINEAR INTERACTIONS OF THE SELF-EXCITED WAVES	83
4.6	CONCLUSION	102

CHAPTER V

EXPERIMENTAL RESULTS OBTAINED WHEN AN EXTERNAL ALTERNATING
VOLTAGE WAS APPLIED ACROSS THE DISCHARGE

5.1	INTRODUCTION	103
5.2	WAVES EXCITED IN FREQUENCY RANGE (b)	103
5.3	CHARACTERISTICS OF THE WAVES EXCITED IN THE LOWER FREQUENCY RANGE (a)	105
5.4	GENERATION OF 'APPARENT' STATIONARY STRIATIONS AND ACCOMPANYING EFFECTS	107
5.5	COUPLING OF THE SELF-EXCITED WAVES WITH THE WAVES PRODUCED BY THE EXTERNALLY APPLIED VOLTAGE	117
5.6	CONCLUSION	119

CHAPTER VI

MODULATION OF A PLANE WAVE

6.1	INTRODUCTION	120
6.2	REPRESENTATION OF THE WAVE	120
6.3	SPACE-TIME DIAGRAMS	121
6.4	FREQUENCY SPECTRUM	125

C O N T E N T S

(continued)

Page

CHAPTER VII

INTERPRETATION OF THE NONLINEAR COUPLING BETWEEN
THE WAVES IN THE ARGON DISCHARGE

7.1	INTRODUCTION	130
7.2	GENERAL REMARKS	130
7.3	POSSIBLE EXPLANATIONS FOR THE WAVE INTERACTIONS	131
7.4	INTERPRETATION OF THE WAVE INTERACTIONS: AMPLITUDE AND PHASE MODULATION	134
7.5	PHYSICAL MODEL FOR WAVE COUPLING	146

CHAPTER VIII

THE EXTENSION OF LINEAR THEORY TO
DESCRIBE NONLINEAR EFFECTS

8.1	INTRODUCTION	149
8.2	EXTENSION OF THE LINEAR EQUATION	150
8.3	GENERATION OF HARMONIC TERMS	152
8.4	RELATIVE VALUES OF ELECTRON DENSITY AND TEMPERATURE	153
8.5	NONLINEAR INTERACTION BETWEEN TWO WAVES	154
8.6	NONLINEAR INTERACTIONS: VIRTUAL WAVES	155
8.7	NONLINEAR INTERACTIONS: PHASE MODULATION	156

CHAPTER IX

VARIATIONAL METHODS AND THEIR APPLICATION
TO IONIZATION WAVES

9.1	INTRODUCTION	161
9.2	GENERAL THEORY	161
9.3	NONLINEAR EFFECTS	163
9.4	APPLICATION TO IONIZATION WAVES	164
9.5	INTERPRETATION OF WAVE COUPLING RESULTS IN ARGON	166
9.6	LINEAR EQUATIONS APPLIED TO AN INHOMOGENEOUS MEDIUM	167

C O N T E N T S

(continued)

Page

CHAPTER X

A GENERAL DESCRIPTION OF THE MODE-COUPLING
BETWEEN STRIATIONS

10.1	INTRODUCTION	170
10.2	RESULTS FROM A NEON DISCHARGE	170
10.3	GENERAL DISCUSSION OF MODE COUPLING BETWEEN TWO IONIZATION WAVES	174

CHAPTER XI

<u>CONCLUSIONS</u>	177
--------------------	-----

APPENDICES

App.A.1	SOLUTIONS OF PARTIAL DIFFERENTIAL EQUATIONS BY THE METHOD OF CHARACTERISTICS	181
App.A.2	PUBLISHED PAPERS	185
	REFERENCES	186
	LIST OF SYMBOLS	189

ACKNOWLEDGEMENTS

I wish to express my sincere gratitude to my supervisor, Dr E.R. Wooding, for providing me with the opportunity to carry out research, and for his constant support and encouragement during this work.

Special thanks are due to my parents whose moral and financial support has enabled me to pursue my studies at University.

Financial assistance from the Science Research Council is gratefully acknowledged.

It is a pleasure to record my thanks to Dr P. Lukac, Komensky University, Bratislava, for his friendship, and helpful advice during the early stages of this work. The hospitality and guidance shown to me while a guest at the Institute of Physics, Prague, by Dr L. Pekarek and his colleagues is remembered with pleasure.

The friendly assistance provided by the technical staff, notably Messrs J. Henley and R. Mason, contributed to the smooth running of the experiment.

Finally, I am indebted to Ina Godwin for her excellent typing and layout of the thesis.

CHAPTER I
INTRODUCTION

Striations in the positive column of a glow discharge are one of the most readily observed plasma wave instabilities. In molecular gases stationary layers of alternating light and dark regions can be seen quite distinctly whilst in inert gases the striations are usually travelling waves which move too rapidly to be distinguished by the naked eye; the discharge column appears uniform.

Only within the last decade has the origin and physical nature of striations been understood. They are not acoustic type waves which rely on the inertia of the ions for energy propagation, but rather they are waves resulting from changes in the charged particle or metastable densities which are determined by the electron temperature dependent ionization or excitation rates. For this reason the term ionization wave is often used as an alternative expression to striations.

At pressures greater than about 1 torr the ionization waves are the only surviving low frequency waves since they are independent of the ion inertia and so cannot be damped by the friction between the ions and the neutrals.

The most commonly observed form of ionization wave has a backward wave characteristic: the group velocity is directed towards the anode whereas the phase velocity is directed towards the cathode. Unfortunately early investigations were concerned with self-excited waves and neither their origin nor backward nature were apparent from the observations.

Backward waves are caused by a change in electron temperature which propagates from the cathode end of the positive column towards the anode as a 'stratification' wave. The stratification wave gives rise to changes in the discharge parameters, such as electric field and light intensity, which

propagate as striations towards the cathode. The striations represent the motion of points of equal phase and as such, give information on the phase velocity of the wave motion, the stratification wave represents the propagation of wave energy and is related to the group velocity of the wave motion. In experimental studies it is usually the striations, or 'wave crests', which are observed.

The uniform direct current discharge may be characterized by various state variables such as electron density and temperature, electric potential, molecular weight of the gas, radius of the tube and pressure of the neutral gas. Since relationships exist between certain of these variables they are not all independent.

If the value of one of the appropriate state variables of the uniform discharge, for example the electric potential, is slightly changed from its equilibrium value then a disturbance in the other related state variables will result and a wave may propagate in the discharge. When the initial perturbation is of small amplitude, then it is often the case that the wave will be damped out as it travels through the discharge which will eventually return to its initial state. The frequency and wavelength of the wave are determined by the equilibrium, or averaged values, of the state variables and are related through a dispersion relation. If more than one wave is present then the waves obey the principle of superposition. Theoretically, the essential features of the waves may be determined from the linearised equations of energy and continuity for each particle type, together with the Poisson equation.

For certain discharge regimes, however, the waves observed are of large amplitude and are absolutely unstable, that is, following a localized perturbation the waves exist throughout the length of the positive column for all time. Often many waves exist simultaneously and the resultant

frequency spectrum may be continuous or consist of many discrete lines. For these situations the original perturbation in a state variable gives rise to a wave, initially of small amplitude, which grows as it travels through the discharge.

A point may be reached where the wave itself, now of large amplitude, perturbs the discharge which results in self-modulation of the wave or the generation of different frequencies. This process may be thought of as the wave reacting back on the state variables to produce further perturbations and a change in the averaged value of the state variables. The dispersion relation between the frequency and wavelength now becomes dependent on the amplitude of the waves. Waves governed by such a dispersion relation are termed nonlinear. The linearised continuity equations prove inadequate to explain the nonlinear phenomena, higher order terms must be included. Nonlinear interactions between nonlinear waves can no longer be explained using the principle of linear superposition.

In this thesis the self modulation and the interactions between self-excited waves in an argon discharge will be described. When this work was started there still remained the problem of interpreting a large amount of experimental data on self excited waves. As will be seen in the review chapter, often a continuous frequency spectrum was obtained when the motion of the striations was very irregular. Subsequently Grabec has shown that such a spectrum and irregular motion are a result of the nonlinear evolution of the wave.

In many cases, however, a multiline frequency spectrum, as distinct from a continuous spectrum, was observed when two or more waves were present simultaneously in the discharge. Recent work has shown that sometimes such multiline spectra are due to the excitation of many waves which belong to a single dispersion curve.

The situation when the multiline spectra cannot be related to the excitation of many waves has to be explained. Associated with this problem is the question of the connection between the different types of frequency spectra and the accompanying variation in wave velocity, which, in some cases, gives rise to 'apparent' disturbances moving towards the anode. These problems are dealt with in the present work and an attempt is made to present a general picture of interactions between striations.

The outline of the thesis is as follows: In Chapter II the essential phenomena associated with ionization waves are reviewed. The experimental apparatus and measuring techniques are dealt with in Chapter III.

The observations made on the purely self-excited waves in the argon discharge are described in Chapter IV. An interpretation is given of some of the effects, but the explanation of the nonlinear wave interactions is deferred until a later chapter. The results obtained when an alternating external voltage was applied across the discharge are described in Chapter V.

In Chapter VI, a general discussion of wave modulation is presented. The conclusions drawn are used in Chapter VII as a basis for the explanation of the mode-coupling effects already described in Chapters IV and V. A physical model of the interactions is discussed.

The linear theory of striations is extended, in Chapter VIII, to describe some of the nonlinear effects seen in earlier chapters. Theoretical methods previously used to predict the behaviour of nonlinear water waves are outlined in Chapter IX and applied to striations.

In Chapter X the evolution of the nonlinear coupling between two waves is discussed using as a basis, some recent experimental results from a neon discharge.

The conclusions drawn from the work are presented in Chapter XI.

CHAPTER II

REVIEW

2.1 INTRODUCTION

Although the existence of moving striations has been known for over a century, it was not until the development of pulsed techniques to generate transient small amplitude striations that any significant insight into the physical mechanisms producing the waves was obtained. Such a state of affairs was due largely to the fact that early investigations were concerned with self-excited waves whose origins were concealed by their non-linear nature.

The results obtained from detailed studies of small amplitude waves has enabled recent investigations to turn full circle, in a sense, back to the early days: by extending the linear theory and models, the nonlinear effects associated with self-excited striations can now be explained.

2.2 HISTORICAL SURVEY

2.2.1 Early Work

The work prior to the 1950's was concerned with self-excited striations and no clear picture emerged owing to the difficulty in interpreting the results. An exception to this was the work of Pupp⁽¹⁾ who investigated the occurrence of striations in inert gases for currents of a few amperes and pressures of between 0.1 and 10 torr, and established their limit of spontaneous existence now called the Pupp Limit.[⊙] Further, he found a similarity law connecting frequency (f), tube radius (a), pressure (p), ionization potential (V_i), and molecular weight (μ), that is applicable to all inert gases except helium, $f a \mu = F(pa/V_i)$. Donahue and Dicke⁽²⁾ carried out experiments in argon and observed, in addition to the usual cathode directed striations, faster moving disturbances propagating towards the anode. From their experimental work they concluded that the

[⊙]See 2-6-1; $i_{\text{Pupp}} = \frac{22}{p^{0.8}} \text{ amp Argon}^{(41)}$
torr

stratification of the plasma column was the most common state of the positive column of a glow discharge.

2.2.2 Investigations using Pulsed Techniques

With the development of the pulsed perturbation technique to generate striations, the true nature of the ionization waves became apparent⁽³⁾. A small amplitude voltage pulse applied to an electrode situated near the cathode, generated a transient ionization wave whose development could be directly observed from rotating drum pictures⁽³⁾. The backward nature of the waves was revealed and the physical mechanism involved was elaborated. With these techniques, ionization waves were found in the pressure range 10^{-3} to 10^2 torr, and at currents from fractions of a milliampere to about ten amperes in different gases, gas mixtures with metal vapours, and in mercury vapour. Waves with their phase and group velocity directed in the same direction (forward waves) were observed⁽⁴⁾. In some cases, two or even three types of backward ionization waves were observed simultaneously in a discharge⁽⁵⁾. For these waves over a broad current-pressure range it was found that the product of the d.c. electric field, E_0 , and the wavelength, λ , was a constant for each variety, $E_0 \lambda = C$. This relation is known as Novak's law.

2.2.3 Linear Theories

Pekarek, starting from a modified form of the diffusion equation which took into account the ionization of the gas, showed that a pulse applied to the positive column would generate a backward wave⁽⁶⁾. Crucial to the existence of a wave solution was the influence of the ionization term. Despite the limitations of the theory, other investigators used it to obtain satisfactory agreement with experimental results and showed that forward waves travelling towards the cathode could be obtained formally from the solution of the basic wave equation⁽⁷⁾.

About the same time, Wojaczek⁽⁸⁾ and Nedospasov⁽⁹⁾ developed theories describing small amplitude steady state striations with more detailed equations taking into account thermal diffusion, heat conduction and the effect of metastable atoms. Over the years, Wojaczek has refined and extended the theory with special reference to striations in argon to obtain good agreement between theory and experiment⁽¹⁰⁾. Similar results have been obtained by Tsendin⁽¹¹⁾. By extending their theory to account for the various chains of processes which may exist in producing the disturbance in ion density, Pekarek and co-workers obtained qualitative but not quantitative agreement with the results for the simultaneous excitation of more than one wave type.

2.2.4 Investigations on Self-Excited Waves

During the same period, Emeleus and his group undertook the difficult task of investigating self-excited large amplitude waves⁽¹³⁻¹⁶⁾. They observed branching effects, high speed anode directed disturbances, coupling of striations to anode spots, and complicated disturbances producing irregular motion of the striations. Tentative explanations of these phenomena were given.

2.2.5 Extension of Linear Theory

The various theories derived for small amplitude waves, predicted certain relationships between the phases of the various quantities such as light intensity, electric field and electron density.

The values of these phase angles were dependent on the basic parameters of the discharge gas, for example, diffusion coefficient and particle mobility⁽¹⁷⁾. Excitation of ionization waves and the simultaneous measurement of the various phase angles offered a potentially simple method of measuring some of the parameters of the gas discharge. To this end, Drouet and Sicha used a more complete set of equations than Pekarek to

derive values for the various phase angles which they then compared with their experimental results⁽¹⁸⁾. Surprisingly, the experimentally measured phase angles disagreed in some cases with Pekarek's and their theories which brought the validity of both into doubt. This initial set-back resulted in a fruitful period in the development of the theory which resolved most of the outstanding problems connected with the small amplitude waves. It came to be realized that at low currents the electron temperature was not a meaningful parameter due to changes in the shape of the electron energy distribution function. In such cases the only consistent approach was to solve the Boltzmann equation for the electrons directly. The solution of the Boltzmann equation for an electron gas, taking into account the inhomogeneous electric field, revealed that at certain values of uniform electric field and wavelength, the perturbed electron density suddenly increased in magnitude and its phase angle, relative to the perturbed electric field, jumped to a larger value. This 'space resonance' effect occurred when the electric field and wavelength were almost equal to those values obtained from Novak's law.

When these space resonances were included in the theory of Pekarek et al. for the different ionization wave varieties, the discrepancies between the hydrodynamic theory and experiment were largely resolved⁽²⁰⁾.

2.2.6 Theory of Self-Excited Striations

As far as the theory of large amplitude waves was concerned the subject remained dormant after the early work of Nedospasov. Nedospasov obtained the relation between the length and velocity of striations which was in agreement with his experimental results. However, this agreement only showed the self consistency of his theory rather than elucidating the nonlinear nature of the waves.

Beginning with the work of Grabec, the nonlinear aspects of ionization waves were investigated in some detail^(22,23). The present work belongs to this period. The evolution of ionization waves from a linear to a nonlinear state has been examined theoretically and experimentally⁽²⁴⁻²⁷⁾. Nonlinear coupling between different wave modes has been observed⁽²⁸⁻³¹⁾ and it has been shown that the waves in the positive column can behave as a nonlinear Van der Pol type of oscillator when modulated at other frequencies⁽³²⁾.

2.2.7 Miscellaneous Effects

Besides experiments and theory dealing with the basic processes and origin of ionization waves, investigations were carried out into the factors influencing moving striations. These included the influence of an applied magnetic field^(27,33-35), the tube geometry⁽³⁶⁻³⁸⁾ and the external circuit⁽³⁹⁾. Theories were derived showing the link between ionization waves and ion-acoustic waves at low pressures⁽⁴⁰⁾.

2.3 SMALL AMPLITUDE STRIATIONS

2.3.1 Generation of Continuous and Transient Waves

The region of occurrence of striations for a given tube radius is such that for certain values of pressure and current, a slight change in one of these parameters will result in a transition from a homogeneous column to one containing moving striations, and vice versa. In inert gases there exists, at high currents, an upper critical value of this current, Pupp limit, above which the column is homogeneous. Well away from this limit the striations are self-excited and of large amplitude. In neon, argon and helium, there also exists a lower current limit below which striations are not seen. At these transition boundaries it is possible to excite continuous or transient low amplitude moving striations by slightly changing the current or potential. This may be achieved for the

case of continuous striations by applying a repetitive voltage pulse between the cathode and an internal or external electrode near the head of the positive column.

The amplitude amplification of the waves is a maximum when the repetitive frequency is equal to that of the natural striations occurring near the boundary⁽⁴¹⁾.

A transient wave may be produced in a similar way. A pulse generator is used to feed a short ($\sim 1 \mu\text{s}$) pulse with adjustable amplitude (0-4 kV) to either an external ring which can be moved to any desired position, or an internal electrode⁽⁴²⁾. The resulting wave, which can be detected with a photomultiplier or rotating mirror system, (see Chapter III) is seen to propagate in the region between the ring and the anode. A schematic analogue of a rotating mirror picture of such a case where the pulse is applied at the cathode, is shown in Fig.2.1. Initially in the

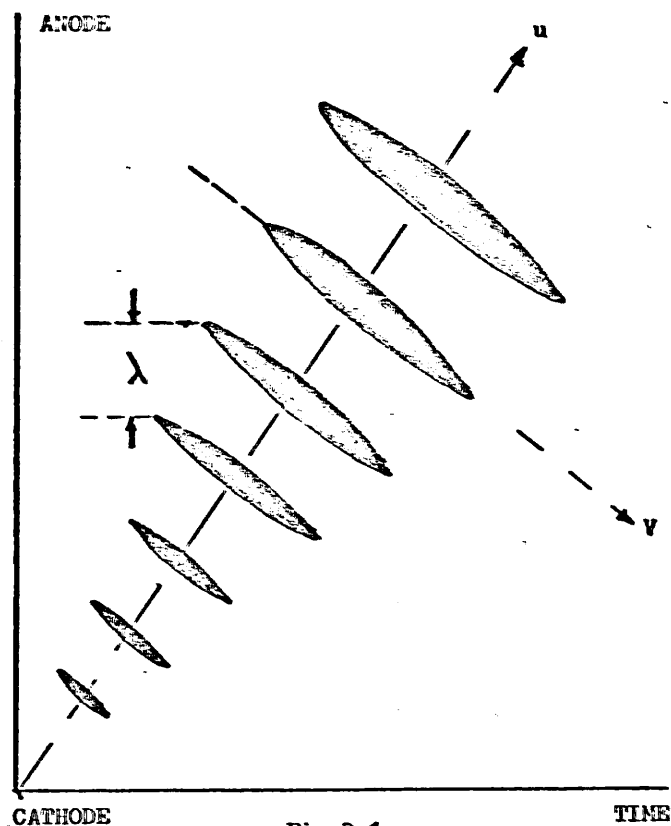


Fig.2.1

Schematic analogue to rotating mirror of a wave of stratification and moving striations in the positive column of an inert gas, V , striation velocity; u , velocity of wave of stratification; λ , striation wavelength

region of the perturbing electrode a packet or region of stratification is seen. With elapsing time, the disturbance producing this stratification moves towards the anode. The individual striations within a packet move towards the cathode. New striations are formed as the 'stratification wave' travels towards the anode. Each striation is observed to have an intensity which is small initially but which gradually increases, reaches a maximum, decreases and ultimately vanishes.

This form of space-time display provides complete information on the dispersion of the wave which may be described by a dispersion equation connecting the complex frequency $\Omega = \omega - i\varphi$ with the complex wave number $K = k + i\gamma$ (3).

2.3.2 General Dispersion Curve and Occurrence of Wave Types

By using pulse techniques a large variety of phenomenological types of ionization waves have been found. These may be summarized in the general dispersion curve proposed by Pekarek, Fig.2.2, where the convention is that k is always positive and ω may be positive or negative to describe waves travelling in opposite directions. The wave type is defined by the direction of the group velocity - the anode to cathode direction being considered positive - and the relationship of the group and phase velocities, parallel velocities, giving a forward wave, anti-parallel a backward. The subscript is related to the curvature of the phase trajectories in this plot: A = accelerating, D = decelerating, in the direction of the group velocity⁽⁴³⁾.

In the high current limit only one wave type is found in an inert gas⁽¹⁰⁾. This is the backward wave, usually B_A - with a phase velocity which increases towards the anode and a dispersion law which is close to the hyperbolic relation $\omega k = \text{constant}$.

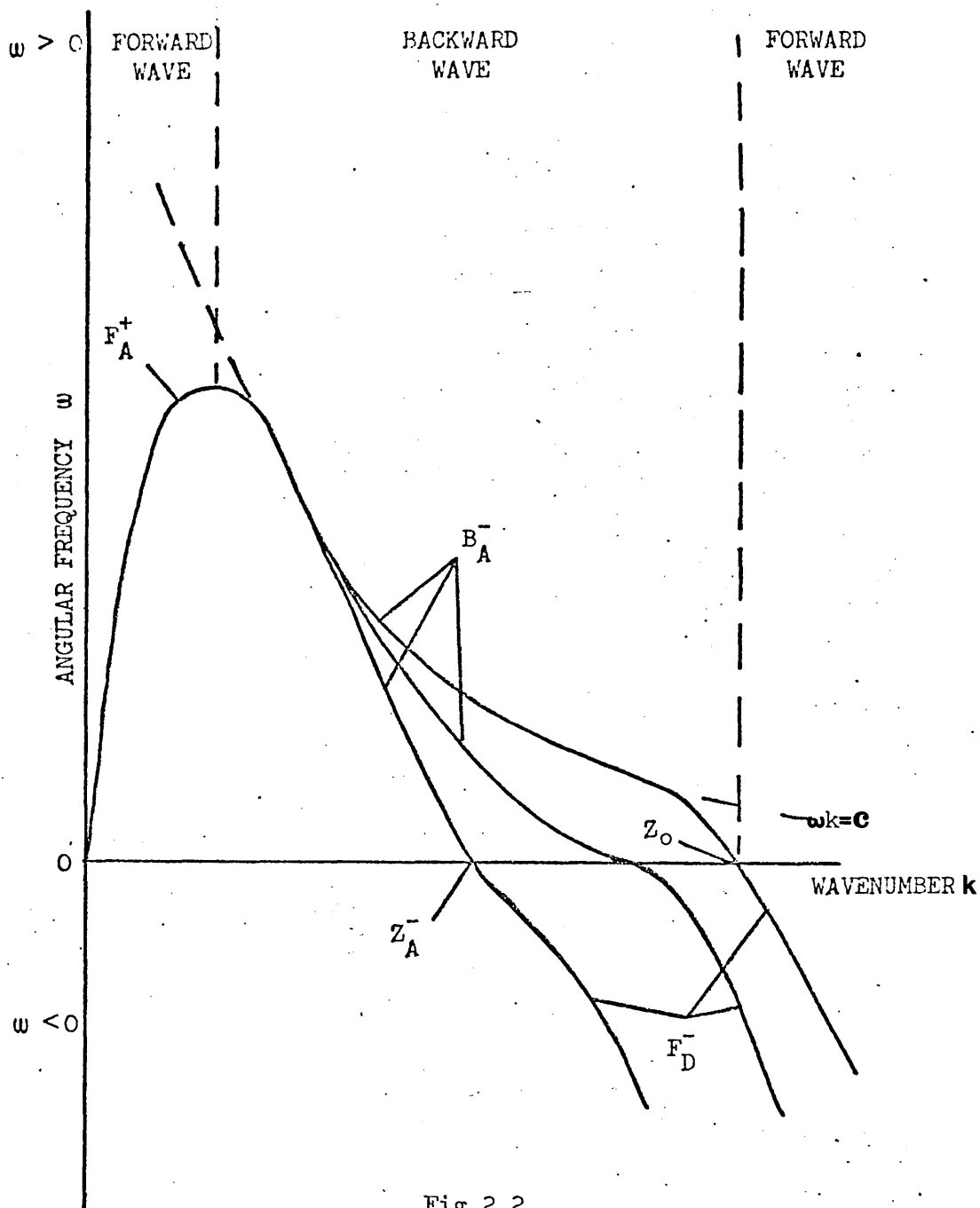


Fig.2.2
 General dispersion curve (after Pekarek 3). Dashed curve - $\omega k = \text{const.}$ By convention k is positive and ω is positive or negative to give cathode or anode directed waves.

Hydrodynamic equations may be used to describe ionization waves in such cases. In the low current region there are, in general, at least four wave types. They may be distinguished between the slow waves s' and p whose frequency grows with increasing current and which are related to changes in the metastable atoms, and the faster waves, s and r , whose frequency decreases with current and which are connected with the ion density.

A feature of these waves is the constancy of the longitudinal field potential measured across the optimum wavelength. The values are characteristic for all the observed waves⁽⁵⁾.

For neon the wave types found are s, s' waves, with $E_0 \lambda \sim 19 \text{ V}$; a p wave, $E_0 \lambda \sim 9 \text{ V}$; and the r wave with $E_0 \lambda \sim 12.6 \text{ V}$.

2.4 DERIVATION OF THE HYDRODYNAMIC EQUATION FOR STRIATIONS

2.4.1 Generalized Diffusion Equation

At high currents only one backward wave variety exists in inert gases. Despite this simplicity, the complete set of equations must include many factors such as heat conduction, viscosity, and metastable atom density. Pekarek, using a simple energy equation, derived in a simple way a basic equation which contains the essential qualitative features of ionization waves. Indeed, when more detailed energy balance equations are used, the resultant equations are essentially the same as Pekarek's, except that the coefficients have different values⁽³⁾.

The waves can be described in terms of the charged particle density N , the electric field intensity E , the mean electron energy T_e and the ionization frequency Z . The equations governing the variation of these quantities are derived from the hydrodynamic equations of continuity, momentum and energy, together with Poisson's equations and an expression for the ionization frequency⁽²⁶⁾. These are:

Ion Continuity

$$\frac{\partial N_i}{\partial t} + \frac{\partial}{\partial z} N_i V_i + \frac{N_i}{t_a} = N_e Z \quad \dots (2.1)$$

Electron Continuity

$$\frac{\partial N_e}{\partial t} + \frac{\partial}{\partial z} N_e V_e + \frac{N_e}{t_a} = N_e Z \quad \dots (2.2)$$

Ion Momentum

$$M N_i \frac{dV_i}{dt} = q N_i E - M N_i \nu_+ V_i - M V_i Z_i N_i \quad \dots (2.3)$$

Electron Momentum

$$m N_e \frac{dV_e}{dt} = -q N_e E - \nabla(N_e kT_e) - m N_e \nu_- V_e - m V_e Z N_e \quad \dots (2.4)$$

Poisson

$$\frac{\partial E}{\partial z} = (N_i - N_e) \frac{q}{\epsilon_0} \quad \dots (2.5)$$

Ionization Frequency

$$Z = A(T_e) \exp(-q V_i / kT_e) \quad \dots (2.6)$$

where the indices i and e refer to ions and electrons, and

N = particle concentration

E = field intensity

V = flow velocity

t = time

z = axial coordinate in the direction of the cathode

Z = ionization frequency: the number of ionizing collisions per second

M = ion mass

m = electron mass

τ_a = ambipolar diffusion lifetime

q = absolute value of electron charge

ν_+ = ion-neutral momentum transfer collision frequency

T_e = electron temperature

ν_- = electron-neutral momentum transfer collision frequency.

The equations are used in one dimensional form. The radial concentration is given by a Bessel function $N(r) = N_0 J_0(2.4 \frac{r}{R})$, and is due to ambipolar diffusion which is accounted for by the relaxation term $1/\tau_a$

determined by the ambipolar diffusion and the tube radius, $\frac{1}{\tau_a} = \left(\frac{2.4}{r_0}\right)^2 D_A$. Only direct ionization is considered. The collision frequencies are much larger than the frequencies of the striations and the ionization frequency and so the time derivatives and the ionization terms in the momentum equations are neglected. In addition the establishment of the electron concentration is considered quasi-stationary since the time to establish it is of the order of 10^{-10} - 10^{-9} secs, in comparison with that of the ion concentration of 10^{-5} to 10^{-6} sec.

With these simplifications the equations reduce to:

$$\frac{\partial N_i}{\partial t} + \frac{\partial}{\partial z} N_i V_i = N_e Z - \frac{N_i}{\tau_a} \quad \dots (2.7)$$

$$\frac{\partial}{\partial z} N_e V_e = 0 \quad \dots (2.8)$$

$$N_i V_i = \frac{q N_i E}{M v_+} = \mu_i N_i E \quad \dots (2.9)$$

$$\begin{aligned} N_e V_e &= -\frac{q N_e E}{m v_-} - \frac{\kappa T_e \nabla N_e}{m v_-} \\ &= -\mu_e N_e E - \frac{\mu_e \kappa T_e}{q} \frac{\partial N_e}{\partial z} \quad \dots (2.10) \end{aligned}$$

Using equation (2.8) in (2.10) gives

$$\frac{\partial}{\partial z} (N_e V_e) = \left[\frac{\partial N_e E}{\partial z} - \frac{\partial}{\partial z} \frac{\kappa T_e}{q} \frac{\partial N_e}{\partial z} \right] \mu_e = 0 \quad \dots (2.11)$$

When inserted in Poisson's equation this gives

$$N_i - N_e = \frac{q E}{\kappa T_e} L^2 \frac{\partial N_e}{\partial z} - L^2 \frac{\partial^2 N_e}{\partial z^2} \quad \dots (2.12)$$

where $L = (\epsilon_0 \kappa T_e / N_e q^2)^{\frac{1}{2}}$, the Debye length. The quantity $\kappa T_e / q E$ is of the order of the striation wavelength λ_0 which is several orders of magnitude larger than L . Approximating

$$\frac{dN_e}{dz} \approx \frac{N_e}{\lambda_0}$$

gives

$$(N_i - N_e) / N_e \approx (L / \lambda_0)^2 \ll 1,$$

which shows that $N_i \approx N_e$ may be substituted everywhere except in Poisson's equation.

The discharge current is mainly determined by the flow of electrons and is assumed constant, in equilibrium it is equal to $N_0 V_{e0} = -\mu_e N_0 E_0$ so that equation (2.10) may be expressed as

$$N_e E + \frac{\kappa T_e}{q} \frac{\partial N_e}{\partial z} = N_0 E_0 .$$

Putting $E = E_0 + e$, $N = N_0 + n$ and linearizing the above equation, gives:

$$e = -\frac{E_0 n}{N_0} - \frac{\kappa T_e}{N_0 q} \frac{\partial n}{\partial z} . \quad \dots (2.13)$$

From equations (2.9) and (2.10), using $N_i = N_e = N$ one obtains

$$\frac{\partial N_i V_i}{\partial z} = \frac{\partial}{\partial z} \mu_i N E = -\frac{\partial}{\partial z} \mu_i \frac{\kappa T_e}{q} \frac{\partial N_e}{\partial z} = -\frac{\partial}{\partial z} D_a \frac{\partial N_e}{\partial z} \quad \dots (2.14)$$

since

$$D_a = \frac{\kappa T_e \mu_i}{q} ;$$

so that equation (2.7) becomes

$$\frac{\partial N}{\partial t} = \frac{\partial}{\partial z} \left(D_a \frac{\partial N}{\partial z} \right) + N \left(Z - \frac{1}{t_a} \right) . \quad \dots (2.15)$$

This equation is basic to the theory of striations and shows that the changes in ion and electron densities are essentially due to ambipolar diffusion of the particles augmented by an ionization term⁽³⁾.

The next stage in determining the nature of the waves from the equations is to introduce an appropriate equation for the mean electron energy (temperature) and to make some assumption on the form of Z for the perturbed state. The first step distinguishes the various linear theories according to the complexity of the equation employed, and the second step determines whether linear or nonlinear (large amplitude) phenomena are to be considered since the expression for the ionization frequency is highly nonlinear due to the exponential term^(6,8,9,11,23). A small increase in the electron temperature will produce a large increase in the ionization

frequency, whereas a small decrease will cause the production rate to drop almost to zero. However, for sufficiently small variations in electron temperature, Z may be expanded to

$$Z = Z_0 + \frac{\partial Z}{\partial T_e} (T_e - T_{e0})$$

where Z_0 equals $1/\tau_{a0}$ from the homogeneous column. This situation corresponds to linear theory.

2.4.2 Pekarek's Solution of the Diffusion Equation

The most simple equation for the electron temperature⁽⁴⁵⁾ is:

$$\frac{\partial \theta}{\partial z} - a\theta = -be \quad \dots (2.16)$$

where $\theta = T_e - T_{e0}$

$e = E - E_0$

$a =$ reciprocal of the electron temperature relaxation length

$b =$ constant approximately equal to $\frac{3}{2}q$.

Upon substituting for e from equation (2.13) and integrating over z , one finds

$$\theta e^{-az} = -b \int_z^\infty e^{-a\xi} \left[\frac{E_0 n(\xi)}{N_0} + \frac{\kappa T_{e0}}{N_0 q} \frac{\partial n}{\partial \xi} \right] d\xi .$$

$$\theta = \frac{b \cdot \kappa T_{e0} n}{N_0 q} - b \left[\frac{E_0}{N_0} + \frac{a \kappa T_{e0}}{N_0 q} \right] \int_z^\infty e^{-a(\xi-z)} n d\xi \quad \dots (2.17)$$

When this expression is substituted into the linearized form of Z , the basic diffusion equation (2.15) becomes, after linearization:

$$\frac{\partial n}{\partial t} = D_a \frac{\partial^2 n}{\partial z^2} + \bar{\alpha} n - A \int_z^\infty e^{a(z-\xi)} n(\xi) d\xi \quad \dots (2.18)$$

where

$$\bar{\alpha} = \frac{\partial Z}{\partial T_e} \frac{b \kappa T_{e0}}{q}$$

$$A = \frac{\partial Z}{\partial T_e} b \left[E_0 + \frac{a \kappa T_{e0}}{q} \right] .$$

The first term on the right-hand-side of equation (2.18) represents ambipolar diffusion of the charged particles in the axial direction. The second term expresses the local influence of the ion concentration on the production of new charge carriers in the same place. The last integral

term expresses the long-distance effect of the concentration of the charge carriers in the positive column on the formation of ions.

The diffusion term damps mostly very short wavelengths, whilst the last term can damp the amplitude of long wavelengths. The second term alone would lead to an instability of the whole column.

By numerically integrating the above equation, Pekarek examined the response of a plasma column to an initial aperiodic pulse applied in the cathode region. The solution obtained reflected the backward wave characteristics of a transient ionization wave and showed that the periodicity of the waves was due to the ionization term⁽⁶⁾.

More generally, for a solution of the form $\exp[i(\omega t - kz) + \varphi t]$, periodic in space, the following expressions for the dispersion $\omega(k)$ and the temporal increment $\varphi(k)$ are obtained:

$$\omega = \frac{A k}{k^2 + a^2} \quad \dots (2.19)$$

$$\varphi = -D_a k^2 + \alpha - \frac{A a}{k^2 + a^2} \quad \dots (2.20)$$

If $a \ll k$, the dispersion relation assumes the form $\omega k \approx A$. The corresponding backward wave has a phase velocity $= -\frac{A}{k^2}$ (see reference (10).)

The equation derived above represents the most simple equation which can describe ionization waves. Omission of any of the terms on the right-hand-side would lead to an equation which cannot have a solution even qualitatively corresponding to the ionization wave⁽⁴⁶⁾.

2.5 PHYSICAL MECHANISM OF BACKWARD WAVES

2.5.1 Wave of Stratification

The physical mechanism responsible for the stratification spreading from the cathode towards the anode can be understood by considering what happens after an initial perturbation in ion and electron (particle) densities close to the cathode⁽³⁾.

Following an increase in particle densities due to a perturbation, a space charge is created as a result of the difference in ion and electron densities brought about by the different mobilities of the ions and electrons.

The space charge field ties the electrons to the ions and ambipolar diffusion takes place in the axial direction leading to damping of the original perturbation. In order to obtain wave behaviour, the changes in ionization must be considered.

The perturbation in space charge reduces the electric field in the region of the perturbation. Electrons arriving from the cathode side of the perturbed region lose their energy by collisions as usual but owing to the decreased electric field their energy balance is changed and their temperature decreases. The electrons emerge from the region with a lower temperature and only recover their original temperature after travelling through a certain space interval. Since the ionization rate is strongly dependent on the electron temperature, the production of charged particles is reduced in the region of lower electron temperature. So an initial increase in particle densities produces, on the anode side of the original perturbation, a region with decreased particle densities. In turn, the decrease in particle densities gives rise to a region of increased electron temperature which produces a region of increased particle densities closer to the anode. The above process is repeated leading to the stratification of the plasma column into alternate regions of increasing and decreasing electron temperature, particle densities, light intensity, and electric field.

2.5.2 Motion of the Striations

The subsequent motion of the striations, which have been produced by the 'stratification wave' as described above, is towards the cathode due to the phase shift between the particle densities and the electron temperature^(3,11). The relative phase shifts for a backward wave are shown in Fig.2.3 at a particular instant (t_0). Since the ionization rate is proportional to the electron temperature, it can be seen that more ions are produced on the cathode side of the ion maximum, so that at a slightly later time $t_0 + \Delta t$ ($\Delta t \ll t_0$) the ion maximum, given approximately by

$$n(t_0 + \Delta t) = n(t_0) + \Delta t \frac{\partial n}{\partial t} \Big|_{t=t_0},$$

moves towards the **cathode**.

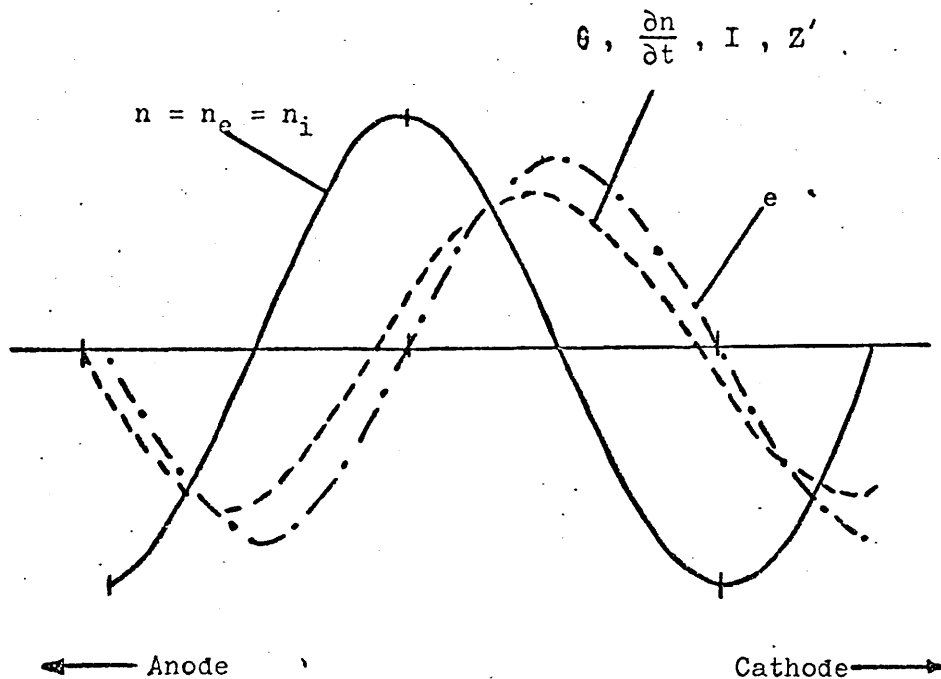


Fig.2.3

Phase shift between the electron (n_e) and ion (n_i) densities; the electric field e ; the electron temperature θ , rate of change of particle density $\frac{\partial n}{\partial t}$, the change in the number of ionizing collisions per second Z' , and I the light intensity, for a backward wave

2.5.3 Amplification of the Disturbance

The phase shift between the electron temperature and particle densities can lead to amplification of the disturbance as it moves towards the anode. This may be seen by considering the initial development of the disturbance at some point x_0 well away from the position of the initial perturbation, at times t_0 and $t_0 + \Delta t$. The relative phase shift ψ between electron temperature and particle densities is shown, in Fig.2.4(a), for the case when $\psi < 90^\circ$. The deviation in electron temperature has produced the increase in particle density (n) on its anode side at x_0 .

At a time $t_0 + \Delta t$, the particle density $n(t_0 + \Delta t)$ is given by

$$n(t_0 + \Delta t) = n(t_0) + \Delta t \left. \frac{\partial n}{\partial t} \right|_{t=t_0}$$

where

$$\left. \frac{\partial n}{\partial t} \right|_{t=t_0} = -k^2 D_a n(t_0) + ZN_0 \theta(t_0)$$

from the linearized form of equation (2.15). Owing to the relative phases, the ionization term $ZN_0 \theta(t_0)$ is positive at x_0 : more ions are produced so that, providing the damping effects of diffusion are much smaller than the increased ionization, $\left. \frac{\partial n}{\partial t} \right|_{t=t_0}$ is positive at x_0 and the particle density $n(t_0 + \Delta t)$ increases.

As described in the previous section, the maxima in particle density and electron temperature move towards the cathode. The increased deviation in particle density $n(x_0, t_0 + \Delta t)$ at x_0 will lead to larger deviations in electric field and electron temperature on the anode side of the position x_0 ; these deviations are larger than those which originally produced the increase in particle density at x_0 , $n(x_0, t_0)$, that is, they have been amplified. A new, larger perturbation in particle density is produced beyond x_0 , Fig.2.4(b), and the process is repeated in the way described in section 2.5.2. Each new deviation in the plasma parameters

nearer the anode, is larger than the one before it leading to amplification of the 'stratification' wave.

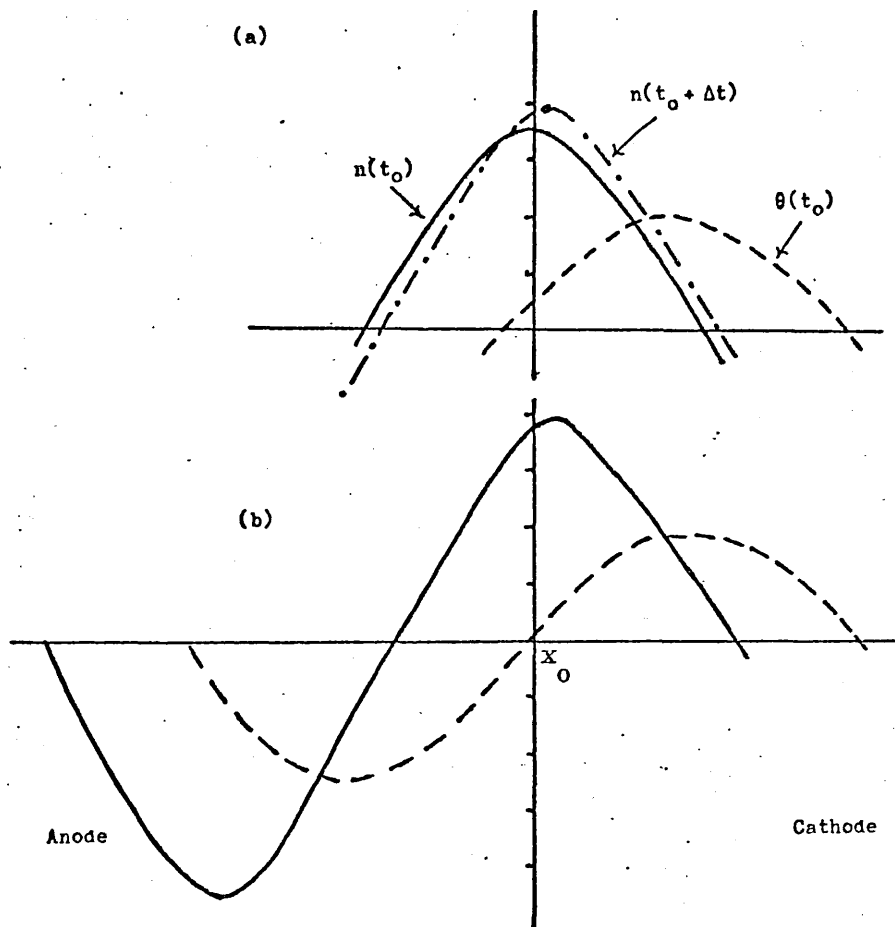


Fig.2.4

Phase shift between particle densities n and the electron temperature θ when the increased ionization is larger than the losses due to ambipolar diffusion.

(a) At time t_0

(b) Subsequent development at $t > t_0$

The amplification can occur only in a certain wavelength interval. At short wavelengths the ambipolar diffusion prevails over the increased ionization, and at large wavelengths the phase shift of the electron temperature always exceeds $\pi/2$ which leads to damping.

The term amplification when applied to the actual ionization wave or striation refers to the fact that the wave energy, that is the amplitude of the 'stratification' wave, increases in travelling from the cathode to the anode. The corresponding amplitude of the striation will decrease as the latter moves towards the cathode.

If the striation is represented as $\exp \alpha x \cos(\omega t - kx)$, where the symbols have the usual meaning, then, since x is measured from the anode to the cathode, the amplification coefficient α will be negative for amplified waves and positive for damped waves.

2.6 LIMITATIONS OF THE BASIC DIFFUSION MODEL

2.6.1 Influence of Metastable Atoms and Electron Energy Function

Although Pekarek's solution reproduces the general behaviour and time scales of the phase and group velocity of the striations, it omits several important factors, e.g. the effect of metastable atoms is not included and the electron thermal conductivity is neglected. However, in argon, for example, at the higher current limit both these terms are important⁽⁹⁾. The effect of the thermal conductivity alone would damp out the waves. It becomes necessary to include indirect ionization due to the metastables as well as the direct ionization. More important still, is the distortion of the tail of the electron distribution function above the first inelastic threshold where the depletion by inelastic collisions is very rapid^(11,44).

Nedospasov has shown that when the metastables are taken into account, the time increment can be positive even for a fairly large thermal conductivity, provided there is considerable step-wise ionization and the excited atoms decay without collisions with electrons⁽⁹⁾. However, near the Pupp limit the metastable lifetime τ_m is less than τ_{a0} which removes the influence of the metastables on the instability⁽¹¹⁾. In this case the instability is due to the distortion of the distribution function⁽⁴⁴⁾. With increasing electron density more electrons are transferred into the depleted tail of the distribution owing to the fact that the distribution becomes Maxwellian, and the ionization rate increases⁽⁴⁷⁾. According to Gentle, the Pupp limit where striations are no longer observed,

corresponds to the point where the electron distribution becomes nearly Maxwellian, causing damping, and the metastables relax to local thermal equilibrium quickly.

By including the above effects the following expressions for the angular frequency ω_0 and wavenumber k_0 for the minimum attenuation, were obtained by Wojaczek and Tsendin^(8,11),

$$\omega_0 = \frac{s b_p E (Z_T - 1)}{a' R^2 k_0} \quad \dots (2.21)$$

$$k_0 = \sqrt{\frac{eE}{R a' T} \sqrt{(Z_T - 1)(2a' - 1.5)s}}$$

where $a' = 1.35$, $s = (2.405)^2 \times 0.87$

b_p = ion mobility (cm s⁻¹)

E = Electric field (V/cm)

$Z_T = V^*/T$

V^* = excitation potential of the metastable level (volts)

T = electron temperature in energy units (eV)

R = tube radius (cms)

e = magnitude of electron charge.

2.7 WAVE VARIETIES AT LOW CURRENTS: EFFECT OF THE ELECTRON GAS

2.7.1 Time Scales of the Ionization Processes

At the lower current limit of wave excitation, of the order of a few milliamperes, the direct ionization predominates and the metastables play a new role since they now contribute essentially an admixture of another gas with a very low ionization potential. The lifetime of the metastables becomes larger than that of the positive ions, and the gas of metastables becomes distinct from the ions, and this can give rise to a slow ionization wave. The scheme of the two branches of ionization is assumed to be :

DISTURBANCE DUE TO PERTURBATION OF PLASMA PARAMETER

Change in the ion density
(life-time τ_{R0})

↓
'r' wave space charge field
↓
disturbance

Change in the metastable density
(life-time τ_m)
'p' wave ion density ($\tau_{a0} \ll \tau_m$)

↓
space charge field
↓
disturbance

2.7.2 Non-Maxwellian Electron Energy Distribution

Another aspect of the discharge which must be included, is the non-Maxwellian form of the electron energy distribution function; this is crucial for explaining the wave types and discrepancies in the observed phase relations between the wave parameters.

Measurements at different phases in small amplitude ionization waves in neon at low current revealed a strongly non-Maxwellian electron energy distribution above 12 eV; similarly in the homogeneous column⁽⁴⁸⁾. Flat but distinct peaks on the curve located at a different position on the energy axis, depending on the phase of the wave, were seen.

This change in shape of the distribution function accounts for the discrepancy between the hydrodynamic theory and the experimental measurements, and in such situations the mean electron energy ceases to be a particularly meaningful parameter⁽¹⁰⁾.

2.7.3 Computed "Resonances" in the Distribution Function

Since the electron drift velocity is much larger than the velocity of the ionization waves, the latter can be considered to give rise to a spatial modulation of the electric field, of the form:

$$E = E_0 \left(1 + \epsilon \cos \frac{2\pi}{\lambda} Z \right) \quad \dots (2.22)$$

through which the electrons move.

Using such a configuration Ruzicka computed the electron distribution function and found peaks appearing in agreement with the experimental results⁽¹⁹⁾. Particularly striking was the fact that at values of λ , given by

$$\lambda = \frac{U_a}{gE_0} (1+p) \quad \dots (2.23)$$

where U_a = energy of lowest excited level

$g = 1, 2, \text{integer}^\ominus$

E_0 = electric field of homoge column

p = the ratio of elastic to inelastic energy loss $\ll 1$,

the amplitude of the perturbed electron density increased greatly and was accompanied by a sudden change in the phase between the perturbed density and electric field. For values of λ away from these resonance values, the hydrodynamic equation predicted the same values of phase and amplitude⁽¹⁰⁾.

2.7.4 Effect of Resonances on the Wave Dispersion

The resonance value corresponded to a value of $E_0\lambda$, close to Novak's potentials. When these 'space resonances' were included in the equation for a low current neon discharge describing the ions and metastables, six possible wave types were obtained depending on the combination of the time scale and space resonance, as shown below:

TABLE 2.1
TIME SCALES AND RESONANCES FOR A NON-MAXWELLIAN
ELECTRON ENERGY DISTRIBUTION FUNCTION

Space Selection	First Resonance $g = 1$ $E\lambda = 19 \text{ V}$	Hydrodynamic Maximum $E\lambda = 13 \text{ V}$	Second Resonance $g = 2$ $E\lambda = 9.5 \text{ V}$
Time Scale Selection			
Slow (metastable guided wave)	s' observed	r' not observed	p observed
Fast (ion guided)	s observed	r observed	p' not observed

$^\ominus$ Integral number λ fit inelastic scattering length $\frac{U(1+p)}{E_0}$

For the particular parameter values chosen, on the slow time scale the s' wave had a positive time increment whilst that for the p wave was zero. Between these two resonances a flat hydrodynamic resonance was seen with a negative time increment corresponding to an r' variety. On the fast time scale the wave at the first resonance (s type) and at the hydrodynamic maximum, represented amplified waves, whilst at the second resonance (p' type) the wave was damped.

Since the s' , s , p waves represent unattenuated waves, it is to be expected that in a discharge the ionization waves would 'lock-in' to these resonant wavelengths rather than the hydrodynamic values representing damped waves. The appearance of waves with Novak's potentials is thus explained. In addition, since the wavelength is nearly constant the $\omega(k)$ dispersion curve would be steeper than for the hydrodynamic case, so that the absolute value of the ratio of group to phase velocity would be larger in accordance with experiment⁽¹⁰⁾.

2.7.5 Experimental Evidence for Resonant Behaviour

Recently Rayment has found similar variations in the electron energy distribution in neon for p and s waves⁽⁵⁰⁾. It was seen that there was a spatial shift of the maximum of the direct ionization rate towards the anode, relative to the electric field maximum corresponding to the physical model presented earlier for amplification. Further, the spatial shift was associated with the arrival of a bump in the electron energy distribution near to the ionization potential.

The presence of a bump enhanced the increase in the direct ionization rate produced by the action of the electric field maximum on the distribution function. The measurements suggested that the resonant wavelengths were such that the bumps in the distribution were accelerated by the field to arrive near the excitation and ionization potentials in the

right phase, with respect to the electric field maximum, leading to wave amplification.

Clearly the inclusion of the non-hydrodynamic behaviour of the electron gas was necessary in order to achieve any success in understanding the ionization waves at low currents.

2.8 LARGE AMPLITUDE STRIATIONS AND NONLINEAR EFFECTS

2.8.1 Characteristics of Large Amplitude Self-Excited Waves

A distinct characteristic of large amplitude striations is the fact that they consist of two regions: a rather narrow head with which is associated a considerable potential gradient and intense ionization and excitation of the gas, and a broad tail on the anode side where the electric field is weak and the presence of ions and electrons is due mainly to ambipolar diffusion^(21,51).

From an examination of Pupp's experimental work on large amplitude striations, Farris came to the conclusion that the equation of ambipolar diffusion should be applicable,

$$\frac{\partial n}{\partial t} - D_a \frac{\partial^2 n}{\partial x^2} = Z \quad \dots (2.24)$$

where n is the charged particle density ($n = n_e = n_i$), Z is the rate of production of ion pairs per unit volume, and D_a is the mean ambipolar diffusion coefficient. Stewart measured the plasma potential, electron temperature and electron concentration as functions of time and position in the positive column of argon⁽⁵³⁾. In analysing the results he used the above equation which, when transformed, gave an expression which allowed the ionization function to be calculated from the experimental measurements. The ionization rate Z had a δ -function like character, varying in time and space in the same way as the emitted light. Following from these results, Nedospasov solved the diffusion equation by assuming that Z could be expressed as the sum of delta functions⁽⁵¹⁾. He obtained

the result that within an individual striation n decreased exponentially in the anode direction. Further the relationship between the length of the striation and its velocity, showed that the waves were backward.

Whilst these results indicated the nature of the wave, they did not give any insight into the transition from the small amplitude waves to the large amplitude waves and the accompanying steepening of the wavefront and other associated effects.

2.8.2 Evolution from Small to Large Amplitude Waves

The transition from low amplitude self-excited ionization waves to large amplitude waves occurs in three stages⁽²⁵⁾. Waves generated in the cathode region, corresponding to the natural modes having a positive gain increment, can initially be described by the linear theory. As the ionization waves propagate towards the anode they are amplified and in a second transition, region nonlinear effects become effective and harmonic generation occurs and mode-mode coupling may be present. In the third region the waves stop growing due to saturation and the spectrum becomes constant in space and time^(24,26).

Sato examined experimentally this evolution to a saturated state and found, for his results at least, that the behaviour of the modes could be represented by a Landau amplitude equation

$$\frac{d|A|^2}{dx} = 2\gamma|A|^2 - \alpha|A|^4 - \beta|A|^6 \quad \dots (2.25)$$

where $|A|$ represents the magnitude of the wave amplitude, γ the linear growth rate, α and β the first and second nonlinear saturation coefficients. The wave grows exponentially as $|A| = |A_1| \exp[\gamma(x - x_1)]$ until for $2\gamma(x - x_1) \gg 1$ it reaches a saturated or equilibrium amplitude $|A_2|^2 \approx 2\gamma/\alpha$, a value independent of the initial amplitude A_1 . Further experiments concerned with the variation of the saturated amplitude A_2 and spatial growth rate k_1 with the change in current I , showed that as

the current was decreased from the Pupp limit I_c , both k_i and A_2^2 increased as $I - I_c$ initially⁽²⁷⁾. Upon decreasing the current further, the above parameters reached maximum values and then decreased. In the linear region the waveforms were linear whilst when A_2^2 and k_i decreased due to nonlinear stabilization, the waveforms had the characteristic nonlinear saw tooth shape.

2.8.3 Regular and Irregular Waves

Depending on the extent of stabilization by inelastic losses, the ionization waves may develop into regular or irregular turbulent large amplitude striations. In the latter case the spectrum seen in the saturated region is broadened and is asymmetric about the fundamental modes. Much of the fluctuation energy is contained in modes outside the interval of unstable mode numbers. The velocity of the striations is amplitude dependent which gives rise to 'collisions' of striations. These random striations have the same 'shock-like' structure as the periodic striations. All these effects have been observed experimentally but not always interpreted^(25,51).

2.8.4 The Nature of Self-Excited Waves as Derived from Nonlinear Equations

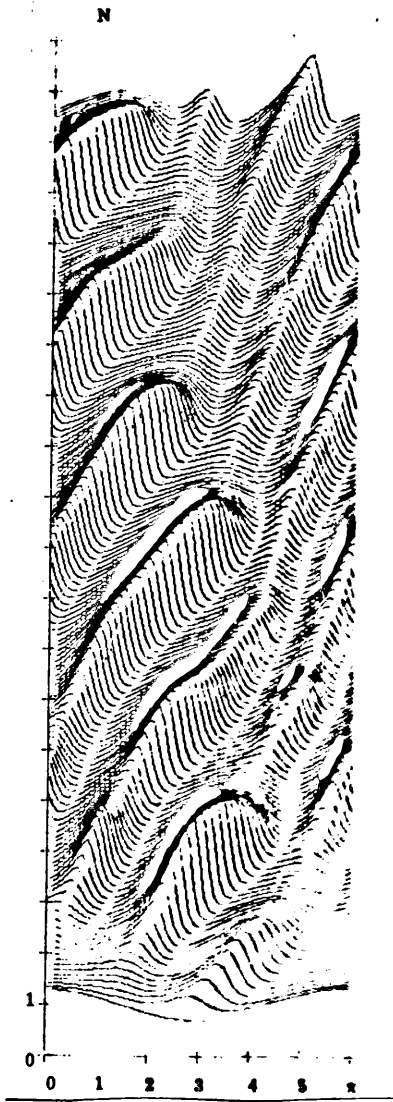
In a series of papers, Grabec has shown that the structure and other basic effects of large amplitude regular and irregular striations may be obtained from the nonlinear form of the expressions derived earlier, equation (2.15), in which the form of the ionization function is not approximated^(23,24,26). The variations of the particle density, ionization frequency and electron temperature were computed from the equations to give the space-time dependence following an initial perturbation of the homogeneous column. The energy equation used for the electrons was still relatively simple, and was of the form:

$$\frac{\partial n_e}{\partial z} V_e u = -q n_e V_e E - \frac{n_e u}{t_1} - n_e Z q V_i \quad \dots (2.26)$$

where n_e = electron density
 V_e = electron flow velocity
 u = mean electron energy
 q = charge on an electron
 E = electric field
 t_1 = relaxation time for elastic collisions
 Z = ionization frequency
 V_i = ionization potential.

The electrons are heated by the electric field and cooled by elastic and inelastic collisions. The loss of mean electron energy in elastic collisions is described by the relaxation time t_1 . In terms of relative variables the losses for the homogeneous state are given by $C + C_1 = 1$, where C represents the inelastic losses due to ionization and C_1 the elastic losses, and $C_1 \cong 1$, $C \ll C_1$. In the linear theory the ionization losses can be neglected but they prove vital in the nonlinear development even though they are small, $C \sim 0.01$.

The response of the column to a low amplitude Gaussian pulse applied near the cathode is initially similar to Pekarek's linear theory. However, it is seen that the growth rate depends on the amplitude which grows rapidly due to the nonlinear dependence of the ionization function on the other quantities. Without the inclusion of the inelastic losses, the calculated deviations quickly reach values too high in comparison with the experimentally observed values. The inelastic losses which depend on Z stabilize the wave and lead to saturation. The space-time diagram following an initial sinusoidal disturbance is shown in Fig. 2.5⁽⁵⁵⁾. It can be seen that the original pulse moves towards the anode whilst the ionization waves generated move towards the cathode. The deviations of the electron concentration above the equilibrium value, grow more quickly than below it. As



(a)

(b)

Fig.2.5
 Computed space-time display (after Grabec) showing
 the evolution of a sinusoidal disturbance
 (a) Ion concentration; (b) Ionization Frequency

the amplitude grows its slope on the cathode side grows and a saw-tooth shaped striation is formed. The steeper the slope the faster the striation moves.

The computations show that for the large amplitude waves the ionization occurs in a narrow region since the distribution of the ionization resembles a delta function. At high electron density the electric field is low and vice-versa, due to the conservation of electric current.

The slope of the striation head is related to the ionization frequency:- the larger the ionization frequency the more quickly the density changes and the more quickly the striation moves towards the cathode. Collisions result when the head of a fast moving striation falls into the low temperature tail of a slower striation. The peak temperature, ionization and hence velocity of the faster striation are diminished, whilst the opposite happens to the previously slower striation. If the drop in temperature is sufficient the ionization may fall to zero and the striation is annihilated since the amplitude is reduced to zero by diffusion.

This variation in amplitude due to collisions gives the appearance of a disturbance moving towards the anode. In the absence of collisions, a modulation of the amplitude which resembles that seen for nonlinear periodic water waves, is sometimes possible⁽²⁴⁾. As the elastic losses are increased a value is reached, depending on the spatial period of the initial perturbation, at which the striations are stabilized, so that their motion is regular and the amplitude saturates to a constant value.

2.9 MODE-COUPPLING AND MODULATION OF SELF-EXCITED WAVES

2.9.1 Harmonic and Heterodyne Generation of Waves

It was remarked in the last section that higher harmonic generation and mode-mode coupling occur in the transition and saturated regions. Heterodyne and harmonic generation produced by the interaction of two waves was demonstrated by exciting two waves at frequencies ω_1 and ω_2 in a neon discharge in a region where the waves were not heavily damped. Harmonics at $2\omega_1, 2\omega_2$ were seen together with satellite frequencies at $\omega_1 \pm \omega_2$. Again in neon, the interaction between p and s waves gave rise to a multi line spectrum⁽²⁸⁾. When two waves of slightly differing frequencies were excited in argon, as expected in the linear region, the waves were superimposed. As they travelled towards the anode, harmonic and sum and difference frequencies were generated until, in the saturated region, a broad spectrum was observed⁽⁵⁶⁾. The difficulty in interpreting these results was that a space-time display was not obtained simultaneously with the frequency spectrum display. Recent measurements which have combined the two measurements to examine the evolution from a linear to non-linear random state in a neon discharge when two wave types are present, will be discussed in Chapter X.

For backward ionization waves resonant interactions of the form

$$\omega_3 = \omega_1 + \omega_2 \quad , \quad k_3 = k_1 + k_2 \quad \dots \quad (2.27)$$

are not possible and so other explanations must be found for the coupling⁽²⁴⁾.

2.9.2 Excitation of Multi-Component Spectrum

By using selective amplifiers, Ohe and Takeda⁽⁵⁷⁾, Krasa and Pekarek⁽⁵⁸⁾, were able to examine individual frequency components from, in one case, a discrete multiline spectrum, and in the other, a broad turbulent spectrum. They showed that the waves were excited from one or more dispersion curves. It was suggested that the multiline spectrum was due to amplitude and frequency modulation and in both cases forced pumping was effective.

2.9.3 External Modulation and Nonlinear Van der Pol Characteristics of the Discharge

The modulation of the discharge current or voltage can have pronounced effects. For a noisy argon discharge it was found that when a signal was applied to the anode and tuned to a frequency characteristic of the discharge, the spectrum became well defined, consisting of the fundamental and harmonics of the characteristic frequency ⁽⁷³⁾.

More recently, Ohe and Takeda have shown that effects such as frequency pulling and synchronization to the applied frequency occur, and may be explained in terms of a Van der Pol type of oscillator solution ⁽²⁹⁾.

When a forced oscillation of frequency ω is applied to the positive column where an ionization wave of frequency ω_0 is self excited, the Van der Pol equation describing the ion density (n) may be expressed as

$$\frac{d^2n}{dt^2} - (\alpha_0 - 2\beta n - 3\gamma n^2) \frac{dn}{dt} + \omega_0^2 n = A\omega^2 \sin \omega t \quad \dots (2.28)$$

where A is the amplitude of the forced oscillation, and the ionization function (S) has been expressed in terms of the electric field which in turn has been expanded in a series

$$\delta S = \frac{\partial S}{\partial E} \delta E = \alpha n - \beta n^2 - \gamma n^3. \quad \dots (2.29)$$

This equation is similar in principle to that found for ion acoustic waves and the solution has similar characteristics ⁽³²⁾. For example, the amplitude of the self-excited wave (a) is related to the applied driving amplitude A and the frequencies ω, ω_0 by

$$\left(\frac{a}{2}\right)^2 = 1 - \frac{2(\omega/\omega_0)^4 A^2}{\left\{1 - \left(\frac{\omega}{\omega_0}\right)^2\right\}^2 a_0^2} \quad \dots (2.30)$$

2.9.4 Apparent and Actual Anode Directed 'Disturbances'

External modulation can also result in a regular modulation of the striation velocity giving the appearance of anode directed disturbances and resulting in the generation of satellite frequencies on the spectrum displays ⁽³¹⁾.

In some cases self-excited waves actually travelling towards the anode are seen. As already mentioned, Donahue and Dicke reported anode directed oscillations moving much faster than the backward ionization waves⁽²⁾. On the other hand, anode-directed disturbances in helium of comparable velocity to the ionization waves were found⁽⁵⁹⁾. At those places where a disturbance and a striation met, the striation was brought to rest for a few microseconds and the result of the interaction was a visible region of increased light intensity. The origin of these disturbances was thought to be connected with low velocity ions. Similar interactions were found in neon as a result of an anode directed disturbance, found in the cathode region, interacting with the normal striations. In this case the disturbances had a velocity approximately ten times that of the striations and were explained in terms of bunches of negative space-charges moving towards the anode in the normal electric field⁽¹⁴⁾.

2.10. FACTORS INFLUENCING MOVING STRIATIONS

2.10.1 External Circuit

The external circuit can, by the provision of a path for feedback between the anode and cathode region, affect the moving striations. By suitably controlling the phase of the feedback it is possible to suppress the moving striation in the discharge⁽²⁷⁾. Pekarek demonstrated that the amplitude and frequency of self-excited moving striations, were slightly modified by the presence of a capacitor in parallel with the circuit resistor⁽³⁹⁾. For absolute instabilities the waves are not dependent on the feedback for their existence, although they may still be modified by oscillations occurring in the external circuit.

2.10.2 Tube Radius

Since the loss of particles by diffusion depends on the radius (R) of the tube, this is one of the parameters upon which the striations are dependent.

In a discharge tube consisting of sections of different diameter, it was found that the striations changed frequency and wavelength upon passing from one tube to another⁽³⁷⁾.

Measurements made on tapered tubes showed that the wavelength was proportional to R^N , where N varied from 1.5 to 2.0, whilst the frequency remained constant, independent of radius, in contrast to the results for constant diameter tubes^(36,38). This apparent discrepancy can be accounted for when the influence of the feedback and synchronization of the waves is taken into account⁽³³⁾.

2.10.3 Applied Magnetic Field

The influence of a longitudinal magnetic field has been investigated in detail by Sato⁽³⁶⁾. With increasing magnetic field, the electric field decreased rapidly and then levelled out to a constant value. The frequency of the ionization waves followed a similar dependence as the electric field, whilst the wavelength increased with increasing magnetic field. For large magnetic fields, in Sato's case 1.6 - 4.0 kG depending on the gas, the waves were damped out. By suitably modifying Wojaczek's theory to account for the magnetic field, reasonable agreement was found for the variations in frequency and wavelength.

The effect of a transverse field has not been studied so thoroughly. Rutscher has observed that the velocity and wavelength are reduced, whilst the frequency increases in the region of the applied field⁽³⁴⁾. A local magnetic field has been shown to decrease the amplification factor whilst leaving the characteristics of the remainder of the discharge unchanged.

Pfan and Rutscher observed that the amplification coefficient in neon decreased initially, reached a minimum, and then increased rapidly with increasing magnetic field⁽³⁵⁾. Sato used a local transverse field to suppress the striations in a localized region of the discharge. Outside this region on the anode side, the waves were seen to grow once more showing that the instability was a property of the positive column, independent of the electrode system in that particular case⁽²⁷⁾.

2.11 THE UNIFORM GLOW DISCHARGE

Some features of the uniform glow discharge must be mentioned so that the results of later chapters can be interpreted. The positive column can behave as if it were a combination of capacitance, resistance and inductance. As with conventional alternating current circuits, the resulting frequency dependent impedance has certain resonant frequencies which in the case of the discharge depend on the plasma parameters.

2.11.1 General Impedance Characteristics of the Positive Column

If the current of a homogeneous positive column is modulated externally according to $I = I_0 (1 + \beta \sin \omega t)$, the electron temperature and electric field will likewise be modulated; these space independent oscillations are known as synchronous oscillations. Provided $\beta \ll 1$ the changes may be derived from the linearised time dependent hydrodynamic equations assuming that the column remains axially homogeneous. The amplitudes of the resulting changes in electric field, electron temperature and density, are constant along the tube axis.

An impedance at a frequency ω may be defined as $Z(\omega) = dE/dJ$ where dE and dJ are the changes in electric field and current. Crawford, in some early work⁽⁶⁰⁾, derived an expression for Z using the equation of motion of the electrons in the axial direction, the expression for the current in terms of electron charge density and velocity, and the diffusion

for the electron density:

$$Z(\omega) = \frac{dE}{dJ} = j \omega \frac{R_0}{\nu} \left[\frac{j\omega + \nu}{b + j\omega} \right] \quad \dots (2.31)$$

where $R_0 = \frac{E_0}{I_0}$, the ratio of the equilibrium values of the electric field and current,

ν = collision frequency for momentum transfer between electrons and neutrals

b = rate of loss of electrons by recombination or escape to the walls.

For low frequencies ω/ν tends to zero and the equivalent circuit consists of a resistance and inductance in parallel; Z has a semicircular locus when plotted on real and imaginary axes. At high frequencies b/ω tends to zero, the collision term dominates and the locus of the impedance is a vertical line parallel to the imaginary axis.

The simple theory of Crawford gave a good approximation to his experimental results of the impedance characteristics of a low pressure mercury-vapour discharge⁽⁶⁰⁾. Later studies have used more complete equations which account for the different ionization processes and the behaviour of the electron gas⁽⁴⁷⁾.

When the applied modulation is not small, β cannot be taken as much less than one⁽⁶¹⁾. Nonlinear effects give rise to a non-sinusoidal waveform of the discharge parameters and a change in their time-averaged values. As for ionization waves, these non-linearities are a result of the exponential dependence of the ionization and excitation frequencies on the electron temperature. Experiments performed by Polman⁽⁶¹⁾ showed that the discharge was influenced by nonlinear effects even for small modulation depths, $\beta = 0.2$. Calculations made without linearising the equations were in reasonable agreement with the experiments.

2.11.2 Resonant Frequency of Synchronous Oscillations

At low frequencies there is a resonant frequency of the equivalent circuit such that if the homogeneous column is perturbed, damped oscillations will be seen at this resonant frequency.

For the circuit shown in Fig.2.6, Krejci⁽⁶²⁾, using the results of

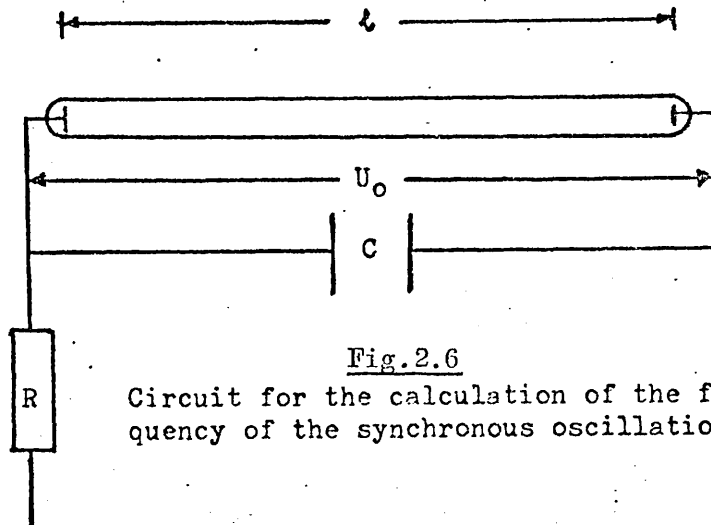


Fig.2.6
Circuit for the calculation of the frequency of the synchronous oscillations

Granowski which were based on the simple continuity equations, derived an equation relating the change in voltage U to the circuit parameters and the direct ionization processes:

$$\frac{d^2U}{dt^2} + 2\beta \frac{dU}{dt} + \omega^2 U = 0 \quad \dots (2.32)$$

where $\beta = \frac{1}{2C} \left(\frac{I_0}{U_0} + \frac{1}{R} \right)$

$$\omega^2 = \frac{I_0}{C} \left(\frac{U_i}{GU_0} - 1 \right) D$$

$$G = \frac{U_e}{U_0} \text{ with } U_e, \text{ the electron temperature in electron volts and } U \text{ in volts.}$$

$$D = \frac{1}{\tau_a U_0}, \text{ where } \tau_a = \text{ambipolar diffusion lifetime.}$$

The expression for the resonant frequency reduces to:

$$f = \frac{0.38}{r} \sqrt{\frac{I_0 b U_i}{C p l E}} \text{ Hz,} \quad \dots (2.33)$$

where r = radius of the tube (cms)
 b = ion mobility at 1 torr (cm/s)
 U_i = ionization potential (volts)
 l = length of tube (cms)
 p = pressure (torr)
 E = electric field (volts/cm)
 I_o = discharge current (amps)
 C = capacitance (farads) .

A comparison of the calculated values of the resonant frequency with experimental results obtained from an argon discharge, gave an order of magnitude agreement⁽⁶²⁾ .

CHAPTER III

EXPERIMENTAL APPARATUS AND MEASURING TECHNIQUES

3.1 INTRODUCTION

The striations were produced in a direct current discharge in argon, the discharge being struck between a hollow cathode and a plane anode with a stabilized direct current power supply.

The system could be pumped down to a pressure of 10^{-6} torr. Experiments were performed at gas pressures between 0.1 and 1.5 torr.

Measurements were made with the aim of studying the waves in the discharge and their interaction with one another. Frequency spectra of the waves together with measurements related to the amplitude of the waves were obtained for different discharge conditions.

Electron temperatures were measured with the aid of a double Langmuir probe. The frequency and relative amplitude of the waves in the discharge were determined from the signal produced from a pick-up coil or photomultiplier and fed to a spectrum analyser. A space-time display of the waves was obtained in some cases using the Stirand method⁽⁶²⁾.

3.2 DISCHARGE TUBE AND VACUUM APPARATUS

The complete discharge, pumping, and gas filling system is shown in Fig.3.1. The discharge tube made from Pyrex glass, had an internal diameter of 5 cms and a length of 110 cms. The tube was connected to the pumping system by a pyrex cross-piece of 5 cm internal diameter.

The discharge system was evacuated using an Edwards oil diffusion pump, backed by an Edwards rotary pump (Speedivac ES 35). A liquid nitrogen trap was mounted above the diffusion pump and directly below a block containing a baffle valve which, when closed, isolated the discharge from the pumping system. An additional line by-passing the diffusion pump,

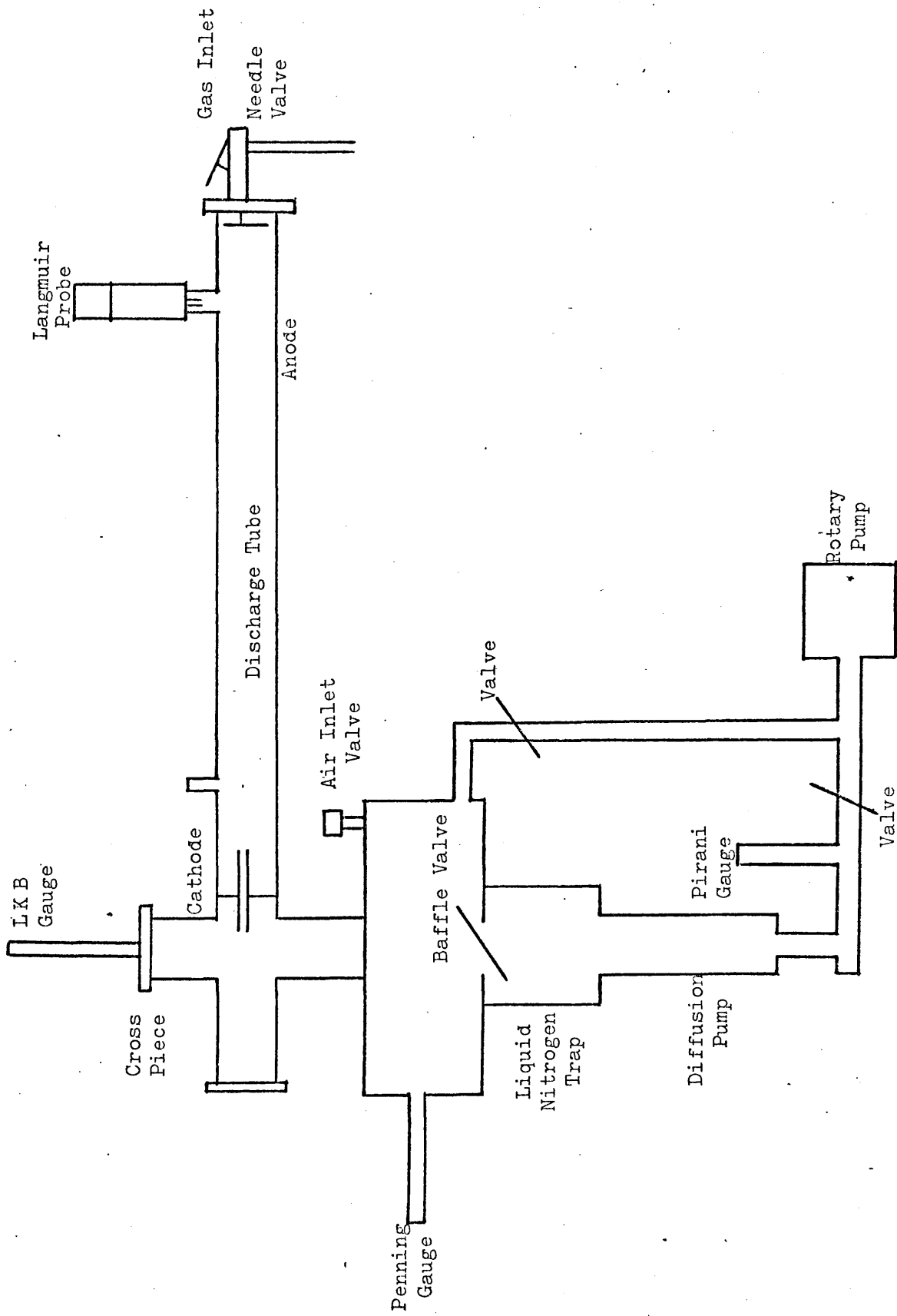


Fig. 3.1
Schematic of the Discharge System

trap and baffle valve enabled the tube to be 'roughed out' with the rotary pump.

The backing pressure was measured with a Pirani gauge mounted between the rotary and diffusion pumps. Lower vacua were measured by a Penning gauge mounted on the block housing the baffle valve. The neutral gas pressure in the discharge tube was measured with an LKB gauge connected to a side-arm of the cross-piece and protected from the discharge by a metal gauze sheet across its aperture.

The gas used in the experiments was admitted to the discharge tube through a hole in the anode with a needle valve used to control the flow rate.

The cathode was a hollow steel wire mesh (10 per cm) of 4mm diameter and 10 cms length. The anode was an aluminium disc of 4 cm diameter.

The system could be let up to atmospheric pressure by an inlet valve on the baffle block. Typically a pressure of 5×10^{-6} torr could be attained when using the diffusion pump and cold trap.

The gas used in the experiments was British Oxygen technical quality argon which is quoted as 99.9% pure. Impurities can affect the properties of striations and their limits of occurrence. However, the results to be presented are concerned with the interaction of the waves so that their origin, as far as impurities were concerned, was not important.

3.3 ELECTRICAL CIRCUIT

A stabilised power supply capable of giving 500 mA at 3 kV was used; this was connected in series with a chain of six 1 K Ω resistors and the discharge tube. A capacitor of 1.5 μ F was connected in parallel to the tube and the negative terminal of the power supply was earthed, see Fig.3.2.

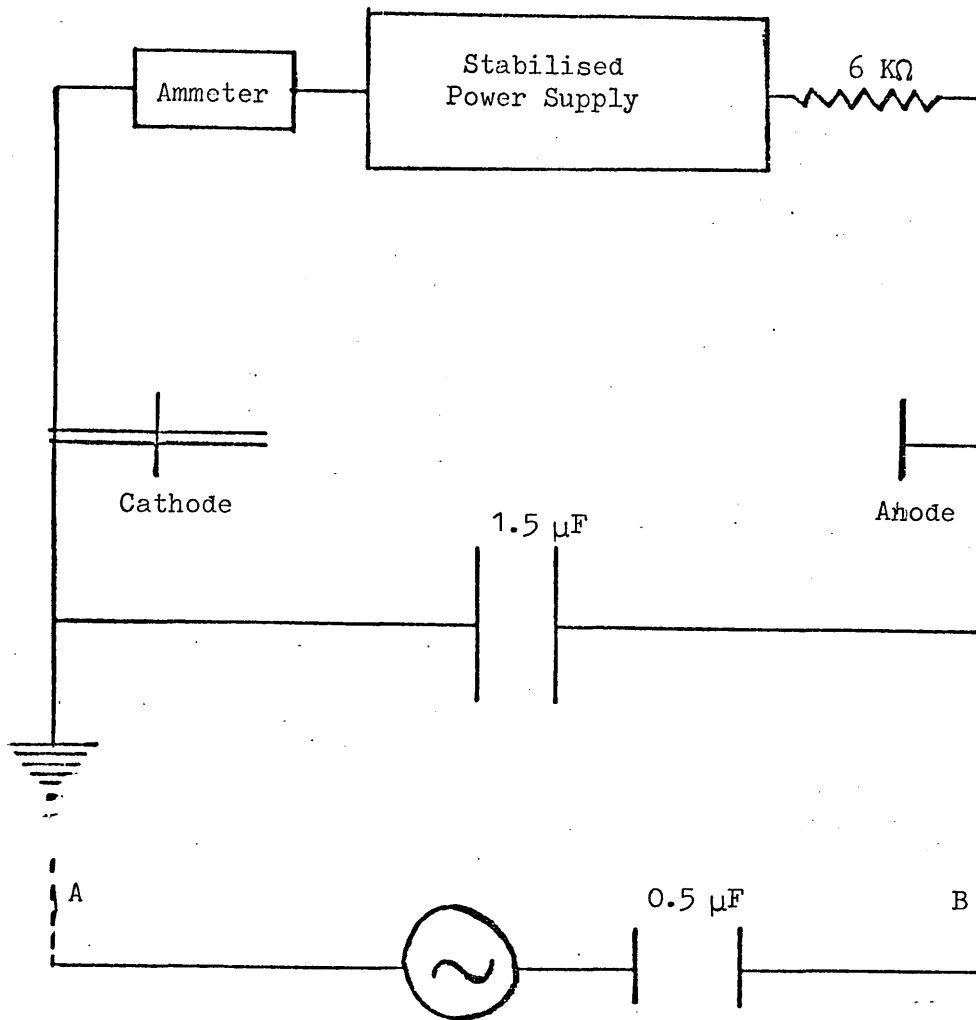


Fig.3.2

Schematic of the electrical circuit for the discharge

3.4 ARTIFICIAL EXCITATION OF STRIATIONS

Striations may be excited by varying the discharge current or voltage⁽⁴¹⁾. In the present case the voltage was varied by using a sinusoidal generator with a variable output, maximum voltage 25V peak to peak, connected between the cathode and the anode, points A and B in Fig.3.2. To prevent large d.c. voltages appearing on the output of the oscillator a blocking condenser of 0.5 μF was connected between the generator and anode.

3.5 FILLING THE SYSTEM WITH GAS

In a typical run the whole system up to the regulator on the gas cylinder was pumped down to about 5×10^{-6} torr. The gas admittance needle valve was then closed and the line between the cylinder and tube was filled with argon. After this the baffle valve was closed, isolating the tube from the pumping system, and the needle valve was opened and the tube filled to a pressure of a few torr. By using the by-pass pipe, gas was then pumped continuously through the discharge tube with the rotary pump. The pressure as measured with the LKB gauge was set by adjusting the needle valve.

Finally a discharge of about 100 mA was struck and allowed to run for about 15 minutes to achieve steady conditions before measurements at the desired current were taken.

3.6 RUNNING THE DISCHARGE

The operating range of the system was between 0.1 - 4.0 torr and 10 - 350 mA.

At lower pressures the discharge became unsteady since it would sometimes strike to the pumping system. At pressures higher than 4 torr the discharge column constricted and required currents larger than 400 mA to sustain it.

3.7 DOUBLE LANGMUIR PROBE

A double Langmuir probe of glass construction was used to measure the electron temperature⁽⁶⁵⁾. The electrodes of the probe consisted of two tungsten rods, diameter 0.5 mm, with their axes separated by 2mm. The electrodes were positioned on the axis of the discharge tube and at right angles to it. The voltage-current characteristics were obtained using the circuit shown in Fig.3.3(a).

The electron temperature (T_e) was then calculated from⁽⁶⁵⁾

$$T_e = 0.252 \Delta \text{ eV}$$

where Δ (volts) is obtained from the voltage-current characteristic, Fig. 3.3(b). The variation of T_e with pressure and current is shown in Fig.3.4.

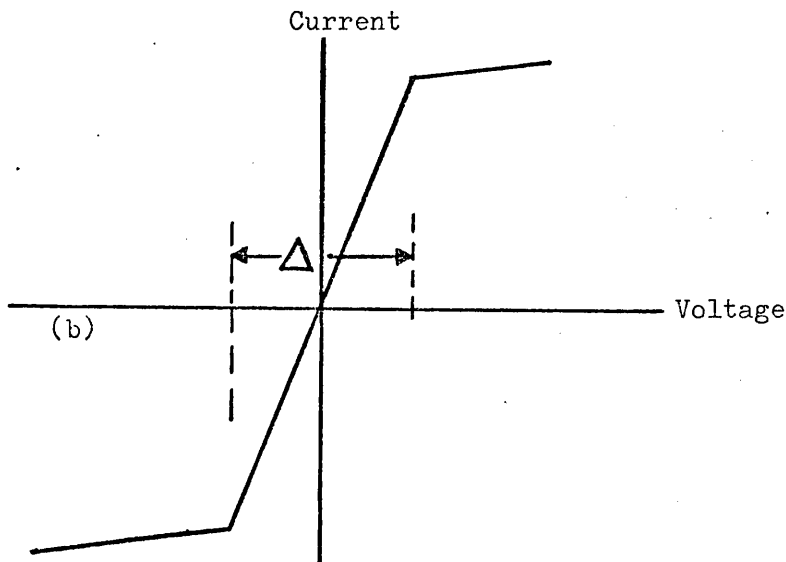
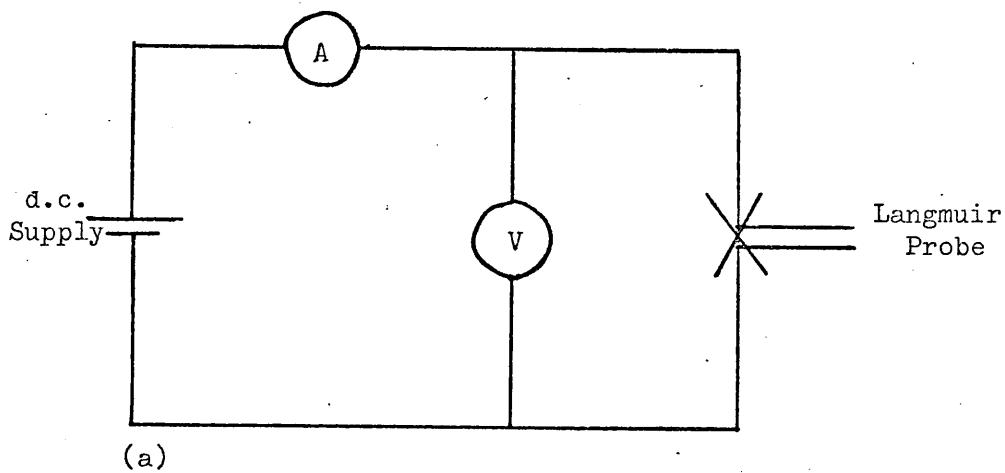


Fig.3.3

- (a) Langmuir probe circuit
A - Ammeter, V - Voltmeter
- (b) Current-voltage characteristic

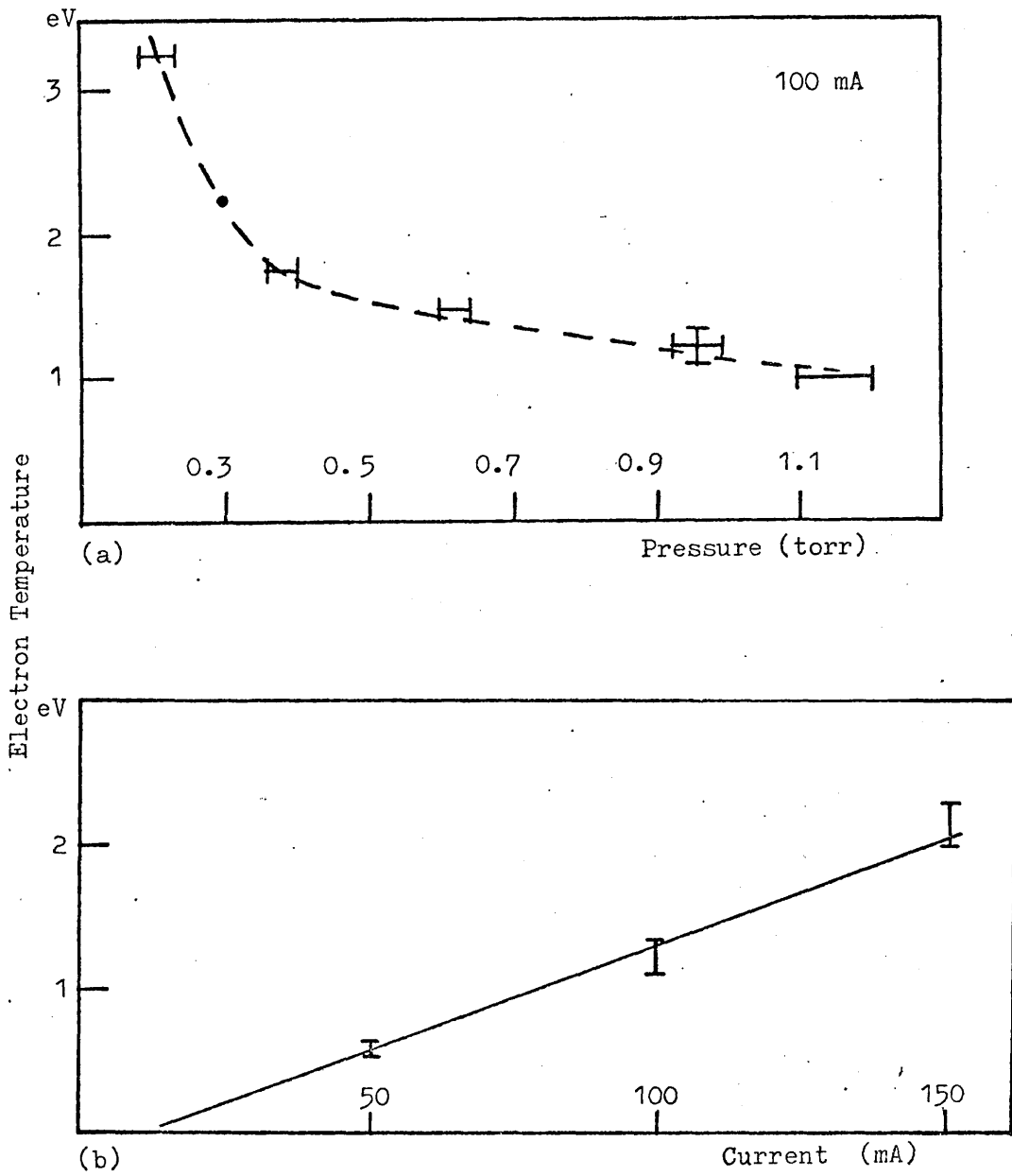


Fig.3.4
 Variation of electron temperature
 (a) With pressure, current = 100 mA
 (b) With current, pressure = 1 torr

3.8 DETECTION OF THE WAVES

The striations (waves) in the discharge produced changes in the electron temperature and particle (electron and ion) densities which in turn resulted in variations of the emitted light intensity and the electric potential of the discharge, respectively. These changes occurred with the frequency and wavelength of the waves so that by monitoring the light intensity and electric potential, the frequency, and in some cases the wavelength, could be determined. In addition the relative changes in amplitude along the tube could be obtained from the above measurements.

3.9 CAPACITIVE PICK-UP PROBE

The changes in potential could be detected by using a capacitive pick-up probe close to the tube⁽⁶⁰⁾. Such a probe was made by wrapping five turns of copper wire on a cylindrical paper former which was concentric with the discharge tube and free to run along it. One end of the wire was left free on the former, whilst the other end was connected to a low frequency spectrum analyser, Tektronix 1L5.

The width of the capacitive probe was 3mm, and so could resolve spatial variations larger than its width. The signal received by the spectrum analyser from the probe was proportional to the alternating component of the electric potential at the position of the probe along the tube. That the probe could respond to the frequencies of the waves was confirmed by externally modulating the voltage at a known frequency and obtaining a probe signal at the same frequency.

3.10 PHOTOMULTIPLIER

The emitted light intensity was detected with the aid of an EMI 9592B photomultiplier. Saturation of the photomultiplier was avoided by keeping the output d.c. current below 0.1 mA by attenuating the incident light with neutral filters and small apertures.

The signal from the load resistor of the photomultiplier was fed to the spectrum analyser.

By mounting the photomultiplier on an optical bench, parallel to the tube, axial variations in the light intensity from the discharge could be measured by changing the position of the photomultiplier. It proved convenient to use a light pipe, one end of which was attached to a slide on the tube while the other was mounted in front of the photomultiplier window.

The alternating signal from a photomultiplier, proportional to the light intensity from the discharge, can usually be related to the change in the ionization function due to the striations. In particular this has been shown experimentally to be the case for self-excited waves in argon⁽⁵³⁾. For small amplitude waves the change in ionization function is proportional to the change in electron temperature⁽¹⁷⁾.

3.11 SPECTRUM ANALYSER

The signals were analysed with a Tektronix 1L5 spectrum analyser having a frequency range of 0-1 MHz. Before each experimental run the standard calibration checks, as given in the manual, were carried out. The accuracy given by the manufacturers is: Centre Frequency: $\pm 5\%$, Dispersion: $\pm 10\%$.

The sweep period required to scan the spectrum is of the order of 0.1 sec and therefore the analyser is not capable of recording 'instantaneous' events. Rather, the input signal is Fourier analysed to give the root mean square of the amplitude of each frequency component and so for aperiodic signals the results must be interpreted with care.

3.12 SPACE-TIME DISPLAY

Time resolved measurements were taken using the space-time display method of Stirand et al⁽⁶⁴⁾, the principles of which are shown in Fig.3.5.

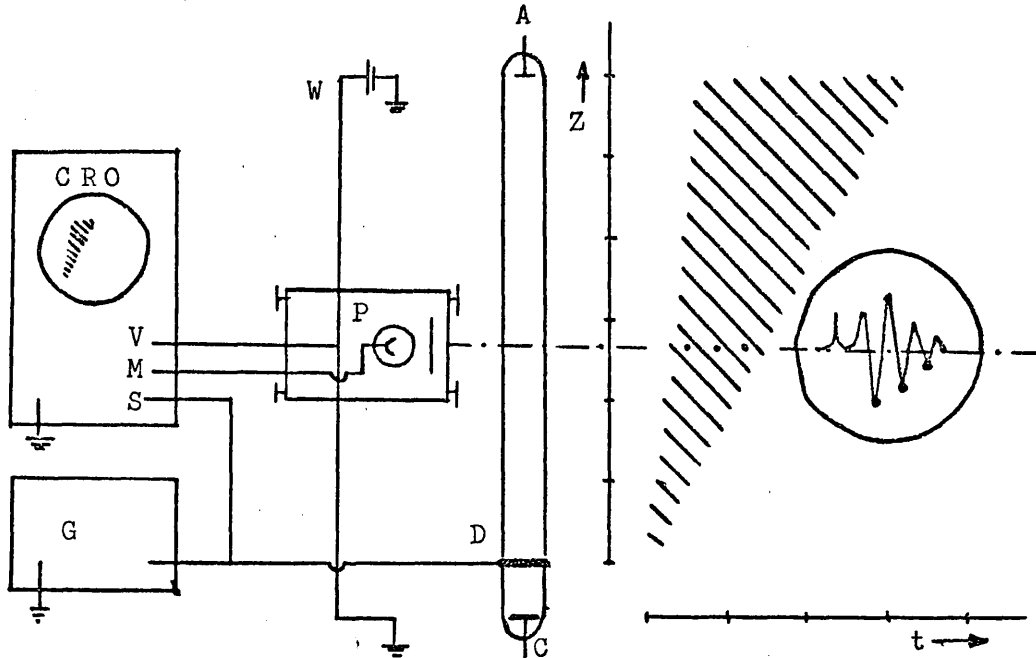


Fig.3.5

Principle of space-time display. G-generator (artificial excitation); CRO - oscilloscope; S - external trigger; V - vertical d.c. input; M - modulation of beam intensity; A - anode; C - cathode; D - ring for reference trigger signal; P - photomultiplier movable along track; W - slide wire voltage divider

The detector, photomultiplier or coil, was moved along the tube, the output representing the light intensity or electric potential at each point at the instant the photomultiplier or coil passed.

In order that the oscilloscope triggering was synchronised with the striations, the signal from a coil mounted at a fixed position on the tube was fed to the external trigger on the oscilloscope.

The slide wire contact gave a voltage proportional to its distance from the cathode. This signal was fed to the y input of the oscilloscope and had the effect of moving the position of the oscilloscope trace up or down the screen as the detector was moved along the discharge.

The signal from the detector was used to modulate the intensity of the trace on the screen so that only the maxima, corresponding to maxima of the input signal, were observed as spots on the screen.

As the detector was moved slowly down the tube, the oscilloscope trace swept across in almost horizontal lines, each line representing the time variation of the maxima in light intensity or electric potential of the striation. The loci of the maximum points thus gave a space and time plot of the striations as they travelled through the discharge. From these space-time pictures the motion of the waves could be observed.

3.13 SPACE-TIME DISPLAY FOR IRREGULARLY MOVING STRIATIONS

When the motion of the waves is aperiodic the Stirand method cannot be used because the oscilloscope triggering cannot be synchronised to the waves. For such a case a rotating drum camera, outlined in Fig.3.6, can sometimes be used. Unfortunately for this type of camera the light intensity from some discharges is insufficient to expose the film. This method could not be used with the argon discharge but was employed successfully to obtain the results, described in Chapter X, for a neon discharge.

The drum, which was rotated by an electric motor, was mounted level with the discharge with its axis parallel to the tube. High speed film, 800 ASA, was mounted around the circumference of the drum and a lens, $f/1.8$, was used to image the discharge onto the film. The image appeared as a horizontal line of negligible breadth.

As the drum was rotated the entire film became exposed to the image of the discharge. At any instant the positions of increased light intensity in the discharge tube due to the striations produced regions of increased exposure along the image of the film. A moment later the film and striations had moved so that a new image with the regions of increased exposure in new positions, was formed on the film adjacent to the previous

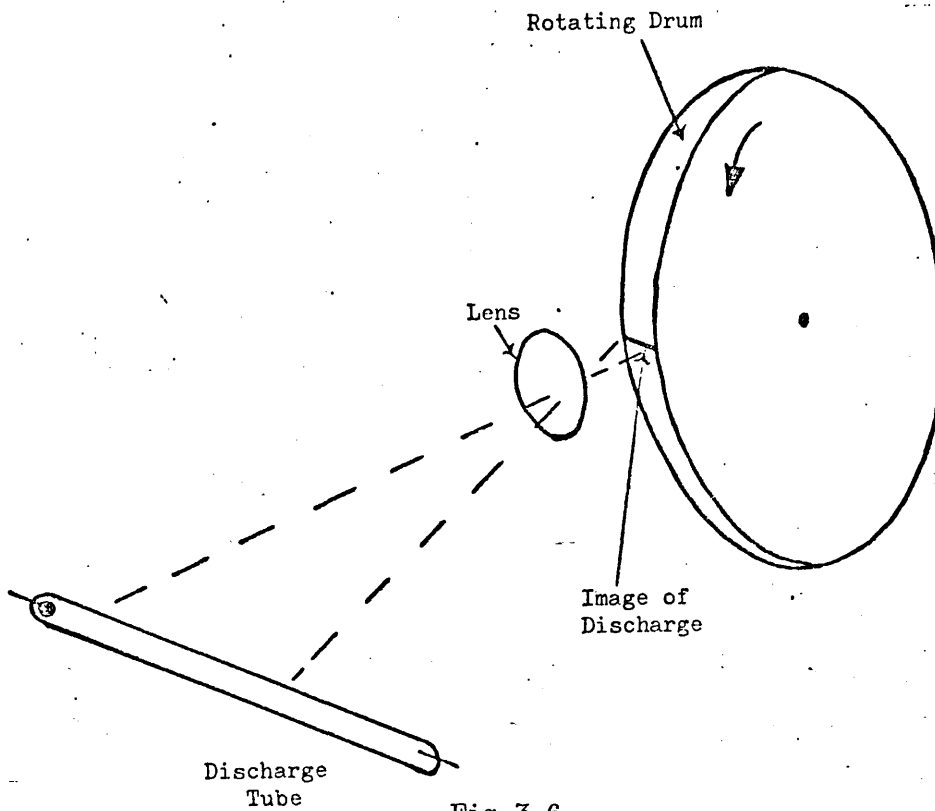


Fig.3.6

Schematic of a rotating drum camera

image. In this way the position of the light intensity maxima of the striations along the tube at different times, was recorded to give a space-time plot of the waves.

The space and time axes were calibrated by placing markers at a known distance apart along the tube, and by using a small neon lamp which was positioned at the end of the tube and pulsed at a known frequency. These markers appeared on the film to give a direct calibration.

A shutter in front of the lens was used to ensure that the film was only exposed for one revolution of the drum.

Since this method does not rely on any synchronisation with the waves, the irregular motion of the striations could be observed from the space-time pictures obtained from the film.

CHAPTER IV

EXPERIMENTAL OBSERVATIONS OF SELF-EXCITED WAVES

IN THE ARGON DISCHARGE

4.1 INTRODUCTION

The linear and nonlinear propagation of regularly moving striations in an argon discharge were studied by recording the frequency spectrum and amplitude variation of the waves.

The general scheme of the investigations will be described before outlining the contents of this chapter.

From preliminary experiments with the 5 cm diameter argon discharge, described in Chapter III, it was seen that discrete multiline frequency spectra resulting from the interaction of self-excited waves could easily be obtained. For this reason more detailed observations were carried out using argon as the discharge gas.

The fundamental frequencies of the self-excited waves fell into three frequency ranges: 200-900 Hz, 1-5 kHz, 10-40 kHz. These will subsequently be referred to as frequency ranges (a), (b) and (c) respectively.

In addition to the interactions between the waves in the different frequency ranges which gave rise to the multiline spectra, it was found that the waves within each frequency range (a) and (b) exhibited spatial variations in amplitude due to both linear and sometimes nonlinear processes.

The experimental results were obtained from measurements of the frequency spectra of the waves taken at different positions along the discharge tube for certain pressure and current settings. The frequency spectra were derived from the coil and photomultiplier output signals as described earlier, Chapter III. By varying the current and pressure different effects were observed.

From the recorded frequency spectra the axial variation of the amplitude of each frequency component could be obtained; this allowed the nature of the linear interactions of the waves within frequency ranges (a) and (b) to be deduced. For the waves in frequency range (b) it was possible to directly observe the interaction using the space-time display technique and so confirm the deductions made from the 'time averaged' standing wave patterns.

Once the linear interactions of the striations were determined it was possible to deduce the nature of the nonlinear interactions from the variation in amplitude of the 'sum and difference' frequency components generated by the interactions. Visual observations made with a rotating mirror supported the proposed form of interaction.

In this chapter, the characteristics of the waves in frequency range (b) and an interpretation of their linear interactions are presented first. The results for the waves in frequency range (a) are then described. Following the description of the nonlinear modulation of the waves in range (b), the nonlinear interactions between the waves in ranges (a) and (b), range (b) and (c), and all three ranges simultaneously, are described. The interpretation of the nonlinear results is dealt with in Chapter VII.

Since the terms 'apparent stationary striations', standing wave patterns and wave patterns are frequently used, it is useful to define them from the outset.

Under certain circumstances it was possible to see with the eye apparent stationary regions of increased light intensity occurring at regular intervals along the discharge tube, these are referred to as 'apparent stationary' striations. The recorded axial variations of the amplitude of the frequency components obtained from the spectrum analyser recordings of the photomultiplier and coil signals, are termed 'standing wave' patterns or

wave patterns. Standing wave patterns were observed with and without the simultaneous observation of apparent stationary striations.

4.2 LINEAR INTERACTIONS: CHARACTERISTICS OF THE SELF-EXCITED WAVES WITH A FUNDAMENTAL FREQUENCY IN RANGE (b) : 1 - 5 KHz

4.2.1 Frequency Variation

Of all the waves seen, those in frequency range (b) had the largest amplitude and were the most easily observed since they existed over almost the entire pressure and current region within which self-excited waves occurred.

The waves had a fundamental frequency between 1 - 5 KHz with harmonics, which in some cases extended up to the seventh order, Fig.4.1. The variation of the fundamental frequency with pressure is shown in Fig.

4.2(b). The corresponding variation with current, Fig.4.2(a), at a given pressure, displays discontinuities, but the general trend is that the frequency increases with current.

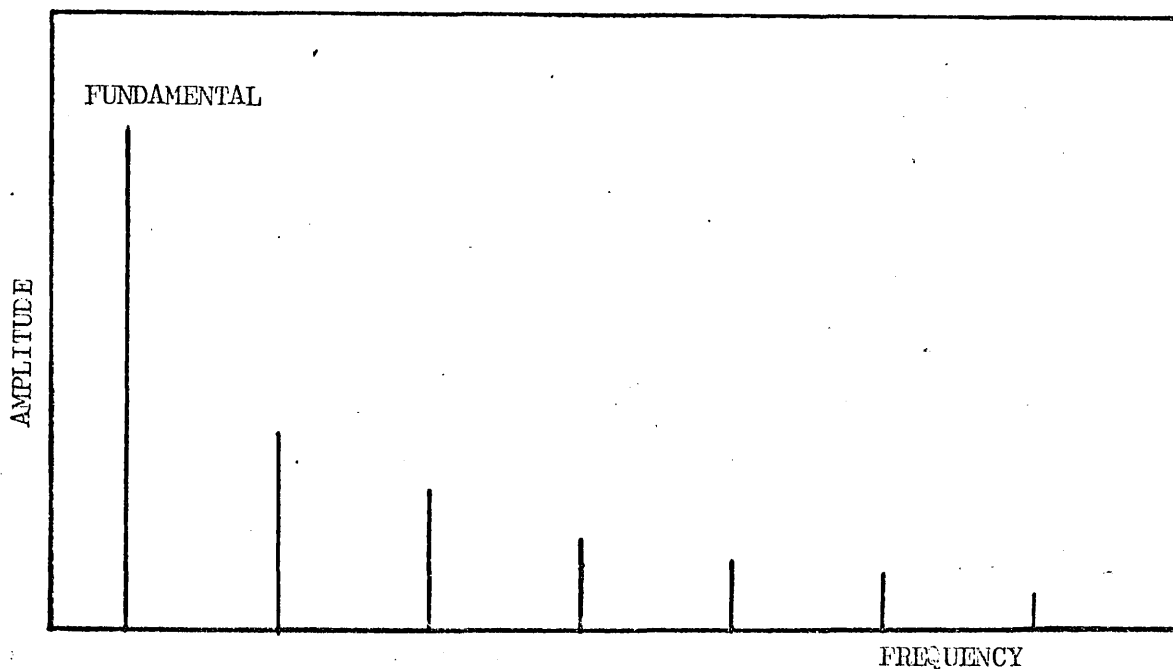


Fig.4.1

Frequency spectra for a wave in frequency (b), showing the fundamental frequency 5.2 KHz, and harmonics $p = 0.15$ torr, $I = 95$ mA

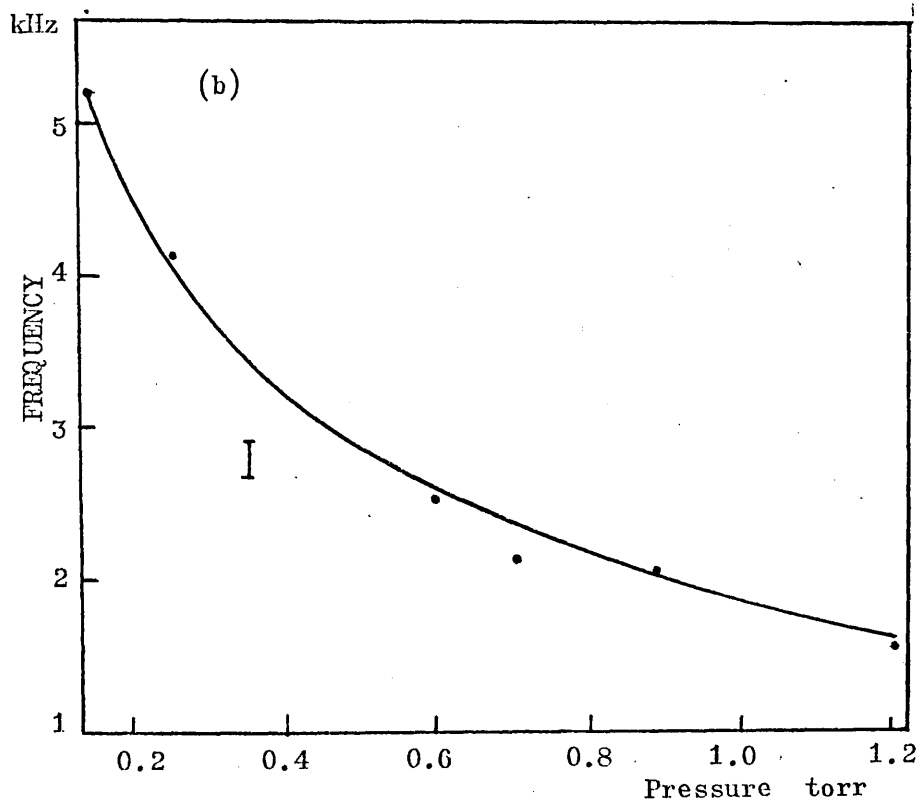
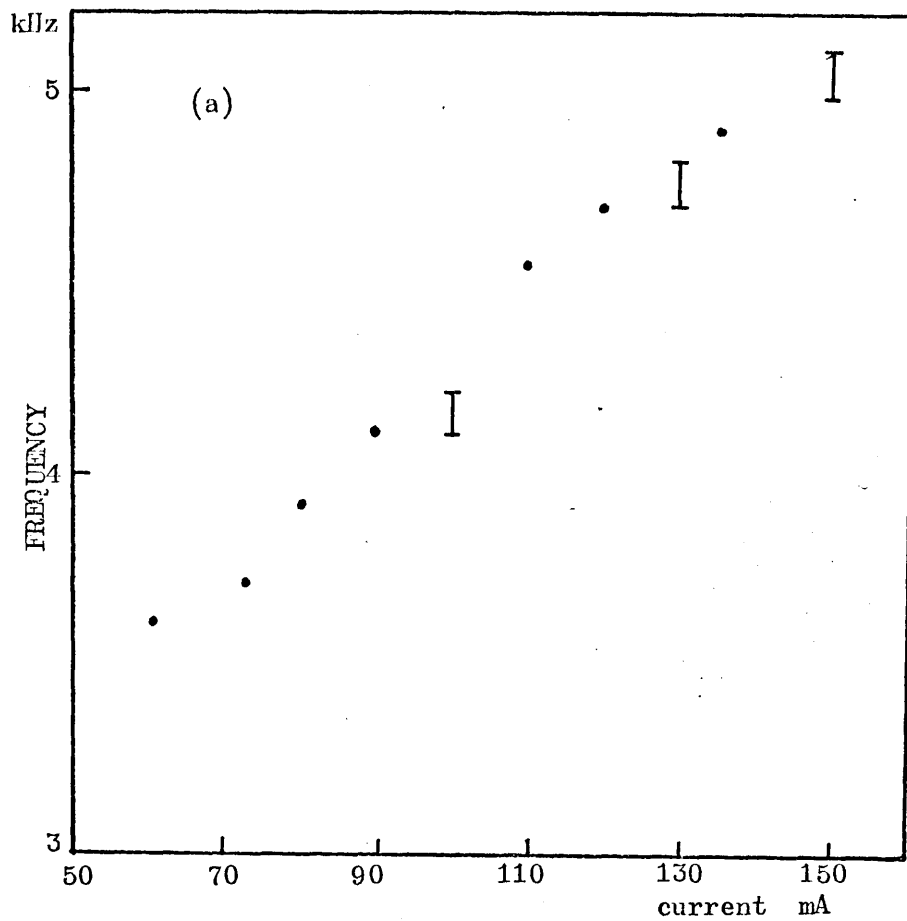


Fig.4.2
 Variation of the fundamental frequency with:
 (a) Current, $p = 0.15$ torr
 (b) Pressure, $I = 92$ mA

4.2.2 Standing-Wave Pattern

The amplitude of the fundamental wave and each harmonic, as measured from the coil and photomultiplier signals, varied with position along the discharge to produce standing wave patterns as the examples in Fig.4.3 show. The standing wave patterns extended the whole length of the positive column; generally the amplitude of the photomultiplier signal decreased with distance from the cathode, whereas the signal from the pick-up coil increased with distance. Furthermore the positions of the maxima and minima for the photomultiplier wave pattern did not coincide with those obtained from the coil signal.

The separation in maxima in the standing wave patterns was inversely proportional to the frequency. For the fundamental frequency this distance was of the order of 15 cm at a pressure of 0.3 torr.

By triggering an oscilloscope with the signal from a coil at a fixed position along the discharge tube and displaying the signal from a second coil which could be moved along the tube, it was possible to measure the relative phase between signals at different positions along the discharge. It was found that at positions corresponding to adjacent maxima in amplitude, as measured in the standing wave pattern, the signals were in phase with one another.

The standing wave patterns obtained from the coil signal were generally more pronounced than those given by the photomultiplier signal. Indeed, the amplitude patterns for the fundamental mode when measured by the photomultiplier, showed hardly any periodic variation in amplitude.

The variation in amplitude of the photomultiplier signal for the fundamental frequency with current at a fixed position is shown in Fig.4.4.

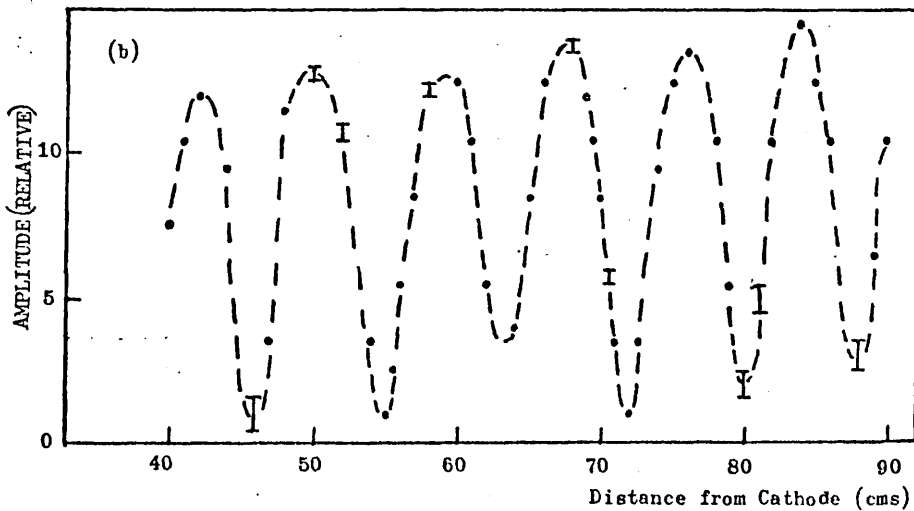
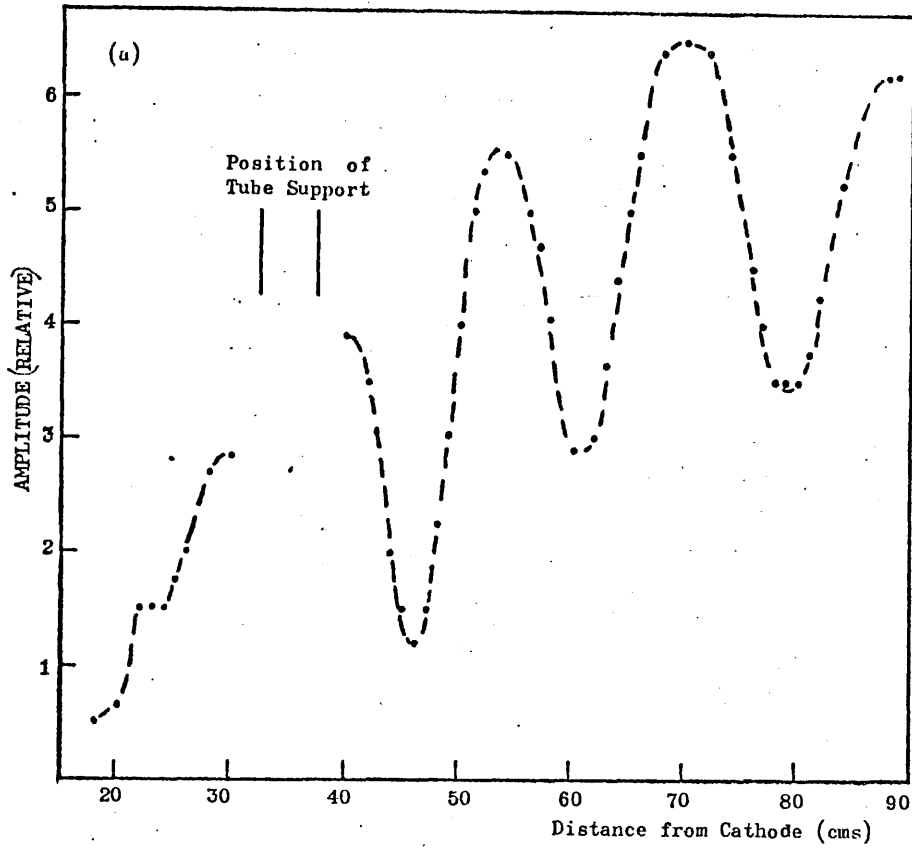


Fig.4.3

Standing-wave patterns of the waves in frequency range (b)

(a) Coil signal; Frequency: 3.4 KHz; Current: 64 mA;
Pressure: 0.15 torr

(b) Coil Signal; Frequency: 5 KHz; Current: 100 mA;
Pressure 0.2 torr

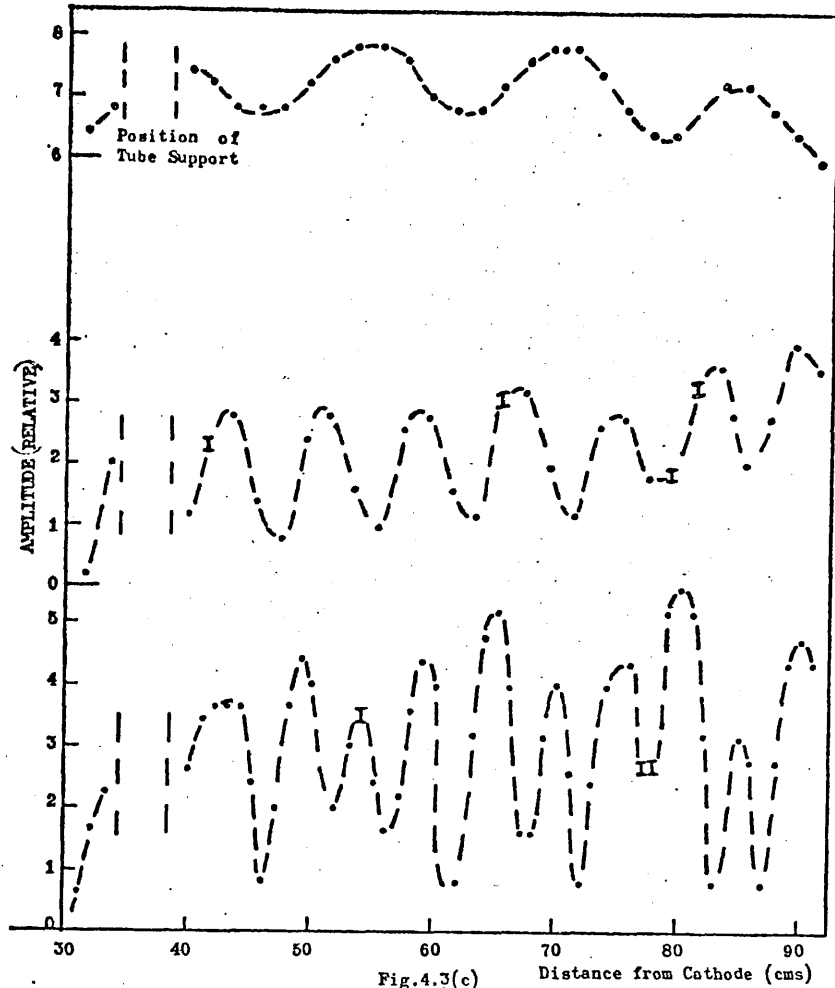


Fig.4.3(c)

Coil signal, Fundamental frequency: 2.6 KHz;
 Current: 98 mA; Pressure: 0.2 torr
 (i) Fundamental, (ii) 1st Harmonic, (ii) 2nd Harmonic.

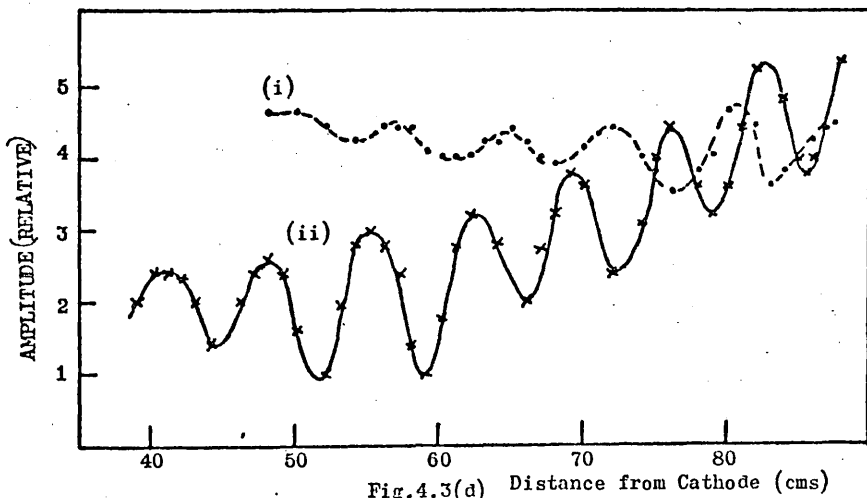


Fig.4.3(d)

Wave pattern for first harmonic. Frequency: 3.62 KHz;
 Current: 76 mA; Pressure: 0.57 torr
 (i) Photomultiplier signal; (ii) Coil signal

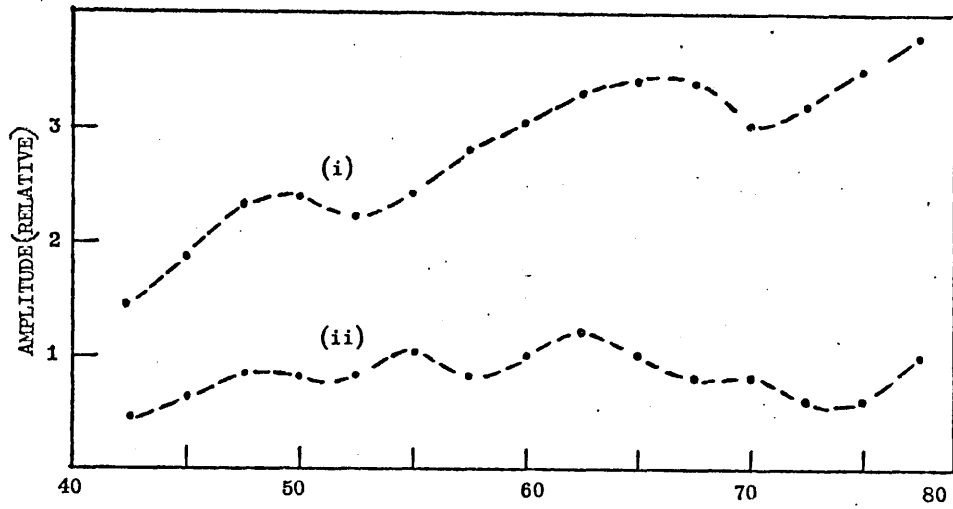


Fig.4.3(e)

Wave pattern from photomultiplier signal. Current: 95 mA;
 Pressure: 0.33 torr; (i) Fundamental, Frequency 3.3 KHz;
 (ii) First harmonic

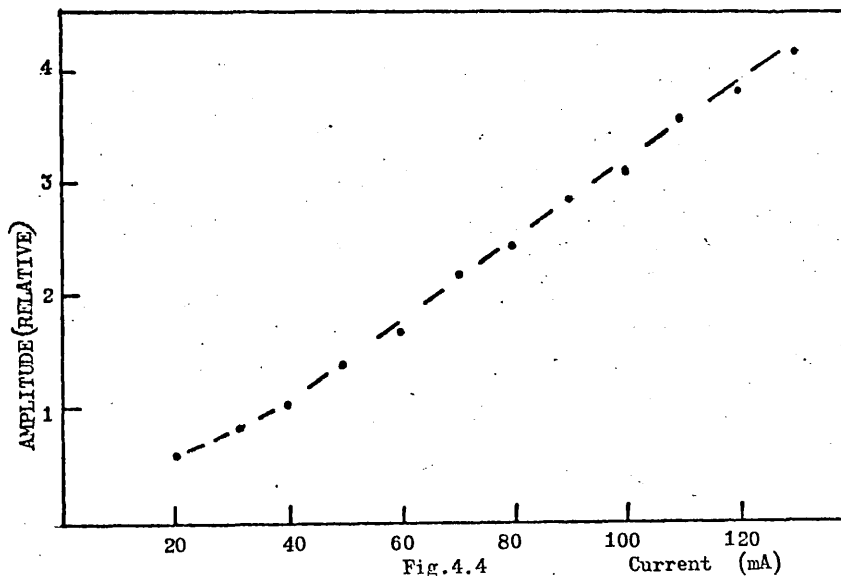


Fig.4.4

Amplitude of fundamental frequency versus current
 for the photomultiplier
 Signal: $p = 0.28$ torr

4.2.3 Interpretation of the Standing Wave Patterns

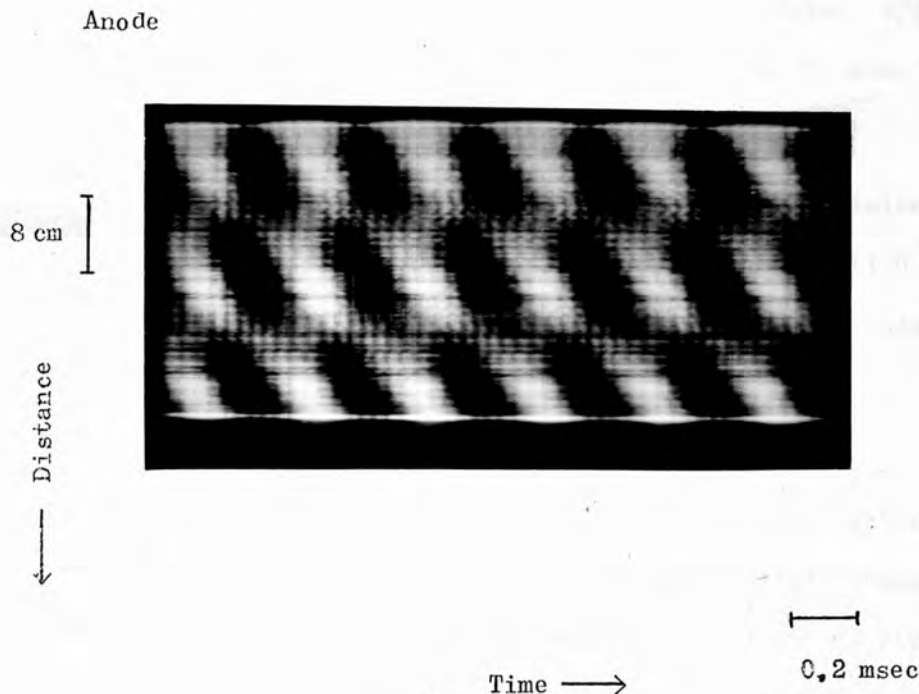


Fig.4.5

Space-time display of the coil signal.
Pressure: 0.3 torr; Current: 57 mA

A space-time display, obtained from the coil signal by using the Stirand method, for the situation when a standing wave pattern was found from the spectrum analyser measurements, is shown in Fig.4.5. It can be seen that in addition to the lines sloping from the left down to the right, which show the path of a striation moving from the anode to the cathode, there are vertical stripes due to synchronous, space-independent, oscillations with the same frequency as the striations.

The space-time display shows that the amplitudes of the travelling waves (striations) and the synchronous oscillations are simply superimposed allowing the variation in amplitude of the standing wave patterns of the coil and photomultiplier signals to be explained in terms of linear interference.

For the general case of two waves which have the same frequency and wavelength (λ) but travel in opposite directions, the adjacent maxima in the standing-wave patterns are separated by a distance $\lambda/2$. In the present case the interference is different since the distance between adjacent maxima is equal to the wavelength λ .

The nature of the interference could have been obtained from the standing-wave pattern and the knowledge of the phase relation between the signals from adjacent maxima in the wave patterns without referring to space-time displays.

4.2.4 Information Obtained from the Wave-Patterns

In interpreting the axial variation in the wave patterns in a way which is consistent with both the coil and photomultiplier measurements, some features of the variations in ionization function and electric potential for the travelling waves and synchronous oscillations are seen. It is worth recalling that the pick-up coil acts capacitively⁽⁶⁰⁾ and that the signal is proportional to the changing electric potential at the point on the tube where the coil is positioned.

For the travelling wave, the light intensity (L_w) and the electric potential (V_w) may be represented by the expression:

$$L_w = A_o e^{\alpha x} \sin(\omega t - kx + \xi) \quad \dots (4.1)$$

$$V_w = C_o e^{\alpha x} \sin(\omega t - kx)$$

where

A_o, C_o are the amplitudes at $x=0$,

x = axial distance measured from the anode,

ω = angular frequency

k = wavenumber

α = spatial amplification coefficient

ξ = phase angle relative to the electric potential.

The electric field (E_s) and light intensity (L_s) for the synchronous oscillation may be represented by:

$$\begin{aligned} E_s &= m \sin(\omega t + \varphi) \\ L_s &= B \sin(\omega t + \delta) \end{aligned} \quad \dots (4.2)$$

where m, B are constants and φ and δ account for any phase difference relative to the electric potential (V_w). From the expression for E_s , the electric potential due to the synchronous oscillation (V_s) is obtained from

$$\frac{\partial V_s}{\partial x} = -E_s,$$

so

$$V_s = [D_0 - mx] \sin(\omega t + \varphi) \quad \dots (4.3)$$

where D_0 is a constant.

The amplitude of the resultant wave pattern for the light intensity is given by

$$L = \sqrt{A^2 + B^2 + 2AB \cos(kx - \xi + \delta)} \quad \dots (4.4)$$

and that for the electric potential is given by

$$V = \sqrt{C^2 + D^2 + 2CD \cos(kx + \varphi)} \quad \dots (4.5)$$

where, $A = A_0 e^{cx}$, $C = C_0 e^{cx}$, $D = D_0 - mx$.

From these expressions for the amplitudes it can be seen that the relative positions of the amplitude maxima for the light intensity and the coil signal depend on the values of the phase angles φ , ξ and δ . It was found that the positions of the maxima of the coil and photomultiplier wave patterns were **either** $\pi/2$ **or** π out of phase, a situation which requires that $(-\xi + \delta) = \varphi + \frac{\pi}{2}$ or $\varphi + \pi$. For moving striations⁽¹⁷⁾ $\xi \approx 0$ which gives values of $\delta = \varphi + \frac{\pi}{2}$ or $\varphi + \pi$.

The coefficients A and C in equations (4.4) and (4.5) for the resultant amplitudes of the light intensity and electric potential are proportional to $\exp cx$. In contrast the coefficient D , which is related to the electric potential of the synchronous oscillation, is linearly proportional to x : it is for this reason that the axial variations of the amplitudes of the standing wave patterns of the photomultiplier and coil signals are different. The following example bears out the above explanation.

4.2.5 Computed Standing Wave Pattern

The axial variations in amplitude for the photomultiplier and coil signal for the first harmonic of 3.7 KHz at a current of 79 mA, are shown in Fig.4.6. Because in this case the changes were so regular it was possible to compute a wave pattern, assuming sinusoidal variations, for the superposition of a travelling wave and a synchronous oscillation.

By taking several maximum and minimum values to calculate α , a curve was fitted to the experimental points for the photomultiplier signal, Fig.4.6(a). This gave a value of $\alpha = 0.01$ and the ratio of the travelling wave amplitude to that of the synchronous oscillation at $x = 0$, was equal to $\frac{A}{B} = 3.4$.

In a similar way α was calculated for the coil signal, Fig.4.6(b), to give a value of 0.011 in agreement with the value found from the other curve. Using the derived value of α and the expression for the potential (V), equation (4.5), the value of m was found to be 0.3 and the ratio of the travelling wave amplitude to the synchronous amplitude at $x=0$ was equal to $\frac{C}{D} = 0.2$. To check the validity of using equation (4.5) several other maxima and minima were calculated and are shown in Fig.4.6(b). From the general shape of the curves in Figs.4.3, 4.6(b) - the decreasing of the maxima and minima values with distance from the anode - and the numerical values obtained, it can be seen that the change in potential due to the synchronous oscillation is larger than that due to the travelling wave. For the light intensity patterns the converse is true. This may be explained by considering the variations in electron temperature since the light intensity is proportional⁽¹⁷⁾ to the electron temperature, which in turn is related to the electric field through the energy equation.

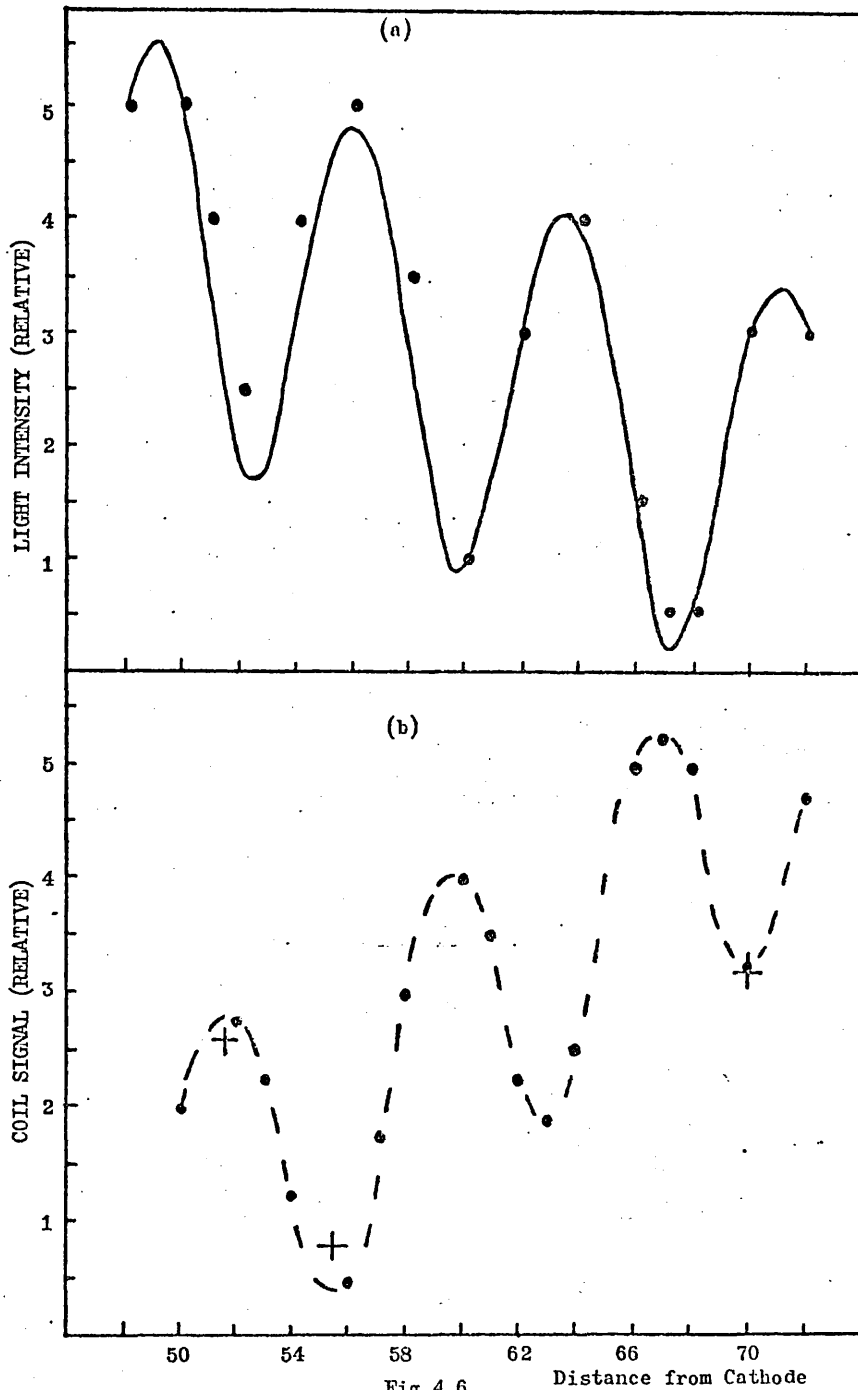


Fig.4.6

Standing-wave pattern for first harmonic
 Frequency = 3.7 KHz; Pressure = 0.58 torr
 (a) Photomultiplier signal ●● experimental — computed
 (b) Coil signal: --●-- experimental + calculated

For a potential (V) given by

$$V = C_0 \sin(\omega t - kx) + (D_0 - mx) \sin(\omega t + \varphi) \quad \dots (4.6)$$

where the symbols have the same meaning as before and $\alpha=0$, for simplicity, the electric field is given by

$$E = -\frac{\partial V}{\partial x} = C_0 k \cos(\omega t - kx) + m \sin(\omega t + \varphi) \quad \dots (4.7)$$

In the example above, $C_0 \approx 2.5$, $k = \frac{2\pi}{7} \text{ cm}^{-1}$ and $m = 0.32$, which give $C_0 k > m$. That is, the electron temperature variation of the travelling wave is larger than that of the synchronous oscillation. Consequently since the electron temperature is proportional to the light intensity, the latter is correspondingly larger for the travelling wave than for the synchronous oscillation, in accord with the experimental results.

Besides the linear interference of waves, other effects were found to produce a standing-wave in the time averaged patterns. These effects will be discussed in connection with doublets and artificial excitation and modulation.

4.2.6 Identification of the Travelling Waves

From the wave patterns at various pressures, and using additional points obtained from phase sensitive measurements, the phase velocity versus pressure (p_0) was obtained, Fig.4.7. The ion drift velocity calculated for argon for a value of $E_0 = 1.5 \text{ V/cm}$ is shown. The fit of the points shows that the

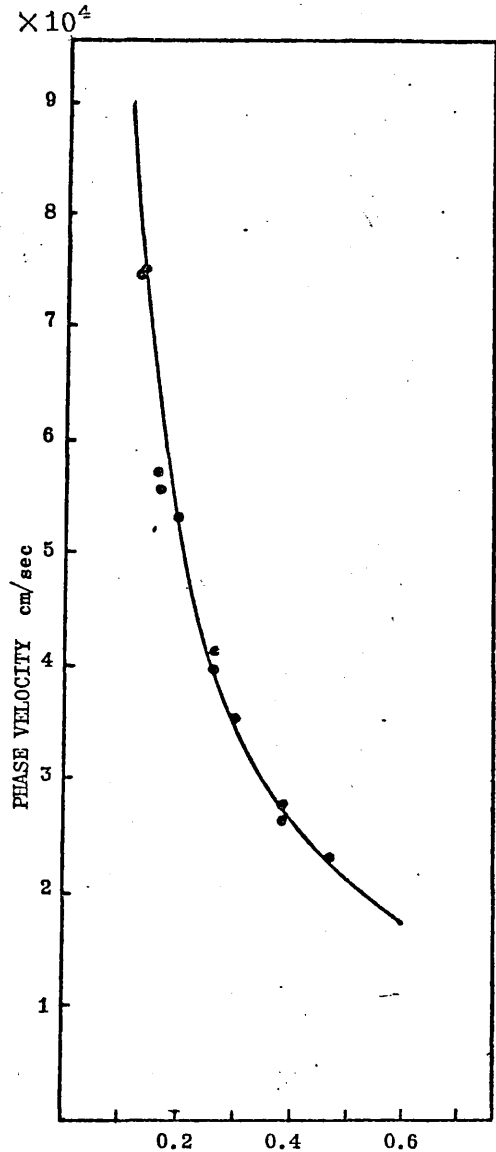


Fig.4.7 Phase velocity against pressure
 o o Experimental
 — Ion drift velocity $\times 7/4$

velocity is proportional to E_0/p_0 , which is a characteristic of striations.

The expressions for ω and k derived by Tsendin, section 2.6.1, give a similar pressure dependence for the phase velocity:

$$\frac{\omega}{k} \approx \text{const. } b_p V^* \sqrt{T_e} \propto \frac{E_0}{p_0} \quad \dots (4.8)$$

since the pressure dependence of T_e is less than that of b_p .

The calculated values of ω and k at 0.3 torr, $T_e = 3$ eV, $E \approx 1.5$ V/cm, $a = 0.85$ cm⁻¹ and $b_p = 1.2 \times 10^3$ cm/sec at 1 torr, are according to Tsendin's theory, equal to

$$\begin{aligned} \omega &= 1.88 \times 10^4 \text{ rad/sec} \\ k &= 0.8 \text{ cm}^{-1} \end{aligned}$$

whereas Pekarek's theory gives

$$\begin{aligned} \omega &= 7 \times 10^4 \text{ rad/sec} \\ k &= 2 \text{ cm}^{-1} \\ \varphi &= 7.65 \times 10^4 \text{ sec}^{-1} \end{aligned}$$

The experimental values were:

$$\begin{aligned} \omega &= 2.5 \times 10^4 \text{ rad/sec} \\ k &= 0.7 \text{ cm}^{-1} \end{aligned}$$

Tsendin's theory is in reasonable agreement, while Pekarek's values are too large. As noted in the review chapter, Pekarek's theory remains qualitatively correct even when considering argon. To obtain quantitative agreement the constants in the equations must be modified. Assuming that Pekarek's theory gives ω and k three times too large, then the adjustment of the constants in equations, will give a corrected $\varphi(k)$ of 3.4×10^4 sec⁻¹. Translating this temporal amplification into a spatial amplification is achieved using

$$\alpha = \frac{\varphi(k)}{\frac{\partial \omega}{\partial k}} = \frac{3.4 \times 10^4}{2.0 \times 10^4} = 1.7 \text{ cm}^{-1}$$

Although only a rough estimate, the large value of α indicates that self-excited waves will grow rapidly as they travel in the discharge.

In the computed example given earlier, a value of $\alpha = 0.01 \text{ cm}^{-1}$ was obtained which seems at variance with the previous statement. However, as the next section will show, this latter α was a measure of the amplitude variation once the nonlinear growth had been fully stabilised to give a constant or diminishing amplitude. Amplitude measurements made using the pick-up coil at the head of the positive column when the travelling wave was growing, gave a value of $\alpha \sim 0.3 \text{ cm}^{-1}$.

4.2.7 Nonlinear Nature of the Travelling Waves

For the pressures used in the experimental investigation, the Pupp limit is of the order of amperes. Since the currents used were of the order of tens or hundreds of milliamperes, well away from the Pupp limit, the linear theory is likely to be inadequate, and nonlinear theories must be used⁽¹⁸⁾.

Indeed, the presence of harmonics of the fundamental wave implies that the waves are nonlinear: when nonlinear terms are retained in the equations describing ionization waves, harmonic frequencies are obtained.

According to the results of Garscadden's stability analysis⁽⁴⁾ of the simplified equations of Pekarek, the discharge should be absolutely unstable for the backward waves in the argon discharge.

As will be seen, in the absence of other waves, the ionization waves of frequency range (b) had a uniform velocity and the frequency spectrum, even with the interactions present, consisted of a discrete line spectrum rather than a broad continuous spectrum. Referring to Grabec's work, section 2.8.4, the above observations imply that the energy losses due to inelastic collisions were sufficient to fully stabilise the nonlinear growth before the 'explosive' instability set in.

It may be concluded that the waves are nonlinear, absolute instabilities of a backward wave nature which are stabilized by energy losses.

4.3 LINEAR INTERACTIONS: SYNCHRONOUS OSCILLATIONS

The variation of space-time diagrams of the synchronous oscillations with current is shown in Fig.4.8. It can be seen that in some cases the amplitude of the synchronous oscillations is larger than the amplitude of the striations.[≡] With increasing current the synchronous oscillations are damped away.

Since standing wave patterns were obtained for each harmonic of the travelling wave, the synchronous oscillations must have had frequency components at the harmonic frequencies. As with the striations, the presence of harmonics implies that the oscillations were nonlinear.

It is known that striations can perturb the anode region and produce oscillations in voltage of the discharge as a whole at the same frequency as the striations⁽¹⁸⁾. The occurrence of these synchronous oscillations may be explained with reference to the work of Krejci, Chapter II.

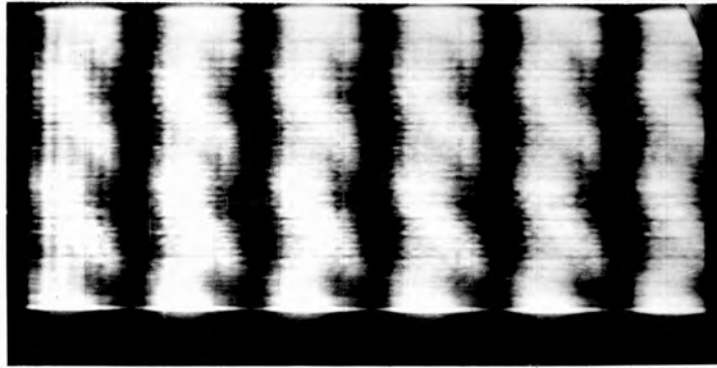
Using the values for argon of $b_p = 3.75 \times 10^3$ cm/sec, $U_i = 15.7$ V, then at 0.3 torr and 60 mA with $E \sim 1.5$ V/cm, $l = 107$ cm to correspond with the present experimental conditions, the resonant frequency from equation (2.33) is of the order of 1 KHz. So, the frequency of the striations is near to the resonant frequency for synchronous oscillations.

In the present case, the perturbation is provided by the striations and so on the right-hand side of equation (2.32) can be added a source term which for simplicity is written as $A e^{i\Omega t}$, where Ω is the frequency of the striations and A is the amplitude of the forcing term dependent in some way upon the amplitude of the striation, to give:

$$\frac{d^2\mathbf{U}}{dt^2} + 2\beta \frac{d\mathbf{U}}{dt} + \omega^2\mathbf{U} = \frac{I}{C} A e^{i\Omega t}, \quad \dots (4.9)$$

[≡] Shown by the destructive interference fig 4.8a.

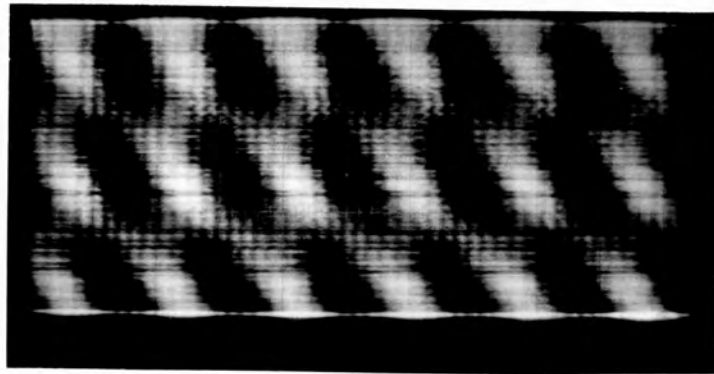
4 cm]



40 mA

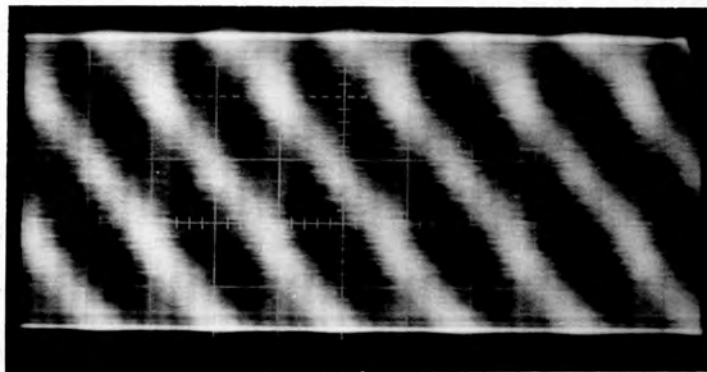
(a)

0.2 msec



57 mA

(b)



120 mA

Anode

(c)

Cathode

Time

Fig.4.8

Space-time display of coil signal. Pressure 0.3 torr

which gives

$$U = \frac{I}{C} \frac{A e^{i\Omega t}}{(\omega^2 - \Omega^2) + 2\beta\Omega i}$$

$$|U| = \frac{AI}{C} \frac{1}{\sqrt{(\omega^2 - \Omega^2)^2 + (4\beta^2 \Omega^2)}} \quad \dots (4.10)$$

From the variation of the amplitude of the photomultiplier signal of the fundamental mode with current, Fig.4.4, it can be seen that, since the travelling wave component is larger than the component due to the synchronous oscillation, the amplitude of the light intensity due to the striations increase linearly with current.

It is assumed that the forcing term is dependent on the amplitude of the striations and so increases with current. In addition the striation frequency Ω increases linearly with current, Fig.4.2, as does β , whilst ω increases as the square root. So the dependence of A , β , ω , Ω on the current, I , may be written most simply as $A = A_0 I$, $\omega = \omega_0 \sqrt{I}$, $\Omega = I\Omega_0$, $\beta = \beta_0 I$. This gives the following expression for $|U|$,

$$|U| = \frac{A_0}{C} \frac{1}{\sqrt{4\beta_0^2 \Omega_0^2 + (\Omega_0^2 - \frac{\omega_0^2}{I})^2}} \quad \dots (4.11)$$

Since Ω is greater than ω from the theoretical value of ω and the experimental values of Ω , as the current increases $|U|$ will decrease to a constant value.

At the higher currents the synchronous oscillations are not seen even though the striations are present to provide the driving force, and the theory predicts the existence of the oscillations. This implies that the coupling of the striations with the anode region to produce the oscillations, is more complicated than the naive assumption made above that the voltage perturbation is proportional to the striation amplitude. Indeed as will be seen in section 4.5 and Chapter V, when the discharge voltage is modulated at the striation frequency, it is possible, by adjusting the

discharge current, to change from a state where synchronous oscillations are generated to one where these oscillations are damped out, and yet the moving striations are modulated to produce a standing wave pattern.

4.4 LINEAR INTERACTIONS: CHARACTERISTICS OF THE WAVES IN FREQUENCY RANGE (a)

At pressures greater than about 0.2 torr, oscillations with frequencies in the range 400-900 Hz were seen for certain values of discharge current in addition to the striations described in section 4.2. Harmonic frequencies of the fundamental frequency were sometimes seen, but the more usual situation was that they were absent.

These waves were detected by both the coil and photomultiplier but the photomultiplier signal proved the more sensitive to axial variations in amplitude. Two examples of the wave patterns are shown in Fig.4.9. The amplitude variation exhibits maxima and minima at positions along the axis.

The frequency of the waves is near to the resonant frequency of the discharge and so the variation in amplitude may be due to linear interference of a synchronous oscillation and a travelling wave. Unfortunately since the larger frequency waves existed simultaneously and were of larger amplitude, they triggered the oscilloscope and so it was not possible to obtain a space-time display of the waves in frequency range (a).

The change in separation between maxima for different frequencies was observed by artificially exciting waves, as will be described in Chapter V. The results show that these waves have a backward nature.

So far, the linear interference of waves, has been observed and interpreted. Under some circumstances, however, effects consistent with nonlinear phenomena were observed and these will be described in the next section.

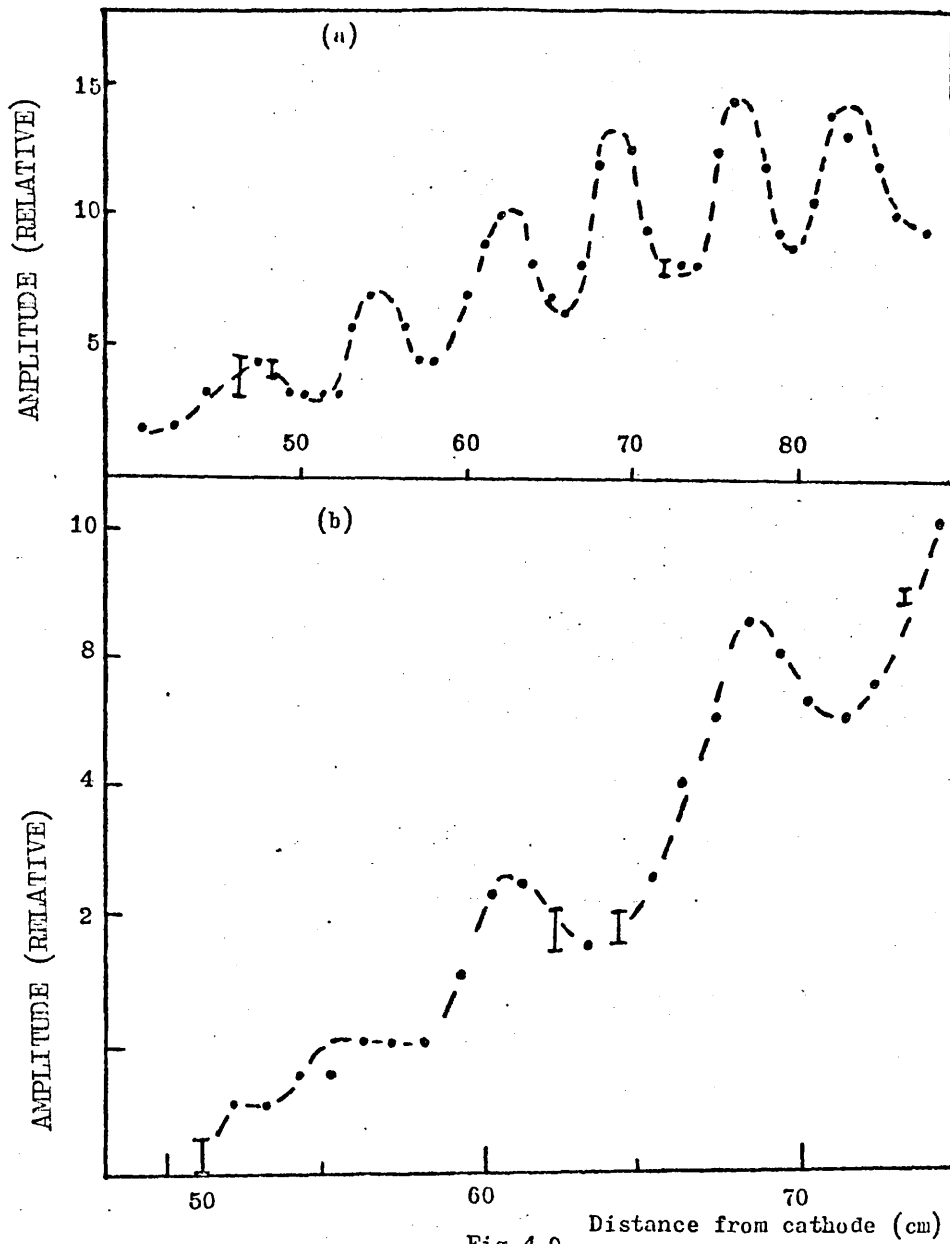


Fig.4.9

Wave patterns of waves in frequency range (a). Photomultiplier signal
 (a) Frequency: 510 Hz; Pressure: 0.37 torr; Current: 81 mA
 (b) Frequency: 630 Hz; Pressure: 0.45 torr; Current: 70 mA

4.5 NONLINEAR INTERACTIONS OF THE SELF-EXCITED WAVES

4.5.1 Apparent Stationary Striations in Frequency Range (b)

Stationary striations, $\omega = 0$, are seen in argon usually only near the cathode end of the positive column, and are heavily damped towards the anode with the result that only one or two can be seen⁽⁴¹⁾. However, in the present experiments it was possible to see, under some circumstances, what appeared to the naked-eye to be stationary striations extending much further into the positive column. Microdensitometer traces of photographs taken of the positive column, representing the time averaged light intensity, are shown for different currents in Fig.4.10 for a pressure of 0.15 torr. The two peaks at the cathode end are the stationary ($\omega = 0$) striations seen for all values of current. As the current was increased above 40 mA, apparent 'stationary' striations were observed as is shown from the presence of peaks in the patterns. From the traces the distance between the light intensity was maxima about the same as the distance between maxima on the standing wave pattern of the first harmonic, which was similar in appearance to the patterns described in section 4.2. From the photomultiplier signal it was found that the apparent stationary pattern was oscillating at the same frequencies as the striations in frequency range (b). Under these circumstances the standing wave patterns for the fundamental and harmonics, had the same separation in maxima, Fig.4.11. Furthermore, the apparent 'stationary' striations sometimes exhibited a binary structure as can be seen from long exposure pictures of the discharge. Fig.4.12, which show the discharge as it appeared to the naked-eye.

The binary structure was best seen at currents between 20-40 mA. At the low currents the striations were highly convex towards the cathode. The **region** of light intensity at the head (cathode side) of each doublet was longer than the second **region**, and the distance separating the maxima



Posn. Discharge Support

Fig. 4.10

Microdensitometer trace of pictures of the discharge
 Pressure 0.15 torr. Current: (a) 39 mA; (b) 43 mA; (c) 56 mA; (d) 69 mA

5 cm

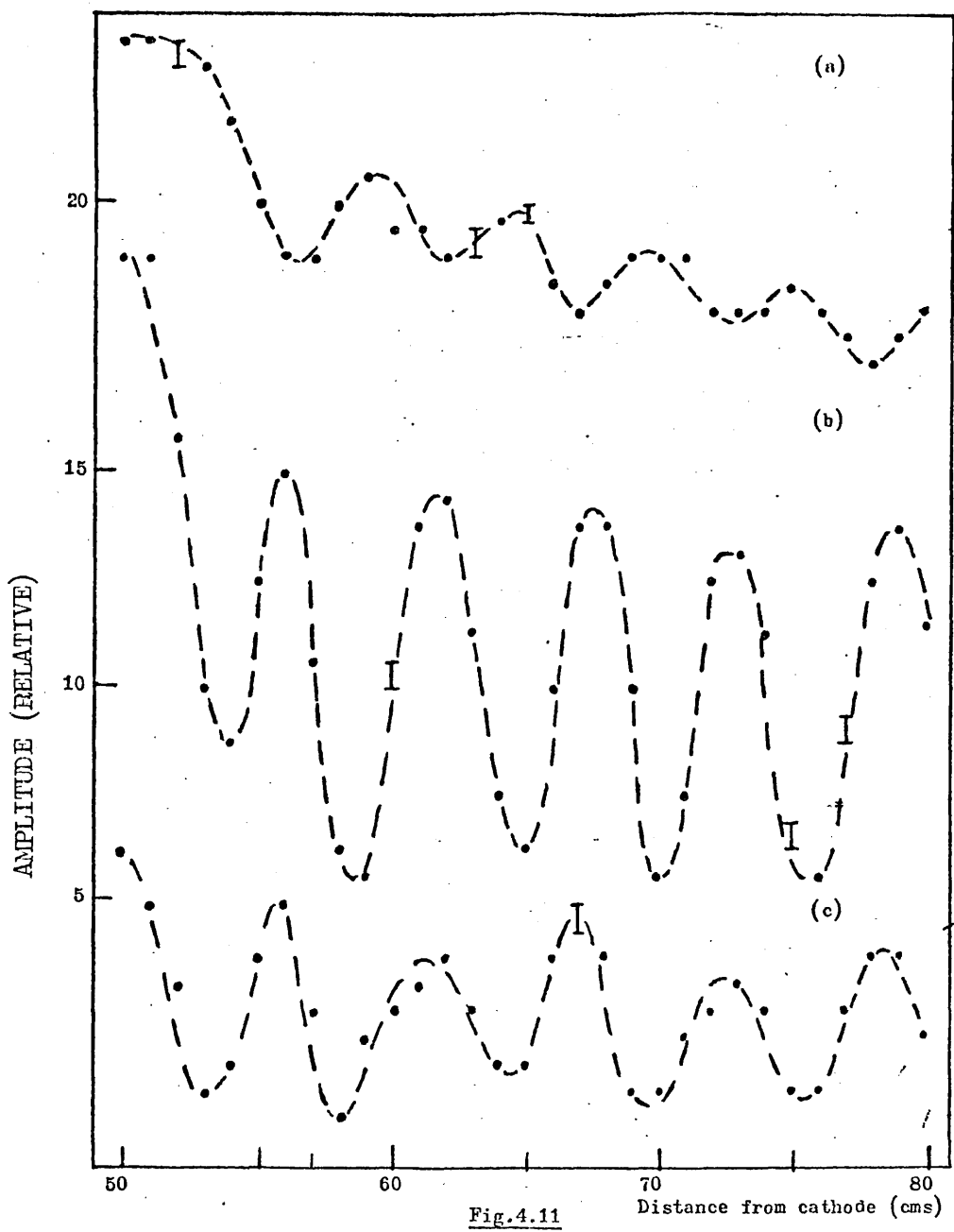


Fig.4.11

Standing wave patterns when 'apparent stationary' striations were seen.
 Photomultiplier signal. Pressure: 0.25 torr; Current: 50 mA;
 (a) Fundamental: 2.25 KHz; (b) First Harmonic; (c) Second Harmonic



a



b



c



d

Fig.4.12

Pictures of the discharge for exposure time of a few seconds.

- (a) Pressure: 0.3 torr; Current: 35 mA
- (b,c) Pressure: 0.33 torr; Current: 42 mA
- (d) Pressure: 0.37 torr; Current: 38 mA

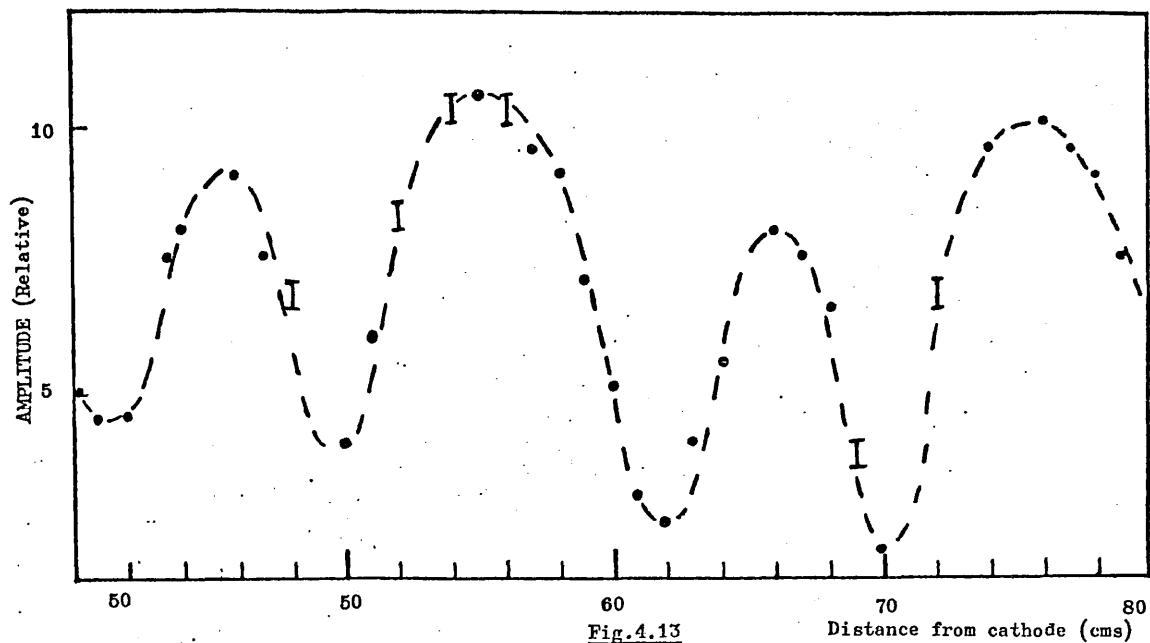


Fig.4.13
 Wave pattern for a doublet structure, photomultiplier signal,
 First harmonic: 5.2 KHz; Current: 34.5 mA; Pressure 0.23 torr

within each doublet was smaller than the distance between the head of one doublet and the head of the adjacent doublet. An example of the standing-pattern for a binary structure is shown in Fig.4.13 as measured with the photomultiplier. Generally the patterns obtained were not so symmetrical but appeared as in Fig.4.14. With increasing current the doublet structure disappeared, since the separation in light intensity maxima were equal, as in Fig.4.15, and the 'stationary' striations were more difficult to see. For the particular pressure of 0.25 torr, the column appeared homogeneous to the eye for currents above 100 mA although the standing pattern was still detected, Fig.4.16.

Linear interference⁽⁶⁶⁾ would not give a time averaged pattern as found here since the integral

$$\int_t^{t+\tau} \sin (wt - kx) = 0 \quad \dots (4.12)$$

The phenomenon is essentially nonlinear and will be discussed in Chapters V and VI.

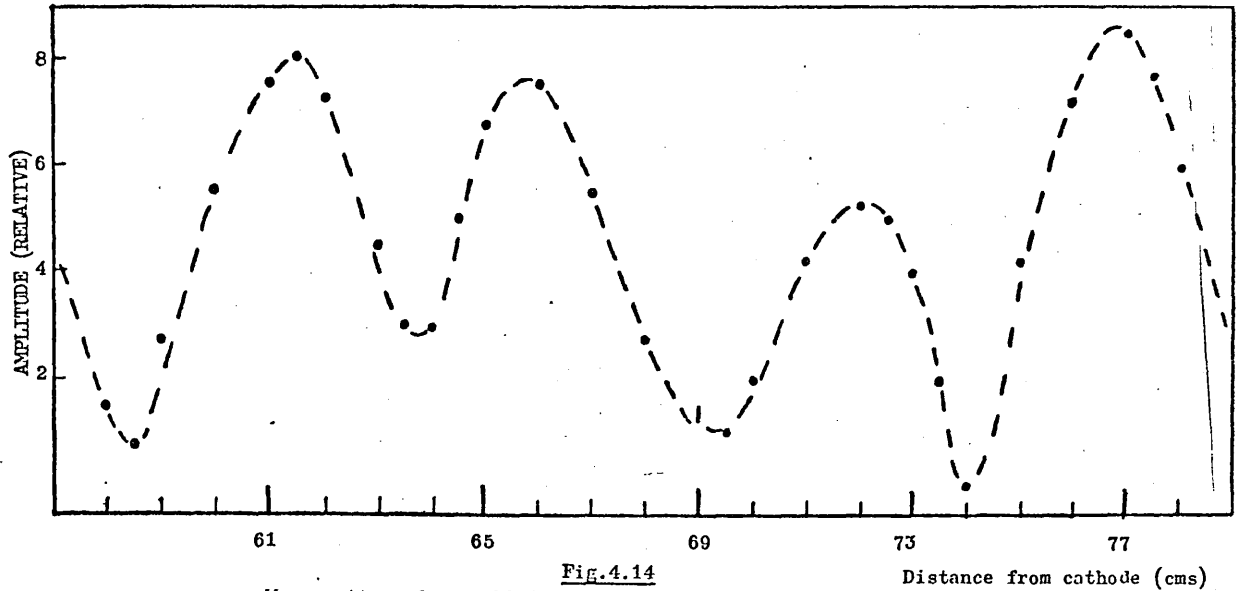


Fig.4.14 Distance from cathode (cms)
 Wave pattern for doublet structure; photomultiplier signal,
 First harmonic: 3.3 KHz; Current: 20 mA; Pressure: 0.37 torr

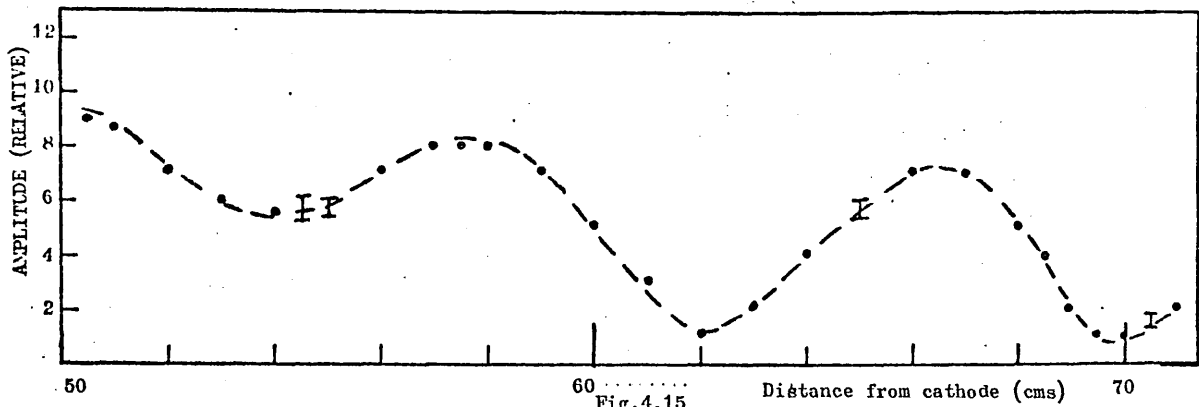


Fig.4.15 Distance from cathode (cms)
 Wave pattern for first harmonic; photomultiplier signal;
 Frequency: 4.3 KHz; Current: 95 mA; Pressure: 0.25 torr

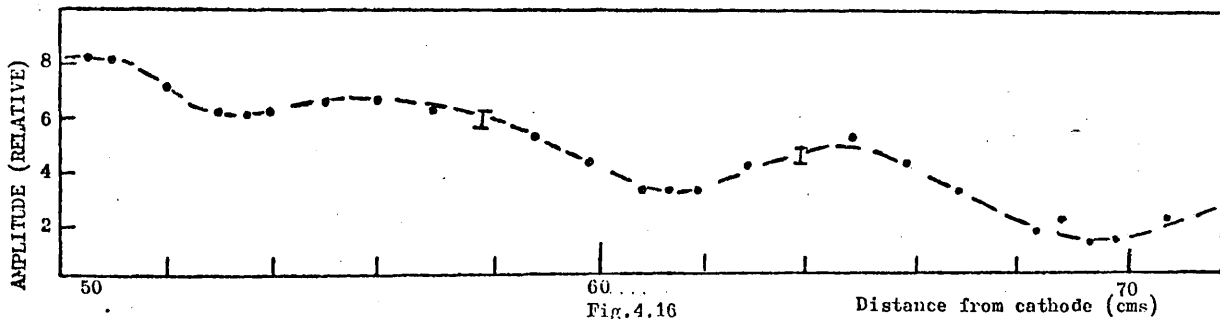


Fig.4.16 Distance from cathode (cms)
 Wave pattern for first harmonic; photomultiplier signal,
 Frequency: 7.2 KHz; Current: 180 mA; Pressure: 0.25 torr

4.5.2 Mode-Coupling between the Waves in the Frequency Ranges (a) and (b)

The change in the frequency spectrum which accompanied the occurrence of the oscillations in the frequency ranges (a) and (b) can be traced from Fig.4.17. At a current of 160 mA the familiar spectra of the self-excited striations with a fundamental frequency of 2.5 KHz with harmonics was seen, Fig.4.17(a). As the current was reduced, an oscillation at about 630 Hz was seen together with satellite frequencies around the first and second harmonics of the 2.5 KHz wave. Upon further reduction of the current, the amplitude of the 630 Hz oscillation increased as did the amplitude of the satellites, whilst the amplitude of the 2.5 KHz oscillation and its harmonics decreased.

In Fig.4.17(d) the frequency of the striations is a few hundred Hertz less than in Fig.4.17(a). This was due to the fundamental frequency decreasing with current. The fundamental frequency, 2.3 KHz has satellites on either side, whilst the first and second harmonics, 4.6 KHz and 6.9 KHz appeared to have only the lower satellites, although with finer resolution the upper satellite could be detected above the noise. Within the accuracy of the spectrum analyser, the separation of these satellites from the basic frequencies is approximately equal to 630 Hz. Although in general both satellites could be detected on either side of the fundamental and harmonics, the occurrence of the lower satellite was more pronounced than that of the upper satellite and its axial variation in amplitude could be measured.

The time-averaged patterns of the amplitude still showed spatial modulation at the satellite as well as the fundamental and harmonic frequencies; some examples are given below. Wave patterns are shown in Fig.4.18 for the fundamental, first harmonic, second harmonic and third harmonic and their lower satellites when the distance between consecutive

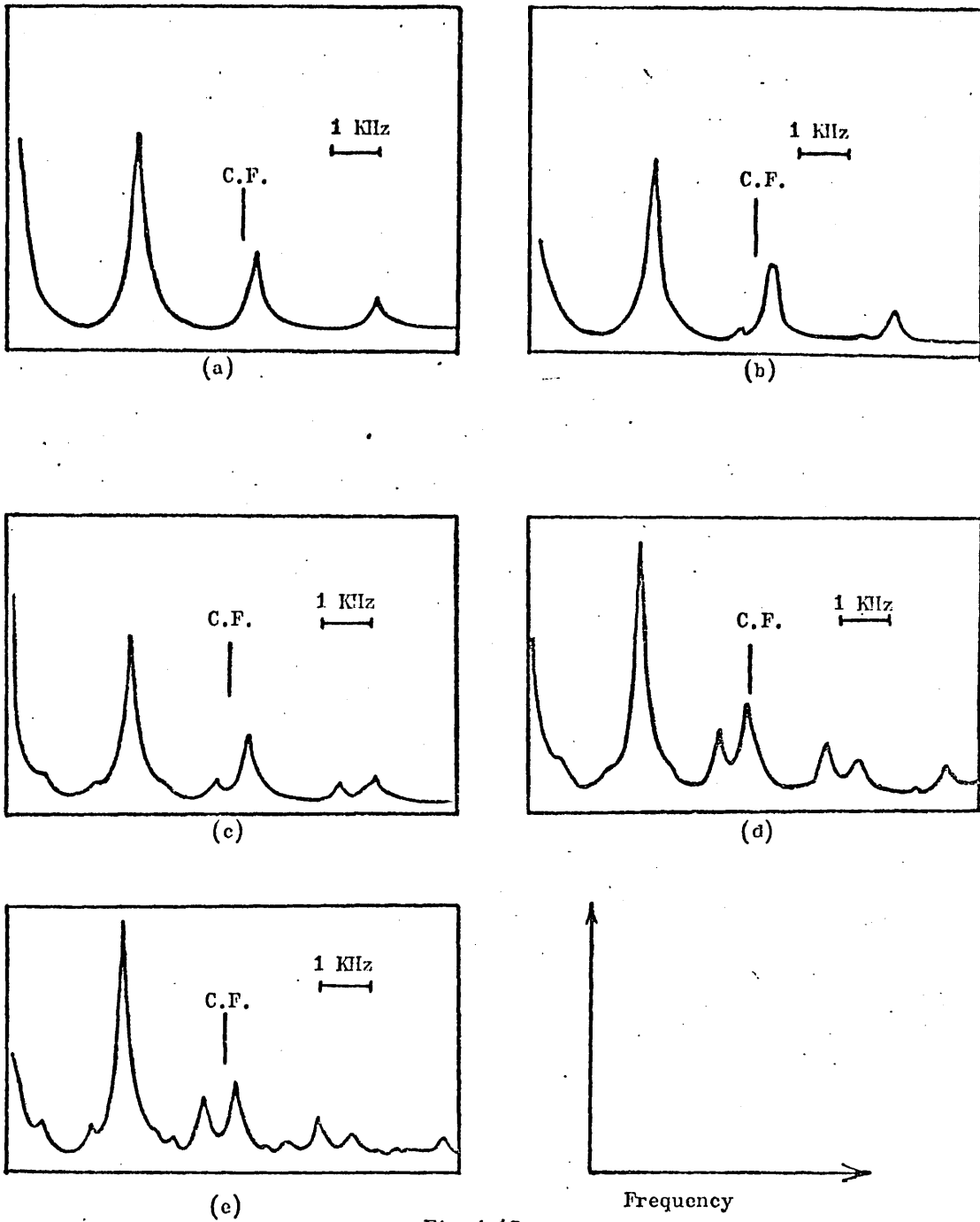


Fig. 4.17

Spectrum of mode coupling of self-excited waves. Coil signal.
 Pressure: 0.42 torr; C.F: Centre frequency = 5 KHz;
 (a) 160 mA, (b) 150 mA, (c) 142 mA, (d) 130 mA, (e) 120 mA.
 Frequency dispersion is the same in all figures;
 In (d),(e) amplitude scale decreased by factor of 2.

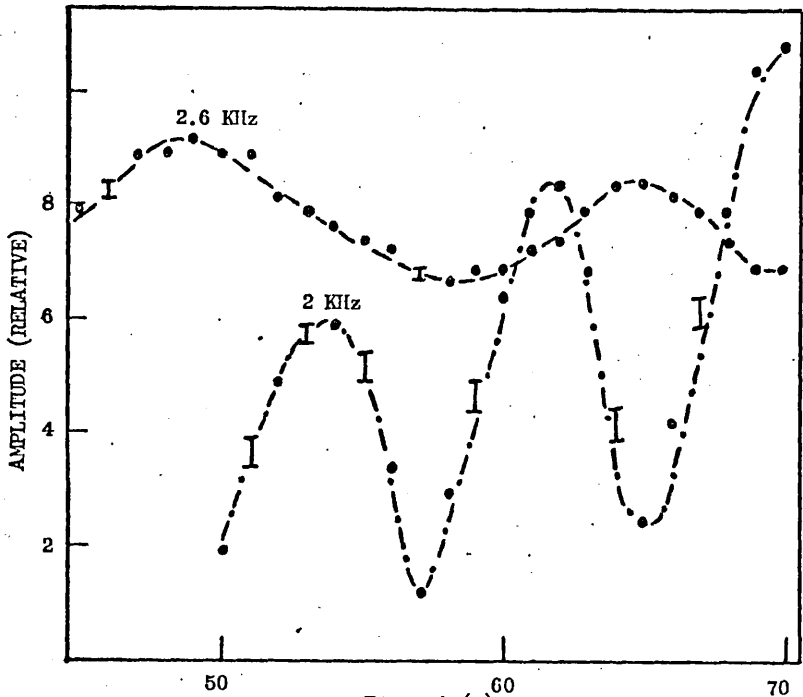


Fig.4.18(a) Distance from cathode (cms)
 Coil signal: wave patterns for fundamental,
 2.6 KHz, and lower satellite, 2.1 KHz
 Pressure: 0.3 torr; Current: 100 mA
 $\lambda_D \approx 5.5$ cms

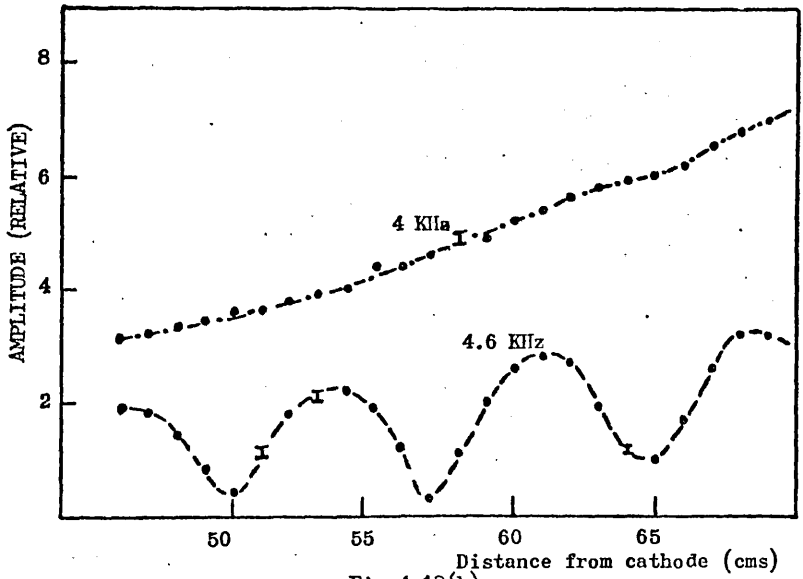


Fig.4.18(b)
 Coil signal: wave patterns for first harmonic
 4.6 KHz and lower satellite 4 KHz
 Pressure = 0.34 torr; Current = 110 mA
 $\lambda_D \approx 7.5$ cm

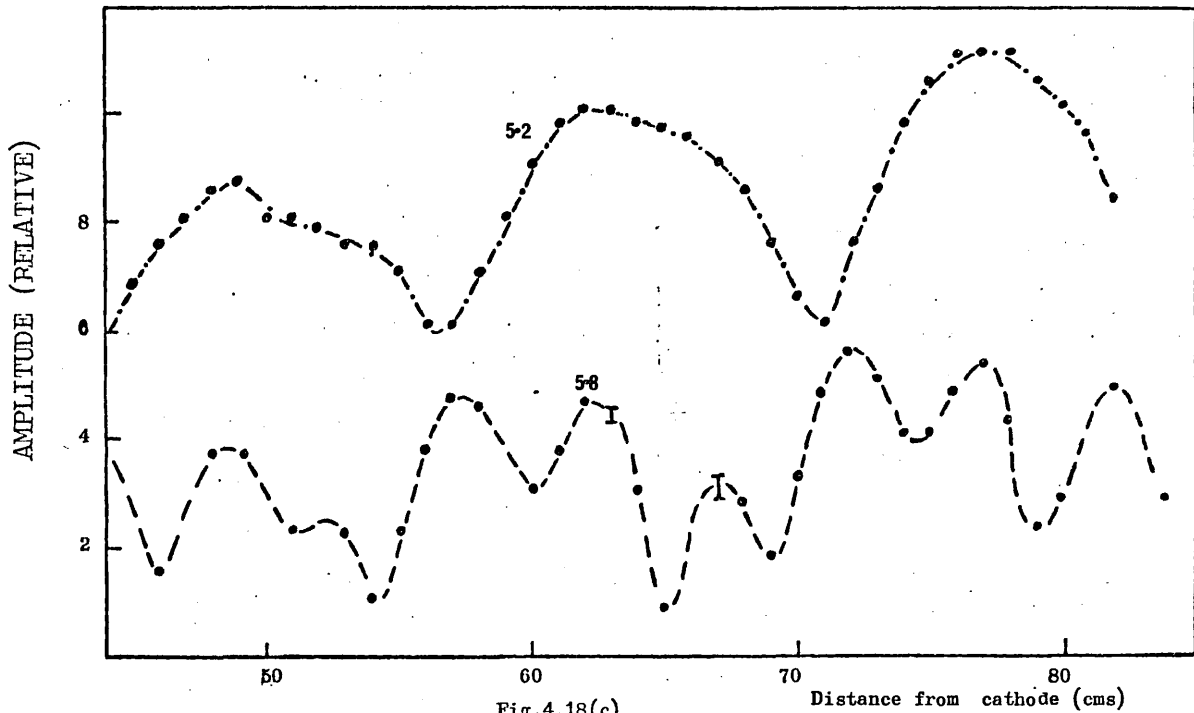


Fig.4.18(c)
 Coil signal: wave patterns for second harmonic
 5.8 KHz and lower satellite 5.2 KHz
 Pressure: 0.3 torr; Current: 80 mA;
 $\lambda_D \approx 8$ cms

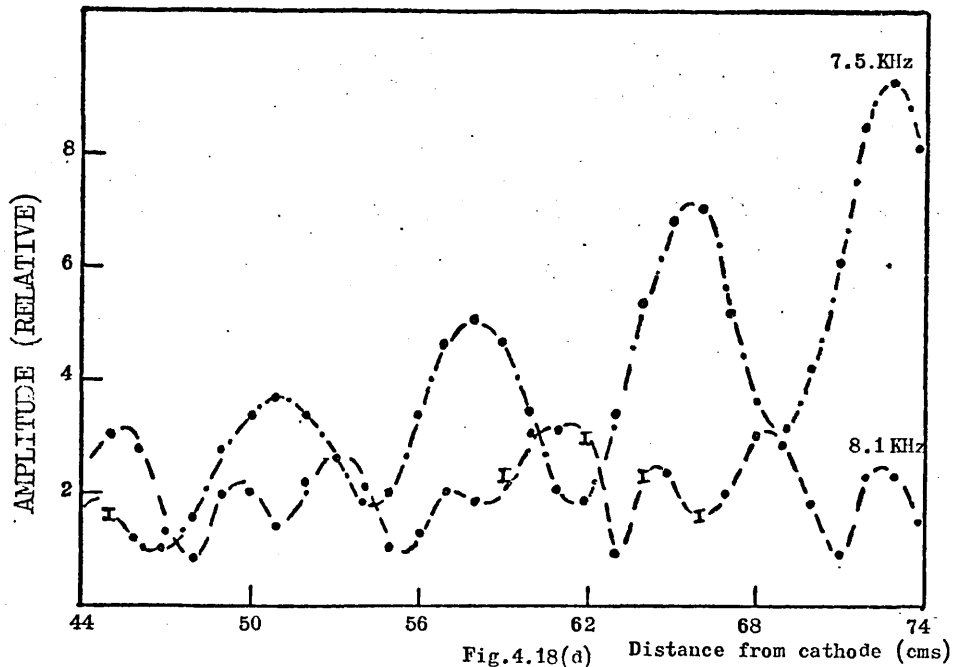


Fig.4.18(a)
 Coil signal: wave pattern for third harmonic
 8.1 KHz and lower satellite 7.5 KHz
 Pressure: 0.33 torr; Current: 100 mA;
 $\lambda_D \approx 7-8$ cms

maxima, λ_D , for the lower frequency 600 Hz wave was in the range 5.5 to 8 cms depending upon the particular current and pressure.

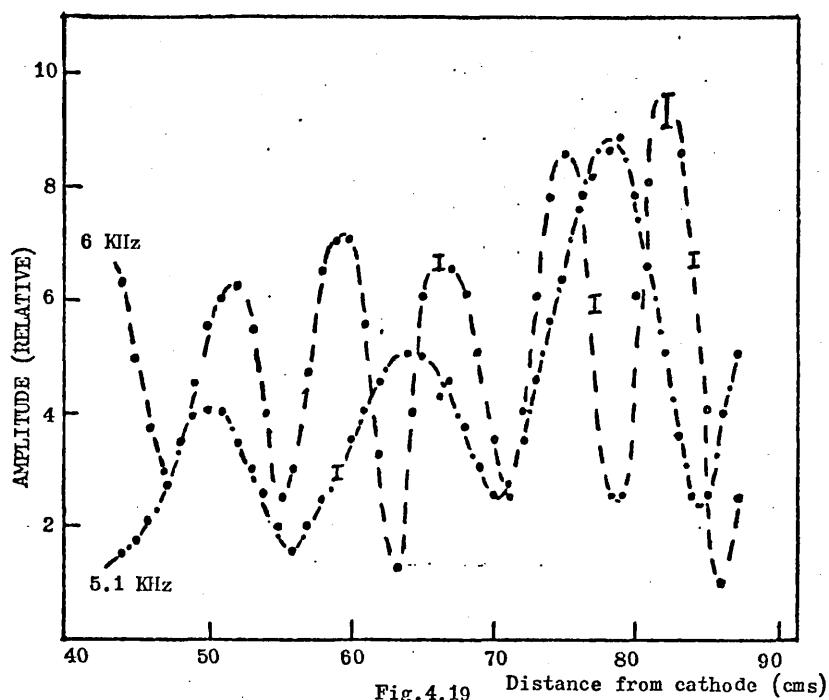


Fig. 4.19
Coil signal: wave pattern for first harmonic, 6 KHz;
and lower satellite, 5.1 KHz. Pressure: 0.25 torr
current: 100 mA; $\lambda_D \approx 14$ cms

The wave patterns obtained for the second harmonic and lower satellite when the frequency of the lower frequency wave was 900 Hz and λ_D was equal to 14-15 cm are shown in Fig. 4.19.

For the wave patterns above, the spacing, λ , between adjacent maxima for the satellite frequencies is related to the spacing, λ_s , between the maxima of the appropriate frequency component of the striations and the spacing λ_D defined above, by

$$\left| \frac{1}{\lambda} \right| = \left| \frac{1}{\lambda_s} - \frac{1}{\lambda_D} \right| \quad \dots (4.13)$$

The observed frequency spectrum and amplitude variations may be represented as the sum of:

$$\sum_{n=1}^{n=N} \sin \left[(n\omega_0 - \Omega)t \right] + \sin \left[(n\omega_0 - \Omega)t - (nk_0 - k)x \right] \quad \dots (4.14)$$

where ω_0, k_0 are the fundamental frequency and wavenumber of the waves

in frequency range (b), and Ω, k are the corresponding values for the waves in frequency range (a). The occurrence of satellite frequencies implies that the phenomenon observed is different from simple linear interference of travelling waves observed by several workers⁽⁷⁴⁾. The origin of the present form of interaction will be discussed in Chapters VI, VII and VIII.

4.5.3 Characteristics of the Waves in Frequency Range (c) and their Coupling with the Lower Frequency Waves

(a) Mode coupling

For currents of 130 mA or less, in the absence of the 400 to 900 Hz oscillations, mode coupling between the striations, frequency range (b), and the waves with frequencies of tens of kilohertz, range (c), was detected. The coupling between a 32 KHz wave and the striations is shown in Fig.4.20. The satellites are separated by the frequencies of the striations.

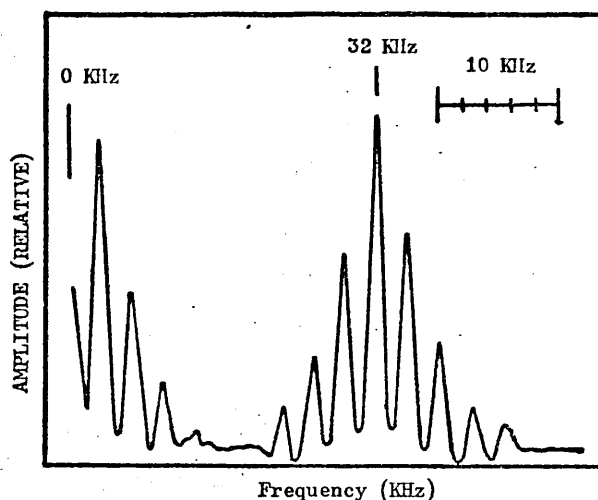


Fig.4.20

Coil signal: spectrum of 32 KHz wave and satellites
Pressure: 0.3 torr; Current: 120 mA

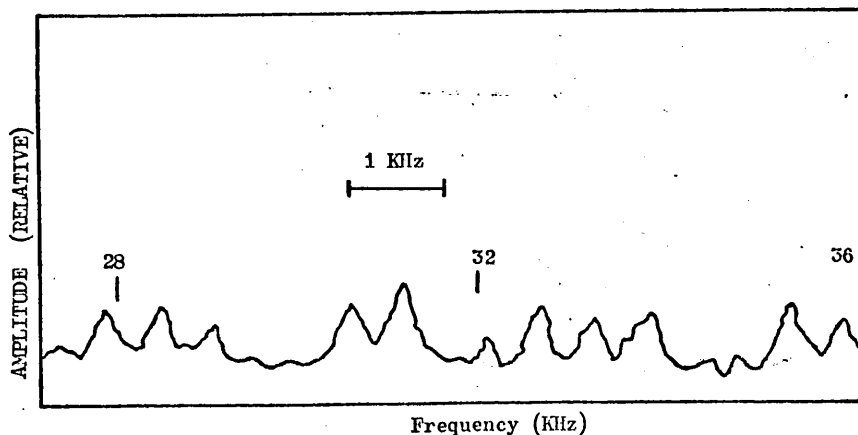


Fig.4.21

Coil signal: spectrum of 32 KHz wave and satellite
Pressure: 0.3 torr; Current: 62 mA

When a 600 Hz wave was present, coupling was observed between the waves for all three frequency ranges to produce the complex display, Fig. 4.21. For such a case the discharge was unstable and a steady spectrum analyser display could not be obtained.

Figure 4.22 shows the wave patterns obtained when the striations were mode-coupled with a 35 KHz wave. The 35KHz oscillation exhibits no standing wave pattern but resembles the noise power diagram obtained for a backward wave in neon. The satellites have standing wave patterns in which the distance between adjacent maxima for a given satellite is approximately equal to the distance for the corresponding striation in the kilohertz range. In this case, the coupling may be represented by

$$\left[\sum_{n=1}^{n=N} \cos \left[(\omega \pm n\omega_0)t - kx \right] + \cos \left[(\omega \pm n\omega_0)t - kx \mp nk_0 x \right] \right] \quad \dots (4.15)$$

where ω_0, k_0 have the same meanings as before, and ω, k now describe the wave in frequency range (c).

The change in the spectrum of the striations of frequency range (b) and the tens of kilohertz waves can be seen in Fig.4.23. At low currents the spectrum is noisy, the striations with frequencies in the range 1.5- 5.0 KHz cannot be seen, but there is a broad peak around 23 KHz. As the current is increased a discrete spectrum appears consisting of the fundamental and harmonics of the 2.5 KHz striation, the oscillation of 23 KHz and harmonics, and the satellites resulting from the coupling of the two oscillations. As the current is increased further, the amplitude of the satellite frequencies decrease as does the harmonics of the 23 KHz wave, until at 74 mA, although the 2.5 KHz striations are present and of large amplitude, mode coupling cannot be seen; there is only a broad peak around 23 KHz of diminished amplitude. No oscillations other than the

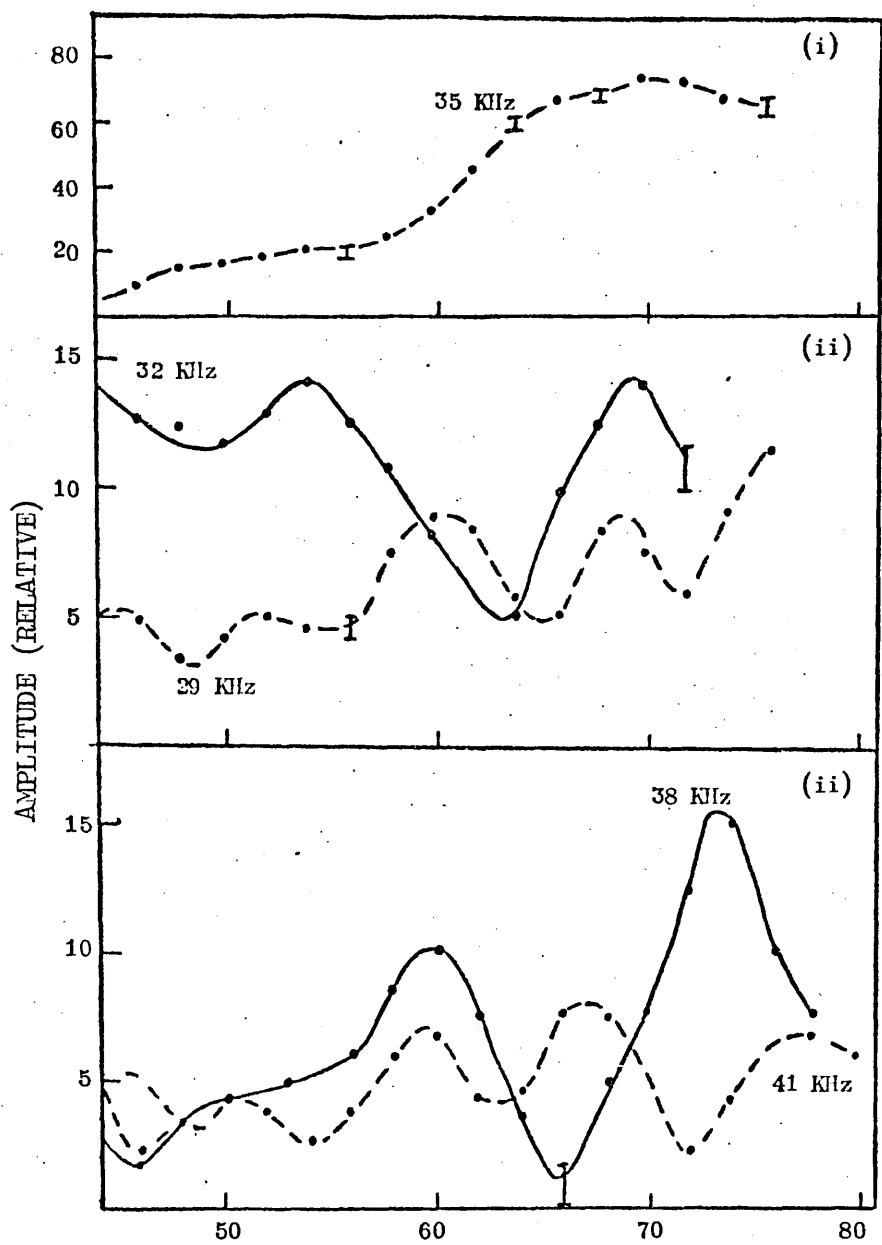


Fig.4.22 Distance from cathode (cms)

Coil signal: wave pattern for (i) 35 KHz wave;
 (ii) Lower satellites 29 KHz, 32 KHz;
 (iii) Upper satellites 38 KHz, 41 KHz;
 Pressure: 0.15 torr; Current: 64 mA

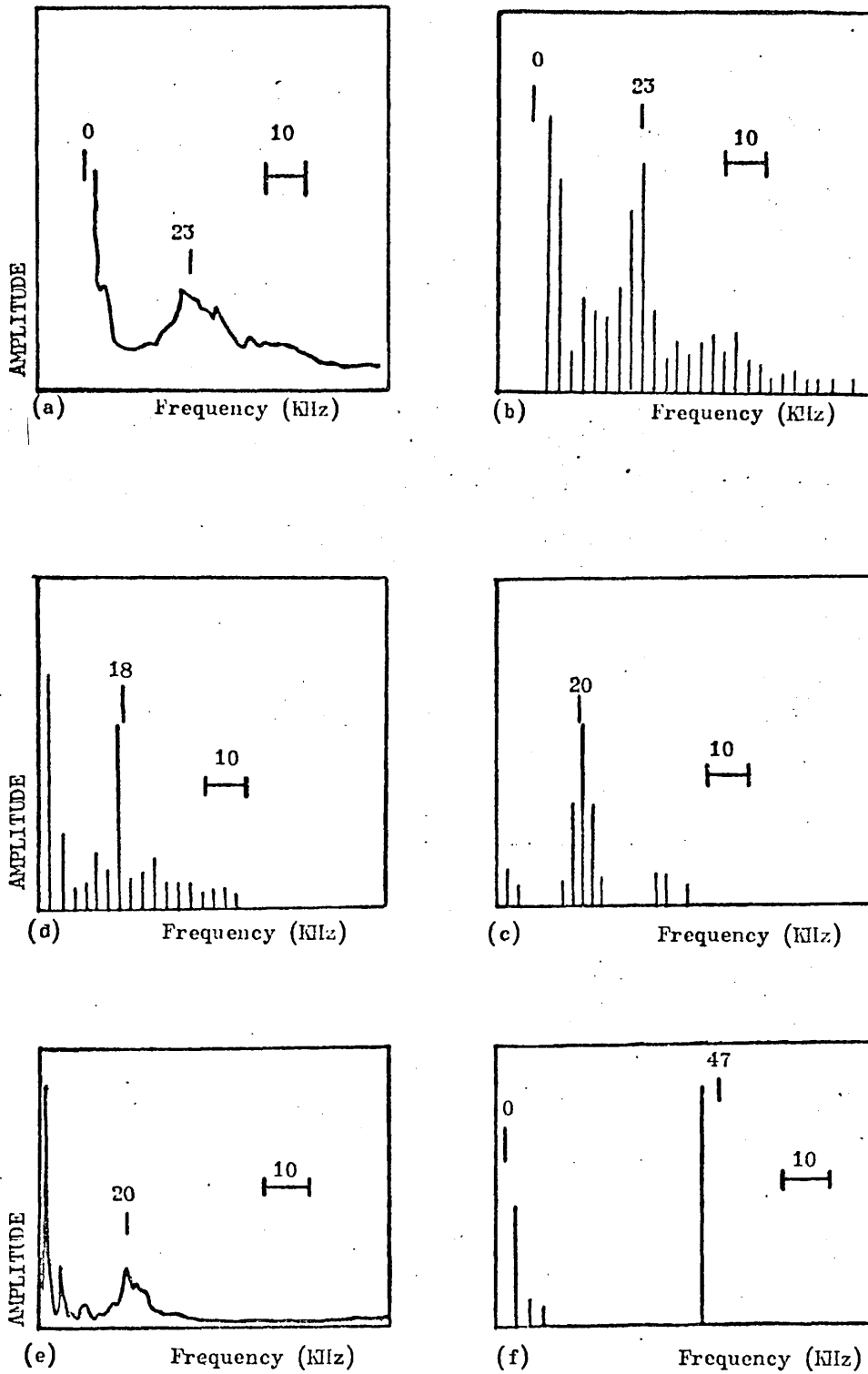


Fig.4.23

Coil signal: spectra for mode coupling between waves
 in frequency ranges (b) and (c)
 Pressure: 0.37 torr. Current: (a) 15 mA, (b) 29 mA,
 (c) 38 mA, (d) 48 mA, (e) 74 mA, (f) 180 mA

striations are seen upon increasing the current further, until at about 180 mA an oscillation with a fundamental frequency of approximately 45 KHz and an amplitude comparable to that of the 23 KHz wave at 29 mA_λ **was seen.** Mode-coupling is not seen at this current.

Using better frequency resolution it could be seen, Fig.4.24, that the change in 'shape' of the amplitude versus frequency spectrum with current for the mode-coupled waves of ranges (b) and (c) was due to a frequency jumping of the higher frequency wave with current.

The asymmetry, Fig.4.23, of the satellite either side of the 23 KHz wave can be traced back to the amplitude versus distance curves, Fig.4.22, where it can be seen that the wave patterns for the upper and lower harmonics show a similar variation, but a lag of one pattern relative to the other exists.

The mode-coupling of the waves appears to depend on the nature of the waves in range (c) and their variation with current. Their nonlinear or linear behaviour can be linked with the occurrence or absence of mode coupling.

(b) Characteristics of the waves in frequency range (c)

Two examples of the amplitude variation, as measured by the coil, with axial position are shown in Fig.4.25. The amplitude variation can be divided into two regions (three for some cases) in accordance with similar observations in neon discharges⁽¹⁴⁾. In the first region the amplitude is constant or grows linearly. The second region is characterized by an exponential growth of the amplitude which increases until reaching the third region where the amplitude saturates then remaining constant, or decreasing with further distance from the cathode.

At a pressure of 0.37 torr and a current of 35 mA, a wave of frequency ~ 20 KHz was detected. Fortunately at this frequency the wave-

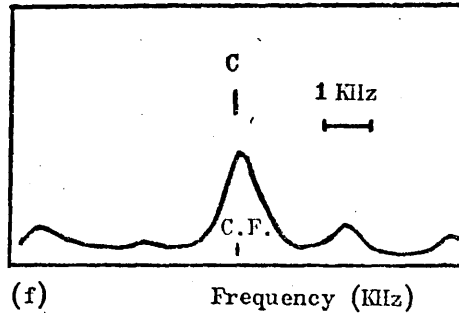
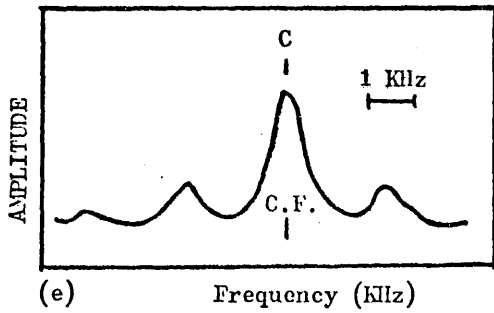
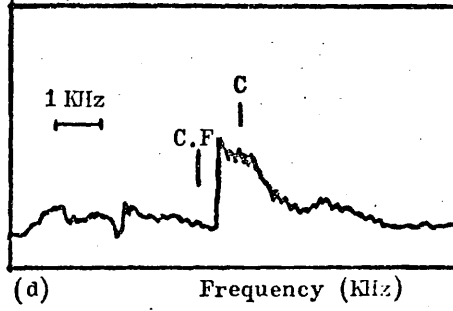
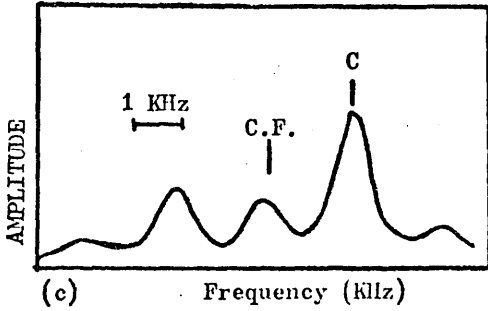
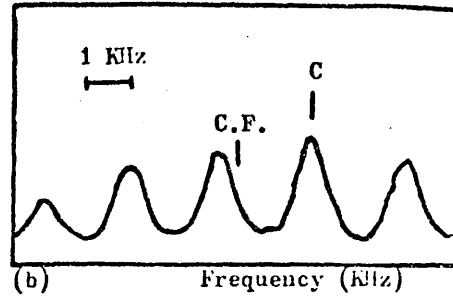
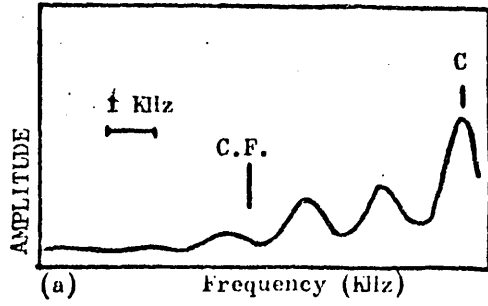


Fig.4.24

Change of frequency of wave in frequency range, C (marked C) and its satellites. Pressure: 0.28 torr; C.F.: Centre frequency 32 kHz; Frequency dispersion the same for all figures;
 Current: (a) 32.5 mA, (b) 42 mA, (c) 48 mA, (d) 60 mA, (e) 73 mA, (f) 91 mA.



Fig.4.25

Coil signal: amplitude variation of waves in frequency range, C:
 (i) Frequency: 20 KHz; Pressure: 0.37 torr; Current: 48 mA
 (ii) Frequency: 23.4 KHz; Pressure: 0.35 torr; Current: 45 mA

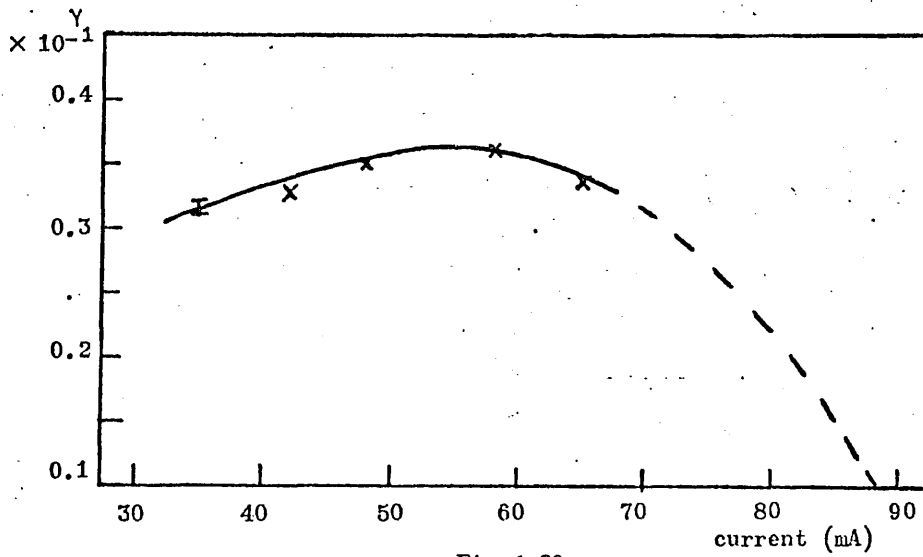


Fig.4.26

Variation of the spatial amplification coefficient γ with current

length could be measured by triggering the oscilloscope with the lower frequency waves. The wavelength at a current of 60 mA was of the order of 1 cm. On other occasions this could not be done since the frequencies were not integrally related.

As the discharge current was increased up to 87 mA, the frequency of the wave remained approximately constant but the amplification coefficient γ for the growth region reached a maximum and then decreased, Fig. 4.26, similar to the variation for backward waves in argon as observed by Sato⁽²⁷⁾. The mode-coupling followed the variation already mentioned. The characteristics, described above, of the waves in frequency range (c) suggest that they are backward waves.

(c) Variation of the frequency spectrum

The change in the frequency spectrum, Fig.4.23, can be related to the change in the amplification coefficient γ with current. The measurements of Fig.4.26 do not correspond to the spectra of Fig.4.23, but the same trend was seen. At the larger currents when γ is small the frequency is centred around 20 KHz, the amplitude is relatively small and although not sharp, the spectrum is not noisy. As γ increases with decreasing current, the spectrum becomes sharp and consists of the 20 KHz wave and the satellites due to mode-coupling; the amplitude of the satellite increases. As the current is decreased further and γ passes through a value corresponding to saturation, the amplitude of the 20 KHz oscillation decreases and the line spectrum is replaced by a noisy spectrum, but still centred around 20 KHz.

4.6 CONCLUSION

In the absence of mode-coupling it has been seen that the presence of the synchronous oscillations gave rise to a standing wave pattern due to linear interference. Consequently it was not essential to use a direct space-time display to obtain information on the moving striations.

Similarly, for the interactions between the waves, it will be seen that because of the presence of the synchronous oscillations, which gave rise to standing wave patterns, it was possible to interpret the nonlinear interactions between the travelling waves without recourse to space-time pictures.

CHAPTER V

EXPERIMENTAL RESULTS OBTAINED WHEN AN EXTERNAL ALTERNATING VOLTAGE WAS APPLIED ACROSS THE DISCHARGE

5.1 INTRODUCTION

Waves could be excited in the d.c. argon discharge by applying a sinusoidal voltage to the anode. Since the frequency and amplitude of these waves could be controlled by merely adjusting the controls of the voltage generator it was possible, in some cases, to easily reproduce and accentuate the linear and nonlinear effects described in the previous chapter, for self excited waves.

The method of superimposing an external voltage has been described in Chapter III. When the frequency of the applied voltage was within 10% of the frequency of the self-excited striations, the frequency of the latter was pulled towards the applied frequency with the result that the striations oscillated at this new frequency. If the value of the applied frequency was sufficiently far away from that of the self-excited striations, then moving striations and synchronous oscillations at both frequencies were seen.

5.2 WAVES EXCITED IN FREQUENCY RANGE (b)

The standing wave patterns obtained from the coil signal for various values of applied voltage and a frequency of 5.2 KHz are shown in Fig.5.1. In addition to the waves at this applied frequency, self-excited waves at a frequency of 3.4 KHz were present in the discharge; their standing wave pattern is included in Fig.5.1 for comparison.

It can be seen that as the applied voltage was increased, well defined maxima and minima appeared in the standing-wave patterns. For an applied voltage of 16V peak-to-peak, the wave patterns for the externally excited wave and the self-excited wave are similar. Using the same

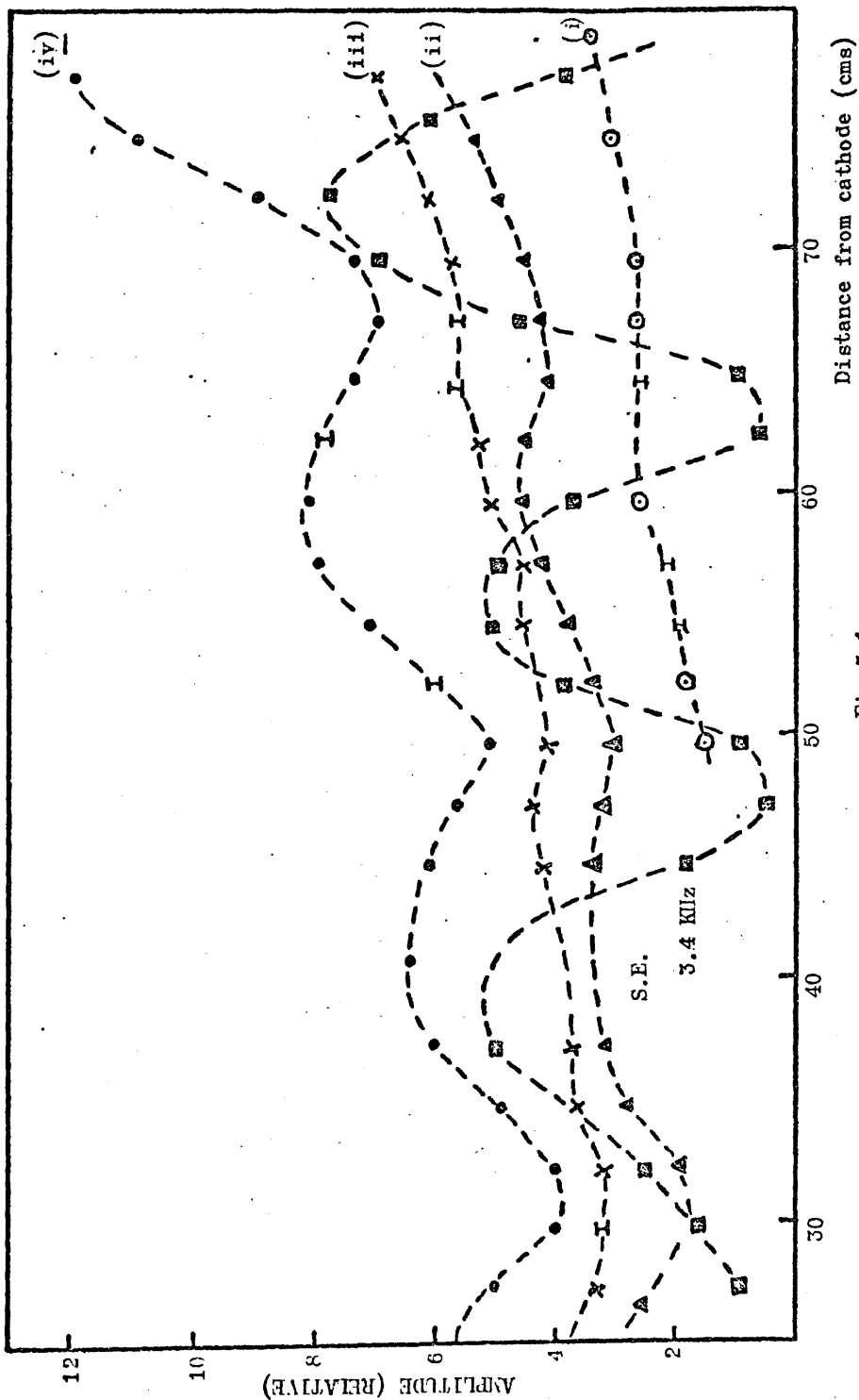


Fig. 5.1

Coil signal: wave patterns for artificial excitation
 Pressure: 0.37 torr; Current: 110 mA; Applied Frequency: 5.2 KHz.
 Applied voltage (p. to p.): (i) 2V; (ii) 4V; (iii) 10V; (iv) 16V
 S.E.: Self-excited striation frequency: 3.4 KHz.

considerations as in Chapter IV, it can be seen that the synchronous oscillations had a larger amplitude than the travelling wave for all values of exciting voltage.

The separation between maxima for the self-excited and artificially excited waves when the applied voltage was 22V peak-to-peak, was found to be approximately 20 cm and 16 cm for the 5.2 KHz and 3.4 KHz waves respectively, indicating that the wave **length** increases with frequency - the characteristic of backward waves.

5.3 CHARACTERISTICS OF THE WAVES EXCITED IN THE LOWER FREQUENCY RANGE (a)

The waves were excited when self excited waves in the same frequency range (a) were present. The variation in the separation of maxima for different applied frequencies is shown in Fig.5.2.

As derived in Chapter IV, the resonant frequency for synchronous oscillations is of the order of 1 KHz. The standing wave patterns may be due to linear interference of a synchronous oscillation and a travelling wave, or caused by velocity modulation of the travelling wave at the same frequency as the wave itself. For the latter case the velocity modulation would result in harmonics of the fundamental frequency of the wave appearing on the spectrum analyser display. These harmonics were not seen experimentally which seems to rule out this interpretation. In any case, for both forms of interaction the spacing between amplitude maxima is equal to or proportional to the wavelength of the wave permitting a dispersion curve to be drawn, Fig.5.3. It can be seen that the waves have a backward characteristic since the wavelength increases with increasing frequency.

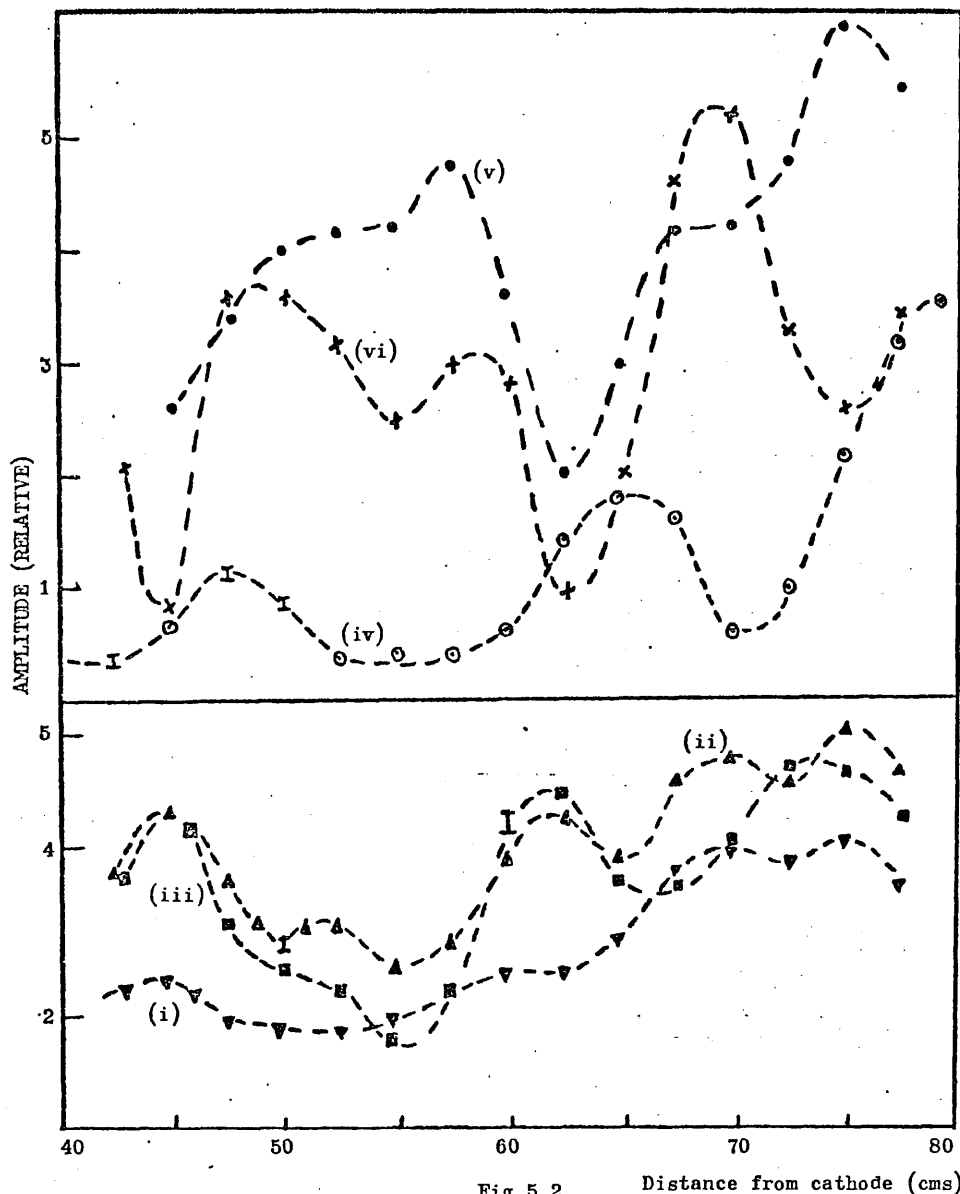


Fig.5.2 Photomultiplier signal: wave patterns of wave excited in frequency range (a). Pressure: 0.32 torr; Current: 110 mA
 Frequency: (i) 300 Hz; (ii) 400 Hz; (iii) 600 Hz;
 (iv) 800 Hz; (v) 1000 Hz; (vi) 1200 Hz

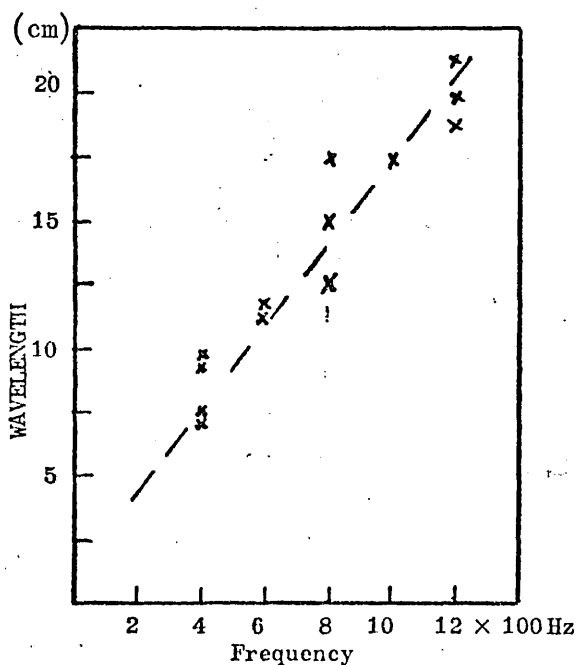


Fig.5.3 Dispersion curve derived from Fig.5.2 for waves in frequency range (a)

5.4 GENERATION OF 'APPARENT' STATIONARY STRIATIONS AND ACCOMPANYING EFFECTS

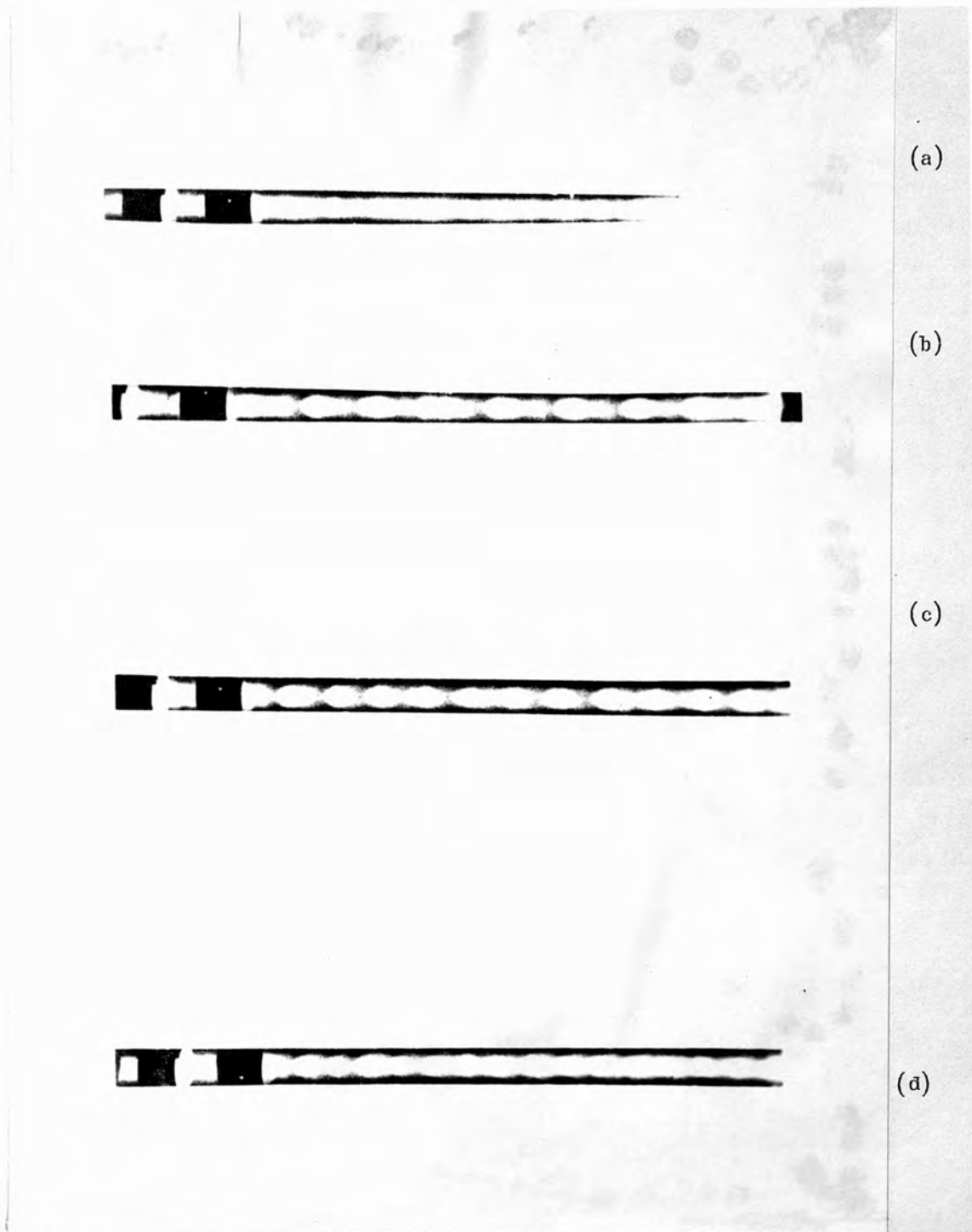
5.4.1 Observations


So far the linear interference, seen in Chapter IV, was reproduced. By suitably varying the discharge current and the exciting voltage, it was possible to change from linear to nonlinear effects as shown by the appearance of 'apparent' stationary striations. Such patterns could only be obtained for the values of current and applied frequency shown in each figure below. If the current or frequency were slightly changed then the stationary pattern would flicker, and with further change there was no longer any nonlinear interaction between the applied voltage and the striations, so the discharge appeared homogeneous.

The photographs of Fig.5.4 show 'apparent' stationary striations which were seen when the external sinusoidal voltage was applied at the fundamental and harmonic frequencies of the self-excited striations. For the fundamental frequency the 'apparent' stationary striations which were not very pronounced, were separated by a distance equal to the wavelength λ of the moving striations. When modulated at harmonics of the natural frequency (f) the spacings between the maxima were equal to λ/n when the modulating frequency was nf , $n = 1, 2, 3$, etc.

It can be seen in Fig.5.4(b) that when modulated at the first harmonic frequency, each 'apparent' stationary striation has a doublet structure: the head (cathode side) of the structure is followed by a less intense more diffuse region of shorter length.

The standing wave patterns as measured from the photomultiplier signal and spectrum analyser are shown in Fig.5.5, when the frequency of the applied voltage was equal to the first harmonic frequency of the waves. The spacing between maxima for each frequency component is equal to $\lambda/2$, the spacing expected for the first harmonic.



Cathode  5 cm

Anode

Fig. 5.4

The discharge as seen by eye: Photographs showing the variation in 'apparent' stationary striations with exciting frequency.

Pressure: 0.3 torr; Exciting voltage: 24 V; p.p: 84 mA;

- (a) Fundamental: 4.2 KHz; Current: 73 mA;
- (b) First harmonic: 6.9 KHz
- (c) Second harmonic: 10.6 KHz, 90 mA;
- (d) Third harmonic: 12.8 KHz, 83 mA

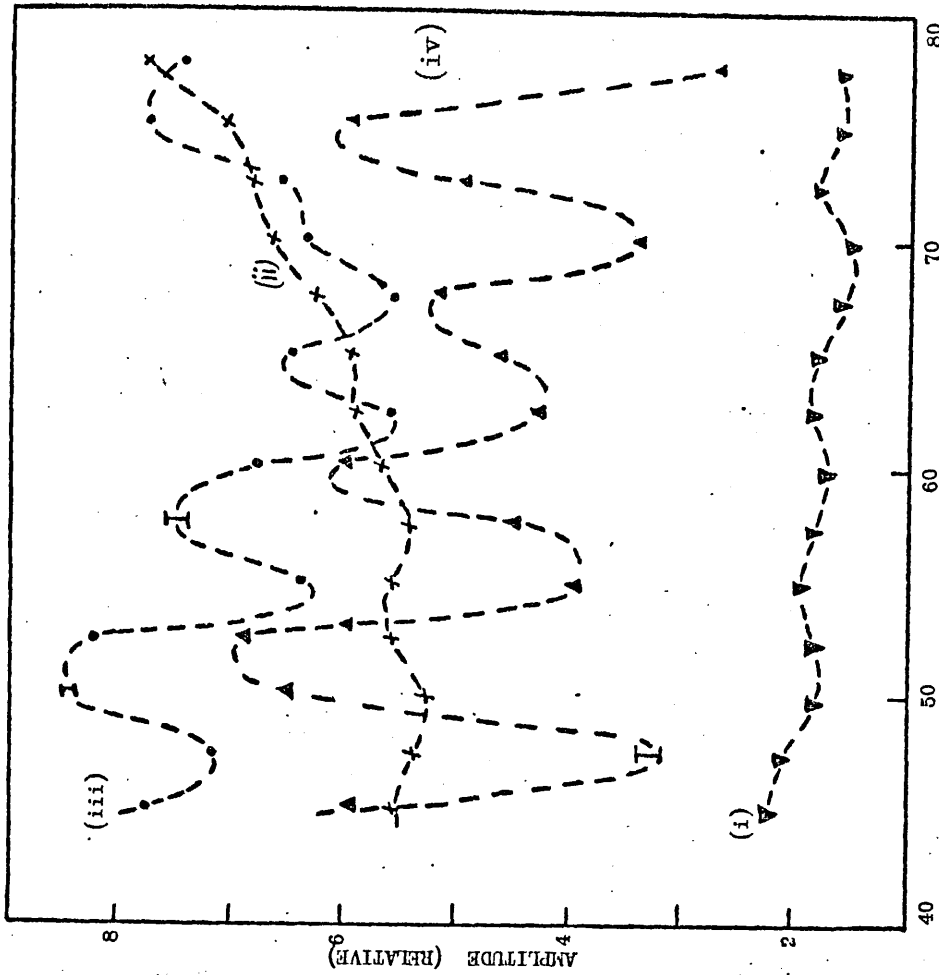


Fig.5.5

Photomultiplier signal: wave patterns when the applied frequency was equal to first harmonic frequency: 7.4 KHz.
 Pressure: 0.3 torr; Current 110 mA; Applied voltage 22V p.p.
 (i) Fundamental Frequency; (ii) First Harmonic;
 (iii) Second Harmonic

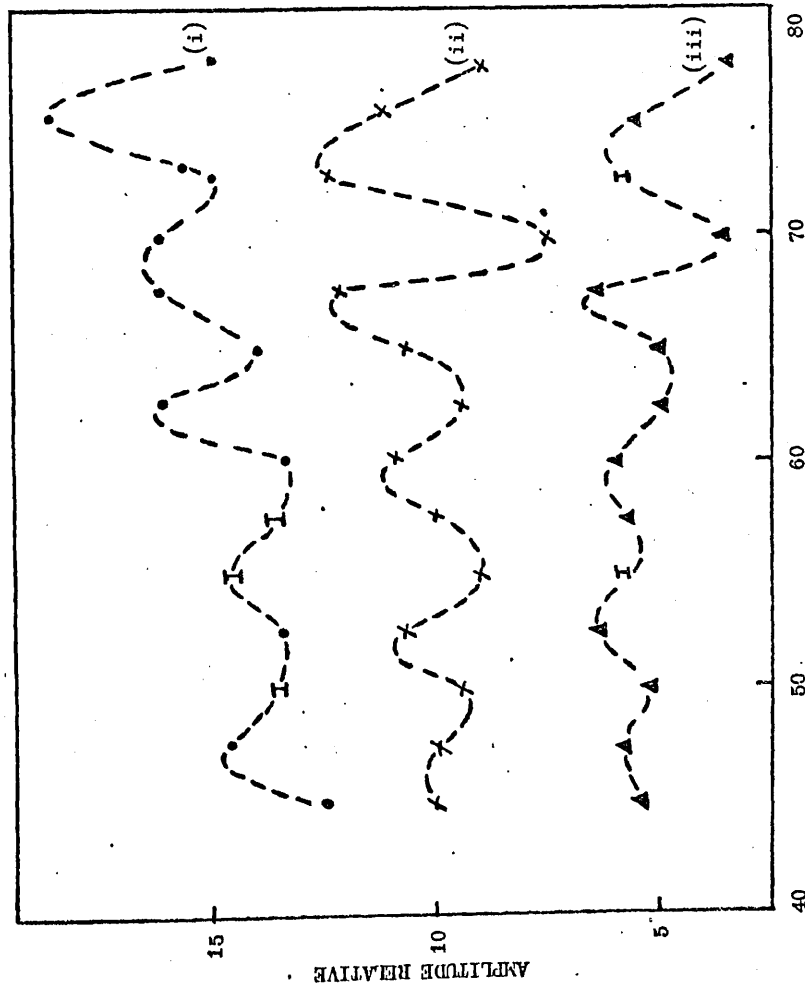


Fig.5.6

Wave patterns for coil and photomultiplier signals.
 Applied frequency at first harmonic: 7.4 KHz;
 Pressure: 0.3 torr; Current: 84 mA; Applied voltage: 24V (p.p.)
 (i) Fundamental coil; (ii) First harmonic coil
 (iii) Fundamental photomultiplier; (iv) First harmonic photomultiplier

The standing wave patterns for the coil and photomultiplier signals for an applied frequency equal to the first harmonic frequency of the striations, are compared in Fig.5.6. The coil signal has the same spacing between maxima as the photomultiplier signal but the difference between maximum and minimum values of amplitude is much smaller than for the photomultiplier signal. This is in contrast to the results for the linear interference where it was seen that the variation in the coil signal amplitude was much more pronounced than that for the photomultiplier signal.

5.4.2 Space Time Display

A space-time diagram, Fig.5.7, obtained when 'apparent' stationary striations, due to external modulation, were seen, reveals that for such conditions the velocity of the striations varies periodically. For Fig. 5.7(a), the discharge was modulated at the fundamental frequency, whilst for Fig.5.7(b), the frequency was equal to the first harmonic frequency. The applied voltage was larger than for the previous figures. For the fundamental frequency 'apparent' stationary striations were spaced $\lambda/2$ apart. Examination of the space-time pictures shows that the velocity is modulated at twice the fundamental frequency and may be represented by:

$$V = V_0 + \Delta \sin 2\omega t \quad \dots (5.1)$$

where V = modulated velocity,
 V_0 = value of the unmodulated velocity,
 Δ = constant,
 ω = angular frequency of the fundamental wave.

5.4.3 Interpretation

Since the waves are nonlinear and so have a non-sinusoidal waveform, the average of their **incremental** light intensity component is not necessarily zero, i.e.

$$I_{av} = \int_0^T f(x-Vt) dt \neq 0 \quad \dots (5.2)$$

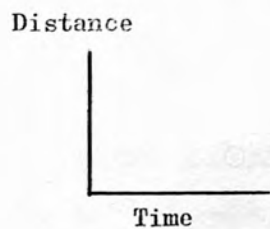
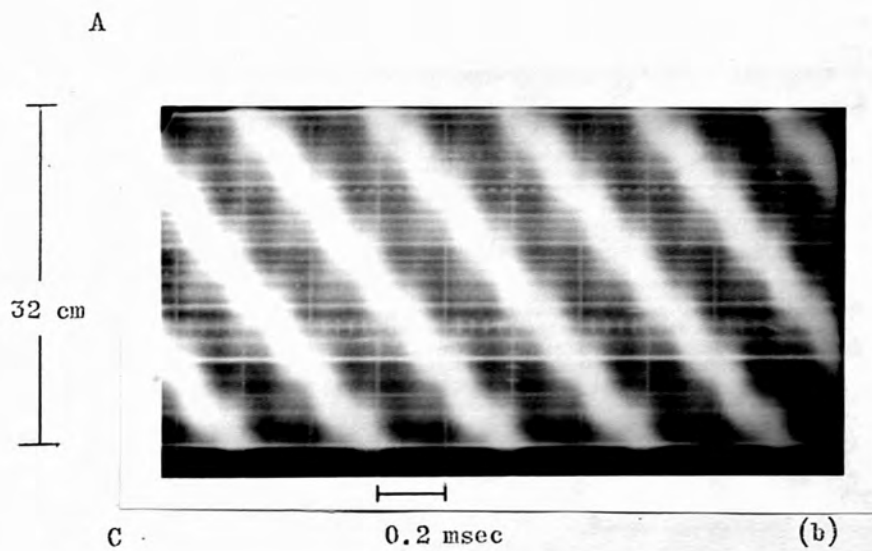
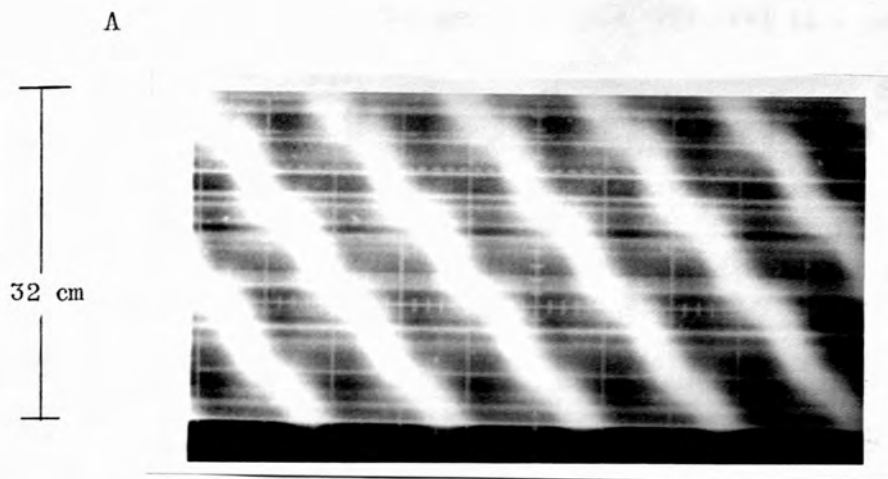


Fig.5.7
 Space-time display for photomultiplier signal. Pressure: 0.46 torr;
 Current: 92 mA; Applied voltage: 40V (p.p.); A: Anode; C: Cathode.
 (a) Modulated at fundamental frequency
 (b) Modulated at first harmonic frequency

where I_{av} is the average light intensity and $f(x-Vt)$ is a periodic function describing the wave. In the absence of any variation in velocity, I_{av} is the same, or increases uniformly, along the discharge tube, and the light intensity from the discharge appears uniform to the eye. With velocity modulation, I_{av} at those points where the striation slows down will be larger than at those points where the velocity has increased. If the velocity is modulated at the same frequency as the wave, those points of increased I_{av} will be spaced λ apart, and will appear as 'apparent' stationary striations.

Returning to Fig.5.6, the difference in the wave patterns for the coil and photomultiplier signals, as compared to the case of linear interference, may be explained. The light intensity variations since they are proportional to $\exp\frac{1}{\theta}$, where θ is the electron temperature, are more non-linear than the electric field changes and so their waveform is more non-sinusoidal as Fig.5.8 shows for the unmodulated discharge. Consequently when the velocity is modulated the variations in the average light intensity along the discharge will be greater than those for the average signal from the coil.

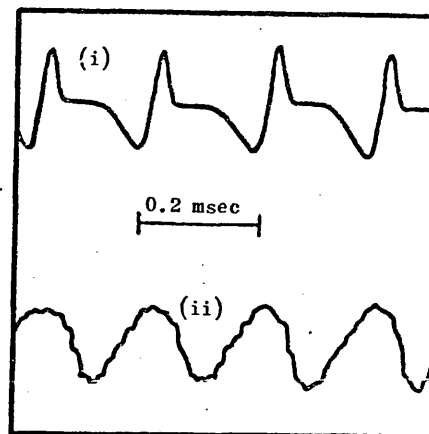


Fig.5.8
Oscilloscope traces of (i) photomultiplier signal and (ii) coil signal waveforms for the self-excited waves. Pressure: 0.2 torr; Current: 85 mA

5.4.4 Linear and Nonlinear Interactions

The above results show that by adjusting the current or frequency, it is possible to change from a state explicable in terms of linear interference between synchronous oscillations and travelling striations to a state where the synchronous oscillations are no longer excited, yet the travelling wave is modulated at the frequency of the applied voltage. In

the latter case the coupling of the external voltage to the striations may be via the anode spots - regions of intense ionization containing a net positive charge^(16,17).

Several authors^(16,67) have shown that the anode spots are linked with the movement of striations in the positive column and that the anode spot frequency can be a simple multiple of the striation frequency.

It is significant that although the synchronous oscillations are of large amplitude, no nonlinear interaction between them and the striations **was seen**. The mechanism by which the striations are coupled to the anode voltage fluctuations, appears to exclude the simultaneous generation of synchronous oscillations at the same frequency.

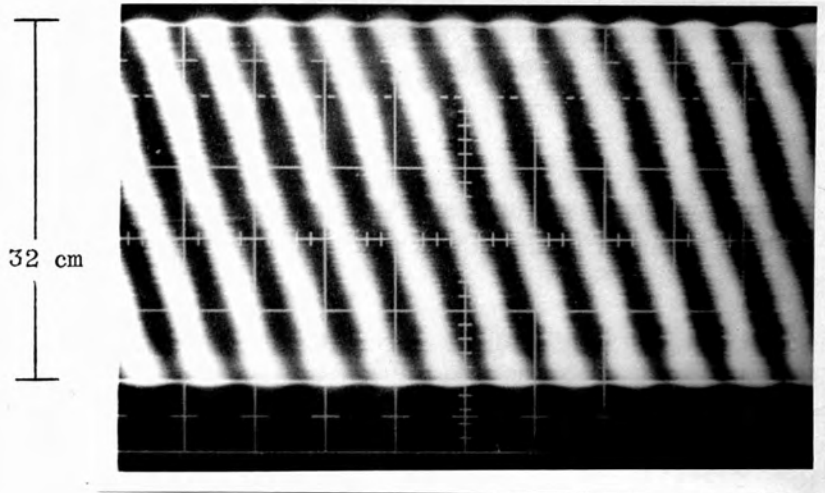
5.4.5 Self-Excited Waves

The 'apparent' stationary striations described in Chapter IV, when there was no externally applied modulating voltage, may be explained in terms of velocity modulation in the same way as described in the preceding sections. A space-time display, Fig.5.9 of the coil signal for a self excited wave shows velocity modulation. 'Apparent' stationary waves were seen 7 cm apart. The results of the artificial modulation suggest that the observed doublet structure arose because the striations were modulated at the first harmonic frequency rather than the fundamental frequency.

5.4.6 Comparison of the Present Results with those of Other Authors

The space-time displays of the velocity modulated motion of the striations differ considerably from those obtained earlier by Stewart⁽⁶⁸⁾. In his results the motion of the striations changed abruptly: for periods of up to 200 μ s there were no striations moving in the discharge. Stationary striations were seen and interpreted as due to the interaction of

A



C



0.2 msec

Time

Fig.5.9

Space-time display for coil signal. Self-excited wave, no applied voltage.
Pressure: 0.44 torr; Current: 92 mA.

'positive' striations - ions travelling from the anode to the cathode - and faster 'negative' striations consisting of electrons travelling towards the anode. Subsequently it was suggested⁽⁷⁾ that the anode directed waves were not a separate phenomenon but could be explained in terms of modulation of the wave.

As far as the present results are concerned it has been shown that the 'apparent' stationary striations were due to velocity modulation. However, closer inspection of Fig.5.7 reveals that where a striation slows down, there is a much fainter, almost vertical streak, originating from this point and which moves at high speed, $\sim 10^5$ cm/s towards the anode. As these lines are very faint, the space-time display is sketched in Fig. 5.10. The magnitude of the velocity suggests that the anode directed 'waves' are associated with electrons drifting in the electric field. For a field of 1.5 V/cm and a pressure of 0.46 torr, the data for argon⁽⁶⁹⁾ gives an electron velocity of the order of 10^6 cm/s.

In the absence of the external voltage, the waves in the discharge appeared as in Fig.5.11; there are no 'negative' striations. In these experiments, at least, the 'negative' waves appear as a consequence of the external modulation.

The anode directed waves described above, appear to be distinct from the observations of Jackson⁽⁵⁹⁾ where anode directed disturbances travelling with the same speed as the cathode directed waves, were seen. As will be seen in Chapter IX, such disturbances can arise from 'self-modulation' of the cathode directed striation.

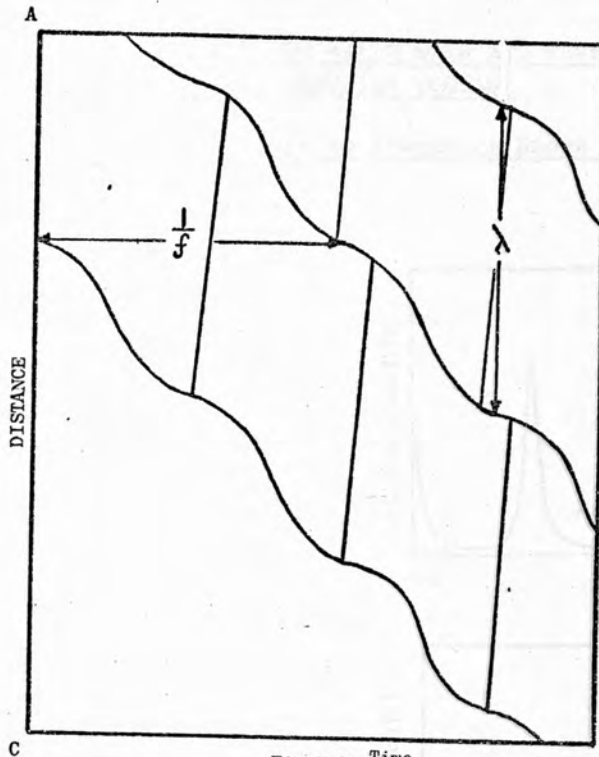


Fig.5.10 Time
Space-time display. Schematic of Fig.5.7(a)
showing anode directed 'waves'

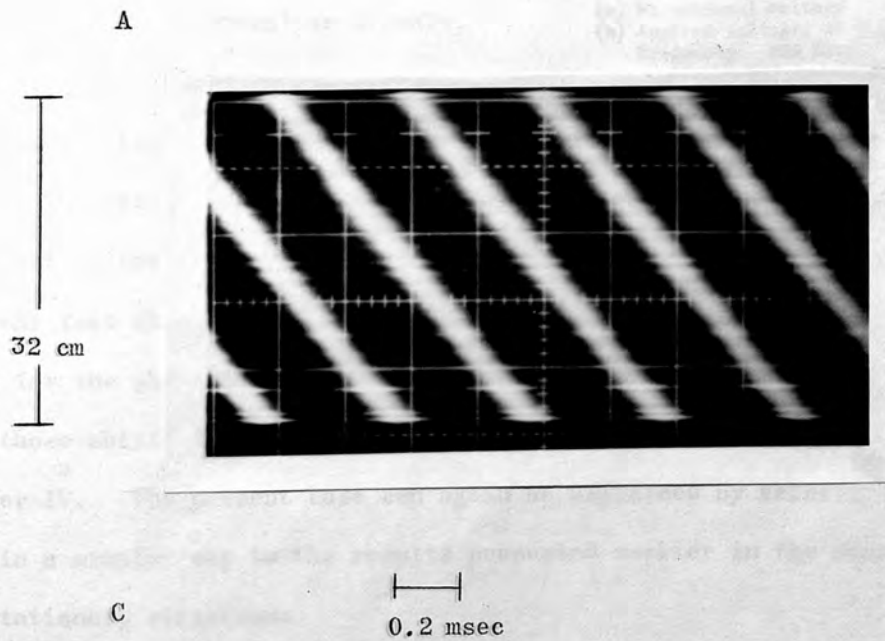


Fig.5.11
Space time display for photomultiplier signal. Para-
meters as for Fig.5.7. No externally applied voltage

5.5 COUPLING OF THE SELF-EXCITED WAVES WITH THE WAVES
PRODUCED BY THE EXTERNALLY APPLIED VOLTAGE

5.5.1 Frequency of Applied Voltage in Frequency Range (a)

The effect of applying a voltage to the anode at a frequency of 600 Hz is shown in Fig.5.12. For an applied voltage of 18V, peak-to-peak, satellite frequencies appear either side of the 3.4 KHz striation, and its harmonics, spaced 600 Hz away from the appropriate frequency component.

With increased voltage modulation the first harmonic of the 600 Hz oscillation was seen and the spectrum became more complex as now there were two satellite frequencies spaced each side at separations equal to 600 Hz and 1200 Hz. The wave patterns of the coil and photomultiplier signals, when the applied voltage was 18 V, are shown in Fig.5.13.

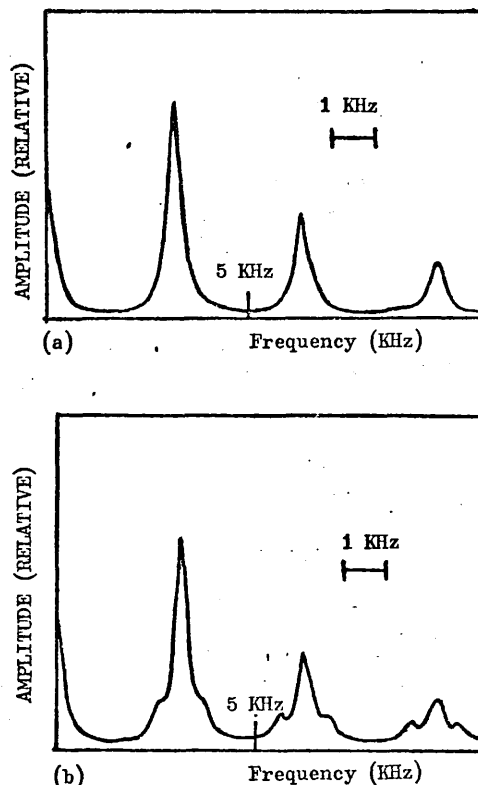


Fig.5.12
Photomultiplier signal: spectra for mode coupling. Pressure: 0.32 torr; Current: 105 mA
(a) No external voltage
(b) Applied voltage: 18 V (p.p.)
Frequency: 600 kHz

The satellite frequencies retain the spacing between maxima of the component of the self-excited striation with which they are coupled, despite the fact that the 600 Hz wave exhibits a standing wave pattern, at least for the photomultiplier signal. In this point these results differ from those obtained for the coupling of the purely self-excited waves, Chapter IV. The present case can again be explained by velocity modulation in a similar way to the results presented earlier in the chapter for the stationary striations.

An interpretation of the results will be given in Chapter VII.

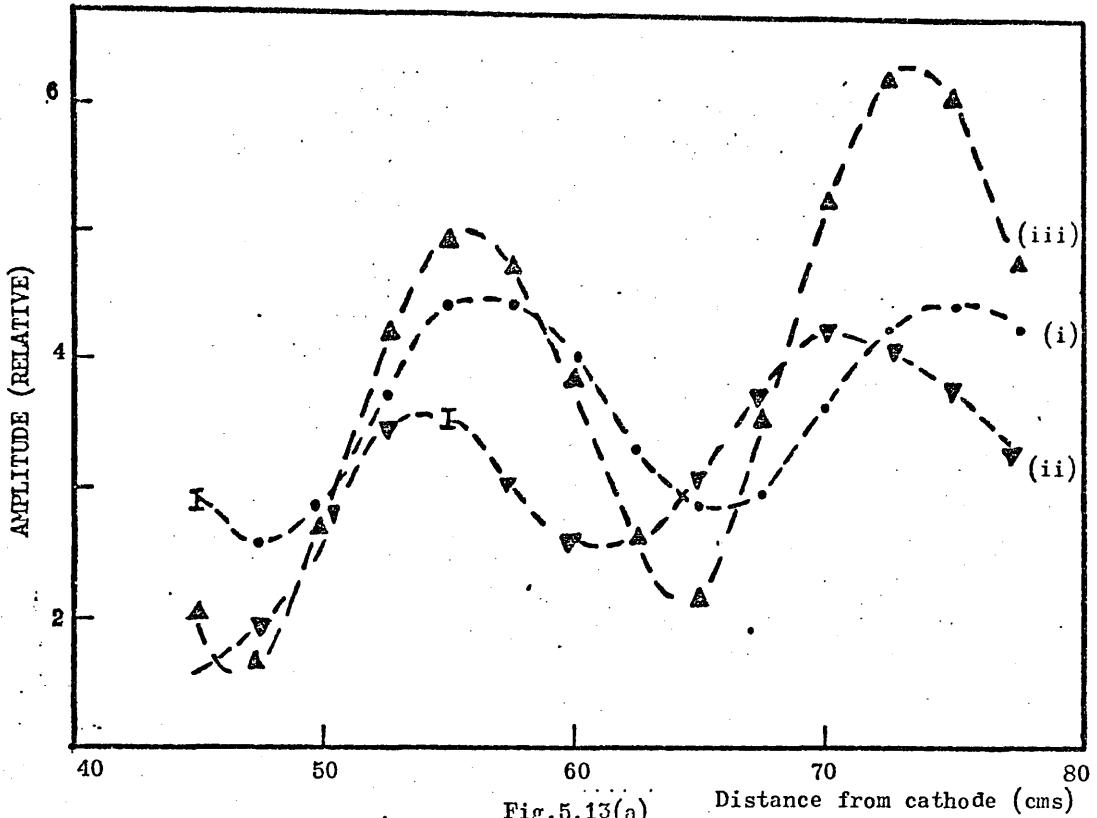


Fig.5.13(a)
 Wave pattern for coil signal for (i) fundamental frequency: 3.4 KHz;
 (ii) Lower satellite: 2.8 KHz, and (iii) Upper satellite: 4 KHz.
 Current: 105 mA; Pressure: 0.32 torr
 Applied voltage: 18 V (p.p.); Frequency: 600 KHz

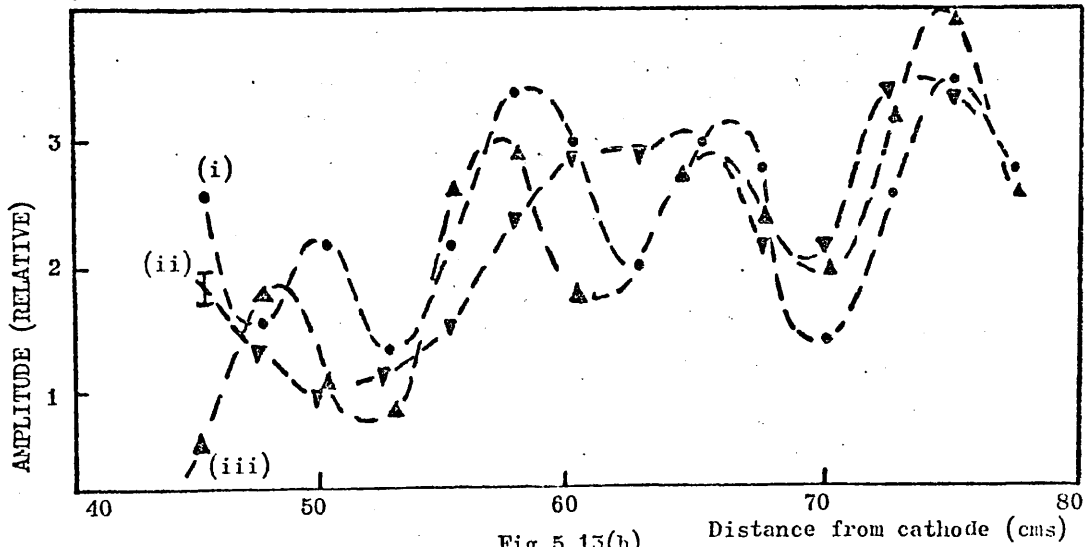


Fig.5.13(b)
 As for Fig.5.13(a)
 (i) First harmonic frequency: 6.9 KHz
 (ii) Lower satellite: 6.2 KHz
 (iii) Upper satellite: 7.4 KHz

5.5.2 Frequency of Applied Voltage in Frequency Range (c)

Results obtained when the frequency of the applied voltage was equal to 30 KHz and the self-excited waves in this frequency range were absent are shown in Fig.5.14. For comparison the self-excited spectrum obtained at a slightly lower current is shown. In the former case there is hardly any coupling between the lower frequency striations and the 30 KHz waves as compared to the self-excited case. Since the artificially excited case differs from the self-excited case it was not pursued further.

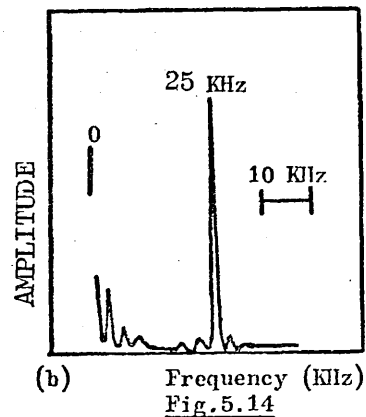
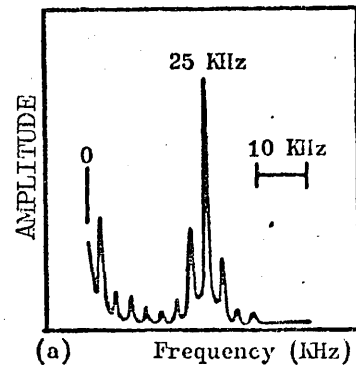


Fig.5.14

Frequency spectra for frequency range (c). Pressure: 0.54 torr;
(a) Self-excited; Current: 90 mA
(b) Externally excited; Current: 110 mA; Frequency: 25 KHz.

5.6 CONCLUSION

The results of this chapter have shown that velocity modulation of the striations may give rise to some of the effects seen in discharges.

Expressions which describe the modulation of a wave will be examined in the next chapter.

CHAPTER VI

MODULATION OF A PLANE WAVE

6.1 INTRODUCTION

The well known sinusoidal expression used to describe a uniformly travelling wave can easily be extended to account for modulation of the wave. The characteristics of a general expression which includes modulation of the amplitude and phase will be examined in this chapter.

The results obtained will be presented in the form of space-time diagrams and frequency spectra so that they may be compared, in the next chapter, with the experimental observations of the nonlinear interactions between waves. It should be emphasized, however, that the conclusions drawn in this chapter are general and do not apply specifically or necessarily to striations.

6.2 REPRESENTATION OF THE WAVE

A travelling wave of constant amplitude and velocity may be represented by $\psi(x,t) = A \cos(\omega t - kx)$, where A is the amplitude, ω and k the angular frequency and wavenumber respectively. When periodic variations in frequency, wavenumber and amplitude occur, the expression may be generalized to:

$$\psi(x,t) = A(1 + m \sin pt) \cos F(x,t) \quad \dots (6.1)$$

where $F(x,t)$ is the phase of the wave, and

$$\frac{\partial F}{\partial t} = \omega(t) = \omega + m_{\Omega} \Omega \cos \Omega t \quad \dots (6.2)$$

$$- \frac{\partial F}{\partial x} = k(x) = k - m_{\kappa} \kappa \cos \kappa x \quad \dots (6.3)$$

giving
$$F(x,t) = \omega t - kx + m_{\Omega} \sin \Omega t + m_{\kappa} \sin \kappa x \quad \dots (6.4)$$

In the absence of modulation, $m = m_{\Omega} = m_{\kappa} = 0$ and $\psi(x,t)$ reduces to the normal cosine expression for a travelling wave.

6.3 SPACE-TIME DIAGRAMS

Experimentally, space-time diagrams represent the loci in time and position of the maximum values of some quantity related to the wave (e.g. light intensity). So, for comparison the space-time diagram may be found in the absence of amplitude modulation from the loci of $\psi(x,t) = A$. When amplitude modulation is included the method is essentially the same but with the addition that the changes in amplitude are superimposed on the velocity modulated loci as will be seen.

Without modulation the loci of $\psi(x,t)$ are straight lines with slope ω/k separated from one another by the wavelength and time period along the space and time axes respectively, Fig.6.1(a).

6.3.1 Phase Modulation

If the amplitude modulation is assumed to be zero, then Fig.6.1(b) shows the space-time diagram when $m_\kappa = 0$ while Fig.6.1(c) shows the diagram when $m_\Omega = 0$. For self-excited striations which are not exactly sinusoidal, the wavenumber modulation will give rise to the 'apparent' stationary striations for any value of κ , while for frequency modulation the occurrence of 'apparent' stationary striations will depend on the relative values of ω and Ω . For example, when $\Omega = n\omega$, n is an integer, they will be seen.

For simultaneous frequency and wave number modulation for arbitrary values of Ω and κ the motion will be more complicated since in this case the changes will appear to propagate in a complex way. Of interest is the case⁽¹⁵⁾ when $\left| \frac{\Omega}{\kappa} \right| = \left| \frac{\omega}{k} \right|$ which is shown in Fig.6.1 for $\kappa = \frac{k}{3}$. The changes in the wave motion occur with an 'apparent' velocity directed towards the anode and equal in magnitude to $|\omega/k|$. The space-time diagram while resembling those of Stewart et al⁽¹⁵⁾ does not reproduce the essential features.

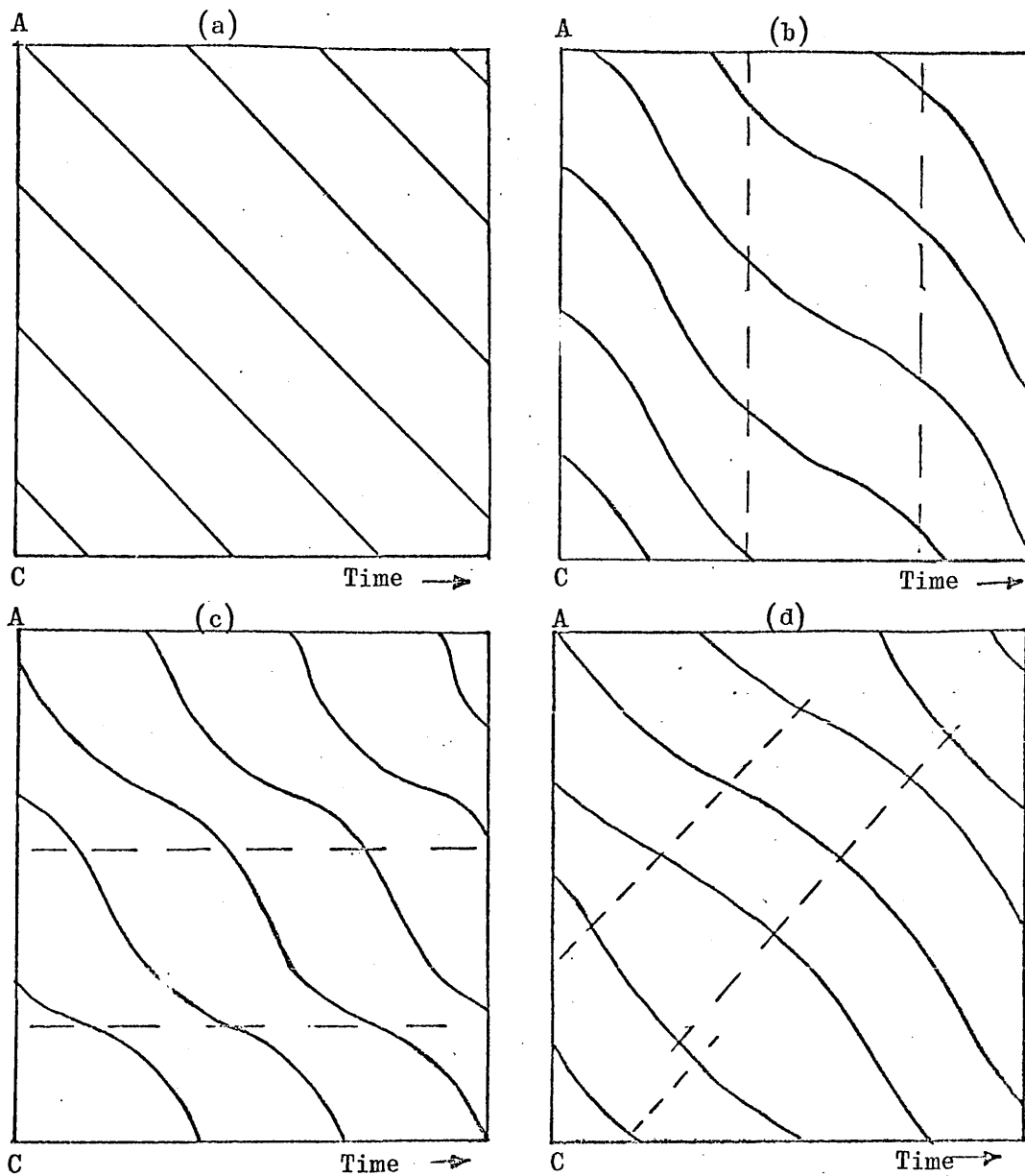


Fig.6.1

Space-time diagrams: (a) Unmodulated wave;
 (b) Frequency modulated; (c) Wavenumber
 modulated; (d) Simultaneous frequency and
 wave-number modulation
 A: Anode, C: Cathode

6.3.2 Phase and Amplitude Modulation

Simultaneous phase, $F(x,t)$, and amplitude modulation are shown in Fig.6.2 when (a) the frequency of the amplitude modulation is equal to the striation frequency, $\omega = p$, and (b) the frequency of amplitude modulation is arbitrary. For the cases shown, $m_\kappa = 0$ and $\Omega = \omega$ in equations (6.2) and (6.3).

The resultant space-time diagrams consist of the phase modulated pattern upon which are superimposed areas of decreased and increased amplitude due to the amplitude modulation. For case (b) the regions of increased amplitude give the appearance of a disturbance moving towards the anode, but a comparison of this diagram with observations⁽¹⁵⁾ shows that the experimental results are different and cannot be explained by such modulation alone.

6.3.3 Phase Modulation: Velocity Modulation by a Travelling Wave

The modulations represented in Fig.6.1 gave rise to velocity changes which occurred in the same positions along the discharge tube. Finally, the space-time diagram when the velocity modulation is of the form:

$$V = V_0 + V_m \cos(\Omega t - \kappa x), \quad \dots (6.5)$$

where $V_0 = \frac{\omega}{k}$ is the phase velocity of the unmodulated wave, is examined.

Such an expression can be obtained when

$$F(x,t) = \omega t - \kappa x + \Delta \sin(\Omega t - \kappa x) \quad \dots (6.6)$$

since the velocity is given by

$$\begin{aligned} \text{velocity} &= - \frac{\frac{\partial F}{\partial t}}{\frac{\partial F}{\partial x}} = \frac{\omega + \Omega \Delta \cos(\Omega t - \kappa x)}{k + \kappa \Delta \cos(\Omega t - \kappa x)} \quad \dots (6.7) \\ &= V_0 + V_m \cos(\Omega t - \kappa x) \end{aligned}$$

when $\Omega \leq \omega$, $\kappa \leq k$, $\Delta < 1$.

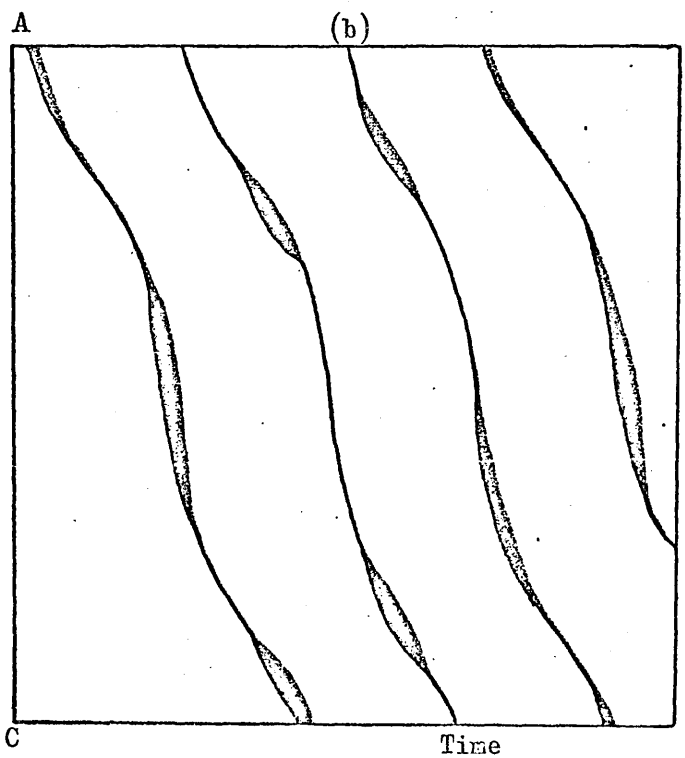
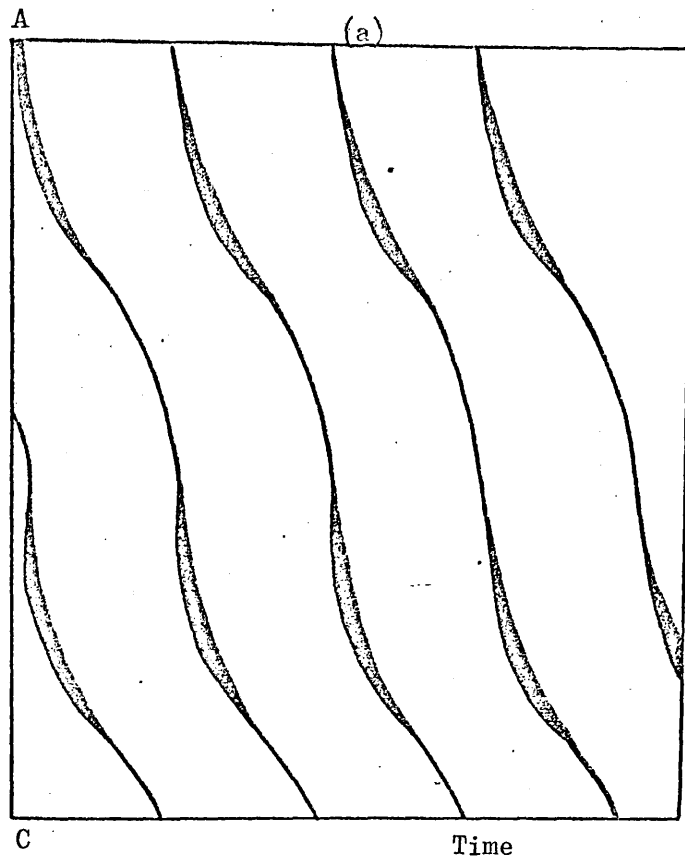


Fig.6.2
 Space-time diagrams: simultaneous amplitude and phase modulation; (a) Modulating frequencies equal; (b) Frequency of amplitude modulation arbitrary

The resulting space-time diagram is shown in Fig.6.3. In Fig. 6.3(a), the continuous lines depict the motion of the maxima of the unmodulated striations. The dashed lines show the loci of the maxima of $V_m \cos(\Omega t - \kappa x)$ for the case when $\Omega/\kappa < \omega/k$.

The points where the two sets of lines intersect correspond to the positions and times when $V = V_0 + V_m$: the velocity has increased from the unmodulated value V_0 to its maximum value. The positions of the maximum values of velocity are depicted in Fig.6.4(b). Similarly by plotting the minima of $V_m \cos(\Omega t - \kappa x)$ the points where the modulated velocity is a minimum can be found - these are not shown in Fig.6.4(b). The perturbations in velocity appear at successive intervals of time $\frac{2\pi}{\delta\omega}$ to approach the anode in steps of $\frac{2\pi}{\delta k}$ leading to an apparent velocity $\frac{\delta\omega}{\delta k}$ where $\delta k = c \left| \frac{k \kappa}{k - \kappa} \right|$, $\delta\omega = c |(\omega - \Omega)|$, c is an unknown constant.

6.4 FREQUENCY SPECTRUM

Experimental results are often obtained in the form of a frequency spectrum display of the output signal from a detector which monitors the waves. This type of display represents the Fourier analysis of the output signal and records the amplitude of the various frequency components.

6.4.1 Expansion of the General Expression for the Waves

The general expression which will be used is:

$$\psi(x, t) = A \left[1 + m \sin(pt + \varphi) \right] \cos \left[\omega t - kx + \Delta \sin(pt - \beta x) \right] \quad \dots (6.8)$$

where the basic wave $A \cos(\omega t - kx)$ is phase modulated by the travelling wave $\sin(pt - \beta x)$ and amplitude modulated by the term $\sin(pt + \varphi)$. The expression may be analysed by making use of the expansion:

$$\cos(\theta + \Delta \sin \alpha) = J_0(\Delta) \cos \theta + \sum_{n=1}^{\infty} J_n(\Delta) \left[\cos(\theta + n\alpha) + (-1)^n \cos(\theta - n\alpha) \right], \quad \dots (6.9)$$

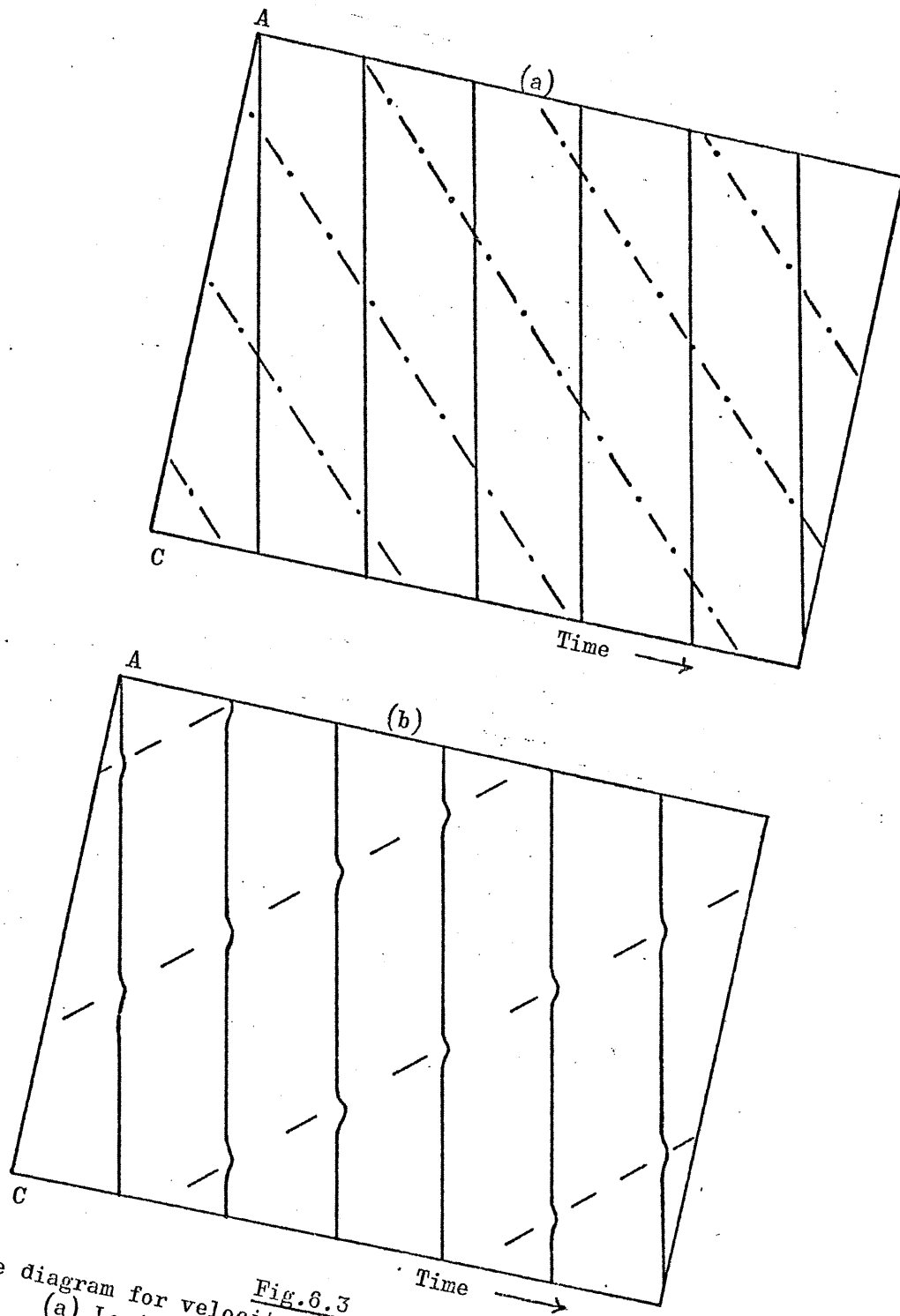


Fig. 6.3
 Space diagram for velocity modulation by a travelling wave. (a) Loci of wave maxima and maxima of the modulating term; (b) Modulated wave showing schematically the positions of increased velocity

where the J's are Bessel functions of the first kind. Terms at frequencies $\omega \pm n\beta$ are generated by the expansion of equation (6.8) using equation (6.9). The following expressions are obtained for the frequency components ω , $\omega - \beta$, $\omega + \beta$:

$$\left. \begin{aligned}
 & \underline{\omega} \\
 & J_0(\Delta) \cos(\omega t - kx) - J_1(\Delta) \frac{m}{2} \left[\sin[\omega t + \varphi - (k - \beta)x] + \sin[(\omega t - \varphi - (k + \beta)x] \right] \\
 & \underline{\omega - \beta} \\
 & - J_1(\Delta) \cos[(\omega - \beta)t - (k - \beta)x] \\
 & \quad - \frac{m}{2} J_0(\Delta) \sin[(\omega - \beta)t - \varphi - kx] + J_2(\Delta) \frac{m}{2} \sin[(\omega - \beta)t + \varphi - (k - 2\beta)x] \\
 & \underline{\omega + \beta} \\
 & + J_1(\Delta) \cos[(\omega + \beta)t - (k + \beta)x] + \frac{m}{2} J_0(\Delta) \sin[(\omega + \beta)t + \varphi - kx] \\
 & \quad - J_2(\Delta) \frac{m}{2} \sin[(\omega + \beta)t - \varphi - (k + 2\beta)x]
 \end{aligned} \right\} \dots (6.10)$$

The amplitude of the higher order satellites is assumed to be negligible compared with the above terms. In addition the $J_2(\Delta)$ terms in the above expressions can be neglected for the values of $\Delta \leq 0.5$ which are likely to be met. The amplitudes of the frequency components are then given by:

$$\left. \begin{aligned}
 & \underline{\text{Frequency } \omega} \\
 & \left[J_0^2(\Delta) + \frac{m^2}{2} J_1^2(\Delta) [1 + \cos(2\beta x + 2\varphi)] \right]^{\frac{1}{2}} \\
 & \underline{\text{Frequency } \omega - \beta} \\
 & \left[J_1^2(\Delta) + \frac{m^2}{4} J_0^2(\Delta) - m J_0(\Delta) J_1(\Delta) \sin(\beta x + \varphi) \right]^{\frac{1}{2}} \\
 & \underline{\text{Frequency } \omega + \beta} \\
 & \left[J_1^2(\Delta) + \frac{m^2}{4} J_0^2(\Delta) + m J_1(\Delta) J_0(\Delta) \sin(\beta x + \varphi) \right]^{\frac{1}{2}}
 \end{aligned} \right\} \dots (6.11)$$

The expressions show that the amplitude of each frequency component oscillates between maximum and minimum values as x varies. For the frequencies $\omega + \beta$, $\omega - \beta$, the distance between consecutive maxima is $\frac{2\pi}{\beta}$ whereas for the frequency ω the spacing is π/β .

In the absence of amplitude modulation, $m = 0$, or phase modulation, $\Delta = 0$, the amplitudes do not change with position and the amplitudes of the frequency components $\omega \pm p$ are equal.

Similarly if the phase varies with time only, $\beta = 0$, the amplitudes are not spatially dependent but the amplitudes of the satellite frequencies $\omega \pm p$ are not equal. As an example of the latter case, the resultant amplitude for different values of the phase angle ϕ is shown in Fig.6.4 for values of $m = \Delta = 0.5$.

6.4.2 Non-Sinusoidal waves

The expression for the modulated wave may be extended to include non-sinusoidal waves:

$$\psi(x, t) = [1 + m \sin(pt + \phi)] G[\omega t - kx + \Delta \sin(pt - \beta x)] \quad \dots (6.12)$$

where $G(\omega t - kx)$ represents an unmodulated travelling wave which is periodic but no longer sinusoidal. The resulting spectrum can still be found by first expressing $G[\omega t - kx + \Delta \sin(pt - \beta x)]$ in a Fourier expansion to give:

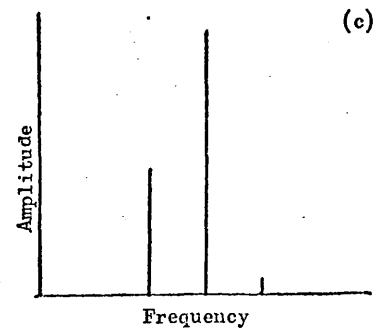
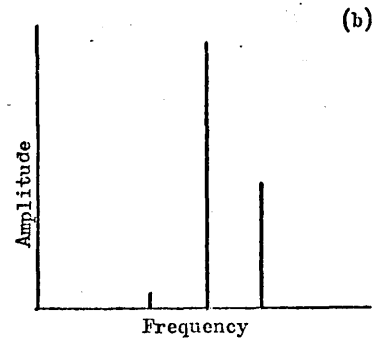
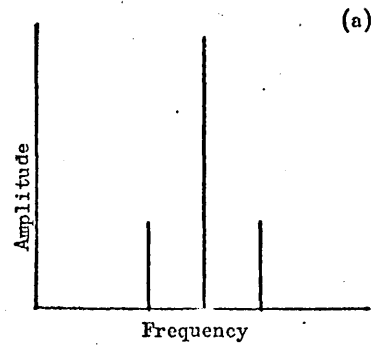


Fig.6.4
Frequency spectra for amplitude and phase modulation when $\beta = 0$, $m = \Delta = 0.5$
(a) $\phi = 0, \pi, 2\pi$; (b) $\phi = \pi/2$; (c) $\phi = 3\pi/2$

$$\begin{aligned}
& G \left[\omega t - kx + \Delta \sin (pt - \beta x) \right] \\
& = A_1 \sin \left[\omega t - kx + \theta_1 + \Delta \sin (pt - \beta x) \right] \\
& + A_2 \sin \left[2\omega t - 2kx + \theta_2 + 2\Delta \sin (pt - \beta x) \right] \\
& \cdot \\
& \cdot \\
& + A_N \sin \left[N(\omega t - kx) + \theta_N + N \Delta \sin (pt - \beta x) \right] .
\end{aligned}$$

Following the same procedure as in the previous section, it can be seen that satellite frequencies $\omega \pm p$, $2\omega \pm p$, $3\omega \pm p$, $N\omega \pm p$, are produced either side of the fundamental frequency ω and its harmonics 2ω , 3ω , $N\omega$.

For the frequency $N\omega$ and its satellites, the amplitudes may be found by replacing Δ by $N\Delta$ in the argument of the Bessel functions in equations (6.11). The amplitude of each satellite frequency varies periodically with a spacing between maxima of $2\pi/\beta$ while the amplitudes of the fundamental frequency ω and its harmonics vary periodically with a spacing of π/β .

CHAPTER VII

INTERPRETATION OF THE NONLINEAR COUPLING BETWEEN THE WAVES IN THE ARGON DISCHARGE

7.1 INTRODUCTION

The nonlinear wave coupling will now be interpreted in terms of amplitude and phase modulation of the waves using the results of the previous chapter. However, it is first necessary to discuss several other effects which can give rise to multiline spectra. Following the interpretation of the results, a physical mechanism for the coupling will be given.

7.2 GENERAL REMARKS

It has been seen that when there were interactions between the waves, the resulting frequency spectrum consisted of discrete lines except for the case when waves from all three frequency ranges were present. The frequency components resulting from the interactions were seen throughout the length of the positive column and yet at the same time there was no region where the spectrum developed into a broad frequency continuum. This may be contrasted with the results in argon of Grabec⁽⁵⁶⁾ and those in neon, see Chapter X, where the initial line spectrum develops into a broad spectrum due to nonlinear effects. As mentioned in Chapter IV, the striations in frequency range (b) saturated close to the cathode end of the positive column due to the stabilization by energy losses. The fact that the spectrum, although multilined, did not degenerate into a broad spectrum suggests that the interaction between the waves took place in a 'regular' way and that fusion and splitting of the striations did not take place.

7.3 POSSIBLE EXPLANATIONS FOR THE WAVE INTERACTIONS

7.3.1 Resonant Coupling

Three wave resonant coupling requires the following relations to be satisfied between the frequencies and wavenumbers

$$\omega_1 + \omega_2 \rightarrow \omega_3, \quad \underline{k}_1 + \underline{k}_2 = \underline{k}_3 \quad \dots (7.1)$$

with the possibility for a small mismatch. Shown in Fig.7.1 are the different regions in the ω, k space occupied by the three groups of waves which have been observed. For these waves the conditions (7.1) leads to values of k_3 which would give a different spatial amplitude variation from that seen experimentally.

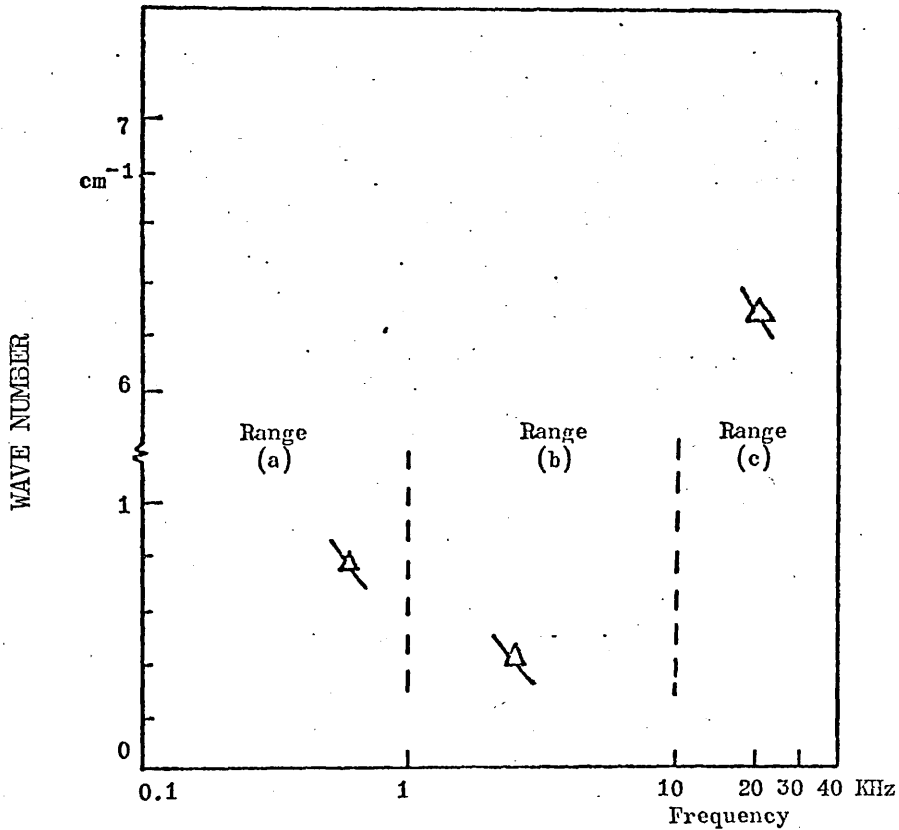


Fig.7.1
Frequency ranges of the observed
Oscillations and Waves

Indeed, for backward waves having dispersion relations of the form $\omega_i k_i = C_i$ these conditions will not be met as can be seen in the following. Suppose that the resultant wave due to the interaction of ω_1, k_1 and

ω_2, k_2 lies on the dispersion curve of $\omega_1 k_1 = C_1$, then the resultant k is given by

$$k_3 = \frac{C_1 k_1 k_2}{C_1 k_2 + k_1 C_2} \neq k_1 + k_2 .$$

Likewise for the interaction between a forward and backward wave resulting in a forward or backward wave, the condition (7.1) will not in general be satisfied.

7.3.2 Excitation of Waves from a Single Dispersion Curve

In the work of Ohe and Takeda⁽⁵⁷⁾ and Krasa and Pekarek⁽⁷⁰⁾, multiline spectra were observed and it was found that the components of the spectrum had frequencies and wavenumbers which lay on a single dispersion curve. In the first case the origin of the spectra was attributed to the response of the positive column when the discharge current was modulated in phase and amplitude. In the second case it was suggested that the discharge was 'pumped' by a synchronous oscillation, the frequency of which was related to the frequency of the multiline spectra.

For the argon discharge, in the absence of mode-coupling between the waves in frequency ranges (a) and (b), the waves of frequency range (b) could be represented as

$$(A + B \sin kx) \sin [\omega t + \varphi(x, t)] \quad \dots (7.2)$$

due to the linear interference between the travelling wave of frequency ω and wavenumber k and the synchronous oscillation at the same frequency, see Chapter IV.

If the results for the mode coupling were interpreted as due to the excitation of travelling waves belonging to the single dispersion curve of the waves of frequency range (b), then it could be supposed that the multiline spectrum, seen when the frequency range (a) wave was present, represented the response of the positive column when the discharge current was modulated at a frequency $\omega + \Delta \sin pt$, where p is the frequency of the

waves in frequency range (a). All the waves so generated would lie on a single dispersion curve.

Experimentally it was seen that the additional frequency components which were generated by the nonlinear interaction, had the same form of axial amplitude variation as the unmodulated waves as given above. Such a variation could then be due to the linear interference of a synchronous oscillation at the frequency $\omega - p$ with a travelling striation at the frequency $\omega - p$ and wavenumber $k + \delta k$. The resulting amplitude variation would vary as $\sin(k + \delta k) x$ and since the striations are assumed to belong to the same dispersion curve $\omega k = C$, the distance d between adjacent maxima would be given by $d = \lambda(1 - \frac{p}{\omega})$ where λ is the wavelength at frequency ω . Using the data from Fig. 4.18(a), for example, $p = 600$ Hz, $\omega = 2.6$ KHz, $\lambda = 16$ cm, the spacing d is equal to 12 cms in contrast to the experimentally observed value of 8 cms.

When an external voltage was applied, both the upper and lower satellites had the same spacing between maxima, contrary to the conclusions of the present interpretation.

Similarly, for the interaction of the waves in frequency range (c), and the waves in range (b), the observed amplitude variation is not consistent with the supposed form of interaction since d would be of the order of 1 cm, the wavelength of the waves of range (c).

It may be concluded that the effects seen in the argon discharge were not due to the excitation of waves from a single dispersion curve.

7.3.3 Excitation of Virtual Waves

Another possibility is that the waves observed at the sum and difference frequencies are a result of forced modulation from nonlinear terms of the form $n^{(1)} \theta^{(1)}$ where n, θ are the electron density and temperature of the waves, see Chapter VIII.

The resultant waves formed by two waves ω_1, k_1 and ω_2, k_2 would have frequencies $\omega_2 \pm \omega_1$ and $k_3 = k_2 \pm k_1$ obtained from the product $\theta^{(1)}_n(1)$ and are termed virtual waves.

Although such an explanation may be given for the wave interactions, it will be seen that velocity modulation is the likelier effect.

7.4 INTERPRETATION OF THE WAVE INTERACTIONS: AMPLITUDE AND PHASE MODULATION

It will now be shown that the experimental observations for the mode coupling can be interpreted in terms of phase (velocity) and amplitude modulation.

From the time-averaged spectrum analyser results of Chapters IV and V it is not possible to differentiate between virtual wave excitation or velocity modulation. However, the arguments of Chapter VIII show that the discharge is likely to be more stable to velocity modulation than to virtual wave excitation, and so the former is more probable. In addition the observations of section 7.4.2(d) support velocity modulation. Both interpretations require that there is no nonlinear interaction between synchronous oscillations and travelling striations.

7.4.1 Summary of Nonlinear Results

For convenience the experimental results to be explained are summarised below.

The interaction between the self-excited waves of frequency ranges (a) and (b) produced satellite frequencies spaced either side of the fundamental frequency of the wave in range (b) and its harmonics. The amplitude of the lower frequency was larger than the amplitude of the corresponding upper satellite. For the fundamental frequency, the amplitude of the lower satellite was much smaller than the amplitude of the fundamental frequency. The relative amplitudes for the harmonic frequencies increased

so that, in some cases, the satellite amplitude was almost as large as that of the corresponding harmonic frequency.

The axial variation in amplitude of the fundamental wave and its harmonics was not altered by the mode-coupling, while the amplitude variation seen for the satellite frequencies was related to the amplitude variations of the waves in ranges (a) and (b). For some values of current the second order satellite frequencies were seen but their amplitude was too small to measure any variation.

In the case of the interactions between the waves in ranges (c) and (b) the upper satellites, as well as the lower, were easily seen. The satellite frequencies on either side of the waves in range (c) were spaced at frequency intervals equal to the frequency of the wave in range (b) and its harmonics. The amplitude variation of the upper and lower satellites was directly related to the variation in amplitude of the corresponding lower frequency wave.

When an external voltage was applied at the same frequency as the self-excited striations in range (b) 'apparent' stationary striations due to velocity modulation were seen for certain values of discharge current. Upon reducing the applied frequency to correspond to the same value as the frequency for the self-excited waves in range (a), mode coupling was seen with lower and upper satellites about the fundamental frequency in range (b) and its harmonics.

The amplitude variation of a satellite frequency, unlike the self-excited case, was essentially the same as that for the frequency component to which it was coupled.

7.4.2 Interactions of the Waves in Frequency Ranges (a) and (b)

The fact that when the externally applied electric potential was of the same frequency as the striations in range (b), the latter were velocity modulated, suggests that at other exciting frequencies velocity and amplitude modulation may have produced the observed effects.

(a) Amplitude variation of the coil signal

Since the waves in frequency range (b) were periodic but non-sinusoidal, the appropriate expression to represent simultaneous amplitude and velocity modulation, of the form $V = V_0 + V_m \sin(pt - \beta x)$ may be found from equations (6.7) and (6.8). It was seen in Chapter VIII, that periodic amplitude variations proportional to $\sin \beta x$ are obtained for all the satellite frequencies.

For such modulation the amplitude of the frequency components $\omega, 2\omega, 3\omega, \dots$, vary as $\cos 2\beta x$ which is contrary to the experimental observations. If however for the travelling wave there is no amplitude modulation, $m=0$, then the desired frequency components are still obtained but the unwanted amplitude variations are removed. However, for such a case none of the amplitudes vary spatially. At this point the role of the synchronous oscillations must be introduced.

The considerations in Chapter IV which showed that moving striations become nonlinear for relatively small perturbations in the electron temperature applies equally for synchronous oscillations. Polman has shown, for example, how the time averaged value of the electron density is influenced by nonlinear effects when the applied current modulation is still small (Chapter II). As the linear interference between the travelling waves and the synchronous oscillations has shown, (Chapter IV), the synchronous oscillations consisted of a fundamental frequency and harmonics.

The general expression to describe amplitude and phase modulation of a synchronous oscillation is found from equations (6.7) and (6.8) by putting $k = \beta = 0$. The resulting frequency components ω , $\omega \pm p$ have amplitudes given by:

Frequency ω

$$\left[J_0^2(\Delta) + \frac{m^2}{2} J_1^2(\Delta) [1 + \cos 2\varphi] \right]^{\frac{1}{2}} \quad \dots (7.3)$$

Frequency $\omega \pm p$

$$\left[J_1^2(\Delta) + \frac{m^2}{4} J_0^2(\Delta) \pm m J_0(\Delta) J_1(\Delta) \sin \varphi \right]^{\frac{1}{2}} \quad \dots (7.4)$$

The satellite frequencies for harmonics of ω can be found from equations (7.3) and (7.4) as explained in Chapter VI. It is assumed that higher order terms with frequencies $\omega \pm np$, $n = 2, 3, 4$ are small enough to be neglected which corresponds to the majority of experimental observations when such frequencies were not seen in the spectra.

By themselves neither the modulated moving striations nor the synchronous oscillations provide the desired amplitude variation of the frequency spectra components. However, taken together they provide just the variation which is sought.

The modulated synchronous oscillations give rise to a spectrum of the form:

$$\left. \begin{aligned} \sum_{n=1}^N A_N \sin \left[(n\omega - p)t + \varphi_{AN} \right] \\ + B_N \sin \left[(n\omega + p)t + \varphi_{BN} \right] \end{aligned} \right\} \quad \dots (7.5)$$

and similarly the velocity modulated striations result in a frequency spectrum

$$\left. \begin{aligned} \sum_{n=1}^N C_N \sin \left[(n\omega - p)t - (nk - \beta)x \right] \\ + D_N \sin \left[(n\omega + p)t - (nk + \beta)x \right] \end{aligned} \right\} \quad \dots (7.6)$$

where the amplitudes A_N, B_N, C_N and D_N can be found from equations (7.3), (7.4) and (6.6).

The resultant amplitude of a synchronous and travelling wave component at a given frequency gives rise to a periodic variation in amplitude as can be seen, for example, by taking the components $A_1 \sin(\omega - p)t$, and $B_1 \sin[(\omega - p)t - (k - \beta)x]$ giving a resultant amplitude

$$\sqrt{A^2 + B^2 + 2AB \cos(k - \beta)x} \quad \dots (7.7)$$

which corresponds to the experimental observations for the spatial variation in amplitude, (section 4.52). Likewise the amplitude variations for the frequency components $2\omega - p$, $3\omega - p$, etc, give the desired spacing between maxima in the standing wave pattern.

(b) Asymmetry of the frequency spectra

The difference in amplitude for corresponding upper and lower satellite frequencies - the latter amplitude was much larger - is not due to the velocity modulation of the travelling wave which would give rise to equal amplitudes for both satellite frequencies. Rather the asymmetry is due to the modulation of the synchronous oscillation and the difference in amplitudes is determined by the value of the phase angle φ . For given values of m and Δ , when $\varphi = 270^\circ$ the amplitude of the component at $\omega - p$ is maximum, while that for the frequency $\omega + p$ is a minimum, see Fig.6.4.

The spectra resulting from various values of Δ and $\varphi = 270^\circ$ has been calculated from equations (6.6) for synchronous oscillations, Fig.7.2. The amplitudes of the fundamental frequency and its harmonics, in the absence of modulation, have been chosen arbitrarily. The asymmetry of the satellite amplitudes is apparent. Another feature seen is the way in which the relative amplitude of the satellite frequency $2\omega - p$ and the first harmonic 2ω is larger than the corresponding ratio for the fundamental frequency ω and smaller than that for the second harmonic 3ω .

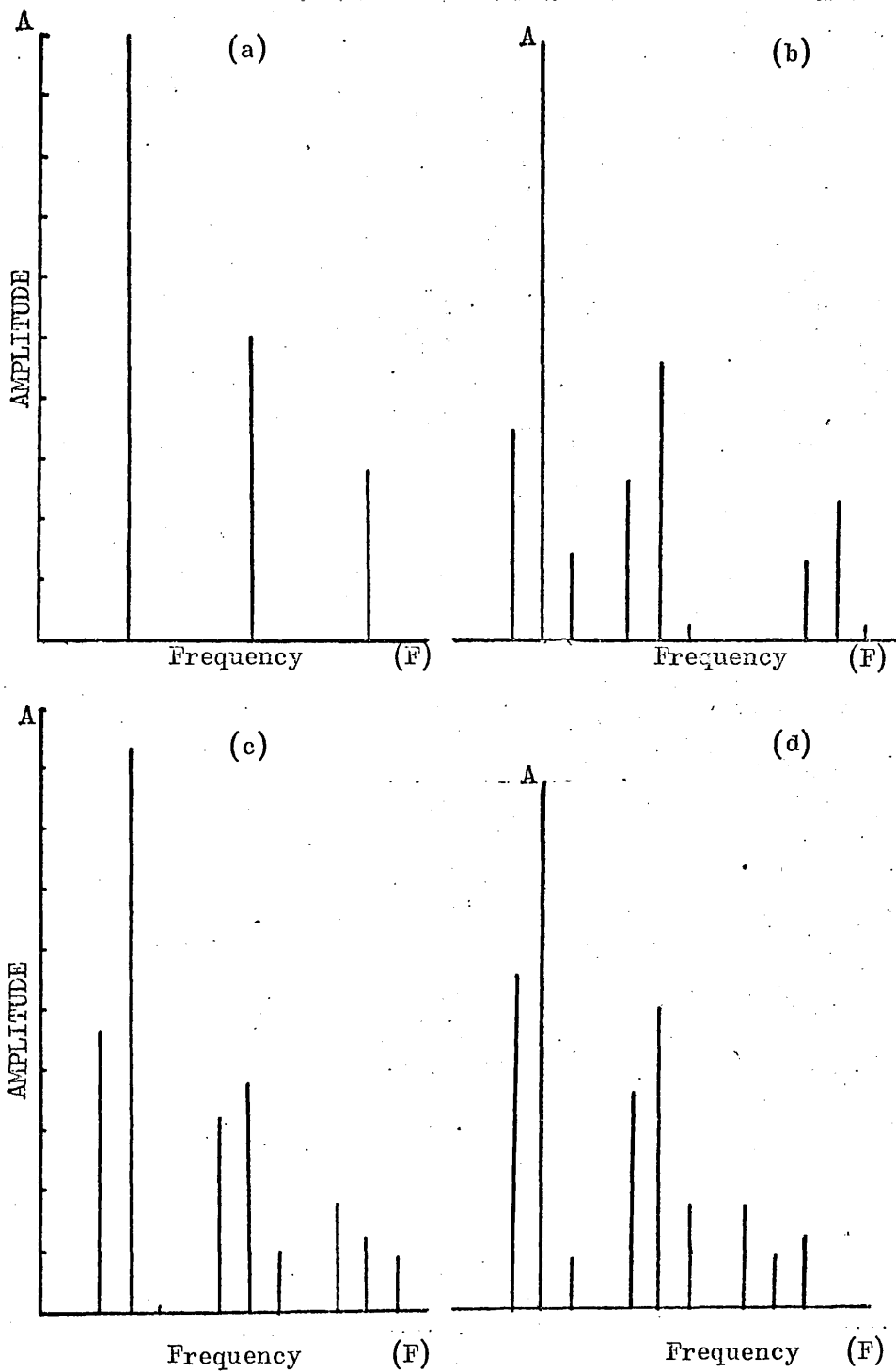


Fig.7.2

Amplitude and phase modulation of a synchronous oscillation

- (a) Unmodulated: shows fundamental and harmonics
- (b) $\varphi = 270^\circ$, $\Delta = 0.2$, $m = 0.5$
- (c) $\varphi = 270^\circ$, $\Delta = 0.5$, $m = 0.5$
- (d) $\varphi = 270^\circ$, $\Delta = 0.7$, $m = 0.5$

Similar variations in amplitude as those described above for synchronous oscillations were seen experimentally for the frequency spectra from the pick-up coil signal. This implies that the synchronous oscillation amplitude components at the satellite frequencies were as large or larger than the corresponding amplitudes of the moving striations. Such is the case in Fig.4.18(a) for the lower satellite frequency where the amplitude of the synchronous oscillation A_{SS} is larger than the amplitude of the travelling wave component at the same frequency B_{TS} :-

$$\frac{\text{Amplitude Synch. Osc. at Satellite Frequency}}{\text{Amplitude Travelling Wave at Satellite Frequency}} = \frac{A_{SS}}{B_{TS}} = 1.3.$$

For the fundamental frequency the relative amplitude of the synchronous C_{SF} and the travelling wave D_{TF} is given by

$$\frac{\text{Amplitude Synch. Osc. at Fund. Frequency}}{\text{Amplitude Travelling Wave at Fund. Frequency}} = \frac{C_{SF}}{D_{TF}} = \frac{1}{7}.$$

Rearranging the above expressions gives

$$\frac{B_{TS}}{D_{TF}} = \frac{A_{SS}}{9C_{SF}} \quad \dots (7.8)$$

An alternative expression for the ratio of the travelling wave amplitudes at the satellite and fundamental frequencies is given by

$$\frac{B_{TS}}{D_{TF}} = \frac{J_1(\Delta)}{J_0(\Delta)} \quad \dots (7.9)$$

derived from the expansion of $\sin(\omega t - kx + \Delta \sin(pt - \beta x))$, see section 6.4.1.

By using limits for A_{SS}/C_{SF} obtained from Fig.7.2, the value of Δ and hence the extent of the velocity modulation can be estimated. Taking

$$\frac{1}{3} \leq \frac{A_{SS}}{C_{SF}} \leq \frac{2}{3}$$

then

$$\frac{1}{27} \leq \frac{B_{TS}}{D_{TF}} = \frac{J_1(\Delta)}{J_0(\Delta)} \leq \frac{2}{27}$$

which gives $0.05 \leq \Delta \leq 0.15$.

The values for Δ give a velocity modulation between 5 to 15% which is consistent with the view that the interaction is due to 'intermediate' nonlinear effects rather than fully developed turbulence.

The corresponding amplitudes for the coupling of Fig.4.18(c) are:

$$\frac{A_{SS}}{B_{TS}} \approx 1.7, \quad \frac{C_{SF}}{D_{TF}} \approx 0.5 \quad \text{and} \quad \frac{C_{SF}}{A_{SS}} \approx 2,$$

to give

$$\frac{D_{TF}}{B_{TS}} \approx 7 = \frac{J_0(3\Delta)}{J_1(\Delta)}$$

resulting in $\Delta \sim 0.1$.

In the above examples for the variation of the coil signal, the amplitude of the synchronous oscillation at the lower satellite frequency was less than twice as large as the amplitude of the corresponding travelling wave. Consequently the depth of modulation in the standing wave pattern - the difference between the maximum and minimum values divided by the mean value - was pronounced as Fig.4.18 shows.

(c) Amplitude variation of the photomultiplier signal

The lack of spatial amplitude variation for the photomultiplier signal may be understood using the arguments of the previous section. For the same velocity variation and relative amplitude of the synchronous oscillations at the satellite and fundamental frequencies as for the coil signal, the ratio of the amplitudes of the travelling wave and the synchronous oscillation at the lower satellite frequency is given by

$$\frac{B_{TS}}{A_{SS}} = \frac{2}{7} \frac{D_{TF}}{C_{SF}} \quad \dots (7.10)$$

where the symbols have the same meaning as before but now refer to the photomultiplier signal.

An indication of the value of the ratio D_{TF}/C_{SF} may be obtained from the results of Chapter IV where the computed and experimental wave patterns showed that $D_{TF}/C_{SF} \approx 5$ when the amplitude of the synchronous

oscillation as measured with coil was about five times larger than the corresponding amplitude of the travelling wave, that is,

$$\frac{D_{TF}}{C_{SF}} (\text{coil}) \approx \frac{1}{5} .$$

For the examples of mode-coupling given in section 7.4.2(b) the ratio

$$\frac{D_{TF}}{C_{SF}} (\text{coil}) > 1 :$$

the travelling wave had a larger amplitude than the synchronous oscillation. Since the photomultiplier signal is proportional, approximately, to the coil signal (section 4.2.5) the ratio D_{TF}/C_{SF} (photomultiplier) is proportional to D_{TF}/C_{SF} (coil) and will be greater than five in this case.

In Chapter IV it was seen that the above ratio

$$\frac{\text{Amplitude of the travelling wave for the fund. freq. } (D_{TF})}{\text{Amplitude of the Synchronous for the fund. frequency } (C_{SF})}$$

is equal to Ak/m where k is the wave number, A and m are quantities related to the coil signal and represent the amplitude of the travelling wave and the space dependent part of the amplitude of the synchronous oscillation respectively.

In Fig.4.18(a) there is little variation in the minimum values of the amplitude of the wave pattern at the fundamental frequency which implies that $m \ll 1$ and so $Ak/m \gg 1$ leading to D_{TF}/C_{SF} (photomultiplier) $\gg 1$ and B_{TS}/A_{SS} (photomultiplier) $\gg 1$. Consequently the depth of the wave pattern, for the satellite frequency, obtained from the photomultiplier signal and equal to $2A_{SS}/B_{TS}$ will be relatively small compared to that for the coil signal. The reason why the amplitude variation was more easily detected with the coil is thus explained.

(d) Space-time display for the argon discharge

As mentioned in Chapter III, the light intensity from the argon discharge was insufficient to record the space-time display photographically; this was one of the motivations for making use of the interference with the synchronous oscillations. However, subsequent to the experiments described in this work, observations were made on an argon discharge of the same dimensions by the author, while at the Institute of Physics Prague. The tube was filled with spectroscopically pure argon at a pressure of 0.3 torr and then sealed.

Using a rotating-mirror, the space-time picture of the discharge could be seen by eye. Two ionization waves of different frequencies and wavenumbers corresponding to the waves of frequency ranges (a) and (b) were seen. The synchronous oscillations were absent as there was no large condenser in parallel with the discharge and the operational current range of the tube was only 20-60 mA owing to problems with the cathode. As the current was increased, linear interference was seen near the cathode and then progressing from the anode, velocity modulation of one wave by the other similar to Fig.6.3 was seen.

Although these visual observations cannot be directly related to the main results of the present work, they do add support to the proposed interpretation.

(e) Modulation by the externally applied voltage

The spatial variation in amplitude of the satellite frequencies when an external voltage was applied to modulate the self-excited waves in frequency range (b) cannot be explained in exactly the same way as for the purely self-excited case. When the frequency of the exciting voltage was in range (a) the spacing between maxima at the satellite frequencies was equal to that of the corresponding frequency component of the self excited waves in range (b).

If in equations (6.8) $m=0$, $\beta=0$, then the required spacings are found. This form of modulation requires the moving striation to be velocity modulated by a time dependent term only, rather than by a travelling wave type of expression. This form of velocity modulation has already been seen when the applied frequency of the applied voltage was equal to the striation frequency (Chapter V).

The effect of the exciting voltage applied to the anode is to modulate the velocity of the self-excited waves in frequency range (b) and to generate synchronous oscillations and travelling waves at the applied frequency. The amplitude of the travelling waves excited at the applied frequency is insufficient to influence the motion of the moving striations in contrast to the equivalent coupling between purely self-excited waves. This difference may be due to the fact that the externally excited travelling waves in frequency range (a) were generated outside the current-pressure regime for self-excitation, and so it is to be expected that they would be damped and of relatively small amplitude compared to the synchronous oscillations which were excited close to the resonant frequency for the discharge.

7.4.3 Interaction Between the Self-Excited Waves in Frequency Ranges (b) and (c)

The travelling waves in frequency range (c) were not accompanied by synchronous oscillations and so the preceding explanations of the wave patterns of the satellite frequencies in terms of interference between synchronous and travelling wave components is not applicable.

However, simultaneous amplitude and velocity modulation of the waves in range (c), by the travelling waves and synchronous oscillations of frequency range (b) give the required spectra and amplitude variation. Such an interaction may be represented in its most general form by:

$$\left[A + \sum_{n=1}^N B_n \sin n\omega t + C_n \sin(n\omega t - nkx) \right] \cos \left[\alpha t - \beta x + \sum_{n=1}^N m_n \sin n\omega t + m'_n \sin(n\omega t - nkx) \right] \dots (7.11)$$

The term $\sum_{n=1}^N m_n \sin n\omega t$ within the phase expression for the wave can refer to either the synchronous oscillations within the discharge or the anode voltage variations. The results of earlier sections have shown that synchronous oscillations and travelling waves do not appear to interact nonlinearly. For the present results to be consistent with this view requires that $B_N = 0$ and that the term $\sum_{n=1}^N m_n \sin n\omega t$ refers to the anode voltage oscillations which generate the synchronous oscillations rather than the synchronous oscillations within the discharge. This is similar to the situation seen in the previous section.

The travelling wave expression cannot appear in both the phase and amplitude of the wave since the nonlinear interaction would need to be of the third order in the perturbed quantities, that is, proportional to $(n^{(1)})^3$ where $n^{(1)}$ is the perturbed charged particle density, and as will be seen in Chapter VIII the nonlinear interactions are of only the second order.

So, the interaction may be expressed as

$$\left[A + \sum_{n=1}^N C_n \sin(n\omega t - nkx) \right] \cos \left[\alpha t - \beta x + \sum_{n=1}^N m_n \sin n\omega t \right] \dots (7.12)$$

or

$$A \cos \left[\alpha t - \beta x + \sum_{n=1}^N m_n \sin n\omega t + m'_n \sin(n\omega t - nkx) \right], \dots (7.13)$$

Expression (7.12) represents velocity modulation of the wave in range (c) with virtual wave generation, while expression (7.13) represents velocity modulation of the wave by the anode voltage changes and the travelling wave.

Both expressions will give the desired amplitude variation for the frequency components $\alpha \pm n\omega$, $n = 1, 2, 3, \dots$, namely:

$$\sqrt{E_N^2 + F_N^2} \mp 2E_N F_N \sin nkx \quad \dots (7.14)$$

for $m_n, m_n' < 1$, where the constants E_N and F_N are determined from the expansions of (7.12) and (7.13) and involve Bessel functions of the first kind. For the frequency components $\alpha - \omega$, $\alpha + \omega$, for example, there is a phase lag between the peak values of amplitude in agreement with the experimental values.

As mentioned at the beginning of section (7.4), of the two mechanisms, virtual wave excitation or velocity modulation, the latter is the more likely and so equation (7.13) is to be preferred to (7.12).

7.4.4 Conclusion

Owing to the presence of the synchronous oscillations and their nonlinear modulation it has been possible to interpret the nonlinear interactions between the travelling wave striations as due to velocity modulation.

The expressions used to describe the interactions predicted the discrete line spectrum and showed that the velocity modulation was relatively small, in keeping with the interpretation that the effects are not due to fully developed turbulence. In general when nonlinear striations are not stabilized, the initial nonlinear mode coupling will degenerate into irregular motion as the results of Chapter X will show.

A physical picture which describes the behaviour of the striations when the nonlinear effects are not fully developed will now be described.

7.5 PHYSICAL MODEL FOR WAVE-COUPLING

The 'collision' of striations can produce amplitude and velocity modulation, see Chapter II.

The most nonlinear waves in the discharge were the striations of frequency range (b). The velocity of these waves was an order of magnitude larger than that for the waves of range (a) and several times larger

than the velocity of the waves of range (c). So, it was possible for a faster striation to catch up with a slower wave and 'collide' with it. This kind of collision differs from that described by Grabec for the case of only one wave type. For this latter case the average velocity of each striation is equal and the striations are deflected rather than actually colliding when they encounter each other.

For the present results, since one wave was inherently faster, it would overtake the slower striation and actually 'pass through it'. The problem arises as to what would actually happen in this interaction region. The effect of such a collision would depend on the degree to which the two waves were nonlinear: the extent of their double structure, that is, the variation of electron temperature and density through each wave. If the decrease in electron temperature of the faster striation upon approaching the region of the minimum electron temperature in the slower wave was not too large, then the corresponding amplitude or velocity changes would not be so large and a regular space-time pattern could still be retained.

In the qualitatively similar case of the collision of ion acoustic solitons such a situation exists⁽⁷⁰⁾. For solitons travelling in the same direction the interaction is repulsive and the collision process resembles that described by Grabec for striations. Solitons travelling in opposite directions interact 'attractively' and cross one another and collide. Despite the fact that the interaction is a highly nonlinear process, the solitons take on precisely their old shape after colliding. Such collisions have been observed experimentally⁽⁷¹⁾. The idea of striations retaining their 'identity' is further supported by the view that nonlinear striations can be approximately treated as particles⁽²⁴⁾.

So, the coupling in the argon discharge was intermediate between the linear case, where the striations could co-exist at the same point to produce linear interference and the turbulent nonlinear case where

destruction and creation of striations could occur. The effect of one striation upon the other was sufficient to modulate but not annihilate.

Another way of looking at this modulation is as a form of 'Luxembourg Effect'. When a striation travels through the discharge its velocity is characterised by the properties of the discharge medium. When the medium is homogeneous the velocity is uniform. If the medium is inhomogeneous then it is to be expected that the velocity may change. The presence of a second oscillation, not necessarily a striation, changes the properties of the discharge sufficiently so that the striation now sees a non-uniform discharge and its velocity is changed accordingly.

As with the Luxembourg effect, the wave perturbing the medium can be localised and so need not exist throughout the tube. For example the perturbation could be provided by anode fluctuations or changes occurring at the boundary between two wave types.

The modulational effects described for the moving striations above will be obtained from a modified form of the Pekarek equation for striations, in the next chapter.

CHAPTER VIII

THE EXTENSION OF LINEAR THEORY TO DESCRIBE NONLINEAR EFFECTS

8.1 INTRODUCTION

By retaining nonlinear terms in the diffusion equation for ionization waves, expressions will be derived which describe some of the 'intermediate' nonlinear effects seen in previous chapters.

The basic equation is just the ambipolar diffusion equation for the charged particles with the addition of an ionization term given by:

$$\left[Z(\theta_0 + \Delta\theta) - Z(\theta_0) \right] N \quad \dots (8.1)$$

where $Z \approx \text{constant} \times \exp - \frac{V_i}{\theta_0}$ is the number of ionizing collisions per second for an electron temperature θ_0 (eV) and ionization potential V_i (volts); $\Delta\theta$ is the change in electron temperature, and N is the charged particle density ($N = N_i = N_e$).

Owing to the exponential dependence of Z on electron temperature, the ionization term is nonlinear for large enough deviations in electron temperature.

Grabec⁽⁵⁵⁾, solved the diffusion equation taking full account of the nonlinear ionization term. His results for argon predicted the broad turbulent spectrum and irregular motion of the striations.

By using the first nonlinear term from a series expansion of Z , expressions will be obtained which predict discrete multiline spectra of the form seen in the argon discharge and in the initial evolution of the mode-coupling in the neon discharge, see Chapter X.

The results describe the intermediate state of the striations when their amplitude is large enough for the linearised theory to be inadequate, but not large enough to warrant the use of the full nonlinear equation.

8.2 EXTENSION OF THE LINEAR EQUATION

The ionization term may be expanded in a Taylor series:

$$\left[Z(\theta_0 + \Delta\theta) - Z(\theta_0) \right] N = \left[\underbrace{Z' \Delta\theta}_A + \underbrace{\frac{Z''(\Delta\theta)^2}{2!}}_B + \underbrace{\frac{Z'''(\Delta\theta)^3}{3!}}_C \dots \right] (N_0 + n), \quad \dots (8.2)$$

where N_0, θ_0 are the charged particle density and electron temperature of the uniform discharge; $\Delta\theta$ and n are the corresponding deviations,

$$Z' = \left. \frac{\partial Z}{\partial \theta} \right|_{\theta=\theta_0}, \quad Z'' = \left. \frac{\partial^2 Z}{\partial \theta^2} \right|_{\theta=\theta_0} = \left(\frac{V_i - 2\theta_0}{\theta_0^2} \right) Z'$$

$$Z''' = \left[\left(\frac{2\theta_0 - 2V_i}{\theta_0^3} \right) + \left(\frac{V_i - 2\theta_0}{\theta_0^2} \right)^2 \right] Z'.$$

The values of the terms A, B, C in equation (8.2) are shown in Table 8.1 for various values of $\Delta\theta/\theta_0$ for an argon discharge with $\theta_0 = 3$ eV and $V_i = 15.8$ eV. The expressions for Z, Z', Z''' etc, assume that the electron gas has a Maxwellian distribution function.

TABLE 8.1

RELATIVE VALUES OF THE COEFFICIENTS IN THE EXPANSION OF Z

$\frac{\Delta\theta}{\theta_0}$	A	B	C
	in units of Z'		
0.05	0.15	0.012	0
0.1	0.3	0.049	0.0025
0.2	0.6	0.196	0.02
0.25	0.75	0.306	0.039
0.3	0.9	0.54	0.0675
0.4	1.2	0.8	0.16
0.5	1.5	1.22	0.312

It can be seen that for $\frac{\Delta\theta}{\theta_0} \leq 0.1$, only the term A, which gives the linear term $Z' \Delta\theta N_0$, need be retained. According to Grabec⁽²³⁾, non-linear effects become operative when $\frac{\Delta\theta}{\theta_0} \approx \frac{\theta_0}{V_i} = 0.19$, in the present case.

For the purposes of the present work only the first nonlinear term $Z' n \Delta\theta$ will be included in the otherwise linear equation. The next nonlinear term $\frac{Z''(\Delta\theta)^2}{2} N_0$ will give rise to similar effects as the first term since they are both of the same order in the perturbed parameters, and $\Delta\theta$ is proportional to n . As only a qualitative description is sought, the term $\frac{Z''(\Delta\theta^2)}{2} N_0$ is not included.

The equation to be considered is

$$\frac{\partial N}{\partial t} = \frac{D_a}{\partial x^2} \frac{\partial^2 N}{\partial x^2} + Z' \Delta\theta N_0 + Z' \Delta\theta n \quad \dots (8.3)$$

which is just the linear equation for ionization waves plus the nonlinear term $Z' \Delta\theta n$. As defined earlier, section 2.4.1, D_a is the ambipolar diffusion coefficient and x is the distance as measured from the anode. The other symbols have been given above.

Such a simple extension of the linear equation cannot be used to describe the nonlinear evolution of a self excited wave. In such a case the spatial amplification coefficient α is of the order of 0.1, which means that the values of $\Delta\theta$ and n proportional to $\exp \alpha x$ will increase rapidly in the cathode to anode direction as Table 8.2 shows.

TABLE 8.2
VALUE OF $\exp \alpha x$ FOR VALUES OF α (POSITIVE
BECAUSE x IS MEASURED FROM CATHODE TO ANODE

Amplification Coefficient α	Distance from Cathode x cms					
	10	20	30	40	50	
0.001	1.01	1.02	1.03	1.04	1.05	} $\exp \alpha x$
0.01	1.1	1.22	1.34	1.49	1.64	
0.1	2.7	7.38	20	54		

The theory can only describe those situations where $\Delta\theta$ and n remain relatively small as may be the case for the early development of the nonlinear effects or when the nonlinear waves have been full stabilized and their values of $\Delta\theta$ and n effectively lowered.

8.3 GENERATION OF HARMONIC TERMS

It can easily be seen how harmonics of the fundamental wave may arise if a series solution for N and θ is assumed, that is:

$$\begin{aligned} N &= N_0 + n^{(1)}(x,t) + n^{(2)}(x,t) + n^{(3)}(x,t) \dots n^{(N)}(x,t) \\ \theta &= \theta_0 + \theta^{(1)}(x,t) + \theta^{(2)}(x,t) + \theta^{(3)}(x,t) \dots \theta^{(N)}(x,t) \dots \end{aligned} \quad (8.4)$$

where N_0 and θ_0 are the steady state values and $n^{(N)}(x,t)$ and $\theta^{(N)}(x,t)$ are the N^{th} order perturbations.

Substituting expressions (8.4) into equation (8.3) gives the first order equation:

$$\frac{\partial n^{(1)}(x,t)}{\partial t} - D_A \frac{\partial^2 n^{(1)}(x,t)}{\partial x^2} = Z' \theta^{(1)}(x,t) N_0 \dots \quad (8.5)$$

It is now assumed that $n^{(1)}(x,t)$ and $\theta^{(1)}(x,t)$ are the parameters of the fundamental wave and that

$$n^{(1)}(x,t) = n_1 e^{\alpha x} \sin(\omega t - kx) \dots \quad (8.6)$$

Inspection of (8.5) shows that $\theta^{(1)}(x,t)$ will vary as

$$\theta^{(1)}(x,t) = \theta_1 e^{\alpha x} \sin(\omega t - kx + \varphi) \dots \quad (8.7)$$

where

$$\tan \varphi = \frac{\omega + 2\alpha k D_A}{D_A(k^2 - \alpha^2)} \dots \quad (8.8)$$

$$\theta_1 = \frac{n_1}{N_0 Z'} \left[(\alpha^2 + k^2)^2 D_A^2 + \omega(4\alpha k D_A + \omega) \right]^{-\frac{1}{2}} \dots \quad (8.9)$$

The second order equation is:

$$\frac{\partial n^{(2)}(x,t)}{\partial t} - D_A \frac{\partial^2 n^{(2)}(x,t)}{\partial x^2} - Z' \theta^{(2)}(x,t) N_0 = Z' \theta^{(1)}(x,t) n^{(1)}(x,t) \dots \quad (8.10)$$

The right-hand-side of equation (9.12) acts as a source term which, due to the product $n^{(1)}(x,t) \theta^{(1)}(x,t)$ is proportional to

$$e^{2\alpha x} \left[\cos \varphi - \cos(2\omega t - 2kx + \varphi) \right] .$$

For the equation to be satisfied $\theta^{(2)}(x,t)$ must be proportional to

$$e^{2\alpha x} [\cos \varphi - \cos(2\omega t - 2kx + \varphi)]$$

whilst $n^{(2)}(x,t)$ will be proportional to $e^{2\alpha x} \cos(2\omega t - 2kx + \varphi + \beta)$ where β is the phase difference between $\theta^{(2)}(x,t)$ and $n^{(2)}(x,t)$. Thus, the first harmonic in particle density and electron temperature is generated. Higher order equations will give rise to source terms proportional to

$$\theta^{(2)}(x,t) n^{(1)}(x,t), \theta^{(1)}(x,t) n^{(2)}(x,t), \theta^{(3)}(x,t) n^{(1)}(x,t)$$

which will produce higher harmonics of the fundamental frequency. These equations show how the harmonics are generated; the full expansion for Z must be used to derive the complete set of harmonics.

8.4 RELATIVE VALUES OF ELECTRON DENSITY AND TEMPERATURE

It is useful to obtain some estimate of the relative values of $\frac{\theta_1}{\theta_0}$ for values of $\frac{n_1}{N_0}$ so that the magnitude of the nonlinear terms can be found. From equation (8.9) for $\alpha \ll 1, k < 1$ and $D_a \leq \omega$, θ_1 is given by

$$\theta_1 \approx \frac{n_1 \omega}{N_0 Z'} \quad \dots (8.11)$$

Von Engel's expressions⁽⁶⁵⁾ for Z and $\exp \frac{V_i}{\theta_0}$ give:

$$\frac{1}{Z' \theta_0} = \frac{(1.2)(cR)^2 p}{9 A_z V_I^{\frac{3}{2}}} \quad \dots (8.12)$$

where R is the radius of the tube, in cms, p is the gas pressure in torr, A_z and c are constants which for argon are equal to 71.10^{-2} and 4.10^{-2} respectively.

Substituting the above values and expression gives

$$\frac{\theta_1}{\theta_0} = \frac{n_1}{n_0} 3.10^{-5} \omega p \quad \dots (8.13)$$

The relative values of θ_1/θ_0 and n_1/n_0 for the striations in frequency range (b) at 0.3 torr and $\omega = 2\pi \cdot 4.10^3$ rad/sec are shown in Table 8.3:

TABLE 8.3
RELATIVE VALUES OF ELECTRON TEMPERATURE AND DENSITY FOR
THE STRIATIONS IN FREQUENCY RANGE (b)

$\frac{\theta_1}{\theta_0}$	$\frac{n_1}{n_0}$
0.002	0.0088
0.01	0.044
0.02	0.088
0.1	0.44
0.15	0.665
0.2	0.88
0.3	1.32
0.4	1.76

8.5 NONLINEAR INTERACTIONS BETWEEN TWO WAVES

If one considers the simultaneous occurrence of two waves, then it is to be expected that the nonlinear term in equation (8.3) will generate, in addition to the harmonics of each wave, new frequencies and wavenumbers due to the cross-products of the terms representing the two fundamental waves.

Representing the changes in the electron temperature and density for the fundamental of each wave by $\theta_1(x,t)$, $n_1(x,t)$ and $\theta_2(x,t)$, $n_2(x,t)$ respectively, equation (8.3) becomes:

$$\begin{aligned} \frac{\partial n_1(x,t)}{\partial t} + \frac{\partial n_2(x,t)}{\partial t} = D_a \frac{\partial^2 n_1(x,t)}{\partial x^2} + Z' N_0 \theta_1(x,t) \\ + Z' n_1(x,t) \theta_1(x,t) + Z' \theta_2(x,t) n_1(x,t) \\ + D_a \frac{\partial^2 n_2(x,t)}{\partial x^2} + Z' N_0 \theta_2(x,t) + Z' n_2(x,t) \theta_2(x,t) \\ + Z' \theta_1(x,t) n_2(x,t). \end{aligned} \dots (8.14)$$

For small amplitude waves the nonlinear terms can be neglected and equation (8.14) represents the addition of two separate diffusion equations which describe the waves $n_1(x,t)$ and $n_2(x,t)$ respectively. When the nonlinear effects are operative the two equations become coupled.

The nonlinear terms in equation (8.14) can be related to the physical model discussed in Chapter VII. The term $Z'\theta_2(x,t) n_1(x,t)$ expresses the influence on wave 1 of the perturbation in ionization, due to wave 2, while the term $Z'\theta_1(x,t) n_2(x,t)$ describes the corresponding effect of wave 1 on wave 2. The coupling of the equations shows that there is a mutual interaction between the two waves. Ignoring the term $Z'\theta_1(x,t) n_1(x,t)$ which will produce the first harmonic of wave 1, the equation for $n_1(x,t)$ is:

$$\frac{\partial n_1(x,t)}{\partial t} = D_a \frac{\partial^2 n_1(x,t)}{\partial x^2} + Z'N_0 \theta_1(x,t) + Z'\theta_2(x,t) n_1(x,t). \dots (8.15)$$

8.6 NONLINEAR INTERACTIONS : VIRTUAL WAVES

One solution of equation (8.15) can be found if the fundamental components for $n_1(x,t)$ and $\theta_2(x,t)$ are represented by

$$\begin{aligned} n_1(x,t) &= n_1 \sin(\omega t - kx) \\ \theta_2(x,t) &= \theta_2 \cos(p t - \beta x) \end{aligned} \dots (8.16)$$

The nonlinear term acts as a forcing term to produce virtual waves at frequencies $\omega \pm p$ and wavenumbers $k \pm \beta$. The term 'virtual' is used in the sense that $\omega \pm p$ and $k \pm \beta$ are not related through a dispersion relation. As noted in Chapter VII, such waves are not due to a resonant interaction.

For the virtual waves to propagate the discharge must oscillate at unnatural modes $\omega \pm p$, $k \pm \beta$ which do not lie on either of the dispersion curves for the fundamental waves. The discharge will be unstable and frequency jumping may result⁽³¹⁾. The virtual waves will be damped at a rate appropriate for an ionization wave at the frequencies $\omega \pm p$.

In the next section it will be shown how the discharge can accommodate the two waves in such a way that the resulting changes in frequency and wavenumber are relatively small enabling the waves to propagate at frequencies and wavenumbers close to the optimum values.

In so far as the harmonics of the fundamental frequency do not lie on the dispersion curve for the self-excited waves, they are virtual waves. Yet they differ from the waves described above in that the discharge often remains stable when harmonic frequencies are present, and the harmonics are of large amplitude rather than damped waves.

These differences may be related to the fact that the harmonics travel with the same velocity as the fundamental wave and may be thought of as lying on virtual dispersion curves of the form:

$$(\omega_n)(kn) = n^2 C \quad , \quad \alpha_n = n\alpha \quad \dots (8.17)$$

where ω_n , kn and α_n are the frequency, wavenumber and amplification coefficient of the n^{th} harmonic, and $\omega k = C$ is the dispersion relation for the fundamental wave which has an amplification coefficient α .

When the harmonics have grown sufficiently, they can lead to an unstable discharge due to the generation of waves at harmonics of the wave-number or frequency which lie on the original dispersion curve, (A2).

8.7 NONLINEAR INTERACTIONS: PHASE MODULATION

If two waves can interact nonlinearly so that their resultant wave-numbers and frequencies are only slightly changed, then the discharge will be more stable than for the excitation of virtual waves. Such an interaction may be achieved if the effect of the waves is to phase modulate each other. This form of modulation is equivalent to velocity modulation and is consistent with the interpretation of the experimental results in argon.

The effects may be derived as follows. In equation (8.15) let

$$n_1(x,t) = n_1 \sin U \quad , \quad \theta_1(x,t) = \theta_1 \sin (U + \varphi) \quad \dots (8.18)$$

where

$$U = \omega_0 t - k_0 x + \Delta_1 \cos (p_0 t - \beta_0 x + \alpha_1) \quad *$$

is the phase of wave 1 which is modulated by an expression proportional to

* Here α_1 is used to denote a phase angle.

the unmodulated expression for wave 2. The value of θ_1 is equal to its unmodulated value. The generalised expressions for the frequency and wave-number are given by

$$\omega = \frac{\partial U}{\partial t} = \omega_0 - \Delta_1 p_0 \sin(p_0 t - \beta_0 x + \alpha_1)$$

and

$$k = -\frac{\partial U}{\partial x} = k_0 - \Delta_1 \beta_0 \sin(p_0 t - \beta_0 x + \alpha_1) \quad \dots (8.19)$$

Substituting equation (8.18) into equation (8.15) gives:

$$n_1 \cos U \left[\omega_0 - \Delta_1 p_0 \sin(p_0 t + \alpha_1 - \beta x) \right]$$

$$= -D_a \sin U k_0^2 + Z' N_0 \theta_1 \sin(U + \varphi)$$

$$+ Z' n_1 \sin U \theta_2(x, t) \quad \dots (8.20)$$

where for simplicity the value of k in the term

$$D_a \frac{\partial^2 n_1(x, t)}{\partial x^2}$$

has been put equal to k_0 . This is justified on the grounds that Δ_1 is assumed to be < 1 and that the characteristics of the ionization wave are determined by the ionization term. The omission of the full expression for k does not alter the results qualitatively.

Since a mutual interaction takes place, the corresponding expressions for wave 2 are:

$$n_2(x, t) = n_2 \cos(p_0 t - \beta_0 x + \Delta_2 \cos(\omega_0 t - k_0 x + \alpha_2))$$

$$\theta_2(x, t) = \theta_2 \cos(p_0 t - \beta_0 x + \Delta_2 \cos(\omega_0 t - k_0 x + \alpha_2) + \eta) \quad \dots (8.21)$$

Assuming that Δ_2 is small, $\theta_2(x, t)$ can be represented in equation (8.20) by its unmodulated form.

For the assumed solutions to be satisfied, like temporal terms on the right and left-hand-sides, must be equal. For the frequency ω_0 the condition reduces to the linear equation, while for the frequencies $\omega_0 \pm p_0$ the equations lead to values for Δ_1 and α_1 . Using equation (8.11) for θ_2 leads to

$$\Delta_1 = \frac{n_2}{N_0}, \quad \tan \alpha_1 = \tan \eta \quad \dots (8.22)$$

In the same way the equation for $n_2(x,t)$ gives

$$\Delta_2 = \frac{n_1}{N_0}, \quad \alpha_2 = \varphi - \frac{\pi}{2} \quad \dots (8.23)$$

The physical quantities which were measured for the waves in argon were the oscillating components of the emitted light intensity and the electric potential which are proportional to the changes in ionization rate and electron temperature respectively. Therefore, the emitted light intensity will be proportional to $Z'N_0\theta_1$, and $Z'n_1\theta_2$ for wave 1. The relative magnitudes are given by:

$$\begin{aligned} |Z'\theta_1 N_0| &= |\omega_0 n_1| \\ |Z'\theta_2 n_1| &= \left| p_0 \frac{n_2}{N_0} n_1 \right| \quad \dots (8.24) \\ |\theta_1| &= \left| \frac{n_1 \omega_0}{N_0 Z'} \right| \end{aligned}$$

for wave 1, and for wave 2

$$\begin{aligned} |Z'\theta_2 N_0| &= |p_0 n_2| \\ |Z'\theta_1 n_2| &= \left| \omega_0 \frac{n_1}{N_0} n_2 \right| \quad \dots (8.25) \\ |\theta_2| &= \left| \frac{n_2 p_0}{N_0 Z'} \right| \end{aligned}$$

If wave 1 is taken as the striation in frequency range (b), and wave 2 as the wave in frequency range (a), then $\omega_0 \approx 6 p_0$ and $n_1 > n_2$. The expressions for wave 1 will be larger than those for wave 2.

In the experimental studies however, the signals proportional to the electric potential were Fourier analysed and the components at the satellite frequencies $\omega \pm p$ observed. The magnitudes of the amplitudes of $\theta_1(x,t)$ and $\theta_2(x,t)$ at frequencies $\omega \pm p$ are given by

$$A_1 = |\text{Amplitude of } \theta_1| = \left| \frac{n_1}{N_0} \frac{\omega_0}{Z'} J_1(\Delta_1) \right| \quad \dots (8.26)$$

$$A_2 = |\text{Amplitude of } \theta_2| = \left| \frac{n_2}{N_0} \frac{p_0}{Z'} J_1(\Delta_2) \right| \quad \dots (8.27)$$

An order of magnitude estimate with $\Delta_1 = 0.1$ and $\Delta_2 = 0.6$ gives:

$$A_1 = \left| \frac{0.6 \times 6 p_0}{Z'} 0.05 \right| = \frac{6.0 \times 0.03 p_0}{Z'} \quad \dots (8.28)$$

$$A_2 = \left| \frac{p_0}{Z'} 0.1 \times 0.3 \right| = \frac{0.03 p_0}{Z'} \quad \dots (8.29)$$

which means that the modulation of wave 1, the striation in frequency range b , gives the larger terms at the satellite frequencies in accord with the interpretation of the results in Chapter VII, where a value of $\Delta_1 = 0.1$ was found. The value of Δ_2 was taken as an upper limit.

For wave 1 the frequency and wavenumber are given by:

$$\omega = \omega_0 + \Delta_1 p_0 \sin(p_0 t - \beta_0 x + \alpha_1) \quad \dots (8.30)$$

$$k = k_0 + \Delta_1 \beta_0 \sin(p_0 t - \beta_0 x + \alpha_1)$$

which since $\Delta_1 \approx 0.1$ remain close to the unmodulated values ω_0 , k_0 and the wave suffers no additional damping.

The corresponding frequency and wavenumber for wave 2 are given by:

$$p = p_0 + \Delta_2 \omega_0 \sin(\omega_0 t - k_0 x + \alpha_2) \quad \dots (8.31)$$

$$\beta = \beta_0 + \Delta_2 k_0 \sin(\omega_0 t - k_0 x + \alpha_2)$$

Since $\omega_0 \approx 6 p_0$, the deviation of p from p_0 will be considerable even for moderate values of Δ_2 . As the frequency p begins to deviate, the damping terms appropriate to ionization waves at the frequency p will come into play. Since the waves at frequency p_0 are observed, despite the damping, the net effect of the latter must be to keep p and β closer to p_0 and β_0 than the above expressions suggest.

If in the above derivation the amplification of the waves had been included, then the Δ 's would have been proportional to $\exp \alpha x$.^{*} This shows that the changes in the frequency and wavenumber would increase with distance from the cathode and for large enough changes might lead to an unstable discharge.

* This α is not to be confused with α_1, α_2 which are phase angles.

It should be remembered that for argon the theory derived above is qualitative. More complete expressions which, however, would tend to obscure the physical picture of the interactions, would be required in order to obtain quantitative results.

The expressions derived in this chapter deal only with the striations (phase velocity) rather than the 'stratification wave' (group velocity) and so give no insight into anode-directed disturbances. By including an equation to describe the continuity of 'wave energy' it will be seen in the following chapter how such disturbances may arise.

CHAPTER IX
VARIATIONAL METHODS AND THEIR APPLICATIONS
TO IONIZATION WAVES

9.1 INTRODUCTION

A novel approach in predicting the nonlinear behaviour of ionization waves is to use the variational methods developed principally by Whitham to determine the propagation of nonlinear water waves (75). This approach is suggested by the fact that water waves and striations often exhibit similar features. For example, the turbulent state of the positive column due to random ionization waves, is similar to the case of nonlinear Stokes waves.

The results obtained give information on the motion of the striations and are similar to those obtained from the computations of Grabec.

9.2 GENERAL THEORY

For a conservative system the most simple travelling wave solution is of the form:

$$u = a e^{i\theta}$$

where

$$\theta = kx - \omega t + \alpha$$

and

$$\frac{\partial \theta}{\partial x} = k, \quad \frac{\partial \theta}{\partial t} = -\omega$$

and the amplitude a , frequency ω , and wavenumber k , are constant. A dispersion relation of the form $\omega = \omega(k)$ relates ω and k . The group velocity $\partial\omega/\partial k$ is the propagation velocity of the wave energy, and the phase velocity ω/k is the velocity at which a particular crest travels. A continuity equation for the conservation of wave 'crests' is given by

$$\frac{\partial k}{\partial t} + \frac{\partial \omega}{\partial x} = 0 \quad \dots (9.1)$$

assuming that waves are not created or destroyed.

The aim of Whitham's analysis was to obtain equations describing the motion in the case where a, ω, k vary slowly in time and space, that is over one time or space period the changes in a, ω, k are relatively

small. In this case ω and k are defined in the same way and the dispersion relation is still satisfied.

Whitham's method consists of using the variational principle

$$\delta \iint L(u_t, u_x, u) dt dx = 0$$

from classical mechanics, where L is the Lagrange function and is equal to the kinetic energy minus the potential energy. The non-varying solution obtained is of the form

$$u = U(\theta)$$

where $\theta_x = k$, $\theta_t = -\omega$, $\theta = kx - \omega t - \alpha$ are constants and the solution $U(\theta)$ brings in another constant A which is equivalent to the amplitude, so that

$$L^{(0)} = L(-\omega U_\theta, k U_\theta, U) \quad \dots (9.2)$$

To find equations for ω, k, A when they are allowed to vary, an 'average Lagrangian' is used

$$\mathcal{L}(\omega, k, A) = \frac{1}{2\pi} \int_0^{2\pi} L(-\omega U_\theta, k U_\theta, U) d\theta \quad \dots (9.3)$$

in terms of the constant parameters ω, k, A . It is then assumed that the slowly varying functions ω, k, A satisfy the variational equations given by the 'averaged variational principle':

$$\delta \iint \mathcal{L}(\omega, k, A) = 0 \quad .$$

The variational equations are then

$$\delta A : \mathcal{L}_A = 0 \quad \dots (9.4)$$

$$\delta \theta : \frac{\partial}{\partial t} \mathcal{L}_\omega - \frac{\partial \mathcal{L}_k}{\partial x} = 0 \quad .$$

Further, from linear problems it is found that $\mathcal{L} = G(\omega, k)a^2$, where a is proportional to the amplitude, so that the above equations give:

$$G(\omega, k) = 0 \quad \dots (9.5)$$

and

$$\frac{\partial}{\partial t} (G_\omega a^2) - \frac{\partial}{\partial x} (G_k a^2) = 0 \quad \dots (9.6)$$

The first of these equations gives the dispersion relation for ω and k whilst the second expresses the conservation of wave action, and is an equation connecting ω , k and a .

Equation (9.6) can be put in the form:

$$\frac{\partial a^2}{\partial t} + \frac{\partial}{\partial x} \{C(k)a^2\} = 0 \quad \dots (9.7)$$

where $C(k)$ is the group velocity

$$\frac{\partial \omega}{\partial k} = - \frac{G_k}{G_\omega} .$$

9.3 NONLINEAR EFFECTS

To include nonlinear effects, additional terms must be added to the expression \mathcal{L} :

$$\mathcal{L} = G(\omega, k) a^2 + G_2(\omega, k) a^4 . \quad \dots (9.8)$$

This is equivalent to adding an amplitude dependent term in the dispersion relation

$$\omega = \omega_0(k) + \omega_2(k) a^2 \quad \dots (9.9)$$

where

$$\omega_2 = - \frac{2G_2(\omega_0, k)}{G_\omega(\omega_0, k)} .$$

These equations are valid for moderately small amplitudes and do not account for any higher order dispersive effects. The nonlinear equivalent of equation (9.1) is:

$$\frac{\partial k}{\partial t} + \omega'_0(k) \frac{\partial k}{\partial x} + \omega_2(k) \frac{\partial a^2}{\partial x} = 0 \quad \dots (9.10)$$

and the linear form of equation (9.7) is still used to give:

$$\frac{\partial a^2}{\partial t} + \omega'_0(k) \frac{\partial a^2}{\partial x} + \omega''_0(k) a^2 \frac{\partial k}{\partial x} = 0 . \quad \dots (9.11)$$

In these equations terms which would provide corrections of relative order a^2 have been omitted.

These two equations which are now coupled, may be solved by the method of characteristics (see Appendix A.1) to find the changes in k and a . These changes in a and k will propagate along paths defined by:

$$\frac{dx}{dt} = \omega'_0(k) \pm \left\{ \omega_2 \omega''_0(k) \right\}^{\frac{1}{2}} a \quad \dots (9.12)$$

and they are related in the following way:

$$\frac{1}{2} \left\{ \frac{\omega''_0(k)}{\omega_2(k)} \right\}^{\frac{1}{2}} dk \pm da = 0 \quad \dots (9.13)$$

For the linear case the equations give the usual result that k and a propagate with the group velocity.

9.4 APPLICATION TO IONIZATION WAVES

For backward ionization waves the expression for the dispersion relation $G(\omega, k)$ is given most simply by:

$$G(\omega, k) = \omega k - c = 0 \quad \dots (9.14)$$

where c is a constant. So $\omega'_0(k)$ is given by $-\frac{c}{k^2}$, i.e. $-\omega/k$ and $\omega''_0(k)$ is given by $\frac{2c}{k^3}$. In determining the sign of $\omega_2(k)$ it is necessary to appeal to experimental results and the computation work which show that ω decreases, that is ω_2 is negative, as nonlinear terms become effective. In this case it can be seen immediately from equation (9.12) that the velocity of propagation of the changes is complex, which implies that the wave train is unstable. In this case solutions for k and a must be found in the form:

$$\begin{aligned} k &= k_0 + k_1 e^{i\mu(x-CT)} \\ a &= a_0 + a_1 e^{i\mu(x-CT)} \end{aligned} \quad \dots (9.15)$$

and it is further found that C is just the characteristic velocity given by equation (9.12). So, a and k will be proportional to:

$$e^{\left(\omega_2 \omega''_0 \right)^{\frac{1}{2}} a t} e^{i\mu[x - \omega'_0(k)T]}$$

Changes in a and k will appear to move towards the anode with the group velocity, which in this case is equal to the phase velocity in magnitude.

The striation may be expressed as:

$$\left[a_0 + a_1 e^{\alpha t} \frac{\cos}{\sin} (\omega_1 t - \vec{k}_1 \cdot \vec{x}) \right] \frac{\cos}{\sin} \left[\omega_0 t - \vec{k}_0 \cdot \vec{x} + \beta e^{\alpha t} \frac{\cos}{\sin} (\omega_1 t - \vec{k}_1 \cdot \vec{x}) \right] \dots (9.16)$$

where

$$\left| \frac{\omega_1}{k_1} \right| = \left| \omega'_0 \right| .$$

So, a modulational instability is obtained in agreement with Grabec's results. Obviously as k and a grow in time, this simple analysis would break down since, for example, the terms neglected initially would have to be retained, and the generation of harmonics due to the growth and other stabilizing effects would have to be included in the equations.

Bearing these limitations in mind, the results obtained can explain the experimental observations of 'disturbances' travelling towards the anode with the group velocity. In Fig.2(a) of Krasa et al, (J. Phys. D, 7, 2541 (1974), see Appendix A.2) the space-time display is given for an s' type wave in neon for the case where the nonlinear effects are only effective near the anode, such disturbances are easily seen.

If α in equation (9.16) is assumed to be small enough so that $\exp \alpha t$ is approximately constant for the time that the solution can be used, or the time taken for the wave to travel the length of the tube, and using the fact that

$$\frac{\omega_1}{k_1} = \frac{\partial \omega}{\partial k} = - \frac{\omega_0}{k_0}$$

the expression for the waves becomes:

$$\left[a_0 + a_1 \cos(\omega_1 t + k_1 x) \right] \cos \left[\omega_0 t - k_0 x + \beta \sin(\omega_1 t + k_1 x) \right] \dots (9.17)$$

where the $\exp \alpha t$ has been absorbed in the constants; the particular cosine/sine dependence has been chosen for convenience and the fact that the disturbances travel in the opposite direction to the waves has been taken into account.

Expanding in terms of Bessel functions and neglecting terms of the order of $a_1 J_1(\beta)$ gives:

$$\begin{aligned}
& a_0 J_0(\beta) \cos(\omega_0 t - k_0 x) \\
& + a_0 J_1(\beta) \left[\cos(\omega_0 + \omega_1)t - (k_0 - k_1)x \right] \\
& + \frac{a_1 J_0(\beta)}{2} \left[\cos(\omega_0 + \omega_1)t - (k_0 - k_1)x \right] \dots (9.18) \\
& - a_0 J_1(\beta) \left[\cos(\omega_0 - \omega_1)t - (k_0 + k_1)x \right] \\
& + \frac{a_1 J_0(\beta)}{2} \left[\cos(\omega_0 - \omega_1)t - (k_0 + k_1)x \right] .
\end{aligned}$$

If the modulation is at the same frequency as the wave, then $\omega_1 = \omega_0$ and k_1 will equal k_0 .

From the above expression it is seen that a time independent component of the wave pattern with a spacing of $\lambda/2$ is seen. As pointed out by Grabec, this readily explains the apparent stationary striations. As noted earlier, modulations of the form $\exp i(\omega t - kx + \beta \sin \omega t)$ also give such 'stationary' striations with the difference that the spacing is equal to λ . Such differences in the form of modulation, give a reason for the different spacing seen experimentally by various authors⁽⁴¹⁾.

9.5 INTERPRETATION OF WAVE COUPLING RESULTS IN ARGON

In the argon discharge, the coupling of the waves in frequency ranges (a), (b), has been attributed to velocity modulation and the standing pattern as due to the linear interference between the time modulated synchronous oscillation and the modulated travelling wave. This phenomenon is distinct from the nonlinear modulational instability just described but the question arises as to whether the results can be explained in terms of the linear interference of synchronous oscillations and the nonlinear modulational instability of the travelling wave.

For example, if it is assumed that synchronous oscillations are present at frequencies $\omega_0 \pm \omega_1$ then from equation (9.18) it is found that the standing patterns will have spacings of (L) given by

$$\frac{1}{L} = \left| \frac{1}{\lambda_0} \pm \frac{1}{\lambda_1} \right| \quad \dots (9.19)$$

where the minus corresponds to $\omega_0 + \omega_1$ (sum frequency) and the plus to $\omega_0 - \omega_1$ (difference frequency). Since $\frac{\omega_0}{\omega_1} = \frac{k_1}{k_0}$ this gives:

$$L_{\text{sum}} = \left| \frac{\lambda_0}{1 - \frac{f_1}{f_0}} \right|, \quad L_{\text{difference}} = \left| \frac{\lambda_0}{1 + \frac{f_1}{f_0}} \right| \quad \dots (9.20)$$

where f is the frequency. From the experiments, f_1 is smaller than f_0 and so

$$L_{\text{difference}} < \lambda_0 < L_{\text{sum}}$$

which does not correspond to the experimental results where $L_{\text{dif.}} > \lambda_0$.

It may be concluded that the nonlinear modulational instability is not responsible for the coupling.

9.6 LINEAR EQUATIONS APPLIED TO AN INHOMOGENEOUS MEDIUM

The equations derived so far were for a homogeneous medium. If an inhomogeneous medium is considered then even in the linear case, ω , k and a will change with x and t . Equation (9.1) is now given by

$$\frac{\partial k}{\partial t} + \frac{\partial W}{\partial k} \frac{\partial k}{\partial x} = - \frac{\partial W}{\partial x} \quad \dots (9.21)$$

where $\omega = W(k, x, t)$.

In this case changes in k and a will propagate with a velocity $\frac{\partial W(k)}{\partial k}$, where k is found from $\frac{dk}{dt} = - \frac{\partial W}{\partial x}$, and k and a themselves will change along these trajectories (in contrast to the case of the homogeneous medium). So, as with the nonlinear case, the changes propagate towards the anode.

However, the motion of a particular crest will be given by

$$\theta = \text{constant} = kx - W(k)t, \quad \text{that is: } \frac{dx}{dt} = \frac{\omega}{k} = \frac{W(k)}{k}.$$

This case of an inhomogeneous medium can be used to describe, in the simplest approximation, the interaction of two wave types. It is assumed that one wave travels through the medium which is non-homogeneous due to the presence of the other wave. Then ω would be of the form $\omega = W_0(k) + W_1 e^{i\mu(x-vt)}$, where the exponential term describes the wave which perturbs the medium and which travels towards the cathode.

The wavenumber would be given by

$$k = k_0 + k_1 e^{i\mu(x-vt)} \quad \text{on} \quad \frac{dX}{dt} = \frac{\partial W(k)}{\partial k},$$

so that the velocity of a crest is given by:

$$\frac{\omega}{k} = \left[\frac{W_0(k) + W_1 e^{i\mu(x-vt)}}{k_0} \right] \left[1 + \frac{k_1}{k_0} e^{i\mu(x-vt)} \right]^{-1}$$

since the theory requires $k_1 \ll k_0$, then

$$\begin{aligned} \frac{\omega}{k} &\approx \left[\frac{W_0(k_0) + W'_0(k_0)(k-k_0) + W_1 e^{i\mu(x-vt)}}{k_0} \right] \left[1 - \frac{k_1}{k_0} e^{i\mu(x-vt)} \right] \\ &= \frac{W_0(k_0)}{k_0} + \frac{W'_0(k_0)(k-k_0)}{k_0} \\ &\quad + \frac{W_1}{k_0} e^{i\mu(x-vt)} - \left[\frac{W_0(k_0)}{k_0} + \frac{W'_0(k_0)k_1}{k_0} \right] \frac{k_1}{k_0} e^{i\mu(x-vt)} \quad \dots (9.22) \end{aligned}$$

It can be seen that the basic phase velocity is modulated by a travelling wave term due to the perturbing wave. For this case, a nonlinear effect is obtained from the linearised equations in contrast to the earlier results. This is due to the fact that the term $\frac{\partial W}{\partial x}$ is included only because one wave is sufficiently nonlinear to affect the medium.

The two-wave interaction considered in Chapter VIII, corresponds to the condition:

$$\omega = W_0(k_0) + W_1 e^{i\mu(x-vt)}$$

that is, the modulated frequency does not necessarily lie on the original dispersion curve. For this case, the deviation of k from k_0 is found from:

$$\frac{\partial k}{\partial t} = - \frac{\partial}{\partial x} W_1 e^{i\mu(x-vt)}$$

and changes moving towards the anode are not found.

It has been seen that the variational methods are capable of predicting various nonlinear effects. The results of the next chapter will show all of these effects occurring in a single discharge.

CHAPTER X

A GENERAL DESCRIPTION OF THE MODE- COUPLING BETWEEN STRIATIONS

10.1 INTRODUCTION

The model used to account for the mode-coupling in the argon discharge described the interaction as a nonlinear process intermediate between the linear and fully nonlinear cases. Such regular velocity modulation can describe the effects observed for striations in other gases as will be shown for results obtained from a neon discharge by the author and a former colleague at the Institute of Physics, Prague. Earlier measurements^(15,31) could have been used, but the results below have the advantage that they combine simultaneous space-time and spectrum analyser displays. The results show how the regular modulation occurs at a certain stage in the nonlinear evolution of the waves.

10.2 RESULTS FROM A NEON DISCHARGE

The space-time diagram display, obtained from a rotating-drum camera, and the spectrum analyser displays of the signal from a photomultiplier at different positions along the tube, are shown for a neon discharge in Figs.10.1, 10.2, and Appendix A.2. The tube was 80 cms in length with an internal diameter of 0.99 cm, and was filled with spectroscopically pure neon.

Two slow waves (metastable-guided) with frequencies of 6.8 KHz and 4.3 KHz are seen belonging to the first resonance (the long 's' wave) and the second resonance (the short 'p' wave). From the space-time display only the short, p variety, is seen in the first 10 cm from the cathode. The corresponding spectrum analyser signal, Fig.10.2, shows the presence of the faster wave which is of small amplitude. At 14 cm from the cathode, both s' and p waves have approximately equal amplitudes, and slightly

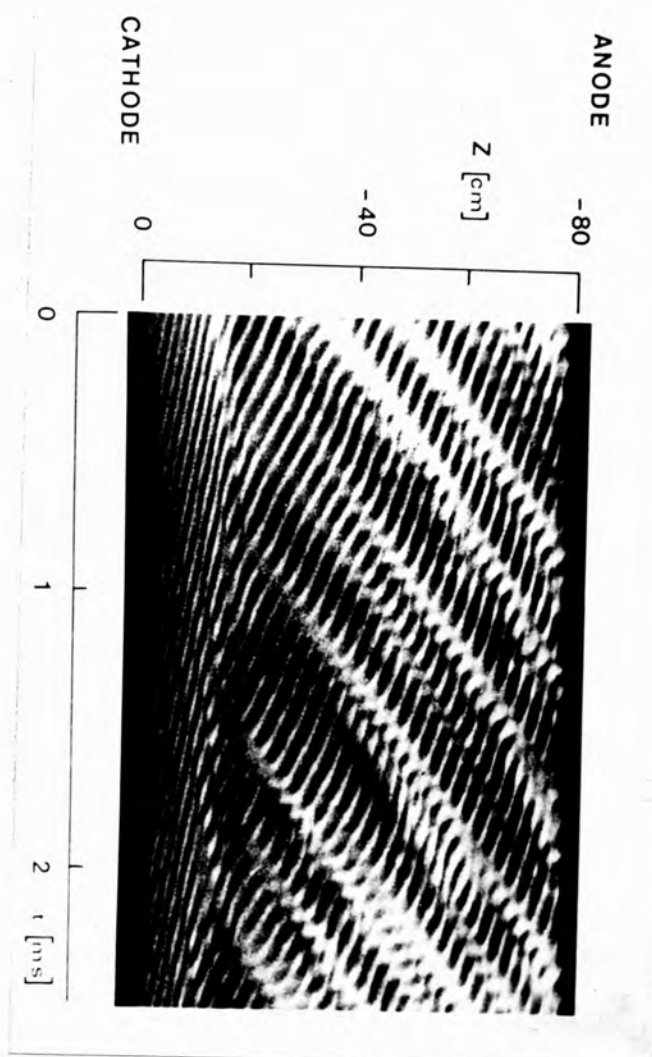


Fig.10.1

Rotating drum (single sweep) photograph
of the neon discharge at $I = 19 \text{ mA}$

pronounced peaks corresponding to sum and difference frequencies are seen. Within the region 14-18 cms from the cathode, a transition from one wave type to the other takes place. The actual boundary position changes with time which causes mis-matching and collisions of the two wave types giving rise to annihilation of striations, and 'dislocations' which propagate as actual disturbances towards the anode. The velocity of propagation is approximately equal to either the group velocity of the s' wave, where this wave is dominant, or the group velocity of the p wave where this is dominant.

On the cathode side of the transition region, and extending to within about 7 cm of the cathode, the p wave is velocity modulated in a regular way as described for the argon discharge. Near the cathode end the modulation is slight but it increases with distance from the cathode. At a lower current setting, where the space-time display exhibited the same features, the frequency spectrum for this interaction was more distinctly resolved showing that the combination frequencies are those obtained from the nonlinear interaction of the s' and p waves, that is the difference frequency, $f_{s'} - f_p = 2.5$ KHZ, and the summation frequency, $f_{s'} + f_p = 11.1$ KHZ, see Fig.10.3.

On the anode side of the 'transition boundary' the frequency spectra become continuous with the central peak occurring near the frequency of the s' wave, Fig.10.2(c). Further along the column towards the anode, the wave motion becomes irregular exhibiting jumps in the phase velocity. The creation and disappearance of the wave crests are observed. Near the anode the spectrum is smooth and continuous, Fig.10.2(d), with its maximum at 5.8 KHZ lying between the frequencies of the two fundamental waves.

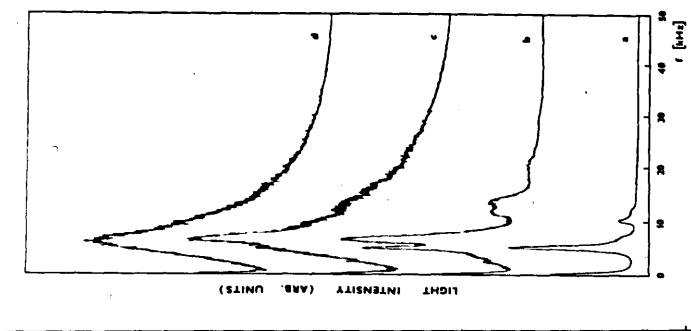


Fig.10.2
 Frequency spectrum at $I = 18$ mA, at various distances from cathode (a) 6 cm, (b) 14 cm, (c) 32 cm, (d) 65 cm

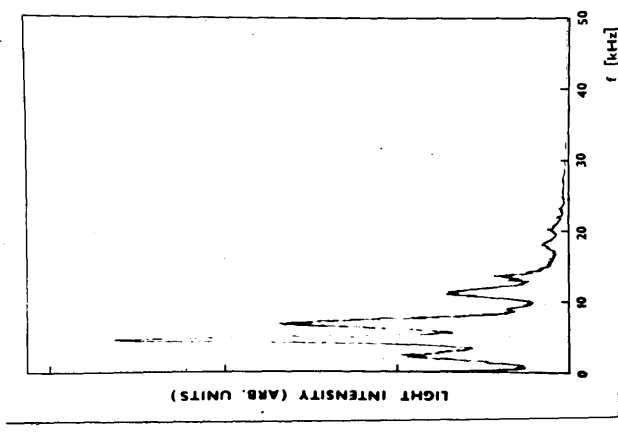


Fig.10.3
 Frequency spectrum 14 cm from cathode at $I = 14$ mA. $f_p = 4.3$ KHz and $f_s = 6.8$ KHz

10.3 GENERAL DISCUSSION OF MODE COUPLING BETWEEN TWO IONIZATION WAVES

The interaction of two waves, which do not belong to the same dispersion curve, will be governed by the principle of linear superposition so long as both waves are of small amplitude⁽²⁶⁾. Only the fundamental frequencies will be seen on the spectrum analyser display.

When the amplitude of one, or both, of the waves is large enough, the first nonlinear effects are seen: these may be the generation of virtual waves due to amplitude modulation or the intermodulation of the phases to give regular velocity modulation of the phase velocity as described by equation (6.5).

If the virtual waves have frequencies or wavenumbers well away from those of the fundamental waves, then phase modulation is the more likely of the two processes. This is because the values of the resulting frequencies and wavenumbers will be close to the optimum values when the amplitudes of the waves are still relatively small. The initial cathode region of the neon discharge is thus described.

As the amplitudes of the waves increase, corresponding to the 'transition' region above, the velocity modulation will increase and the variation in frequencies and wavenumber may no longer be small. The discharge will become unstable in this region for several reasons: since the waves are of comparable amplitudes the discharge at this point can accommodate both wave types equally well, which, when combined with the destabilizing influence of the phase modulation, is likely to lead to mode jumping⁽³¹⁾ between the two wave types. In addition the velocity modulation, due to phase modulation, and the mode jumping make it possible for a 'repulsive collision', of the type described by Grabec⁽²⁶⁾, to take place between the two wave types as is clearly seen between 15-20 cms from the

cathode in Fig.10.1. It is these 'collisions' which lead to the anode directed disturbances with a velocity close to that of the p wave.

For the neon results the p wave ceases to grow after 18 cms and the s' wave which continues to grow, is the dominant wave in the rest of the discharge. As the wave amplitude grows the nonlinear self-modulation effects, Chapter IX, become noticeable. Variations in amplitude and velocity are seen; anode directed disturbances moving with the group velocity of the s' wave are observed. Further interactions between these anode directed disturbances and the cathode directed striations take place; further modes are excited and anode directed wave packets, short in space and time, are produced to give a frequency spectrum which is quite continuous near the anode end of the discharge.

If in the above example both waves had continued to grow, then the regular velocity variation would have still broken down and the nonlinear 'self-modulation' effects for both waves would have given a broad continuous spectrum.

Where a definite but varying 'transition' boundary exists between two wave types, the effects seen at the boundary will depend on whether a smooth transition from one wave type to the other can be achieved⁽³¹⁾. When the overlap region for the two waves is small, then it may be possible for one wave type to branch out into two waves of the other variety with a minimum of velocity variation⁽¹⁶⁾.

If both waves are stabilized to give, in the absence of the other wave, a uniform velocity, see section 2.8.4, then the interaction of the waves is likely to give rise to regular modulation of both waves. A rotating drum camera may, however, only detect the modulation of one of the waves if the relative amplitudes of the two waves are considerably different.

The change from a discrete multiline spectrum to a broad continuous one may thus be explained as due to the different nonlinear effects which become effective as the wave amplitude increases. In the argon discharge, the waves were fully stabilized or of relatively small amplitude so that full turbulence did not develop and the interactions were restricted to regular velocity modulation. The results for the neon discharge were of a more general nature: besides the 'first order' nonlinear effects, other effects which would require the higher order nonlinear terms to be retained in the equations of Chapters VIII and IX were seen.

CHAPTER XI

CONCLUSION

The linear interference between the self-excited synchronous oscillations and the travelling striations in frequency range (b), provided an easy way of obtaining the characteristics of the striations. It is interesting to see that the synchronous oscillations and the striations, both of large amplitude, did not interact nonlinearly: when the striations were velocity modulated, in the purely self excited case and when an external voltage was applied, synchronous oscillations at the same frequency were not seen.

The modified theory for the synchronous oscillations while agreeing qualitatively with the results, does not account for the way in which the striations interact with the anode and cathode regions to produce the voltage oscillations which in turn produce the synchronous oscillations. The influence of the regions of the discharge bounding the positive column has been seen by other authors in the case of anode spot interactions with striations^(14,16,59) branching effects⁽¹⁴⁾, feedback mechanisms⁽²⁷⁾ and matching conditions⁽³¹⁾.

The influence of the anode and cathode regions on the positive column requires a separate study. This would most likely prove to be a difficult task since even for the unperturbed discharge, an adequate explanation of the cathode and anode regions has still to be found.

By applying the external voltage it was possible to simulate the 'apparent' stationary striations seen in the purely self-excited case. The space-time display showed that the effect, which was nonlinear, was due to velocity modulation of the wave at its fundamental frequency or harmonics of this frequency. The 'doublet' patterns which were seen

corresponded to modulation at the first harmonic frequency. In addition, the external modulation gave rise to 'disturbances' moving towards the anode with speeds much faster than the striations. Similar disturbances have been reported by other authors but the present results show that these anode directed waves are a consequence and not a cause of velocity modulation. In some cases such disturbances have the same speed as the striations and may be due to the nonlinear self-modulation of the striation, as described in Chapter IX.

The waves in frequency range (a) were shown to have a backward nature while the characteristics of the waves in range (c) suggested that they too were backward. Theoretically only backward waves would be expected in the discharge.

From the time averaged measurements it was possible to establish the nature of the mode-coupling interactions between the waves in the different frequency ranges. By using expressions representing the modulation of the waves, the degree of velocity modulation, 5-15%, was estimated from the wave patterns of the satellite frequencies. Such relatively small changes in velocity would have been difficult to estimate from a rotating drum photograph. The time-averaged results, which made use of the presence of the synchronous oscillations to give standing wave patterns, afforded a convenient method of measurement for the argon discharge. In general, however, it is preferable to have both types of measurement - space-time displays and frequency spectra - so that any ambiguity can be removed. For the argon results, the visual observations using a rotating mirror supported the proposed form of interaction.

A consistent explanation of the interactions between waves in frequency ranges (a) and (b), frequency ranges (b) and (c) was given in terms of regular velocity modulation. This form of modulation gives rise

to discrete multiline frequency spectra and describes the initial nonlinear effects or, a state when the nonlinear growth of the waves has been fully stabilized to give regularly moving striations. The interactions which give rise to this form of modulation represent the simplest nonlinear effect since theoretically they come from first order nonlinear terms proportional to $[n^{(1)}]^2$, where $n^{(1)}$ is the perturbed ion density. The extension of the linear theory for ionization waves provided expressions to describe the above effects which are intermediate between the linear state and the full developed turbulent state.

The physical model used to interpret the results was consistent with the modified theory and was supported by the fact that a similar interpretation in terms of 'collisions' has been used to describe ion-acoustic solitons. The 'particle-like' structure of the waves which these interpretations suggest, is an interesting feature and one which is being currently studied in the general field of nonlinear waves.

Regular velocity modulation is not peculiar to argon discharges; the idea that this effect is the initial nonlinear response of the discharge to the growth of the waves was born out by the results from the neon discharge which allowed the development of the nonlinear interactions to be followed since both space-time and frequency spectrum displays were obtained. The effects observed for the neon discharge are common to many discharges where the waves grow sufficiently to produce a broad continuous frequency spectrum. The results showed that as the amplitude of the waves grew, different nonlinear effects became operative. The regular velocity modulation and discrete frequency spectra were seen until the waves had grown sufficiently for the velocity variation to be significant, resulting in an unstable region where mode jumping, and the annihilation and splitting of striations occurred. Further growth of the waves gave rise to

anode directed disturbances, and amplitude and velocity modulation as predicted by the variational methods of the present work, Chapter IX, and the computations of Grabec, see Chapter II.

The complexity of the experimental observations and the complete equations required to describe striations meant that any comparison between theory and experiment could only be qualitative. Even so, it has been seen that the essential features of the nonlinear evolution of mode-coupling between two waves can be predicted theoretically to the extent that the many experimental observations of coupling between nonlinear ionization waves can now be interpreted in a unified way.

APPENDIX A.1
SOLUTION OF PARTIAL DIFFERENTIAL EQUATIONS
BY THE METHOD OF CHARACTERISTICS

The method of characteristics enables partial differential equations to be reduced to ordinary differential equations provided certain conditions are met. A simple example will illustrate the method.

Consider the equation,

$$\frac{\partial y}{\partial t} + c(y) \frac{\partial y}{\partial x} = 0 \quad \dots (A1.1)$$

where y is a function of x, t . One approach to the solution is to consider the function $y(x, t)$ at each point on the (x, t) plane and to note that

$$\frac{\partial y}{\partial t} + c(y) \frac{\partial y}{\partial x} = 0 = \frac{dy}{dt}, \quad \dots (A1.2)$$

the total derivative, if

$$c(y) = \frac{dx}{dt} \quad \dots (A1.3)$$

Equation (A1.3) defines a family of curves C , the characteristic curves, in the x, t plane on which (A1.2) is satisfied. Since y remains constant on C , the curves are, in this simple case, straight lines with slope $c(y)$. The curves cannot be found explicitly since the unknown values of y are involved. Thus the general solution of (A1.1) depends on the construction of a family of straight lines in the x, t plane, each line with a slope $c(y)$. For the present work the main feature of this solution is the condition obtained from equation (A1.3).

The above method may be generalised by considering a quasi-linear first order system:

$$A_{ij} \frac{\partial u_j}{\partial t} + a_{ij} \frac{\partial u_j}{\partial x} + b_i = 0, \quad (i = 1, \dots, n) \quad \dots (A1.4)$$

where the matrices A , a and the vector b may be functions of u_1, \dots, u_n , as well as x and t . In general any one of these equations in (A1.4) has different combinations of $\partial u_j / \partial t$ and $\partial u_j / \partial x$ for each u_j . That is, it

couples information about the rates of change of the different u_j in different 'directions'; one cannot deduce information about the increments of all the u_j for a step in any single 'direction'. This can be achieved by manipulating the equations by considering a linear combination

$$\ell_i \left(A_{ij} \frac{\partial u_j}{\partial t} + a_{ij} \frac{\partial u_j}{\partial x} \right) + \ell_i b_i = 0 \quad \dots (A1.5)$$

where the vector $\underline{\ell}$ is a function of x, t, \underline{u} . For a suitable choice of ℓ , equation (A1.5) can be transformed to

$$\ell_j \left(\beta \frac{\partial u_j}{\partial t} + \alpha \frac{\partial u_j}{\partial x} \right) + \ell_j b_j = 0, \quad \dots (A1.6)$$

which provides a relation between the derivatives of all the u_j in the single 'direction' (α, β) . If $x = X(\eta)$, $t = T(\eta)$ is the parametric representation of a curve in the (x, t) plane defined by the α 's and β 's, then

$$\frac{du_j}{d\eta} = \frac{dT}{d\eta} \frac{\partial u_j}{\partial t} + \frac{dX}{d\eta} \frac{\partial u_j}{\partial x} \quad \dots (A1.7)$$

and if $\alpha = \frac{dX}{d\eta}$, $\beta = \frac{dT}{d\eta}$, equation (A1.6) may be written as an ordinary differential equation

$$\ell_j \frac{du_j}{d\eta} + \ell_j b_j = 0 \quad \dots (A1.8)$$

provided

$$\ell_i A_{ij} = \ell_j T', \quad \ell_i a_{ij} = \ell_j X' \quad \dots (A1.9)$$

where

$$T' = \frac{dT}{d\eta}, \quad X' = \frac{dX}{d\eta},$$

which for nontrivial solutions requires

$$|A_{ij} X' - a_{ij} T'| = 0 \quad \dots (A1.10)$$

Equation (A1.9) is the equivalent of (A1.3) in the simple example and is a condition on the curve in the x, t plane on which (A1.8) is satisfied. Such a curve is said to be the characteristic and the corresponding equation (A1.8) is said to be in characteristic form.

The equations for solution are

$$\left. \begin{aligned} \frac{\partial k}{\partial t} + \omega'_0(k) \frac{\partial k}{\partial x} + \omega_2(k) \frac{\partial a^2}{\partial x} &= 0 \\ \frac{\partial a^2}{\partial t} + \omega'_0(k) \frac{\partial a^2}{\partial x} + \omega''_0(k) a^2 \frac{\partial k}{\partial x} &= 0 \end{aligned} \right\} \dots (A1.11)$$

If $u_1 = k$, and $u_2 = a^2$, then the matrices are found from equation (A1.4) to be

$$A = \begin{vmatrix} 1 & 0 \\ 0 & 1 \end{vmatrix}, \quad a = \begin{vmatrix} \omega'_0(k) & \omega_2(k) \\ \omega''_0(k)a^2 & \omega'_0(k) \end{vmatrix} \dots (A1.12)$$

If $\eta = t$ is taken, then $\frac{\partial T}{\partial \eta} = 1$, $\frac{dX}{d\eta} = \frac{dx}{dt} = c$, and it follows after substituting in (A1.9) that the characteristic velocity (c) is given by

$$c = \omega'_0(k) \pm \sqrt{\omega_2(k) \omega''_0(k) a} \dots (A1.13)$$

From equations (A1.9) and (A1.8) the following relation between the charges in a and k are obtained

$$dk \pm 2 da \sqrt{\frac{\omega_2(k)}{\omega''_0(k)}} = 0 \dots (A1.14)$$

Since for the equations (A1.11) A_{ij} reduces $A_{ij} = \delta_{ij}$ and $T' = 1$, $X' = c$, the condition (A1.10) is equivalent to

$$|\delta_{ij} c - a_{ij}| = 0 \dots (A1.15)$$

If in (A1.13) either $\omega_2(k)$ or $\omega''_0(k)$ is negative, then the characteristic velocity c is complex and has no physical meaning. The solution of (A1.11) in this case can be found by considering the equation

$$\frac{\partial u_i}{\partial t} + a_{ij} \frac{\partial u_j}{\partial x} = 0 \dots (A1.16)$$

and assuming a solution

$$u_i = u_i^0 + u_i^{(1)} \quad \text{where } u_i^{(1)} \propto e^{i\mu(x - C't)}$$

to give

$$\frac{\partial u_i^{(1)}}{\partial t} + a_{ij}^{(0)} \frac{\partial u_j^{(1)}}{\partial x} = 0, \quad a_{ij}^{(0)} = a_{ij}(U_0^0) \dots (A1.17)$$

and so

$$-i \mu C' u_i^{(1)} + a_{ij}^{(0)} i \mu u_j^{(1)} = 0$$

and for $C' = C' \delta_{ij}$, a non-trivial solution requires

$$|a_{ij}^{(0)} - C' \delta_{ij}| = 0 \quad \dots (A1.18)$$

Comparison of (A1.18) with (A1.15), which is the condition for non-trivial $u_i^{(0)}$, shows that $C' = c$ (as given by (A1.13)).

Substitution of C' in the sinusoidal wave solution for $u^{(1)}$ shows that the wave moves with a velocity $\omega_0'(k)$ and has a temporal amplification proportional to $\pm \sqrt{\omega_2(k) \omega_0''(k) a}$ which is a complex quantity.

APPENDIX A.II

PUBLISHED PAPERS

- (1) PERKIN, R.M. and WOODING, E.R., Electronics Letts., 7, 781 (1971).
- (2) PERKIN, R.M. and WOODING, E.R., 2nd Int. Conf. Ionized Gases,
(I E E., London), 248 (1972).
- (3) PERKIN, R.M. and WOODING, E.R., Phys. Letts., 41A, 27 (1972).
- (4) PERKIN, R.M. and WOODING, E.R., Phys. Letts., 42A, 367 (1973).
- (5) PERKIN, R.M. and WOODING, E.R., Phys. Letts., 45A, 165 (1973).
- (6) PERKIN, R.M., XIth Int. Conf. Ioniz. Phen. Gases, (Prague),
306 (1973).
- (7) PERKIN, R.M., KRASA, N.J. and PEKAREK, L., J. Phys. D.,
8, 161 (1975).
- (8) KRASA, J., PERKIN, R.M. and PEKAREK, L., J. Phys. D, 7, 2541 (1974).

REFERENCES

- (1) PUPP, W., Zs. Techn. Phys. A F., 257, (1934).
- (2) DONAHUE, T.M. and DICKE, G.H., Phys. Rev., 81, 248 (1951).
- (3) PEKAREK, L., Sov. Phys. Uspekhi, 11, 188 (1968).
- (4) GARSCADDEN, A. and BLETZINGER, P., Phys. Fluids, 12, 1833 (1969).
- (5) NOVAK, M., Czech. J. Physics, B10, 954 (1960).
- (6) PEKAREK, L., Proc. VIth Int. Conf. Ion. Phen. in Gases (Paris), 2, 133 (1963).
- (7) LEE, D.A., BLETZINGER, P. and GARSCADDEN, A., J. Appl. Phys., 37, 377 (1966).
- (8) WOJACZEK, K., Beitr. Plasmaphys., 2, 2 (1962); also 6, 319 (1966).
- (9) NEDOSPASOV, A.V. and PONOMARENKO, Yu.B., High Temperature, 3, 12 (1965).
- (10) PEKAREK, L., Invited Paper, Xth Int. Conf. Phen. Ionized Gases, (Oxford), (1971).
- (11) TSENDIN, L.D., Sov. Phys. Tech. Phys., 15, 1245 (1971).
- (12) PEKAREK, L., MASEK, K. and ROHLENA, K., Czech. J. Phys., B15, 644 (1965).
- (13) COOPER, A.W.M., COULTER, J.R.M. and EMELEUS, K.G., Nature, 181, 1326 (1958).
- (14) COULTER, J.R.M., Physica, 26, 949 (1960).
- (15) STEWART, R.S., MAY, W.F., EMELEUS, K.G., COULTER, J.R.M. and ARMSTRONG, N.H.K., Int. J. Elec., 18, 65 (1965).
- (16) COULTER, J.R.M., ARMSTRONG, N.H.K. and EMELEUS, K.G., Physica, 24, 828 (1958).
- (17) PEKAREK, L.; Invited Paper, Int. Conf. Ioniz. Phen. Gases (Bucharest) (1969).
- (18) DROUET, M.G. and SICHA, M., Canadian J. Phys. 46, 219 (1968).
- (19) RUZICKA, T., Proc. IXth Int. Conf. Phen. Ionized Gases, (Bucharest) 454 (1969)
- (20) ROHLENA, K., RUZICKA, T. and PEKAREK, L., Czech. J. Phys., B22, 920 (1972).
- (21) NEDOSPASOV, A.V., Soviet Phys. Tech. Phys., 3, 153 (1958).
- (22) POBERAJ, S. and GRABEC, I., Proc. IXth Int. Conf. Phen. Ionized Gases, (Bucharest), 463 (1969).
- (23) GRABEC, I., Beitr. Plasmaphysik, 11, 285 (1971).
- (24) GRABEC, I. and MIKAC, S., Plasma Phys., 16, 1155 (1974).
- (25) GRABEC, I. and POBERAJ, S., Zeitschrift fur Natur., 25a, 297 (1970).
- (26) GRABEC, I., Phys. Fluids, 17, 1834 (1974).

- (27) SATO, M., Phys. Rev. Letts., 24, 998 (1970), also
Phys. Letts., 35A, 431 (1971).
- (28) GRABEC, I., Beitr. Plasmaphysik, 12, 83 (1972).
- (29) OHE, K. and TAKEDA, S., Jap. J. Appl. Phys., 11, 1173 (1972).
- (30) PERKIN, R.M., KRASA, J. and PEKAREK, L., J. Phys. D., 8,
161 (1975).
- (31) GARSCADDEN, A. and BLETZINGER, P., Proc. Xth Int. Conf. Phen.
Ionized Gases, (Oxford), 293 (1971).
- (32) OHE, K. and TAKEDA, S., Beitr. Plasmaphysik, 15, 55 (1975).
- (33) SATO, M., Beitr. Plasmaphysik, 10, 371 (1970).
- (34) RUTSHER, A., Naturwissenschaften, 45, 54 (1958).
- (35) PFAU, S. and RUTSCHER, A., Ann. der. Phys. (Leipzig), 6, 244 (1960).
- (36) SATO, M., Beitr. Plasmaphysik, 11, 445 (1971).
- (37) COOPER, A.W., J. App. Phys., 35, 2877 (1964).
- (38) KENJO, T. and HATTA, Y., J. Phys. Soc. Japan, 19, 2313 (1964).
- (39) PEKAREK, L., Czech. J. Phys., 8, 32 (1958).
- (40) SWAIN, D.W. and BROWN, S.C., Phys. Fluids, 14, 1383 (1971).
- (41) OLESON, N.L. and COOPER, A.W., Adv. Electronics and Electron Phys.
24, 155 (1968).
- (42) PEKAREK, L., Czech. J. Phys., 4, 221 (1954).
- (43) PEKAREK, L., Proc. VIIIth Conf. Ion. Phen. Gases (Vienna),
Paper 4.3.14.5, (1967).
- (44) GENTLE, K., Phys. Fluids, 9, 2203 (1966).
- (45) PEKAREK, L. and KREJCI, V., Czech. J. Phys., B12, 296 (1962).
- (46) PEKAREK, L. and KREJCI, V., Czech. J. Phys., B13, 881 (1963).
- (47) RUZICKA, T. and ROHLENA, K., XIth Int. Conf. Ion. Phen. Gases (Prague),
Invited Paper, (1973).
- (48) RAYMENT, S.W. and TWIDDY, N.D., Proc. IXth Int. Conf. Ion. Phen. Gases,
(Bucharest), 455 (1969).
- (49) ROHLENA, K., RUZICKA, T. and PEKAREK, L., Phys. Letts., 40A,
239 (1972).
- (50) RAYMENT, S.W., J. Phys. D., 7, 871 (1974).
- (51) NEDOSPASOV, A.V., Sov. Phys. Uspeki, 11, 174 (1968).
- (52) FARRIS, V.D., Proc. Phys. Soc., B68, 383 (1955).
- (53) STEWART, A.B., J. Appl. Phys., 27, 911 (1956).
- (54) GRABEC, I., Private communication (to be published).
- (55) GRABEC, I., Proc. XIth Int. Conf. Ion. Phen. Gases, (Prague)
309 (1973).
- (56) POBERAJ, S. and GRABEC, I., Proc. Summer School Suppl., Hergegnovi,
153 (1970).
- (57) OHE, K. and TAKEDA, S., Jap. J. Appl. Phys., 11, 1173 (1972).

- (58) KRASA, J. and PEKAREK, L., Czech. J. Phys., B23, 863 (1973).
- (59) JACKSON, A.T. and COULTER, J.R.M., J. Phys. A, 3, 559 (1970).
- (60) CRAWFORD, F.W., J. Appl. Phys., 33, 20 (1962).
- (61) POLMAN, J., Phys. Fluids, 12, 1128 (1969).
- (62) KREJCI, V., Czech. J. Phys., 8, 46 (1958).
- (63) STIRAND, O., KREJCI, V. and LASKA, L., Czech. J. Phys., B16, 65 (1966).
- (64) HAYTER, J., MASON, R. and WOODING, E.R., J. Phys. E, 4, 468 (1971).
- (65) ENGEL, A.V., 'Ionized Gases', 2nd ed., Clarendon Press, Oxford, (1965).
- (66) STIRAND, O., Proc. Xth Int. Conf. Ion. Phen. Gases, (Oxford), 287 (1971).
- (67) JACKSON, A.T., J. Phys. D., 4, 1963 (1971).
- (68) STEWART, A.B., J. Opt. Soc. Am., 45, 651 (1955).
- (69) BROWN, S.C., 'Basic Data Plasma Physics,' Wiley (1961).
- (70) KRASA, J. and PEKAREK, L., Proc. XIth Int. Conf. Phen. Ioniz. Gases, (Prague), 303 (1973).
- (71) BISKAMP, D. and PARKINSON, D., Phys. Fluid., 13, 229 (1970).
- (72) WATANABE, S., ISHIHARA, O. and TANACA, H., Plasma Phys., 17, 345 (1975).
- (73) PAIK, S.P., WALLACE, R.N. and McCLEES, H.C., Phys. Rev. Letts., 110, 78 (1963).
- (74) HINZPETER, G., Beitr Plasmaphysik, 9, 75 (1969).
- (75) WHITHAM, W.B., 'Nonlinear Waves', Wiley (1974).

(A 2) APPENDIX II

LIST OF SYMBOLS

Wave amplitude; Constant	A
Constant	A_z
Wave Amplitude; Backward Wave	B
Wave Amplitude; Characteristic Velocity; Capacitance; Constant	C
Wave Amplitude	D
Ambipolar Diffusion Coefficient	D_a
Wave Amplitude; Electric Field	E
Electric Field	E_0
Wave Amplitude; Phase of Wave; Forward Wave	F
Ratio of Energy Losses; coefficient in Lagrange Function	G
Light Intensity; Discharge Current; Pupp Current Limit	I
Current Density; Bessel function of the first kind	J
Complex Wavenumber	K
Debye Length; Lagrange Function	L
Light Intensity	L_w
Average Lagrangian	\mathcal{L}
Ion Mass	M
Charged Particle Density	N
Tube Radius	R
Ionizing Function	S
Electron Temperature	T_e
Potential of Lowest Excited Level	U_a
Ionizing Potential	U_i
Flow Velocity	V
Ionizing Potential	V_i
Ionization Frequency; Discharge Impedance; Wave with zero phase velocity	Z

Reciprocal of Relaxation Length; Tube Radius; Amplitude	a
Rate of Loss of Electrons; Constant	b
Ion Mobility	b_p
Characteristic Velocity	c
Distance between Maxima in the Wave Patterns	d
Perturbed Electric Field	e
Frequency	f
Integer	g
Wavenumber	k
Spatial Growth Rate	k_i
Distance between Maxima in the Wave Patterns; Length of discharge	ℓ
Electron Mass; Constant	m
Perturbed Charged Particle Density; Integer	n
Pressure; angular Frequency; Ratio of Elastic to Inelastic Collisions	p
Wave Type	p'
Absolute Value Electron Charge	q
Radial Coordinate	r
Wave Type	r'
Constant	s
Wave Type	s'
Time	t
Relaxation Time of Elastic Collisions	t_1
Velocity of Stratification Wave; Electron Temperature; Perturbed Voltage	u
Striation Velocity	v
Axial Coordinate	z
<hr/>	
Phase Angles	$\alpha_{1,2}$
Wavenumber; Second Nonlinear Saturation Coefficient; Constant	β
Spatial Amplification Coefficient	γ
Phase Angle; Variational Change	δ
Constant	ϵ
Permittivity of Air	ϵ_0
Molecular Weight	μ
Ion Mobility	μ_i

Electron Mobility	μ_e
Wavelength	λ
Electron Temperature; Phase Angle	θ
Sinusoidal Expression for a Wave	ψ
Angular Frequency	ω
Angular Frequency	Ω
Ion-Neutral Collision Frequency	ν_+
Electron-Neutral Collision Frequency	ν_-
Phase Angle; Temporal Amplification Coefficient	φ
Phase Angle	ψ
Phase Angle	ξ
Constant	Δ
Boltzmann's Constant; Wavenumber	κ
Time Period	τ
Ambipolar Diffusion Life-time	τ_a
Metastable Life-time	τ_m

Subscripts

i:	Ion
e:	Electron
S:	Synchronous oscillation
T:	Travelling wave
W:	Wave
F:	Fundamental
S:	Satellite

GLOSSARY OF TERMS

Ion-Acoustic Wave: Analogous to an acoustic wave in a gas with a temperature equal to that of the electrons and a mass equal to the ion mass.

Striation(Ionization Wave): A periodic variation of the degree of ionization in a plasma resulting from changes in the electron temperature.

Wave of Stratification: The initial disturbance in the electron temperature which travels from the cathode towards the anode and produces the striations.

Self-Excited Wave: A wave which occurs spontaneously in the discharge without any externally applied pulse.

Backward Wave: A travelling wave which has its group velocity and phase velocity in opposite directions. Usually the group velocity is in the cathode to anode direction and the phase velocity is directed from the anode to the cathode.

Synchronous Oscillation: An oscillation which is dependent on time but not on space and is determined by the A.C. impedance of the positive column.

Definition of the nth harmonic as used in this thesis: For a fundamental frequency f , the n^{th} harmonic is defined in this work as that component which has a frequency $(n + 1) f$ where n is an integer from $1 \dots N$. For example the first harmonic ($n = 1$) has a frequency $2f$. However, following the standard convention such a frequency component ($2f$) should be termed the second harmonic.

To convert to the standard notation requires that n^{th} harmonic (this work) = $(n + 1)^{\text{th}}$ harmonic standard notation.

INTERFERENCE OF LOW-FREQUENCY WAVES IN A POSITIVE COLUMN

Indexing terms: Gas-discharge tubes, Interference, Oscillators

Standing waves have been observed in an argon positive column. From the wave patterns, it is deduced that these waves are striations of the type described by Nedospasov.

Standing waves due to interference between backward waves in an argon positive column have recently been observed by Stirand.¹ A wave pattern is now described which could be the result of an amplified wave travelling from anode to cathode accompanied by an undamped wave travelling in the reverse direction.

The discharge was produced in technical-quality argon at pressures of 0.1 to 2 torr in a pyrex tube of 5 cm internal diameter and 107 cm in length. A current of between 60 and 130 mA flowed between a hollow steel-wire mesh cathode of 4 mm diameter and an aluminium anode of 4 cm diameter. Self-excited oscillations were detected by imaging the discharge on a photomultiplier and by a 5-turn copper coil wound round the pyrex tube. The signals were displayed on

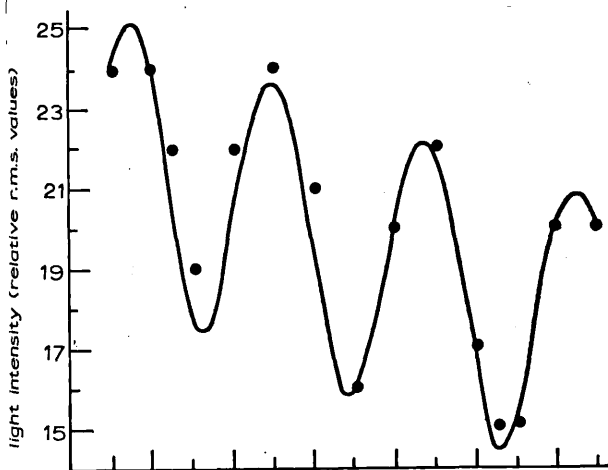
a Tektronix 1L5 spectrum analyser. Reproducibility throughout the experiment was good.

Oscillations occurred at a fundamental frequency between 1.5 and 4 kHz with harmonics, up to the seventh order in some cases. Each mode formed a standing-wave pattern which extended the whole length of the positive column. It is seen in Figs. 1a and b that the light intensity decreased with distance from the cathode, whereas the signal from the pick-up coil increased with distance, a trend which was seen in all the measurements. The separation of the maxima in the standing-wave pattern was inversely proportional to the frequency. For the fundamental frequency, this distance was of the order of 30 cm.

Emeelus* has shown that striations can be reflected at the Faraday dark space. If the standing-wave pattern is due to the reflection of a single wave of wavelength λ , the maxima are separated by a distance $\lambda/2$, allowing the phase velocity to be plotted against the pressure (Fig. 2). In the same Figure, a curve is drawn of the ion drift velocity $\times 7/2$, the velocity being calculated from the average electric field in the plasma. The field was determined from the potentials of two probes separated by a known distance in the positive column. The excellent fit of the experimental points to this curve indicates that the oscillations were striations of the type described by Nedospasov.²

A wave pattern has been computed, assuming sinusoidal variations, for the superposition of a wave with an amplification coefficient of 0.01 cm^{-1} travelling from anode to cathode, and an undamped wave, with zero amplification coefficient,

*EMEELUS, K. G.: 'Low frequency waves'. Culham Laboratory study group on plasma waves, 1964 (unpublished)



travelling from cathode to anode. The close fit of this curve to the experimental points in Fig. 1a supports the authors' view that the standing waves are produced by the superposition of an undamped wave on an amplified wave travelling in the opposite direction.

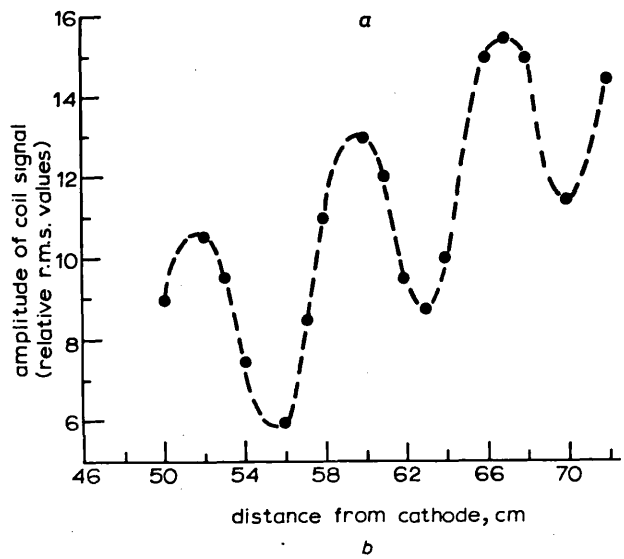


Fig. 1 Standing-wave pattern for first harmonic

Frequency = 3.7 kHz
Current = 79 mA
Pressure = 0.38 torr
a Photomultiplier signal
● experimental
— computed
b Coil signal
● experimental

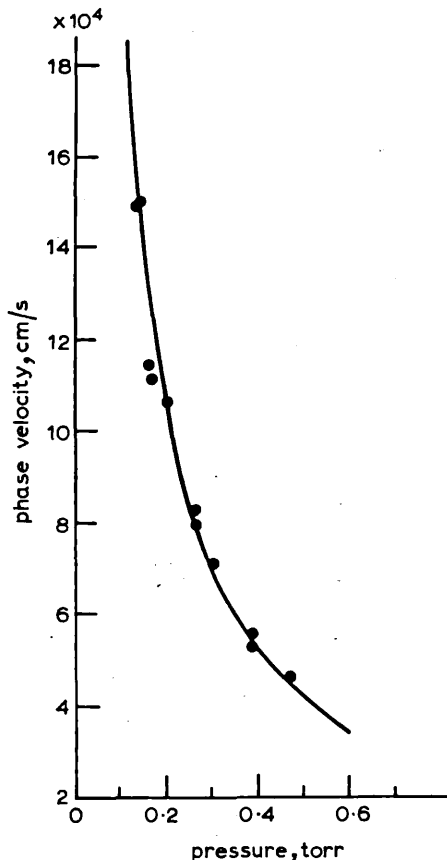


Fig. 2 Phase velocity against pressure

● experimental
— ion drift velocity $\times 7/2$

Acknowledgment: R. M. Perkin expresses gratitude to the UK Science Research Council for their support.

R. M. PERKIN
E. R. WOODING

19th November 1971

Department of Physics
Royal Holloway College
University of London
Englefield Green, Surrey, England

References

- 1 STIRAND, O.: 'Time and space interference of the forward and backward ionization waves' in '10th conference on ionization phenomena in gases' (Oxford, 1971), p. 291
- 2 NEDOSPASOV, A. V.: 'Striations', *Sov. Phys. Aspekhi*, 1968, **11**, pp. 174-187

MODE-COUPLING OF LOW FREQUENCY WAVES

R M Perkin and E R Wooding

Royal Holloway College, University of London, Englefield Green, Surrey

Introduction

In a recent theory of wave mode-coupling of ionization waves [1,2] it was pointed out that the resonance condition for mode-coupling,

$$\omega = \omega_1 + \omega_2, \quad k = k_1 + k_2 \quad (1)$$

is practically impossible to satisfy exactly although virtual waves may be easily observed with frequencies and wavenumbers,

$$\omega_v = \omega_1 \mp \omega_2, \quad k_v = k_1 \mp k_2 \quad (2)$$

respectively. In experiments carried out by the same author, harmonic generation and mode-coupling have been observed for externally excited ionization waves [3]. We now report some experimental observations of mode-coupling between self-excited waves having frequencies in the hertz, kilohertz, and tens of kilohertz ranges.

Apparatus

A 5 cm diameter pyrex discharge tube containing technical quality argon at pressures of 0.1 to 1 torr through which currents of 10 to 200 mA passed was used. The oscillations were detected [4] with a pick-up coil wound round the tube and with a photomultiplier. In either case, the signals were displayed on a low frequency spectrum analyser.

Observations

The self-excited striations which were observed [4] consisted of a fundamental frequency of between 2 and 5 kHz, with harmonics; each mode forming a standing wave pattern. Measurements with the pick-up coil showed that the distance between adjacent maxima, l_s , in the wave pattern for a particular frequency was inversely proportional to the frequency, this distance being of the order of 15 cm for the fundamental mode.

When the current was less than about 150 mA, an oscillation occurred, with a frequency in the range 400 to 900 Hz, and at the same time satellite signals accompanied the oscillations in the kilohertz range. Fig.1 shows the spectrum from the photomultiplier signal of the striations (a) in the absence of the lower frequency, and (b) when a 630 Hz oscillation was also present. In Fig.1b the frequency of the striations is a few hundred hertz less than in Fig.1a. This is due to the fundamental frequency decreasing with current. The fundamental frequency, 2.3 kHz, has satellites on either side whilst the first and second harmonics, 4.6 kHz and 6.9 kHz, have only the lower satellite. Within the accuracy of the spectrum analyser, the separation of these satellites from the basic frequencies is approximately equal to 630 Hz. In some cases it was found that the harmonics had both satellites whilst the fundamental had only the lower satellite.

For currents of 130 mA or less, in the absence of the 400 to 900 Hz oscillation, mode-coupling between the striations and waves having frequencies of tens of kilohertz was detected. Fig.2a shows this coupling between a 32 kHz wave and the striations. The satellites are separated by the frequencies of the striations. When a 600 Hz wave was present, coupling was observed between the 32 kHz wave and the striations which were already coupled with the 600 Hz oscillation to produce the more complex display, Fig.2b.

Using the pick-up coil standing wave patterns were obtained for the 600 Hz oscillation, the striations and

satellites. Wave patterns are shown in Figs 3 and 4 for the fundamental and its lower satellite, and the first harmonic and its lower satellite when the distance between consecutive maxima, l_D , for the lower frequency, 600 Hz, was between 7 and 8 cm. The wave pattern for the second harmonic and both its satellites, shown in Fig.5, was obtained when l_D was between 14 cm and 15 cm for a frequency of 900 Hz.

From the wave patterns, the distance between the maxima for the satellite frequencies is given, to within experimental accuracy, by

$$\left| \frac{1}{l} \right| = \left| \frac{1}{l_s} \pm \frac{1}{l_D} \right| \quad (3)$$

which is equivalent to condition (2) for virtual waves.

Fig.6 shows the wave patterns obtained when the striations were mode-coupled with a 35 kHz wave. The 35 kHz oscillation exhibits no standing wave pattern but resembles the noise power diagram obtained in [5] for a backward wave in neon. The satellites have standing wave patterns in which the distance between adjacent maxima for a given satellite is approximately equal to the distance for the corresponding striation in the kilohertz range. In this case, the coupling appears to be between the standing-waves of the striations and a travelling wave which may be a backward wave.

Acknowledgements

One of us, R M Perkin, is in receipt of a Science Research Council maintenance grant. The authors are grateful to Mr J Henley, Mr R Mason and Mr G Waters for assistance in the construction of the apparatus.

References

- 1 S Poberjac. 10th International Conference on Ionization Phenomena in Gases, Oxford 1971, p.292.
- 2 S Poberjac. 10th International Conference on Ionization Phenomena in Gases, Oxford 1971, p.295.
- 3 S Poberjac and I Grabec. 9th International Conference on Ionization Phenomena in Gases, Bucuresti 1969, p.463.
- 4 R M Perkin and E R Wooding. Electronics Letters 7 (26) 1971, 781.
- 5 I Grabec and S Poberjac. Zeitschrift für Naturforschung Band 25a Heft 2, 1970, p.297-298.

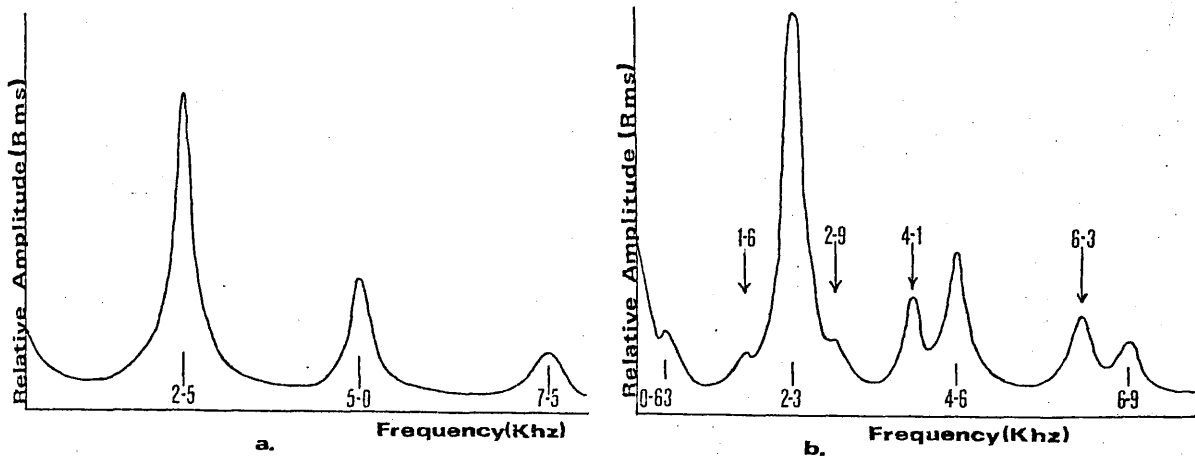


Fig.1. Spectrum of striations. Pressure = 0.43 torr. (a) Current = 160 mA. (b) Current = 130 mA.

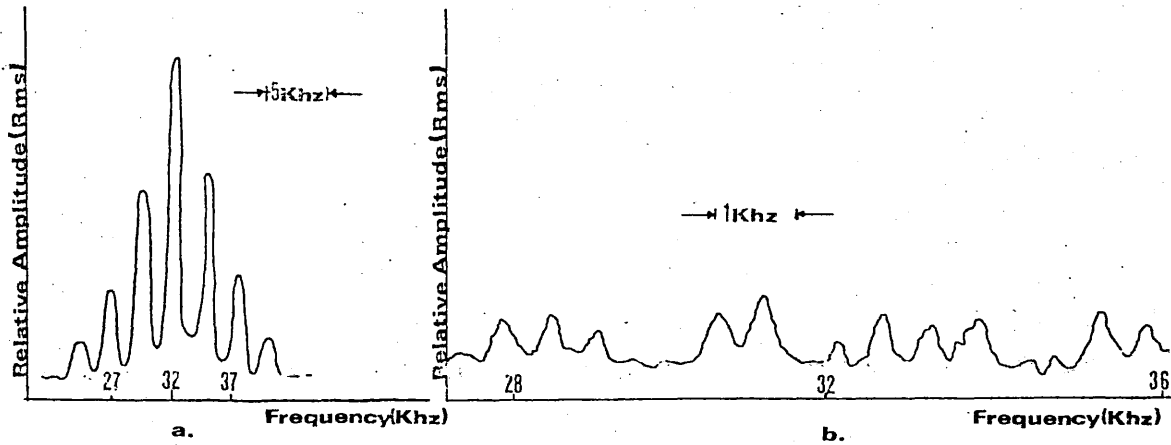


Fig.2. Spectrum of 32 kHz oscillation and satellites. Pressure = 0.3 torr. (a) Current = 120 mA (b) Current = 62 mA

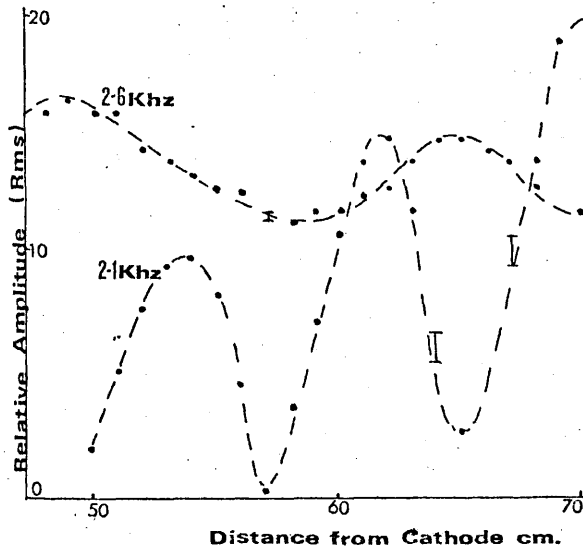


Fig.3. Wave patterns for fundamental, 2.6 kHz and lower satellite 2.1 kHz. Pressure = 0.3 torr. Current = 100 mA

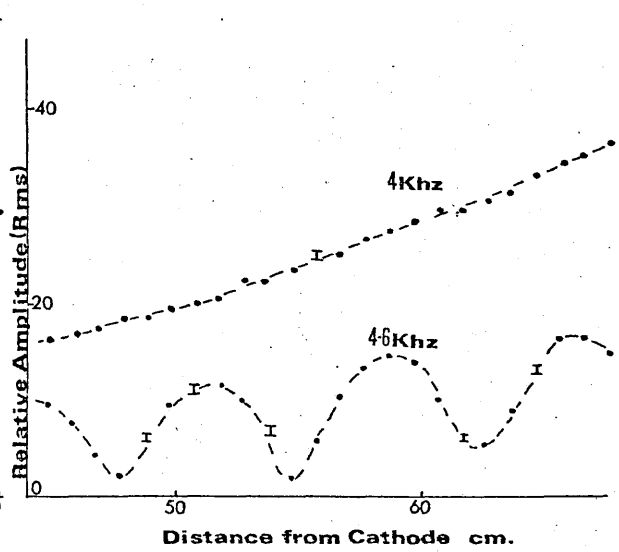


Fig.4. Wave patterns for first harmonic 4.6 kHz and lower satellite 4 kHz. Pressure = 0.34 torr. Current = 110 mA

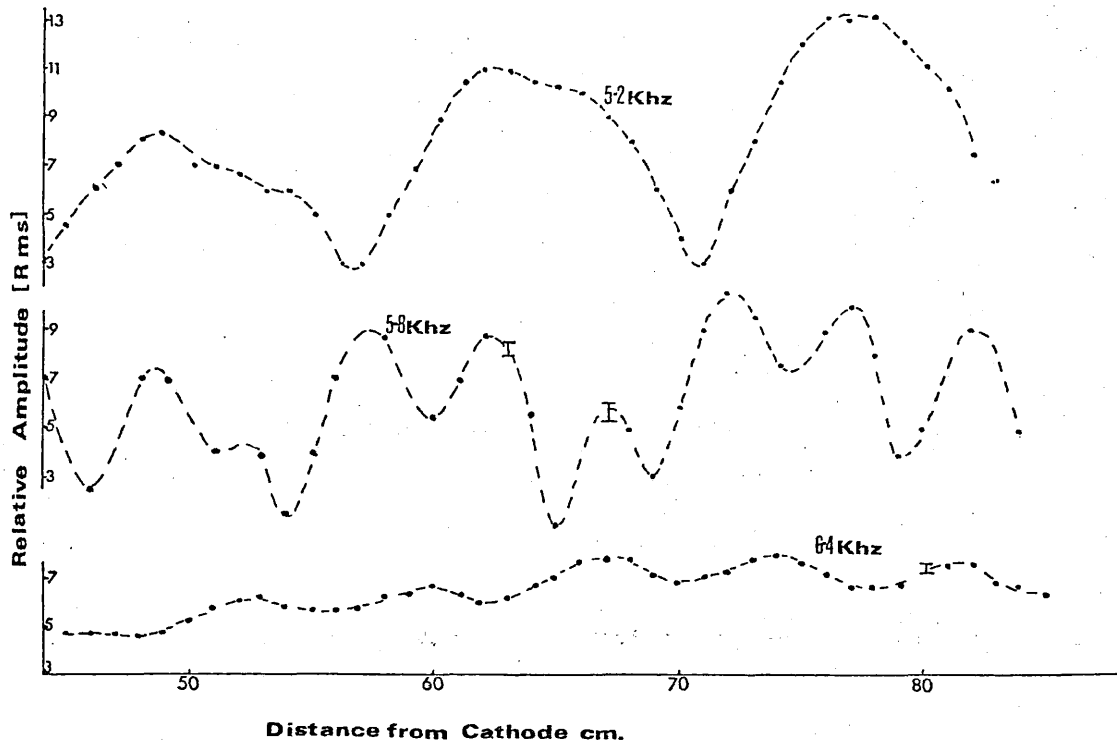


Fig.5. Wave patterns for second harmonic, 5.8 kHz, lower satellite, 5.2 kHz, and upper satellite, 6.4 kHz. Pressure = 0.3 torr. Current = 80 mA.

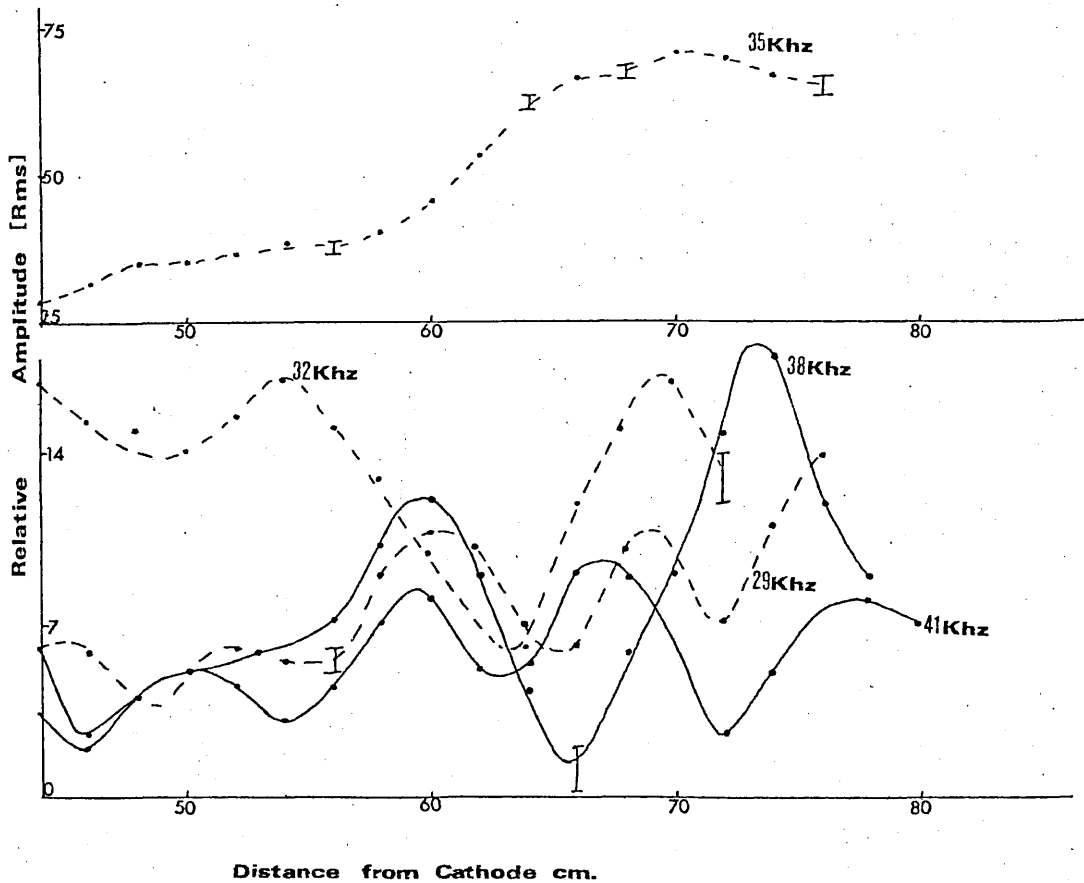


Fig.6. Wave pattern for (a) 35 kHz wave, and (b) wave patterns for lower satellites, 29 kHz, 32 kHz, and upper satellites, 38 kHz, 41 kHz. Pressure = 0.15 torr. Current = 64 mA.

SELF EXCITED STRIATIONS IN A DISCHARGE TUBE OF VARYING DIAMETER

R.M. PERKIN and E.R. WOODING

Department of Physics, Royal Holloway College (University of London) Englefield Green, Surrey, UK

Received 30 June 1972

Observations on striations contained in a discharge tube of varying diameter are reported. The results support Sato's recent work.

This note reports observations on self-excited striations in an argon discharge which support the conclusions of Sato's recent study on backward waves in neon [1].

Whilst some previous workers [2] had shown that the wavelength, frequency, and velocity were all functions of the discharge tube radius, others [3] had found that the frequency was independent of the radius and remained constant. Sato resolved this contradiction by suggesting that in the latter case the striations were synchronised to the frequency of natural oscillations occurring at the electrodes or of external forces applied to the tube.

The present work was carried out using the discharge tube shown in fig. 1; the cathode and anode were the same as those used previously [4] and the argon was of technical quality. The oscillations were detected using a photomultiplier or a pick-up coil [4], and a Tektronix X1000 probe was used to detect fluctuations in anode voltage. The oscillations were detected in the pressure range 0.2 to 8 torr and currents between 0.1 and 0.5 A.

Generally, the signals from tube A were noisy; the noise decreased progressively from tube A to tube D

which was filled mainly by the Faraday dark space. Several anode spots were clearly visible. The nature of the oscillations is best described by quoting specific examples.

At a pressure of 0.22 torr and a current of 0.26 A, anode voltage fluctuations with frequencies of 3.5 and 7 kHz were detected. The photomultiplier signal from tube A consisted of noise with a noticeable peak around 3.5 kHz. Only the higher frequency was detected in the remaining tubes. For a larger current, 0.33 A, the anode oscillations occurred at frequencies of about 4 and 8 kHz, with the amplitude of the 8 kHz oscillation about twice that of the 4 kHz. In tube A both frequencies were detectable above the noise but the 4 kHz has a slightly larger amplitude than the 8 kHz. In tube B both frequencies were seen; the 8 kHz signal was much larger than the 4 kHz and as the photomultiplier was moved towards the cathode end the amplitude of the 8 kHz signal increased whilst that of the 4 kHz decreased. Tube C supported both frequencies with again the amplitude of the 8 kHz oscillation much larger than that of the 4 kHz oscillation. In tube D signals at both frequencies were seen and their amplitudes were approximately equal.

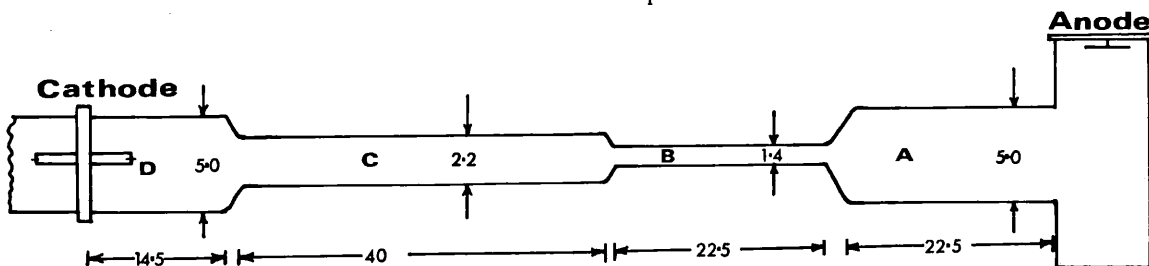


Fig. 1. Discharge tube geometry (dimensions in cm).

At a pressure of 1 torr and current of 0.42 A, the anode voltage oscillations consisted of a fundamental frequency of about 1.5 kHz and harmonics. The signals detected by the coils on the other tubes showed the same frequency spectra although the relative amplitude of the harmonics was not the same for each tube. In tube B, the fundamental and second harmonic were much smaller relative to the first harmonic than in tube C.

Sato found that, whilst the frequency remained constant throughout the tube, the amplitude of the higher harmonics increased with decreasing tube radius. This is related to the fact that the resonance frequency also increases with decreasing radius. The present results may be understood from these points. The tubes act as selective amplifiers. Tube A, with the largest radius, synchronises more readily to the lower frequencies of the anode oscillations. Tubes B and C, on the other hand, with smaller radii, prefer the higher frequencies. In some cases the lower frequency is damped out by tubes B and C so that in tube D, which has the same radius as tube A, only the higher frequency is detectable.

The mechanism by which the anode voltage fluctuations are linked to the striations could be through

the anode spots [5]. The dependence of the wavelength on radius was not investigated but for the first two cases mentioned it was found that "stationary" striations were visible in the narrow tube, originating at the cathode end and extending along about half to three-quarters the length of the tube. These "stationary" striations were, in fact, a standing wave with the frequency of the detected oscillation and with a separation in maxima of about 3 cm. This phenomenon is under further investigation.

The authors are grateful to Mr. R. Mason for constructing the discharge tube, and one of us (R.M. Perkin) is in receipt of a Science Research Council maintenance grant.

References

- [1] M. Sato, Beitr. Plasmaphys. 11 (1971) 445.
- [2] A.W. Cooper, J. Appl. Phys. 35 (1964) 2877.
- [3] T. Kenjo and Y. Hatta, J. Phys. Soc. Japan 19 (1964) 2313.
- [4] R.M. Perkin and E.R. Wooding, Electronics Letters 7 (1971) 781.
- [5] J.R.M. Coulter, N.H.K. Armstrong and K.G. Emeleus, Physica 24 (1958) 828.

NON-LINEAR GENERATION OF IONIZATION WAVES

R.M. PERKIN* and E.R. WOODING

*Department of Physics, Royal Holloway College (University of London),
Englefield Green, Surrey, England*

Received 31 October 1972

By including non-linear terms in the equation for ionization waves it is shown that waves at harmonic and 'sum' and 'difference' frequencies may be generated.

By including non-linear terms in the Pekarek-Krejci equation for ionization waves [1], resonant wave coupling and the non-linear response of an unstable positive column have recently been examined [2, 3]. We now show that by using these non-linear terms and assuming that a sinusoidal oscillation is established that harmonics of this fundamental mode may be produced by forced oscillation. The basic equation which is used is the Pekarek-Krejci equation in the high current limit.

$$\partial N/\partial t = D_{A0} \partial^2 N/\partial x^2 + D' \Delta \theta \partial^2 N/\partial x^2 + A \Delta \theta N \quad (1)$$

where N is the particle density, ($N_e = N_i = N$), D_{A0} is the ambipolar diffusion coefficient, D' equals $\partial D_A/\partial \theta_0$, θ is the electron temperature, $\Delta \theta$ is the deviation in the electron temperature; A equals $(\partial Z/\partial \theta_0 + \tau^{-2} \partial \tau/\partial \theta)$, Z is the ionization rate and τ is the lifetime of the charged carriers. By using the derivatives of $D(\theta_0)$, $Z(\theta_0)$, $\tau(\theta_0)$ in finding $D(\theta_0 + \Delta \theta)$, $Z(\theta_0 + \Delta \theta)$, $\tau(\theta_0 + \Delta \theta)$ we imply that $\Delta \theta \ll \theta_0$.

It is assumed that N and θ may be expanded in a perturbation series,

$$\begin{aligned} N(x, t) &= N_0 + N^{(1)}(x, t) + N^{(2)}(x, t) + \dots + N^{(N)}(x, t) \\ \theta(x, t) &= \theta_0 + \theta^{(1)}(x, t) + \theta^{(2)}(x, t) + \dots + \theta^{(N)}(x, t) \end{aligned} \quad (2)$$

where N_0 and θ_0 are the steady state values and $N^{(N)}(x, t)$ and $\theta^{(N)}(x, t)$ are the N^{th} order perturbations.

Substituting (2) into eq. (1), the first order equation is

$$\frac{\partial N^{(1)}}{\partial t}(x, t) - D_{A0} \frac{\partial^2 N^{(1)}}{\partial x^2}(x, t) = A \theta^{(1)}(x, t) N_0 \quad (3)$$

We suppose that $N^{(1)}(x, t)$ and $\theta^{(1)}(x, t)$ are the parameters of the fundamental oscillation and that

$$N^{(1)}(x, t) = n_1 \exp(\alpha x) \sin(\omega t - kx) \quad (4)$$

Sinusoidal variations are chosen for simplicity and because they correspond, in many cases, to the experimental conditions. Inspection of (3) shows that $\theta^{(1)}(x, t)$ will vary as $\theta_{(1)} \exp(\alpha x) \sin(\omega t - kx + \phi)$ where

$$\tan \phi = (\omega + D_{A0} 2\alpha k) / \{D_{A0} (k^2 - \alpha^2)\}$$

$$\text{and } \theta_{(1)} = \frac{n_1}{N_0 A} [(\alpha^2 + k^2)^2 D_{A0}^2 + \omega(4\alpha k D_{A0} + \omega)]^{1/2}.$$

The second order equation is

$$\begin{aligned} \frac{\partial N^{(2)}}{\partial t}(x, t) - D_{A0} \frac{\partial^2 N^{(2)}}{\partial x^2}(x, t) - D' \theta^{(2)}(x, t) N_0 = \\ = D' \theta^{(1)}(x, t) \frac{\partial^2 N^{(1)}}{\partial x^2}(x, t) + A \theta^{(1)}(x, t) N^{(1)}(x, t). \end{aligned} \quad (5)$$

The right-hand side of (5) acts as a source term which, due to the product $N^{(1)}(x, t) \theta^{(1)}(x, t)$ is proportional to $\exp(2\alpha x) [\cos \theta - \cos(2\omega t - 2kx + \phi)]$. For the equation to be satisfied, $\theta^{(2)}(x, t)$ must be proportional to $\exp(2\alpha x) [\cos \theta - \cos(2\omega t - 2kx + \phi)]$ whilst $N^{(2)}(x, t)$ will be proportional to

* Now at Czech Technical University, Prague.

$\exp(2\alpha x) \cos(2\omega t - 2kx + \phi + \beta)$ where β is the phase difference between $\theta^{(2)}(x, t)$ and $N^{(2)}(x, t)$ as determined from (5). Thus the first harmonics in particle density and electron temperature are generated. In a similar way, higher harmonics will be obtained from higher order equations. In general the n th harmonic in electron density is proportional to

$$\exp\{(n+1)\alpha x\} \exp\{i[(n+1)\omega t - (n+1)kx + \gamma_N]\} \quad (6)$$

Self excited striations consisting of a fundamental mode and harmonics with a frequency and wavenumber dependence of the form of (6) have been observed [4].

If in the expression for $N^{(1)}(x, t)$ a term at another frequency and wavenumber is added, then harmonics of this second frequency will be produced together with 'virtual' waves at the sum and difference frequencies of the two initial waves. The term 'virtual' is used in the sense that the wavenumber and frequen-

cies of these sum and difference modes are not necessarily related through a dispersion relation.

This simple derivation indicates how harmonics and sum and difference frequencies might be generated. An exact solution requires the use of a more complete set of equations rather than the eq. (1) used here.

R.M. Perkin is in receipt of a Science Research Council Maintenance grant.

References

- [1] N.L. Oleson and A.W. Cooper, *Advan. Electron Electron Phys.* 24 (1968) 155.
- [2] S. Poberjac, *Proc. 10th Int. Conf. Phen. Ion. Gas.* Oxford 1971, p. 292.
- [3] I. Grabec, *Beitr. Plasma Physik* 11 (1971) 285.
- [4] R.M. Perkin and E.R. Wooding, *Electron. Lett.* 7 (1971) 781.

FORCED MODULATION OF SELF EXCITED STRIATIONS IN A DISCHARGE TUBE OF VARYING DIAMETER

R.M. PERKIN* and E.R. WOODING

Royal Holloway College (University of London), Egham, Surrey, UK

Received 2 July 1973

Observations on striations contained in a discharge tube of varying diameter are reported and explained in terms of forced modulation.

Recently some results were presented which were concerned with self-excited striations in a discharge tube made from several glass pipes of different diameters [1]. It was observed that the frequency of the striations was constant but that in the narrower tubes the oscillations at the larger frequencies were more prominent. This was explained by the fact that the resonant frequency for striations increases with decreasing tube radius. Further considerations suggest that the higher frequency signal grows in preference to the lower frequency not only because of the smaller tube radius but also because of forced oscillation at this higher frequency. This driving of the striations is in addition to the forced oscillation by which Sato explained the synchronization of frequencies in a tapered tube.

The experimental details have been given elsewhere [1] and here the same nomenclature is used to describe the discharge tube. The spectra of the oscillations found, using an external pick-up coil, in the different tubes for a current of 165 mA and a pressure of 0.3 torr is shown in fig. 1. It can be seen that common to the tubes are oscillations at about 5 kHz and 8.5 kHz. In the narrowest tube (B), apparently standing striations were clearly visible to the naked eye extending from the cathode end nearly to the anode end of the tube. The time-averaged spectrum analyser signal from the coil showed a corresponding "standing" wave pattern at a frequency of 8.5 kHz. Due to a "flickering" of the discharge it was not possible to obtain a space-time display picture of the striations in tube B. However, it was found using an argon discharge in a tube of 5 cm diameter at a similar pressure, that when an external

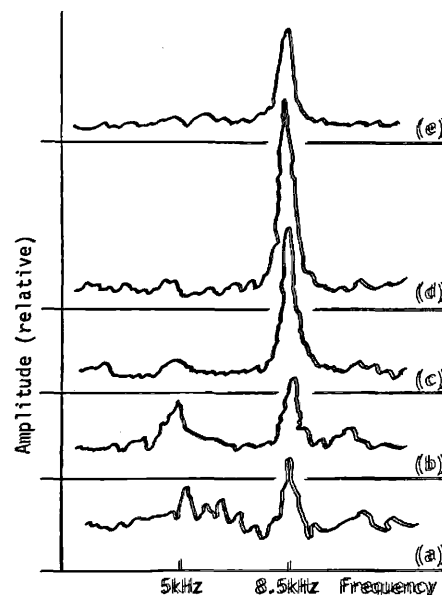


Fig. 1. Spectra in various parts of the tube. Pressure 0.3 torr, current 165 mA. (a) Tube A. (b) Tube B - anode end (86 cm) (c) Tube B - cathode end (68 cm) (d) Tube C - anode end (62 cm) (e) Tube C - cathode end (28 cm).

voltage signal was applied across the discharge at the frequency, or harmonic, of the striations, similar "apparently standing" striations were visible. This was due to forced driving of the striations [3] which can be represented as

$$\exp(i\omega t - kx + \beta \sin \omega t)$$

and which appeared on the space-time display as velocity modulation of the striations. It is suggested that a similar effect occurs in the narrow tube B, the external drive being provided by the feedback to the electrodes.

* Present address: Institute of Physics, Na Slovance 2, Prague 8.

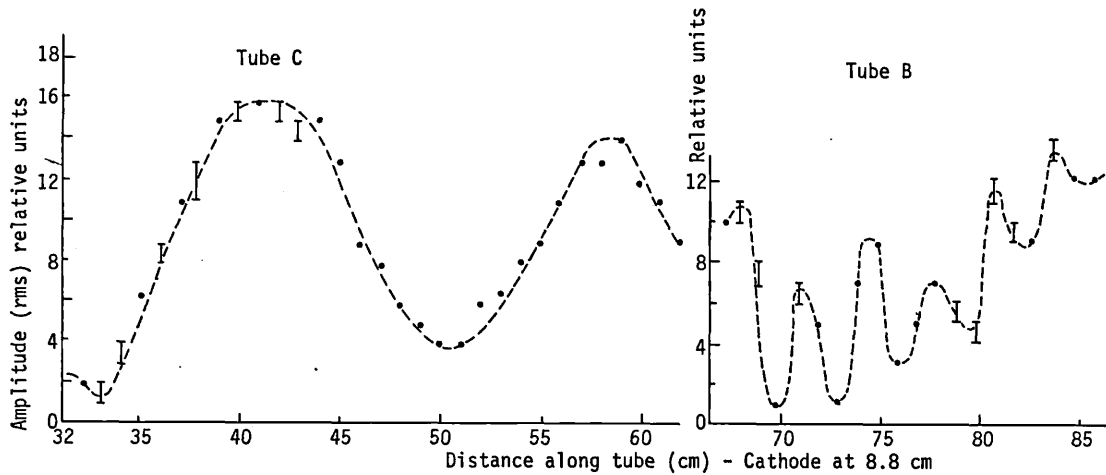


Fig. 2. Amplitude of signal from coil in tubes B, C. Pressure 0.3 torr, current 165 mA, frequency 8.5 kHz.

From fig. 1 it can be seen that in tube A the 5 kHz and 8.5 kHz signals only just appear above the noise. In tube B, the noise and the 5 kHz signal are suppressed progressively towards the cathode end whilst the amplitude of the 8 kHz signal changes as in fig. 2. In tube C the noise level is constant whilst the 5 kHz signal is damped further. The variation in amplitude of the 8.5 kHz signal is shown in fig. 2 but in this case no "apparently standing" striations were visible.

From the present results at least, the forced driving at the higher frequency seems most effective in the narrow tube. This is probably due to the selective effect of tubes B and C [1] resulting in greater feedback of the higher frequency appearing in the anode voltage oscillations. Usually the higher frequency has the larger amplitude.

Forced modulation has been observed for ion sound waves [4] and striations [3]. In the former case a non-linear theory showed that the behaviour

of the waves was similar to a Van der Pol oscillator. The inherent non-linear nature of self-excited striations makes a theoretical explanation difficult and it has yet to be shown that an equation describing striations can be reduced to a Van der Pol type of equation.

R.M. Perkin was in receipt of a Science Research Council maintenance grant when this work was carried out.

References

- [1] R.M. Perkin and E.R. Wooding, *Phys. Lett.* 41A (1972) 27.
- [2] M. Sato, *Beitr. Plasmaphys.* 11 (1971) 445.
- [3] A. Garscadden, P.B. Bletzinger and T.C. Simonen, *Phys. Fluids* 12 (1969) 1833.
- [4] B.E. Keen and W.H.W. Fletcher, *J. Phys. D. Appl. Phys.* 3 (1970) 1868.

4.3.3.6

VELOCITY-MODULATED IONIZATION WAVES (STRIATIONS)

R. M. Perkin

Institute of Physics, Czech.Acad.Sci., Prague, Czechoslovakia

Under certain discharge conditions self-excited striations may be velocity modulated /1, 2/. In some cases, the velocity changes appear to move in the direction of the anode or occur in identical places of the tube giving rise to "apparently standing" striations which are visible to the naked-eye /1, 3/. The latter case is shown in Fig.1 where an external voltage of the same frequency as the striations was applied. The explanation for such motion is not clear but may be connected with the disturbances carried through the stratified column in the direction of the group velocity of the (backward) waves /1/. In /4/ the modulation has been described using the Van Der Pol oscillator as a model, but for striations it has not yet been shown that the equations representing striations can be reduced to a Van Der Pol type of equation.

Since the space-time photographs for such velocity variations often exhibit a regular pattern it seems of interest to examine the motion of striations which have periodic variations in frequency and wavenumber. Such a description cannot account for the highly irregular motion including branching effects (seen in some cases /1/) which are connected with frequency mismatching and changes in the mean velocity.

We suppose that a striation travelling from the anode to the cathode can be represented by,

$$\psi(x,t) = \cos F(x,t)$$

where

$$\frac{\partial F}{\partial t} = \omega(t) = \omega + m_a \Omega \cos(\Omega t)$$

$$-\frac{\partial F}{\partial x} = k(x) = k - m_x K \cos(Kx)$$

giving $F(x,t) = \omega t - kx + m_a \sin(\Omega t) + m_x \sin(Kx) \dots (1)$
 In the absence of modulation, $\psi(x,t)$ reduces to the normal cosine expression for a travelling wave. The space-time diagram is found from $\psi(x,t) = 1$, $F(x,t) = 2\pi n$.

Fig.2 shows the cases (a) $m_x = 0$ and (b) $m_a = 0$. For self-excited striations which are not exactly sinusoidal, the wavenumber modulation will give rise to the "apparently standing" striations for any value of K , while for frequency modulation the occurrence of "apparent standing" striations will depend on the relative values of ω, Ω . For example, when $\Omega = n\omega$ they will be seen.

For simultaneous frequency and wavenumber modulation for arbitrary values of Ω and K the motion will be more complicated since in this case the changes will appear to propagate in a complex way. Of interest is the case when $\frac{\Omega}{\omega} = \frac{K}{k}$, since this corresponds to experimental observations /1/, which is shown in Fig.3 for $K = \frac{k}{2}$. The simplification $m_a = m_x$ was made together with the initial approximation that $\omega t - kx = 2\pi n$ which was substituted in the term $\sin(Kx)$. It can be seen that the changes occur with a velocity directed towards the anode and equal in magnitude to $\frac{\omega}{k}$. However, whilst the picture obtained resembles /1/, it differs in that there is a "jumping" of the motion. Thus to some extent the anode directed disturbances may be described in terms of frequency and wavenumber modulation.

It has been pointed out /5/ that linear ionization waves exhibit interesting phenomenological similarities with water waves. In trying to understand non-linear striations therefore, it may prove useful to draw the analogy with non-linear water waves. For example the instability of Stoke's waves observed in /6/ is similar to the experiment /4/ where an externally excited ionization wave gave rise to a broad spectrum of waves. The more general expressions, from kinematic wave theory /8/, for the relation between wavenumber and frequency which take into account spatial and amplitude dependence when applied to ionization waves may provide the explanation for the highly irregular behaviour of striations /1/ and other non-linear effects which are hitherto unexplained.

REFERENCES:

- /1/ R.S. STEWART et Al., Int.J.Electr. 18 65 (1965)
- /2/ O.A. LEE, P. BLETZINGER, A. GASCADEN, J.App.Phys. 37 377 (1966)
- /3/ M.K. PIGG et Al., 3rd I.C.P.I.G., Venice, 833 (1957)
- /4/ A. GASCADEN, P.B. BLETZINGER, 10th I.C.P.I.G., Oxford (1971)
- /5/ L. PEKÁREK, Invited Paper 9th I.C.P.I.G., Bucharest (1969)
- /6/ T.B. BENJAMIN, Proc.Roy.Soc. 299 59 (1967)
- /7/ S. POBERAJ, I. GRABEC, Summer Sch. Hercegnovi 153 (1970)
- /8/ M.T. LIGHTILL et Al. in "Hyperbolic Equations and Waves" ed.M.Froissart, Springer-Verlag 1970.



Fig.1. Modulated Argon Discharge, Pressure = 0.46 torr Current = 92 mA, Wavelength = 16.5 cm, Frequency = 2.5 kHz.

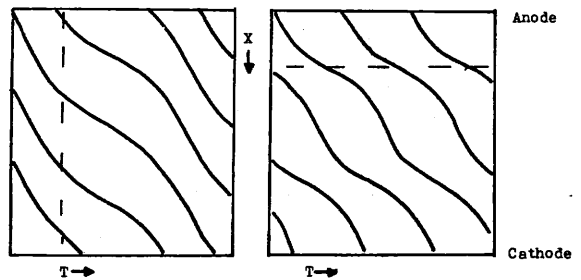


Fig.2. Frequency (a) and Space (b) Modulation.

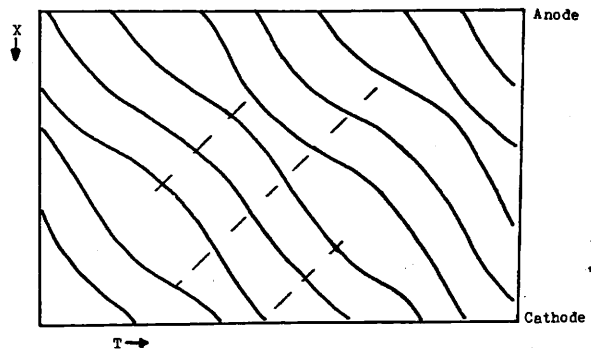


Fig.3. Calculated Space-time diagram for simultaneous frequency and wavenumber modulation.

4.3.3.5

THE DEPENDENCE OF THE BOUNDARY FOR SELF-EXCITATION OF IONIZATION WAVES ON THE POWER OF THE AUXILIARY HIGH FREQUENCY FIELD

J. Šafránková

Faculty of Mathematics and Physics, Charles University Prague, Czechoslovakia

One way to increase the boundary for self-excitation of ionization waves is based upon the local disturbance of axial electrical field in plasma [1]. In order to accomplish this we can, for instance, use the high-frequency field or add a grid of special shape into the region of the anode column, as was shown in [2]. However, in none of these works the displacement of the boundary for self-excitation is studied in dependence on the magnitude of local disturbance.

Thus the object of our work was to measure the dependence of the boundary for the self-excitation of ionization waves upon high-frequency power absorbed in plasma. Quantitative knowledge of this dependence is significant for the operating mode of devices, which use the low-pressure plasma discharge (for instance gas lasers, discharge noise generators).

To derive the expression for the power absorbed in plasma, we start from the telegraph equations describing the propagation of electromagnetic waves in a transmission line. If we consider the case of a line supplied by high-frequency generator and terminated with general impedance:

$$\hat{Z} = R + jX,$$

we receive for the power absorbed in plasma

$$P = \frac{(|U_{max}| + |U_{min}|)^2}{2Z_0} \frac{R}{(R+1)^2 + X^2}$$

where Z_0 is the characteristic impedance of the line used. This expression is valid for an arbitrary loss-free line. The real and imaginary parts R, X of the loading impedance can be determined in classical way from the measurement of standing waves on the line and by the use of the Smith chart of the factor:

$$\frac{(|U_{max}| + |U_{min}|)^2}{(|U_{max}| - |U_{min}|)^2}$$

includes the influence of the variable output-voltage of the feeding generator. U_{max}, U_{min} are respectively the values of voltage corresponding to maxima and minima of standing waves on the measured line. It is, however, necessary to calibrate the line in units of voltage. To this aim we have used a high-frequency voltmeter.

The measurement of the dependence of the boundary for self-excitation of ionization waves upon the power absorbed in plasma has been made in the experimental set-up shown in Fig.1. In order to change the resonance frequency of the resonator with plasma we changed the position of an adjusting impedance. By means of this the power absorbed in plasma changed too and we could observe the displacements of the boundary for self-excitation of the ionization waves. Two of the typical dependences are in Fig.2. They are different in the range of medium power. For too small or sufficiently large power the boundary for self-excitation of ionization waves is the same in both dependences. For large power certain saturation is observed, that is, with increasing value of absorbed power the boundary for self-excitation remains constant. In the range of medium power the dependence in both graphs is qualitatively the same. On both a rapid increase of the boundary for self-excitation of ionization waves occurs, however, on each of them for different power absorbed in plasma. This effect can be explained as a consequence of different values of ignition and extinguishing voltage of the high-frequency discharge superposed upon the D.C. discharge. Suppose the high-frequency discharge is burning, then it extinguishes (which results in decrease of the boundary for self-excitation of ionization waves) at considerably lower power than in the case when we proceed in the opposite sequence, that is, the discharge is not yet burning, but then ignites. This explanation is based on the measured behaviour of light intensity of the auxiliary high-frequency discharge.

From Fig.2 it is obvious that the value of the boundary for self-excitation of ionization waves is closely related to the existence of high-frequency discharge. Therefore the dependence of the boundary for self-excitation of ionization waves upon light

intensity of high-frequency discharge is plotted on graph 3. The saturation at high light intensities (that is, at high absorbed power) is observed also on this dependence.

One of the possible explanations of this saturation is based on work [3], where the dependence of the increment of amplification of ionization waves on the discharge current is measured. From the curve in this work which corresponds with our experimental conditions (pressure of neon 1,3 torr, diameter of the tube 2 cm) we can deduce that rapid increase of the increment of amplification of ionization waves occurs at a current of 7 mA. Our measurement indicates that in the range of lower discharge currents, where the dependence of the increment of amplification upon the discharge current is approximately linear in semilogarithmic scale. The dependence of the boundary of self-excitation of ionization waves upon light intensity of the auxiliary high-frequency discharge is linear. For currents of about 7 mA, where a more pronounced increase of amplification of ionization waves occurs, the boundary for self-excitation of ionization waves increases far slower.

The following conclusion results from our measurement: If we want to use a local high-frequency field for attenuation of self-exciting ionization waves, it is not advantageous to use high power. If we succeed to ignite the high-frequency discharge in plasma, further increase of the power absorbed in plasma does not substantially increase the boundary of self-excitation. In our case absorbed power of tens of mW proved to be sufficient for the attenuation.

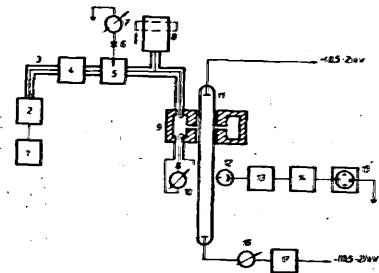


Fig. 1

1. Frequency meter; 2. Microwave generator; 3. Coaxial line;
4. Attenuator; 5. Measuring line; 6. Probe of measuring line;
7. Circuit of probe of measuring line; 8. Matching impedance;
9. Toroidal resonator; 10, 16. Milliammeter; 11. Discharge tube;
12. Photomultiplier; 13. Cathode follower; 14. Noise reductor;
15. Oscillograph; 17. Current stabilizer.

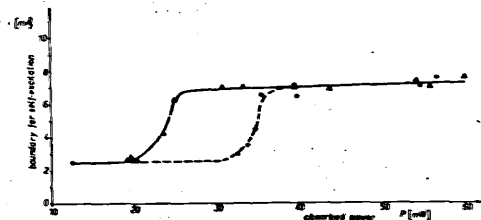


Fig. 2

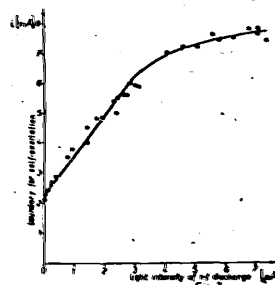


Fig. 3

References:

- [1] Šícha M.: Czech.J.Phys. B 17 (1967) 867
- [2] Takayama K., Ikeda H., Miyake S.: VIII. International Conference on Phenomena in Ionized Gases (1967, Vienna) contributed papers page 553
- [3] Achterberg H., Michel J.: Ann.Phys., 7 Folge, Bd.2 (1959) 365

Nonlinear interference of ionization waves

R M Perkin,† J Krása,‡ and L Pekárek‡

† Culham Laboratory, UKAEA, Abingdon, Berks

‡ Institute of Physics, Czech. Acad. Sci. 180 40 Prague 8, Na Slovance 2, Czechoslovakia

Received 20 July 1974, in final form 25 September 1974

Abstract. The onset of irregular wave motion caused by nonlinear interference of two spontaneously existing ionization wave varieties is described and compared with the situation when only a single wave becomes irregular due to forced modulation by its harmonics. A similar phenomenological explanation for the loss of periodicity based on the influence of combined frequencies and wavenumbers of the fundamental originally periodic waves can be given in this case.

1. Introduction

The onset of irregular wave motion in the case when only one wave variety is observed in a neon discharge has been studied by Krása *et al* (1974). In the present paper, the irregular wave motion caused by nonlinear interference of two varieties existing spontaneously in the discharge is investigated.

Generation of difference and summation frequencies by interaction of two ionization waves, one existing spontaneously and the other externally excited, was reported by Grabec (1972). Ohe and Takeda (1972) found nonlinear mixing of frequencies between a spontaneously existing ionization wave and external periodic modulation of the discharge current. They explained the mixing by a combined modulation of frequency and amplitude of the wave. No other experiments on the connection of the nonlinear interference of ionization waves with the onset of irregular wave motion have been reported.

2. Apparatus

A rotating drum camera and a frequency-spectrum analyser already described (Krása *et al* 1974) were used to visualize the wave motion and find the frequency spectrum.

The mean phase velocity of the self-excited waves and its current dependence was measured using the space-time oscilloscopic method (Štirand *et al* 1966) to obtain the conditional average of the wave pattern (Pekárek *et al* 1969).

The tube was 80 cm in length with internal diameter of 0.99 cm, and was filled by spectroscopically pure neon. The investigated current region was from 6 to 60 mA, the gas pressure being 4.9 Torr.

3. Results

Two wave varieties were observed, existing simultaneously in the current region from 6 to 20 mA. From the dependence of their velocity on the discharge current, both waves were identified as slow (metastable-guided) waves, belonging to the first resonance (the long 's' wave) and the second resonance (the short 'p' wave) (Rohlena *et al* 1972). At lower current, (6 mA) the short 'p' variety was dominant. With increasing current the long s' variety prevailed, and above 20 mA only the s' variety was observed (figure 1).

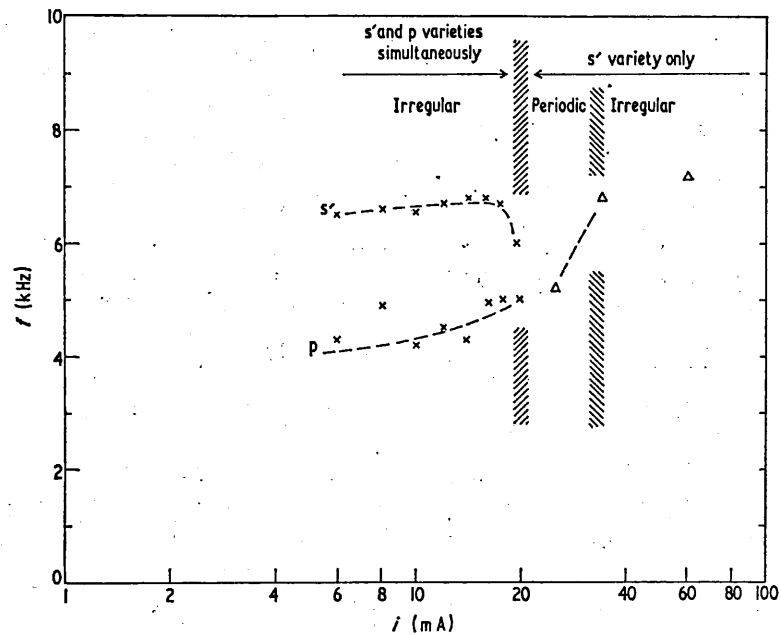


Figure 1. Current dependence of frequency of p and s' wave varieties at $p=4.9$ Torr.

The rotating-drum photographs revealed coherent (periodic-in-time) motion of both wave varieties in the region of the column which was nearest to the cathode, even if in most of the column the wave motion was irregular.

In the region where the waves are periodic, their nonlinear interference expressed itself by combination frequencies appearing in the Fourier spectra (figure 2).

The two fundamental wave-frequencies were $f_{s'}=6.8$ kHz, and $f_p=4.3$ kHz. Maxima belonging to harmonics $2f_{s'}=13.6$ kHz, $2f_p=8.6$ kHz of the s' and p waves, and to difference and summation frequencies of fundamental frequencies $f_{s'}-f_p=2.5$ kHz, $f_{s'}+f_p=11.1$ kHz, were distinctly resolved.

Development of the nonlinear wave interference along the tube axis can be followed in figure 3 (plate), which is a rotating drum photograph of the discharge at 18 mA. Fourier spectra of the wave pattern taken at different distances from the cathode are presented in figure 4.

Near the cathode (figure 3) only the short-wave p variety can be distinctly seen, with a strictly periodic motion and simple line spectrum (figure 4a). At 14 cm from cathode, both s' and p waves have approximately equal amplitudes (figure 4b), and slightly

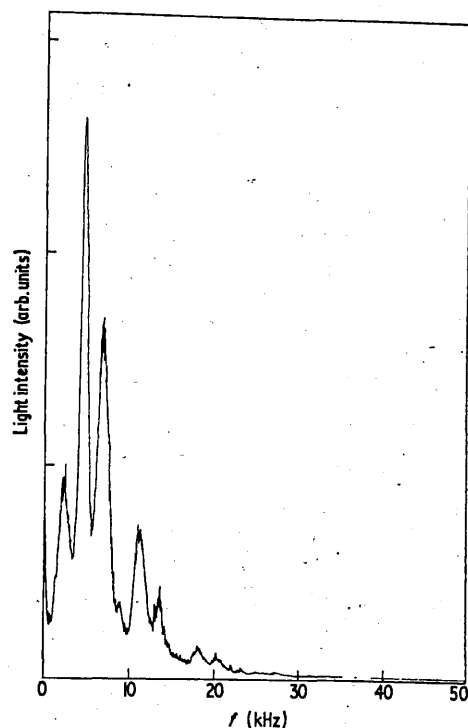


Figure 2. Frequency spectrum 14 cm from cathode at $I=14$ mA. $f_0=4.3$ kHz and $f_{s'}=6.8$ kHz.

pronounced peaks corresponding to summation and difference frequencies appear in the spectrum. Still further from the cathode, only the faster irregularly moving s' wave with continuous spectrum (figure 4c) centring around 6.8 kHz is observed. Approaching the anode, we find a smooth continuous spectrum (figure 4d) with its maximum at 5.8 kHz lying between the frequencies of the two fundamental waves. The wave motion (figure 3) is very irregular, exhibiting quickly following jumps in the phase velocity, and creation and disappearance of the wave crests is observed.

4. Discussion

The irregular wave motion above 30 mA (see figure 1) concerns only one (s') wave variety. This situation was investigated earlier (Krása *et al* 1974) and explained as a consequence of forced modulation of waves by harmonics in frequency and wavelength.

Below 30 mA, the wave becomes strictly periodic, until the regularity of its motion is disturbed again at 20 mA and lower. At this current, the other (p) variety appears simultaneously in the column, and nonlinear mixing of the two waves results in combination frequencies and wave numbers lying closer to the maxima of the growth rates of the two waves than their ordinary harmonics. This makes the forced modulation easier, and it leads again to irregular excitation of waves from different parts of the dispersion curve with different phase velocities. The excited modes propagate as wave packets with anode-directed group velocity and interfere nonlinearly giving rise to excitation of

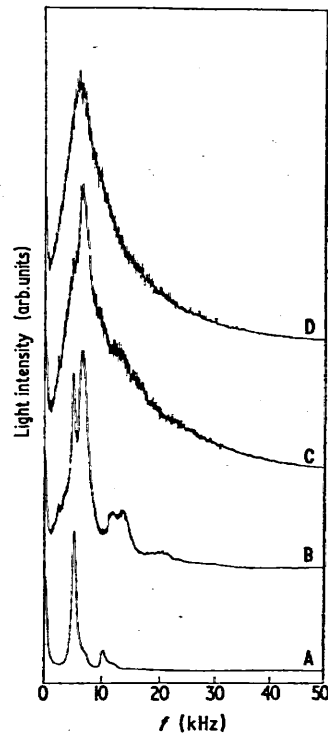


Figure 4. Frequency spectrum at $I=18$ mA, at various distances from cathode: (A) 6 cm; (B) 14 cm; (C) 32 cm; (D) 15 cm.

new wave packets. The irregularity of wave motion grows along the direction of propagation, the wave packets are still shorter in space and time, and, eventually, the frequency spectrum of the whole pattern becomes quite continuous.

5. Conclusions

A nonlinear interference of two wave varieties existing simultaneously in the discharge can disturb the originally periodic motion of the waves and lead to irregular wave motion even more easily than if only one wave variety were present. In both cases, the randomization of wave motion is connected closely with the strong dispersion of ionization waves (usually causing the waves to be backward waves).

References

- Grabec I 1972 *Beitr. Plasmaphys.* **12** 83–6
 Krása J, Perkin R M and Pekárek L 1974 *J. Phys. D: Appl. Phys.* **7** 2541–4
 Ohe K and Takeda S 1972 *Jap. J. Appl. Phys.* **11** 1173–80
 Štirand O, Krejčí V and Láška L 1966 *Rev. Sci. Instrum.* **37** 1481–4
 Pekárek L, Krejčí V, Grabec I and Peřina V 1969, *Proc. 9th Int. Conf. on Phenomena in Ionized Gases, Bucharest* (Bucharest: Ek. Akad. Rep. Soc. Rom.) p 460
 Rohlena K, Růžička T and Pekárek L 1972 *Czech. J. Phys.* **B22** 920–37

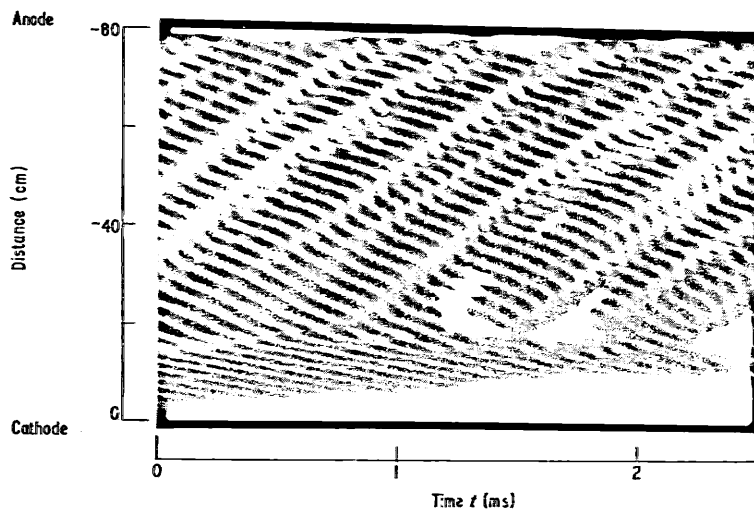


Figure 3. Rotating-drum (single-sweep) photograph of the discharge at $I=18$ mA.

The evolution from regular to irregular motion of ionization waves in neon

J Krása†, R M Perkin‡ and L Pekárek†

† Institute of Physics, Czechoslovakian Academy of Science, 180 40 Prague 8,
Na Slovance 2, Czechoslovakia

‡ Culham Laboratory, UKAEA, Abingdon, Berks

Received 13 May 1974

Abstract. Experimental observations on the motion of s' variety ionization waves in neon are reported. The results are explained in terms of mode-jumping and forced modulation due to nonlinear effects.

1. Introduction

Because of their inherent nonlinearity, self-excited ionization waves (striations) occurring in the positive column of glow discharges offer a readily available source for the observation of nonlinear and turbulent effects (Stewart *et al* 1965, Lee *et al* 1966, Sato 1970, Krása and Pekárek 1973). Examples of this are the nonlinear saturation of an initially linear wave and the generation of a broad frequency spectrum from a single frequency (Poberaj and Grabec 1970). Other effects such as irregular ionization waves or disturbances apparently moving towards the anode have been attributed to the nonlinearity of the ionization term or the nonlinear interference of two different wave varieties (Grabec 1973, Perkin *et al* 1974).

This paper describes the evolution from regular to irregular motion of a single variety of a spontaneously existing ionization wave.

2. Apparatus

The discharge tube was 80 cm in length with a diameter of 0.99 cm. A plane anode was used together with a hollow cathode. The wave motion was recorded by imaging the light from the discharge with an $f/1.8$ lens on to a rotating drum holding film of 800 ASA. In addition, a spectrum analyser and photomultiplier were used to record the frequency spectra of the waves.

The dispersion curves for irregular waves were evaluated from the rotating-drum, single-sweep photographs.

The results described were taken at a pressure of 4.9 Torr.

3. Results

To avoid interference phenomena between several wave varieties, the discharge pressure and current were chosen so that only one wave variety was observed in the column. It

was identified as the s' variety (see Pekárek 1971, Rohlena *et al* 1972a, b), ie the long wave guided by changes in the metastable atom density.

At a current of 25 mA the self-excited wave was periodic and moving regularly, as can be seen from figure 1 (plate). The frequency spectra consisted of a fundamental frequency of 5.2 kHz together with harmonics of this frequency. When the current was increased to 34 mA the motion remained regular throughout most of the discharge, but near the anode the phase velocity fluctuated, giving the appearance of disturbances moving in the direction of the anode (figure 2*a*, plate). The corresponding spectrum in this region is shown in figure 2*(b)*, plate). Besides the fundamental and harmonics there were 'satellite' frequencies with a spacing from the other frequencies equal to half the fundamental frequency. The amplitudes of the fundamental frequency and its harmonics saturated whilst the 'satellite' frequencies grew in amplitude towards the anode. At a current of 61.5 mA, the fluctuations of phase velocity were already apparent at 20 cm from the cathode. Moving towards the anode, the disturbances of phase velocity developed into abrupt changes, and branching and fusion of striations was observed. The motion became quite irregular (figure 3*a*, plate). The frequency spectrum at various points along the tube for this case is shown in figure 3*(b, c)*, plate).

The local frequencies and corresponding wavelengths were found from figure 3*(a)*, and it was then possible to plot a dispersion curve for the waves in the region of irregular motion (figure 3*d*, plate).

The points shown on the dispersion curve were obtained from places at different distances from the cathode (eg the point marked by full triangle in figure 3*(d)* corresponds to the coherent wave near the cathode; the others were taken from the irregular part of wave pattern). Within the error of the evaluation method, all points lie on the same approximately hyperbolic curve. The group velocity of a certain wave-mode is therefore opposite and close in absolute value to the phase velocity. For the fundamental mode, this feature of the wave is distinctly seen on the disturbances propagating towards cathode.

4. Discussion

The harmonics nk_F , nf_F which develop in the coherent wave as a result of the nonlinearity of the ionization term grow in the direction of the group velocity in which the wave is amplified (Perkin and Wooding 1973). For some time, they move with the same phase velocity as the fundamental mode (which has frequency f_F and wavenumber k_F) so that they can be represented as lying on 'virtual' dispersion curves (see figure 4, where the point for $n=2$ is shown and marked by V).

The subharmonic frequency $f_F/2$ in the spectrum (figure 2*b*) appearing at a certain distance from cathode is caused evidently by the second harmonic in wavenumber, which—if its amplitude is high enough—begins to move independently on the fundamental wave with a phase velocity corresponding to the point $k=2k_F$ on the real dispersion curve (figure 3*d*). As the dispersion curve is hyperbolic in this case, a subharmonic frequency $f_F/2$ is generated by the harmonic wavenumber $2k_F$. Wave packets corresponding to this point on the dispersion curve can also be found on the single-sweep photographs (figures 2*a*, 3*a*) in the parts of the column where the wave motion becomes irregular.

The onset of the independent movement of the harmonics depends evidently on the degree of the nonlinearity of the fundamental wave and is sensitive to any fluctuation. The newly excited waves are therefore not exactly periodic from the very beginning. This

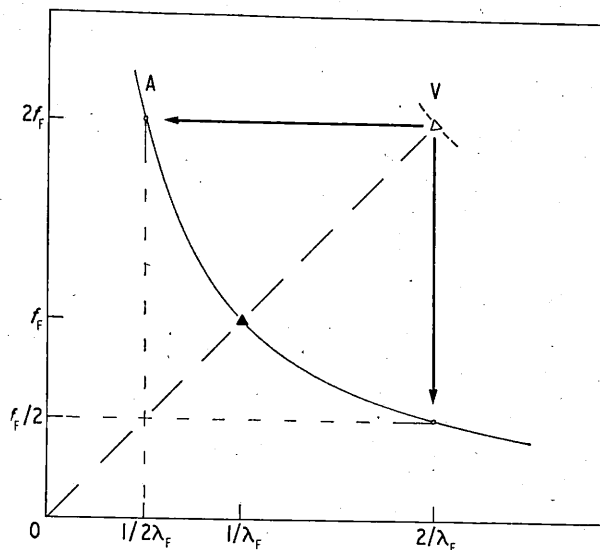


Figure 4. The suggested scheme for forced generation of harmonic and subharmonic waves. A, actual dispersion curve; ▲ fundamental frequency $f_F = \omega_F/2\pi$ and wavenumber $1/\lambda_F = k_F/2\pi$; V, first virtual dispersion curve; △ harmonic frequency $2f_F$ and harmonic wavenumber $2/\lambda_F$.

makes the corresponding frequency peaks broader (figure 2*b*). In addition, the lifetimes of the excited modes are necessarily rather short as their increments are usually negative and, simultaneously, their motion is disturbed by nonlinear interference with the fundamental wave and with other excited modes. The synchronization and selection of discrete frequencies is thus gradually lost in the anode direction (ie in the direction of the group velocities), and the spectrum becomes continuous with a broad maximum around the maximum of the wave-increment. Only a slight peak of frequency f_F remains from the coherent wave.

The extension of the region of the irregular motion towards the cathode with increasing current may be explained thus: the growth rate of the fundamental mode increases with increasing current with the result that nonlinear effects occur nearer the cathode; simultaneously, the increment for the harmonic waves lying on the actual dispersion curve is higher, which makes the forced excitation of harmonic wave modes easier.

From the space-time picture figure 3(*a*), it is observed that when a wavecrest (striation) changes its velocity during its passage from the anode to the cathode, then the adjacent wave crest on the anode side also changes its velocity but at a later time and at point nearer to the anode. The velocity of propagation of this disturbance is evidently closely related to the group velocity of the wave motion.

5. Conclusions

If an originally coherent ionization wave becomes strongly nonsinusoidal due to nonlinear amplitude growth and saturation, it changes into an irregular wave motion with fluctuating phase velocity. Approaching the anode the wave-trains move still more irregularly, giving broad continuous spectra of frequency and wavenumber. As the

local wavenumber and instantaneous frequency of the individual wave-trains lie on one dispersion curve containing the coherent fundamental wave, the decomposition of the wave can be explained as a result of forced modulation by the wavenumber and frequency harmonics and their nonlinear interference.

References

- Grabec I 1973 *Proc. 11th Int. Conf. on Phenomena in Ionized Gases, Prague* (Prague: Czech. Acad. Sci.) p 309
- Krásá J and Pekárek L 1973 *Czech. J. Phys.* **B23** 863–6
- Lee D A, Bletzinger P and Garscadden A 1966 *J. Appl. Phys.* **37** 377–87
- Pekárek L 1971 *Proc. 10th Int. Conf. on Phenomena in Ionized Gases, Oxford* (Oxford: Donald Parsons) pp 365–403
- Perkin R M, Krásá J and Pekárek L 1975 *J. Phys. D: Appl. Phys.* in the press
- Perkin R M and Wooding E R 1973 *Phys. Lett.* **42A** 367–8
- Poberaj S and Grabec I 1970 *Z. Naturf.* **25a** 297–8
- Rohlenská K, Růžička T and Pekárek L 1972a *Czech. J. Phys.* **B22** 920–37
- 1972b *Phys. Lett.* **40A** 239–41
- Sato M 1970 *Phys. Rev. Lett.* **24** 998–1000
- Stewart R S, May W F, Emeleus K G, Cloutier J R M and Armstrong N H K 1965 *Int. J. Electron.* **18** 65–72

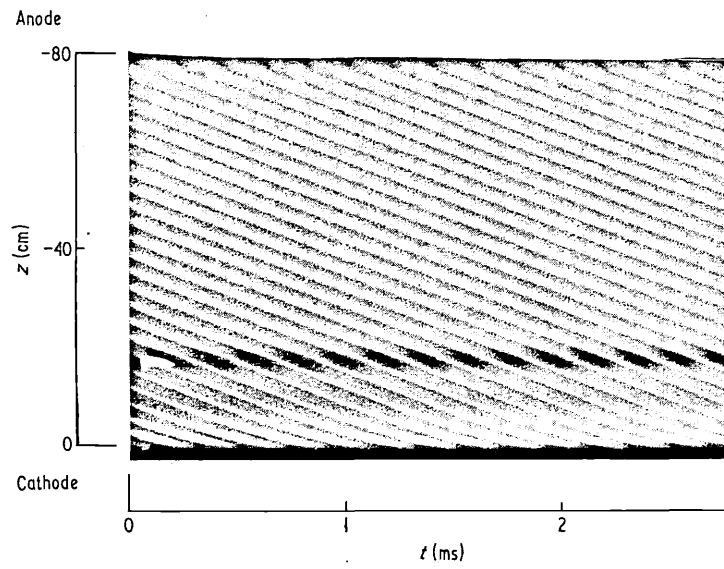
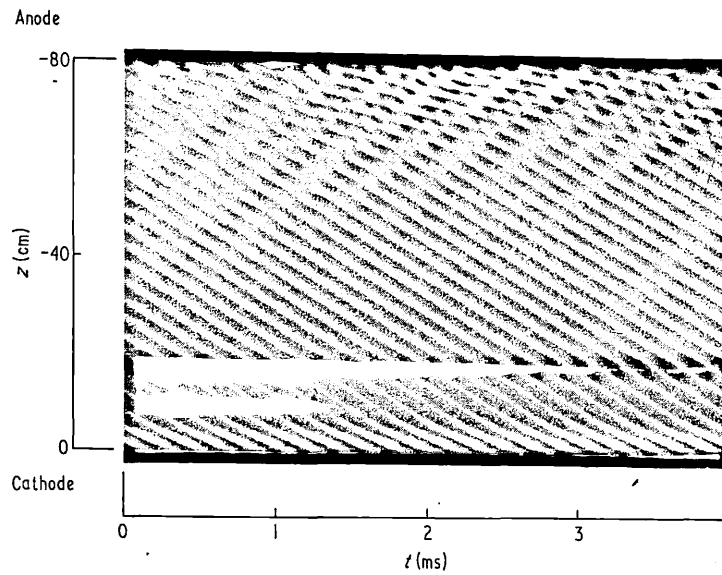
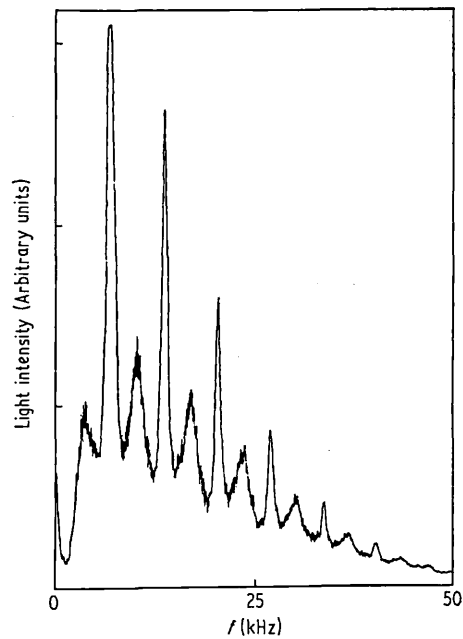


Figure 1. Rotating-drum, single-sweep photograph of the discharge at $I=25$ mA.



(a)



(b)

Figure 2. (a) Rotating-drum, single-sweep photograph of the discharge at $I=34$ mA. (The dark horizontal streak is caused by a clamp on the apparatus.) (b) Frequency spectrum 48 cm from cathode at $I=34$ mA.

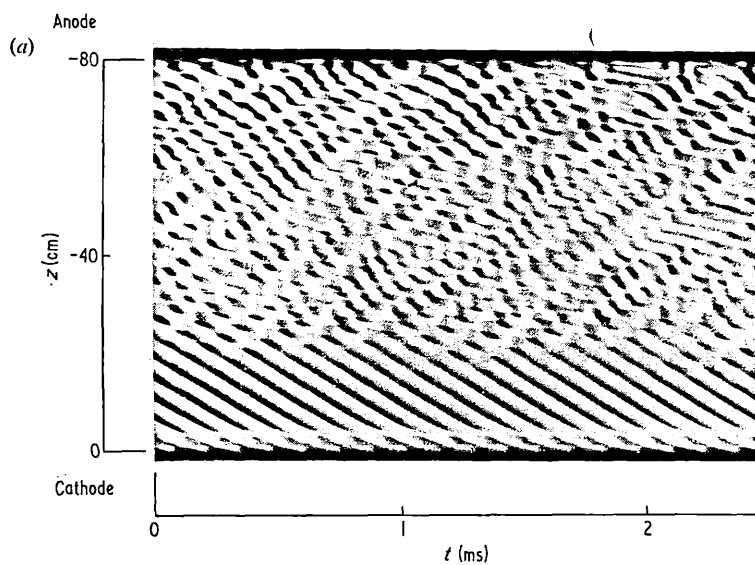


Figure 3. (a) Rotating-drum, single-sweep photograph of the discharge at $I=61.5$ mA; (b) frequency spectrum 11 cm from cathode, $I=61.5$ mA; (c) frequency spectrum 55 cm from cathode, $I=61.5$ mA; (d) dispersion curve of frequency f against wavenumber ($1/\lambda$), $I=61.5$ mA. (\blacktriangle point of fundamental self-excited periodic wave of frequency f_F and wavelength λ_F ; \pm error in wavenumber measurement.)

